

**SYNTHESIS AND STRUCTURE-PHOTOPHYSICAL PROPERTY
RELATIONSHIPS OF T₈, T₁₀, T₁₂ AND OLIGOMERIC ORGANIC
FUNCTIONALIZED SILSESQUIOXANES**

by
Joseph C. Furgal

A dissertation submitted in partial fulfillment
of the requirements for the degree of
Doctor of Philosophy
(Chemistry)
in The University of Michigan
2015

Doctoral Committee:

Professor Theodore G. Goodson III, co-Chair
Professor Richard M. Laine, co-Chair
Associate Professor Bart Bartlett
Associate Professor Jinsang Kim
Professor Melanie Sanford

© Joseph C Furgal

2015

Dedication

This dissertation is dedicated to

Mom and Dad

Granny and Grandaddy

Allison and Charlie

Katie

This work would have been impossible without them!

Acknowledgements

I would like to express my appreciation first to both of my advisors, Professors Ted Goodson III and Rick Laine for their support, guidance, inspiration and patience throughout this work. It was painful having two advisors, but I would not have had it any other way. I extend thanks to my committee members Melanie, Jinsang and Bart for their comments and support. I thank Timothy Scott for his support and future Post Doctoral research opportunities.

I also thank the current and previous members of both the Goodson Group and the Laine Group for their friendship and support, especially Dr. Jae Hwan Jung for his help with getting started on synthetic research in silsesquioxanes, Dr. Jin Zhang for her help with learning laser spectroscopy analysis techniques, as well as Dr. Santy Sulaiman, Dr. Travis Clark, Dr. Sung Hei Yau, Dr. Meng Guo, Dr. Oleg Varnavski, Neranga Abeyasinghe, Eongyu Yi, Nate Taylor, Phi Doan, David Pan and Mozghan Bahrami. I would also like to thank my undergraduate army for all their help with experiments and making research a truly enjoyable experience including Matt Schwartz, Sarah Clark, Tim Odykirk, Felicia Murry, Jeffery Xiong, and Brandon Yik. I thank all of the visiting scientists I have worked with over the years especially Dr. Elma Rodriguez, Dr. Ayako Nakao, and Honami Yamane. I also thank Casey Dougherty and Mark Banaszak-Holl for their collaboration and friendship.

Special thanks are in order to the Chemistry Department and the Macromolecular Science and Engineering Center, especially Nonna Hamilton who was always willing to have random conversations and help solve any administrative challenges that popped up.

I would also like to thank James Windak and Paul Lennon of the Chemistry Department Mass Spec Services Lab for all their help with determining molecule compositions.

Gratitude is also given to the UDM Chemistry Department faculty, especially my advisor Prof. Matt Mio for getting me interested in chemistry and turning me away from

a degree in music, as well conversations about graduate school toward maintaining my sanity.

I also thank my family, my church and God for all of their support over the years and keeping me motivated to become the first doctor in the family. Without my girlfriend Allison and my sweet dog Charlie there is no way I could have handled all the stress of graduate school, and I love them both dearly.

Lastly, I would like to thank the funding that supported my graduate education. This includes the Department of Energy: Energy Frontier Research Center, Boeing Corporation, Intel Corporation, TRW, UM Chemistry for Graduate Instructor opportunities and a Chemistry Research Excellence Fellowship, and finally Rackham Graduate School for the prestigious honor of being chosen for a Rackham Predoctoral Fellowship.

Table of Contents

Dedication.....	ii
Acknowledgements.....	iii
List of Figures.....	x
List of Schemes.....	xx
List of Tables.....	xxiii
List of Appendices.....	xxvii
Abstract.....	xxviii
Chapter 1 Introduction.....	1
1.1 History and Background.....	1
1.2 Routes to Functionalized Alkoxysilanes.....	3
1.2.1 Commercial Methods.....	3
1.2.2 Other Routes to Alkoxysilanes.....	5
1.2.3 R-alkoxysilanes from Spirosiloxanes.....	7
1.3 Introduction to Silsesquioxanes.....	9
1.3.1 Completely Condensed Silsesquioxanes.....	12
1.3.2 General Mechanism of Formation for Silsesquioxanes.....	14
1.3.3 Examples of Post-Synthetic Functionalization.....	15
1.4 Silsesquioxanes and Fluoride.....	17
1.4.1 Theoretical Investigations of Fluoride Encapsulation/Catalysis.....	20
1.5 Silsesquioxane Based Polymers.....	21
1.6 Optical/Electronic Properties of Silsesquioxanes.....	25
1.6.1 Theoretical Investigations.....	33

1.6.2	Non-Linear Optical Properties of Silsesquioxanes.....	35
1.6.3	Fluorescence Lifetime Kinetics.....	40
1.7	Overview of Subsequent Chapters.....	42
	References:.....	44
	Chapter 2 Experimental Methods.....	61
2.1	Analytical Methods.....	61
2.1.1	Standard Characterization.....	61
2.1.2	Photophysical Characterization.....	64
2.2	Materials.....	69
2.3	Synthetic Methods.....	70
2.3.1	Nucleophilic Substitution of Alkoxysilanes.....	70
2.3.2	Decaphenylsilsesquioxane [PhSiO _{1.5}] ₁₀	71
2.3.3	T _{10/12} Stilbenevinylsilsesquioxanes, [stilbenevinylSiO _{1.5}] _{10,12}	73
2.3.4	Separation and Photophysical Properties of T ₁₀ and T ₁₂ StilbenevinylSQs ..	75
2.3.5	Beads on a Chain (BoC) Polymers Based on Mixed Phenyl-vinylSQs	76
	References:.....	81
	Chapter 3 Silsesquioxanes from the Ground Up: Nucleophilic Attack of R-lithium at Tetrahedral Silicon in Alkoxysilanes.....	83
3.1	Abstract.....	83
3.2	Introduction.....	84
3.3	Experimental Methods.....	87
3.4	Results and Discussion.....	87
3.4.1	Reactions with Spirosiloxane I.....	87
3.4.2	Other Nucleophiles.....	99
3.4.3	Nucleophilic Substitution at TEOS.....	104

3.4.4	Summary of Findings	109
3.4.5	Silsesquioxane Synthesis.....	109
3.5	Conclusion.....	112
	References:.....	113
Chapter 4 D_{5h} $[\text{PhSiO}_{1.5}]_{10}$ Synthesis via F^- catalyzed rearrangement of $[\text{PhSiO}_{1.5}]_n$. An Experimental/Computational Analysis of Likely Reaction Pathways, Photophysical Properties and Post Synthetic Functionalization.....		
4.1	Abstract	116
4.2	Introduction	117
4.3	Experimental	119
4.4	Results and Discussion.....	119
4.4.1	Optimized Synthesis of $[\text{PhSiO}_{1.5}]_{10}$	119
4.4.2	Reaction Mechanism Studies.....	123
4.4.3	Modeling Studies.....	141
4.4.4	Photophysical Properties of $[\text{PhenylSiO}_{1.5}]_x$	145
4.4.5	Functionalization of $[\text{PhenylSiO}_{1.5}]_{10,12}$	151
4.5	Conclusions	151
	References:.....	152
Chapter 5 Modification of 3-D molecular mixtures of $[\text{vinylSiO}_{1.5}]_{10}/[\text{vinyl-SiO}_{1.5}]_{12}$, Functionalization to $[\text{R-stilbenevinylSiO}_{1.5}]_{10/12}$, and Photophysical Properties.....		
5.1	Original Publication Information	158
5.2	Abstract	158
5.3	Introduction	159
5.4	Experimental Procedures.....	161
5.5	Results and Discussion.....	161
5.5.1	FTIR Studies.....	165

5.5.2	GPC studies	166
5.5.3	DSC Studies.....	166
5.5.4	Photophysical Studies.....	167
5.5.5	SQs as Electron Acceptors in Photovoltaics.....	184
5.6	Conclusions	187
References:.....		188
Chapter 6 Analyzing Structure-Photophysical Property Relationships for Isolated T ₈ , T ₁₀ and T ₁₂ Stilbenevinyl Silsesquioxanes.....		
		192
6.1	Original Publication Information	192
6.2	Abstract	192
6.3	Introduction	193
6.4	Experimental Procedures.....	195
6.5	Results and Discussion.....	195
6.5.1	Synthesis and Separations	196
6.5.2	Photophysical Characterization	200
6.5.3	Summary of Findings	212
6.5.4	Additions and Future Work.....	213
6.6	Conclusions	215
References:.....		215
Chapter 7 Beads on a Chain (BoC), Phenylsilsesquioxane (SQ), Polymers Via F ⁻ Catalyzed Rearrangements and ADMET or Reverse Heck Cross-coupling Reactions; through chain, extended conjugation in 3-D with potential for dendronization.		
		222
7.1	Original Publication Information	222
7.2	Abstract	222
7.3	Introduction	223
7.4	Experimental Procedures.....	226

7.5	Results and Discussion.....	226
7.5.1	Syntheses of [(vinyl) ₂ (Ph) _{n-2} SiO _{1.5}] _n and [(vinyl) ₂ (<i>p</i> -IPh) _{n-2} SiO _{1.5}] _n (n = 10, 12)	227
7.5.2	Synthesis of Polymers by Metathesis	231
7.5.3	Functionalization of Polymer A with R-styrene.....	234
7.5.4	Synthesis of Polymers by Reverse Heck Cross-coupling	235
7.5.5	Model Compound Syntheses.....	237
7.5.6	Photophysical Studies.....	237
7.5.7	Two-photon Spectroscopy.....	241
7.5.8	Comparison of Steady State Spectroscopy for BoC Polymers.....	241
7.6	Conclusions	244
Chapter 8	Summary and Future Work.....	251
8.1	Summary and Insights.....	251
8.2	Future Work	253
Appendices	263

List of Figures

Figure 1.1. Silsesquioxane publications per year (1988-2014).....	9
Figure 1.2. Silsesquioxane structural motifs.....	11
Figure 1.3. Siloxane nomenclature methodology.....	11
Figure 1.4. Examples of SQ cage structures and their simplified structures.....	13
Figure 1.5. Typical sizes and volumes of silsesquioxane molecules; SQ with R-groups in different octants of Cartesian space.....	13
Figure 1.6. Mechanisms of acid and base catalyzed reactions to form SQs.....	15
Figure 1.7. a. ^{29}Si NMR of mixed $\text{F}^-@[\text{vinyl}(\text{SiO})_{1.5}]_8$ and $\text{F}^-@[\text{phenyl}(\text{SiO})_{1.5}]_8$, b. ^{29}Si NMR of $[\text{phenyl}(\text{SiO})_{1.5}]_8$ and $[\text{vinyl}(\text{SiO})_{1.5}]_8$ equivalent Me_4NF , both in THF.....	19
Figure 1.8. Theoretical energy diagram of fluoride encapsulation within an HSQ core ..	20
Figure 1.9. Hybrid silsesquioxane-silicone polymer, R = cyclohexyl.....	22
Figure 1.10. Epoxy coupling reaction to BoC polymers.....	25
Figure 1.11. Absorption and emission of $\text{T}_{8,10,12}$ Cl-propylSQs.....	26
Figure 1.12. AFM image of an $[\text{PhSiO}_{1.5}]_8$:P3HT:PCBM film (100-150 nm aggregates).	27
Figure 1.13. a. Structure and b. absorption and fluorescence of SQ anchored poly(2-methoxy-5-(2-ethylhexyloxy)-1,4-phenylenevinylene).....	28
Figure 1.14. Absorption and emission comparison of ortho and para (<i>o/p</i>)-MeStilbeneSQs to <i>p</i> -MeStilbene in THF.....	30
Figure 1.15. a. Normalized absorption (empty symbols) and emission (closed symbols) of 4'-vinylbiphenyl-3,5-dimethylalcohol functionalized SQ (Blue) and 4'-vinylbiphenyl-3,5-dimethylalcohol (Red).....	31

Figure 1.16. Absorption and emission of stilbeneoctavinylSQs.....	32
Figure 1.17. (a) Me ₂ NStil-corner, (b) Me ₂ NStil-half, and (c) Me ₂ NStilOS.	32
Figure 1.18. Absorption and emission of T _{10/12} divinylbenzene linked oligomer (BoC). ¹⁴⁰	33
Figure 1.19. Comparison of HOMO and LUMO of silsesquioxane systems, and their charge transfer mechanisms.....	35
Figure 1.20. Comparison of one and two-photon excitation pathways.	36
Figure 1.21. Examples of structural motifs in two-photon absorbing organic systems....	38
Figure 2.1. Redox example curve of pentafluorophenylstilbenevinylSQ; reduction used for calculation of LUMO, oxidation used for calculation of HOMO.	64
Figure 2.2. Two-photon excited fluorescence setup, dash dot line for wavelengths 720- 820 nm, dashed line for wavelength of 650 nm from beam doubled system.	67
Figure 2.3. Fluorescence upconversion setup for 400 nm sample excitation.	69
Figure 3.1. MALDI-ToF of 1:1 Spirosiloxane (I):PhLi (-78 °C), m/z ≈ 344.4 is the parent ion for LiPhSi(2-methyl-2,4-diolato) ₂ , which loses PhLi to give I at m/z = 259.	88
Figure 3.2. ²⁹ Si NMR of synthesized tetraphenylsilane, -14.4 ppm, isolated from a 1:1 PhLi:I reaction run at -78 °C then warmed to room temperature without quenching, and then rinsed with diethyl ether to remove excess I.....	89
Figure 3.3. EI mass spectrum of tetraphenylsilane isolated from a 1:1 PhLi:I reaction run at -78 °C then warmed to room temperature without quenching, and then rinsed with diethyl ether to remove excess I. Tetraphenylsilane is at 336 m/z. The peak at m/z = 259 is Ph ₃ Si and the peak at m/z = 182 is Ph ₂ Si.	89
Figure 3.4. Negative ion ESI mass spectrum of 1:1 PhLi:I after quenching with MeI. ...	90
Figure 3.5. EI-MS of 1:1 PhLi:I (3 h, -78 °C) quenched with MeI, peak at 457.9 m/z is III, and peak at 442.8 m/z is III-Me.	91
Figure 3.6. ²⁹ Si NMR spectrum of the MeI quenched -78 °C 1:1 PhLi:I.	91

Figure 3.7. EI MS of 1:1 PhLi:I after quenching with TMSCl; peaks: 410.3 m/z is IV, 259.1 is I.....	96
Figure 3.8. ²⁹ Si NMR spectrum of the TMSCl quenched -78 °C 1:1 PhLi:I. Peaks: -4.8 ppm, TMS-benzene; -59 ppm PhSi(RO) ₃ ; -65 ppm Ph-Si-OSiMe ₃ (OR) ₂	97
Figure 3.9. EI mass spectrum of 1:1 PhLi:I (4.5 h, -78 °C), quenched with TMSCl; I-Me at 245.1 m/z, V at 310.1 m/z, and V-Me at 295.1 m/z.....	98
Figure 3.10. ²⁹ Si NMR spectrum of 1:1 PhLi:I (4.5 h, -78 °C) quenched with TMSCl, Peaks ≈ 55-65 ppm are PhSi(O) _x units, peak at 9.17 ppm is Si-O-SiMe ₃ , peak at -82 ppm is I.....	98
Figure 3.11. EI mass spectrum of anthracenylLi:I (3 h, -78 °C), quenched with TMSCl; VIII at 410.2 m/z, VIII-Me at 395.2 m/z, VIII-TMS at 338.1 m/z, 438.2 is VIII without TMS group.....	103
Figure 3.12. ²⁹ Si NMR of 1:1 anthracenylLi:I (3 h, -78 °C, VIII) quenched with TMSCl, peak at 57.4 ppm is R-Si(OR) ₃ , peak at 10.0 ppm is Si-O-SiMe ₃ , peak at -2.8 is TMS-anthracene, I is unobserved at -82 ppm.	103
Figure 3.13. EI mass spectrum of 1:1 PhLi:TEOS after quenching with MeI at -78 °C.	104
Figure 3.14. ²⁹ Si NMR of 1:1 Ph:TEOS, -32.2 (18% Ph ₂ TE), -57.9 (Ph ₁ TE), -81.6 (TEOS) after quenching with MeI.	105
Figure 3.15. EI mass spectrum of 0.5:1 PhLi:TEOS at -78 °C (2h) after quenching with MeI. PhSi(OEt) ₃ is at 240.1 m/z, TEOS is at 208.1 m/z, both of ~equal peak height....	108
Figure 3.16. EI mass spectrum of 0.5:1 PhLi:TEOS at -78 °C (2h) without quenching, 272.3 m/z is Ph ₂ Si(OEt) ₂	109
Figure 3.17. GPC trace comparison of oligomeric materials from 1:1 PhLi:I (6 h) compared with an overnight TBAF catalyzed PhSQ synthesis.	110
Figure 3.18. MALDI-ToF spectrum of PhSQs made by TBAF catalyzed reaction of PhI oligomers; all peaks are Ag ⁺ ions.	110

Figure 3.19. MALDI-ToF spectrum of anthraceneSQs made by TBAF catalyzed reaction of AnthraceneI (VIII).....	111
Figure 3.20. Absorption and emission spectra of anthraceneSQ.....	112
Figure 4.1. MALDI-ToF of crude phenylSQ reaction product mixture, $[\text{PhSiO}_{1.5}]_{10}$ at 1400.2 m/z.....	121
Figure 4.2. MALDI-ToF spectrum of $[\text{PhSiO}_{1.5}]_{10}$ (Phenyl T_{10}), Ag^+ peak at 1398.9 m/z $[\text{Ag-Si}_{10}\text{O}_{15}(\text{C}_6\text{H}_5)_{10}]$	122
Figure 4.3. ^{29}Si NMR of $[\text{PhSiO}_{1.5}]_{10}$, peak at -79.61 ppm corresponding to a T_{10} compound.....	122
Figure 4.4. TGA of $[\text{PhSiO}_{1.5}]_{10}$ in air (10°C/min), actual and theoretical ceramic yields are 45.9% and 46.4%, with $T_{d5\%}$ of 490 °C.	123
Figure 4.5. MALDI-ToF of $[\text{PhSiO}_{1.5}]_{18,20,22}$ mixture.	123
Figure 4.6. MALDI-ToF analysis of $[\text{PhSiO}_{1.5}]_{10}$ equilibration with F^- after 3 days, ratio 8:10:12 of 1:3:1.3.....	124
Figure 4.7. MALDI-ToF analysis of $[\text{PhSiO}_{1.5}]_{12}$ equilibration with F^- after 3 days, ratio 8:10:12 of 1:3:1.3.....	124
Figure 4.8. ^{19}F NMR reaction analysis of Reaction 3 conditions (OPS F^- rearrangement) over a 55 min time frame at 0 °C.....	126
Figure 4.9. Structures of exo and endo fluoro T_8 , $[\text{PhSiO}_{1.5}]_8[\text{F}^-]$ and $\text{F}^- @[\text{PhSiO}_{1.5}]_8$ respectively.	126
Figure 4.10. ^{29}Si NMR of OPS+5 mol% TBAF in DCM at -20 °C after 12 h acquisition time.	127
Figure 4.11. MALDI-ToF showing T_8 to T_{10} rearrangement reaction taken after 2 min at RT, with 1141.4 m/z T_8 and 1400.1 m/z T_{10} , Ag^+ ion peaks.	128
Figure 4.12. MALDI-ToF showing T_8 to T_{10} rearrangement reaction taken after 45 min at RT, with 1141.9 m/z T_8 , 1399.4 T_{10} , and 1658 T_{12} all of which are Ag^+ ion peaks.	129

Figure 4.13. [PhSiO _{1.5}] ₁₀ (1400 m/z) composition (relative intensity vs. time) over 36 h under Reaction (3) conditions (60 mM OPS in DCM, 5 mol% F ⁻).	131
Figure 4.14. Comparison of [PhSiO _{1.5}] ₁₀ composition within the first 25 min of reactions (2-6 and 9).....	132
Figure 4.15. T ₁₀ composition at 0, 20 and 35 °C for F ⁻ catalyzed rearrangement of OPS over the first 25 min of reaction.....	132
Figure 4.16. MALDI-ToF of 35 °C OPS rearrangement Reaction 10.....	133
Figure 4.17. MALDI-ToF OPS + TBAF in DCM under anhydrous Reaction (3) conditions (3 days drying with 4Å molecular sieves), showing OPS Ag ⁺ ion at 1142.1 m/z.....	133
Figure 4.18. MALDI-ToF of H ₂ ¹⁸ O isotope study under pseudo reaction (3) conditions; T ₁₀ region shown at 1414.5 m/z, suggesting seven ¹⁸ O are incorporated on average.....	135
Figure 4.19. MALDI-ToF spectrum of OPS + TBAF in DMF after 24 h (Reaction 20).	136
Figure 4.20. EI mass spectrum showing fluoride functionalized free corners (185.1 m/z = tributylammonium), Reaction (3) after 2 min. b. MALDI-ToF showing Ag ⁺ PhSi(OH) ₂ F at 266.2 m/z, Reaction (3) after 1 min.	137
Figure 4.21. MALDI-ToF spectrum of OPS + TBAOH in DCM under pseudo Reaction (3) conditions.	138
Figure 4.22. T ₈ and T ₁₀ concentration vs time for Reaction (3) monitored by MALDI-ToF over the first 50 min of reaction.....	138
Figure 4.23. a. Natural log plot of T ₈ concentration over the first 600 sec giving a slope of -5.2x10 ⁻³ s ⁻¹ . b. Arrhenius plot from T ₈ concentrations at 35°, 20°, 0°, and -35 °C, E _a ~5±1 kcal/mol.	139
Figure 4.24. Reaction (3) intermediate concentrations by MALDI-ToF over the first 25 min and then after 24 h.	140
Figure 4.25a-d. B3LYP optimized structures: a) T ₉ -OH ₁ b) T ₇ -OH ₃ , c) T ₁₀ , d) T ₁₂	141

Figure 4.26. Potential mechanism from observed reaction intermediates and their model [HSiO _{1.5}] _n heats of reaction, ΔH (kcal/mol).....	143
Figure 4.27. Absorption and emission spectra for [PhSiO _{1.5}] _{8,10,12,[18,20,22]} in THF and acetonitrile.....	146
Figure 4.28. Proposed interaction orientations between phenyl groups.	147
Figure 4.29. CIS-6-31G(d,p) calculated a. HOMO (-0.3272 eV) and b. LUMO (0.1062 eV) of [PhSiO _{1.5}] ₈	149
Figure 4.30. CIS-6-31G(d,p) calculated a. HOMO (-0.3221 eV) and b. LUMO (0.1087 eV) of [PhSiO _{1.5}] ₁₀	149
Figure 4.31. CIS-6-31G(d,p) calculated a. HOMO (-0.3174 eV) and b. LUMO (0.1180 eV) of [PhSiO _{1.5}] ₁₂	150
Figure 5.1. Representative FTIR for GEN1 <i>p</i> -MeOStrySQ and GEN2 C ₆ F ₅ stilbenevinylSQ.....	165
Figure 5.2. GPC traces of vinylSQs and styrenylSQs and stilbenevinylSQ (GEN2).	166
Figure 5.3. DSC traces of selected styrenylSQs and stilbenevinylSQ (GEN2), second scan.	167
Figure 5.4. UV-vis absorption and PL spectra for GEN1 T _{10/12} R = S-Ph, and D-Ph in THF.....	169
Figure 5.5. UV-vis absorption and PL spectra of GEN1 T _{10/12} R = S-NP and D-NP (THF).	169
Figure 5.6. UV-vis absorption and PL spectra of GEN1 T _{10/12} R = S-An and D-NP (THF).	169
Figure 5.7. Solvent study of GEN1 T _{10/12} R = S-An by sequential dilution with THF to reduce the amount of acetonitrile and the overall concentration.	171
Figure 5.8. GEN1 T _{10/12} R = An emission spectra at different acetonitrile:THF ratios (1 μM).	172

Figure 5.9. UV-vis absorption spectra of selected GEN2 vinylstilbene compounds in THF.....	174
Figure 5.10. PL emission spectra of selected GEN2 vinylstilbene compounds in THF.	174
Figure 5.11. UV/vis absorption and PL spectrum of GEN2 T _{10/12} R = NH ₂	175
Figure 5.12. Emission studies of T _{10/12} R = H in acetonitrile/THF mixtures at constant 0.86 μM concentration.....	176
Figure 5.13. Emission studies of T _{10/12} R=H in hexane/THF at constant 0.86 μM concentration.....	177
Figure 5.14. T _{10/12} R = H emission in 10:1, 20:1 and 30:1 hexane:THF at various concentrations, suggesting “aggregate” formation.	177
Figure 5.15. Emission spectra of T _{10/12} R=H in 10:1, 20:1 and 30:1 MeOH:THF at various concentrations, showing “aggregate” formation.....	178
Figure 5.16. Possible aggregation or exciplex formation between two GEN2 stilbenevinylSQs.	179
Figure 5.17. Two-photon absorption spectra of selected GEN2 vinylstilbene compounds in THF.....	183
Figure 5.18. Cyclic Voltammetry studies of selected GEN2 compounds, with published data for P3HT and PCBM added.	185
Figure 5.19. Cyclic Voltammetry oxidation and reduction curves of pentafluorostilbenevinylSQ (5F).	186
Figure 5.20. LUMO and HOMO orbitals of C ₆₀	186
Figure 5.21. Cyclic voltammogram of oxidation and reduction of C ₆₀	187
Figure 6.1. StilbenevinylSQ cages, R = stilbenevinyl, R' = H.....	194
Figure 6.2. Solvent study and MALDI-ToF analysis of separated mixed stilbenevinylSQs.	198

Figure 6.3a and b. MALDI-ToF Comparison of the separated T ₁₀ and T ₁₂ stilbenevinylSQ compounds.....	198
Figure 6.4. ²⁹ Si NMR of T ₁₀ stilbenevinylSQ in CDCl ₃	199
Figure 6.5. ²⁹ Si NMR of T ₁₂ stilbenevinylSQ in CDCl ₃	199
Figure 6.6a. Absorption spectra of stilbenevinylSQs, b. Emission spectra (THF, ~3x10 ⁻⁷ M).....	201
Figure 6.7a. Comparison of excitation spectra for T ₁₀ and T ₁₂ stilbenevinylSQ with emission held at 387 and 450 nm, b. Comparison of emission of T ₁₀ stilbenevinylSQ with excitation at 333 or 400 nm, (THF, ~2x10 ⁻⁷ M).....	202
Figure 6.8. TPEF plot comparing T _{8,10,12} stilbenevinylSQs at 800 nm excitation.....	204
Figure 6.9. Log-Log plot for TPA cross-sections at 740 nm.....	205
Figure 6.10. Comparison of short fluorescence lifetime components of T _{8,10,12} stilbenevinylSQs with the instrument response function at 286 nm.....	207
Figure 6.11. Comparison of long decay fluorescence lifetime components of stilbenevinylSQs.....	208
Figure 6.12. Fluorescence decay of T _{10/12} (H) at 400 nm excitation, and 450 nm collection.....	211
Figure 6.13. Fluorescence anisotropy measured at 286 nm excitation and 450 nm fluorescence collection for stilbenevinylSQs.....	212
Figure 6.14. a and b. SEM images of T ₁₀ stilbenevinylSQ aggregates.....	213
Figure 6.15. AFM image of T ₁₀ stilbenevinylSQ aggregates on mica (nm).....	214
Figure 6.16. NSOM image of T ₁₀ stilbenevinylSQ aggregates on mica (nm).....	214
Figure 6.17. NSOM-TPEF spectrum of T ₁₀ stilbenevinylSQ taken on a USB-2000 Ocean Optics Spectrophotometer, with Gaussian fit.....	214

Figure 7.1. Heck cross-coupling synthesis of a BoC oligomer with 1,4-divinyl bridges between phenylT ₁₀ and phenylT ₁₂ SQs	223
Figure 7.2. MALDI-ToF spectrum of [(vinyl) ₂ (Ph) _{n-2} SiO _{1.5}] _n (n = 10, 12).	228
Figure 7.3. MALDI-ToF spectrum of [(vinyl) ₂ (IPh) _{n-2} SiO _{1.5}] _n (n = 10, 12).	228
Figure 7.4. GPC analysis of [(vinyl) ₂ (Ph) _{n-2} SiO _{1.5}] _n and [(vinyl) ₂ (IPh) _{n-2} SiO _{1.5}] _n , (n = 10, 12).	231
Figure 7.5. GPC analysis of polymers A and B.	232
Figure 7.6. GPC analysis of polymers C and D, with characterization data given in Table 7.5.	235
Figure 7.7. GPC of polymers E and F, with 1,4-dibromobenzene and 4,4'-dibromostilbene linkers.	237
Figure 7.8. Steady-state absorption and emission comparison of ADMET linked BoC polymers.	238
Figure 7.9. Absorption and emission comparison of a. polymer F and model 1, and b. polymer E and model 2.	240
Figure 7.10. Absorption and emission of dimethylfluorene polymer derivatives.	243
Figure 8.1. J-V curves of OPV devices fabricated with a mixture of P3HT, PCBM, and di-styryl-pentafluorophenyl ₈ SQ, with device configuration of glass/ITO/PEIE/active layer/MoO ₃ /Ag.	255
Figure 8.2. a. Photocurrent histogram showing an increase in photocurrent up to 15 wt.% SQ, b. Conductive AFM measurement of the mixed P3HT:PCBM:SQ film with SQs theorized to be in black.	256
Figure A.1. Example basic input for benzene single point energy.	263
Figure A.2. Setting up time and memory requirements.	264
Figure A.3. Example for setting up CIS calculations.	265

Figure A.4. GamessQ file que GUI interface.....	265
Figure B.1. 3 rd harmonic upconversion table setup.....	266
Figure B.2. 3 rd harmonic upconversion reflection angle.....	267
Figure B.3. 3 rd harmonic upconversion wall spot positions.....	268
Figure B.4. 3 rd harmonic upconversion pinhole position.....	268
Figure C.1. ²⁹ Si NMR of 1:1.2 2-thienylli:I (IX) quenched with Me ₃ SiCl at -78 °C.....	270
Figure C.2. EI MS of 1:1.2 9,9-dimethylfluorenylli:I (IX) quenched with Me ₃ SiCl at -78 °C.....	271
Figure C.3. ²⁹ Si NMR of 1:1.2 9,9-dimethylfluorenylli:I (IX) quenched with Me ₃ SiCl at -78 °C.	271
Figure C.4. EI MS of 1:1.2 Li-phenylacetylide:I (VII) quenched with Me ₃ SiCl at -78 °C	272
Figure C.5. ²⁹ Si NMR of 1:1.2 Li-phenylacetylide:I (VII) quenched with Me ₃ SiCl at -78 °C.....	272
Figure C.6. EI MS of 1:1.2 methylnaphthalenylli:I (X) quenched with Me ₃ SiCl at -78 °C.....	273
Figure C.7. ²⁹ Si NMR of 1:1.2 methylnaphthalenylli:I (X) quenched with Me ₃ SiCl at -78 °C.....	273
Figure D.1. Absorption and emission of T ₁₀ stilbenevinylSQ.....	274

List of Schemes

Scheme 1.1. Depolymerization of silica by alcohol.	5
Scheme 1.2. Depolymerization of silica with catechol and KOH.	5
Scheme 1.3. Depolymerization of silica with ethylene glycol to form glycolatosilicate. ..	6
Scheme 1.4. Depolymerization of silica with ethylene glycol to form glycolatosilicate. ..	6
Scheme 1.5. Depolymerization of silica with ethylene glycol to form glycolatosilicate. ..	6
Scheme 1.6. Depolymerization of silica with 2-methyl-2,4-pentandiol and catalytic NaOH.	7
Scheme 1.7. Typical reactions of triscatecholato silicate or tetralkoxysilanes with Grignard and lithium reagents	8
Scheme 1.8. Outline of a synthetic process for converting silica to silsesquioxanes	9
Scheme 1.9. Example synthetic method to R-silsesquioxanes.	10
Scheme 1.10. Functionalization of phenylsilsesquioxanes (T ₈): (a, b, c, d, e, and f) Electrophilic aromatic substitution (EAS), (g and p) Buchwald-Hartwig reactions, (h and r) Sonogashira, (j and s) Suzuki, (k, q, t, and u) Heck	16
Scheme 1.11. Reactions of vinylsilsesquioxanes (T ₈): (i) Heck cross-coupling, (ii) Cross-metathesis, (iii) Thiolene reactions, (iv) Hydrosilylation reactions	16
Scheme 1.12. Heck cross-coupling to form stilbeneoctavinylSQs.	17
Scheme 1.13. Synthesis of propylmethacrylate silsesquioxane polymers.	22
Scheme 1.14. Polymerization of difunctional SQs to form BoC polyimides.	23
Scheme 1.15. Heck cross-coupling reaction to form BoC polymers, (phenyl/divinylbenzene).	24

Scheme 3.1. Typical reactions of triscatecholatosilicate or tetraalkoxysilanes with Grignard and lithium reagents	85
Scheme 3.2. Proposed mechanism for nucleophilic substitution at Si via pentacoordinate intermediates	85
Scheme 4.1. Synthesis of [PhSiO _{1.5}] _{8,10,12} by fluoride catalyzed rearrangement.....	118
Scheme 4.2. Synthesis and separation of phenylSQs by the CaCl ₂ quenching method.	120
Scheme 5.1. Heck coupling reactions of vinylT _{10/12} (GEN1).....	162
Scheme 5.2. Metathesis reactions of vinylT _{10/12} (GEN1).....	163
Scheme 5.3. Heck coupling reaction of <i>p</i> -Br-StyrenylvinylT _{10/12} (GEN2).	164
Scheme 6.1. Synthesis of T _{10/12} stilbenevinylSQs.....	196
Scheme 7.1. Synthesis of vinyl/phenyl mixed functional SQ compounds by F ⁻ catalysis.	224
Scheme 7.2. F ⁻ catalyzed rearrangement reaction of I ₈ OPS and OVS.....	227
Scheme 7.3. ADMET coupling of DVB with phenyl and iodophenyl vinyl SQs generating BoC polymers A and B.....	231
Scheme 7.4. Synthesis of R-styrene functionalized oligomers from polymer A.....	234
Scheme 7.5. Synthesis of BoC polymers E and F through Heck cross-coupling with 1,4-dibromobenzene and 4,4'-dibromostilbene.	236
Scheme 7.6. Synthesis of bis-vinyltriethoxysilylbenzene and 4,4'-bis-vinyltriethoxysilylstilbene model compounds 1 and 2.	237
Scheme 7.7. Synthesis of phenyl-fluoreneSQ BoC polymer.....	242
Scheme 8.1. Synthesis of di-styryl-pentafluorophenyl ₈ SQ and its HOMO-LUMO energy levels.	255
Scheme 8.2. Synthesis of mixed donor-acceptor SQs through F ⁻ catalyzed rearrangement.	256

Scheme 8.3. Controlled functionalization of SQs with donor and acceptor moieties. ...	257
Scheme 8.4. Synthesis of donor-acceptor BoC polymers.....	258
Scheme 8.5. Example synthetic methodology for developing squaraine functionalized SQs.....	258
Scheme 8.6. Synthesis of high surface area materials based with methyl functionality by fluoride catalyzed cage formation.....	259
Scheme 8.7. High surface chiral separation polymers based on N-acetyl-L-cysteine functionalized silsesquioxanes by thiol-ene functionalization followed by fluoride catalyzed polymer formation.	261

List of Tables

Table 1.1. Example synthetic parameters to various T ₁₀ and T ₁₂ silsesquioxanes.	12
Table 1.2. TPA properties of silsesquioxane derivatives and quantum efficiencies (Φ)..	40
Table 2.1. Synthesized SQ materials and their chemical makeup.	80
Table 3.1. Literature ²⁹ Si NMR chemical shifts of selected alkoxysilanes in CDCl ₃	92
Table 3.2. Reaction conditions and observed characterization data for PhenylLi reactions with spiroxiloxane, all reactions were conducted at -78 °C for 2 h. (I = spiroxiloxane)...	92
Table 3.3. Reaction conditions and observed characterization data for RLi reactions with I, all reactions were conducted at -78 °C for 3h and quenched with Me ₃ SiCl unless otherwise noted.	100
Table 3.4. Reaction conditions and observed characterization data for PhenylLi reactions with TEOS, all reactions were conducted at -78 °C or -40 °C for 30 min – 2 h. (TE = TEOS).	106
Table 4.1. Literature ¹⁹ F NMR data for select Si-F species.....	126
Table 4.2. Reaction condition studies in DCM MALDI taken at 5 min intervals up to 25 min, and then taken at 24 h for final relative %T ₁₀ (108 mg OPS).....	128
Table 4.3. Observed MALDI-ToF peaks from Reaction (3), predicted formulae and relative peak intensities.....	129
Table 4.4. OPS rearrangement studies in selected solvents without F ⁻ removal. [60 mM concentration (108 mg of OPS in 15 mL of solvent), 20 °C/45μL-1M TBAF DCM/24 h.	134
Table 4.5. Rate constants from T ₈ consumption at different temperatures.....	139

Table 4.6. MP2 and B3LYP (6-31G(d)) total energies in Hartrees (gas and DCM), solvent stabilization energies in kcal/mol and ZPC corrected electronic+thermal enthalpies (Hartrees) of some HSQ structures.	142
Table 4.7. Comparison of cage solvent stabilization energy and their corresponding MALDI ratios.....	145
Table 4.8. Absorption and emission λ_{\max} for [PhSiO _{1.5}] _{8,10,12} and T _{18,20,22} in THF.....	146
Table 4.9. Phenyl-phenyl distances for different cage sizes.....	147
Table 4.10. CIS-6-31G(d,p) calculated HOMO and LUMO energy levels for [PhSiO _{1.5}] _x	150
Table 5.1. Characterization of T _{10/12} GEN 1 Mono (S) and Double (D) Heck coupling compounds.....	163
Table 5.2. Characterization of T _{10/12} GEN1 materials produced by metathesis.	163
Table 5.3. Characterization of T _{10/12} stilbenevinylSQ (GEN2) compounds.....	164
Table 5.4. Absorption and Emission Maxima for GEN1 compounds.....	170
Table 5.5. Photophysical data for GEN1 compounds.....	170
Table 5.6. Emission solvent study comparing GEN1 T _{10/12} R = S-An in acetonitrile, hexanes and THF.	172
Table 5.7. Absorption and Emission Maxima for GEN2 compounds.....	174
Table 5.8. UV/vis absorption and PL for 4-aminovinylstilbene Gen2 SQ as a function of solvent.....	175
Table 5.9. Emission (nm) of T ₈ and T _{10/12} stilbenevinylSQs (\pm 2 nm) in Acetonitrile:THF.	180
Table 5.10. Emission (nm) of T ₈ and T _{10/12} stilbenevinylSQs (\pm 2 nm) in hexane:THF or MeOH:THF of varying concentrations.....	180

Table 5.11. Emission of T ₈ and T _{10/12} vinylstilbene molecules (\pm 2 nm) in hexane:THF or MeOH:THF at constant concentrations.	181
Table 5.12. Two-photon studies of GEN2 compounds with respective cross-sections given.....	184
Table 5.13. Two-photon laser wavelengths studied and respective cross-section per chromophore on GEN2 SQs.	184
Table 6.1. ²⁹ Si NMR for separated stilbenevinylSQ cages.	199
Table 6.2. Comparison of T _{8,10,12} (H)-stilbenevinylSQ steady state properties in THF. .	201
Table 6.3. Comparison of TPA data for T _{8,10,12} (H)-stilbenevinylSQs (cross-sections GM/mol).	203
Table 6.4. TPA data for T _{8,10,12} (H)-stilbenevinylSQs (cross-sections GM/chromophore).	204
Table 6.5. TPEF emission maxima at different two-photon excitation wavelengths.	205
Table 6.6. T _{8,10,12} StilbenevinylSQ quantum yield values for 387 and 450 nm emission bands.	206
Table 6.7. Fluorescence lifetime data for T _{8,10,12} StilbenevinylSQ at 286 nm excitation and 450 nm collection (isotropy).	207
Table 6.8. Fluorescence lifetimes of selected T _{10/12} StilbenevinylSQ components excited at 286 nm with fluorescence collection at 385 nm.	210
Table 6.9. Fluorescence lifetimes of the T _{8,10,12} StilbenevinylSQ systems using fluorescence upconversion spectroscopy from excitation at 400 nm and collection at 450 nm.	211
Table 7.1. MALDI-ToF data for [(vinyl) ₂ (Ph) _{n-2} SiO _{1.5}] _n (n = 10, 12) w/Ag ⁺ ion.	228
Table 7.2. MALDI-ToF data for [(vinyl) ₂ (IPh) _{n-2} SiO _{1.5}] _n (n = 10, 12) without Ag ⁺ ion.†	229

Table 7.3. GPC and TGA data for difunctional SQ monomers for polymerization.	229
Table 7.4. Characterization of BOC polymers synthesized by ADMET.....	233
Table 7.5. GPC and TGA characterization of Polymers C and D.	235
Table 7.6. GPC and TGA characterization of polymers E and F.	236
Table 7.7. Steady-state absorption and emission properties of the BoC polymers (excitation at λ_{\max}).	239
Table 7.8. Spectral data for T ₈ iodophenyl based monomers with divinylbenzene or diethynylbenzene linkers, A-F and 2,7-dibromo-9,9-dimethylfluorene linked polymers in THF.....	244
Table D.1. Approximate distances for $\langle r \rangle$ in Å and hopping time estimate based on $\langle r \rangle$ value given.	275
Table E.1. Possible peak orientations and formulas for OPS rearrangement. Peaks in bold and italics are those observed in MALDI-ToF spectrometry, $(\text{PhSiO}_{1.5})_a(\text{H}_2\text{O})_{0.5b}$	276

List of Appendices

Appendix A. Guide to geometry optimization, single point energy, and excited state energy calculations in the Gamess software Package.....	263
Appendix B. Third Harmonic Generation Fluorescence Upconversion Setup:.....	266
Appendix C. Supplemental Reaction Schemes, Mass Spec and NMR Data for Chapter 3:	270
Appendix D. Förster radius determination for Chapter 6:	274
Appendix E. MALDI-ToF data for Chapter 4.	276

Abstract

Silsesquioxanes with conjugated organic tethers (chromophores) offer high orders of functionality (> 8 tethers), unusual enhanced absorption, emission and charge separation over free chromophores, excited state electron delocalization, and high thermal stability. This dissertation presents the synthesis and characterization of organic functionalized T_{10} and T_{12} $[\text{RSiO}_{1.5}]_{10,12}$ molecules, with emphasis on their synthesis by fluoride catalyzed rearrangement from $[\text{RSiO}_{1.5}]_n$ and an understanding of their unique photophysical properties targeting components in optoelectronic devices.

Initial discussion focuses on the synthesis of silsesquioxanes from silica via conversion of rice hull ash (RHA) silica to spiroxiloxanes [i.e. $\text{Si}(\text{2-methyl-2,4-pentane-diolato})_2$] by reaction with 2-Me-2,4-pentanediol and catalytic NaOH. The resulting spiroxiloxane reacts with selected arylLi reagents to form mono-aryl-spiroxiloxane, suggesting a pentacoordinate silicon based mechanism. These aryl-spiroxiloxanes are then converted through fluoride catalysis to novel aryl-silsesquioxanes $[\text{RSiO}_{1.5}]_{8,10,12}$.

Thereafter we detail the development of $[\text{RSiO}_{1.5}]_{10,12}$ materials by fluoride catalyzed rearrangement and its mechanisms. F⁻-catalyzed rearrangement of polymeric and octameric SQs is indispensable to the synthesis of $[\text{RSiO}_{1.5}]_{10/12}$, and mixed $[\text{R}_1\text{R}_2\text{SiO}_{1.5}]_{10,12}$ molecules in up to 95% yield. $[\text{PhSiO}_{1.5}]_{10}$ is synthesized in the highest reported yield to date (~50%), and is used as a model system for mechanism studies. The likely mechanistic paths taken to form T_{10} and T_{12} SQs are analyzed by experiment with MALDI/NMR to identify intermediates and computational modeling for the most likely pathways. The most favorable pathway to T_{10} from T_8 involves coincidental participation of fluoride and water with a net enthalpy of ~-24 kcal/mol.

We also present an extensive analysis of the photophysical properties of phenyl, stilbene, and stilbenevinylsilsesquioxanes $[\text{RSiO}_{1.5}]_{10/12}$ (R = phenyl, stilbene, stilbenvinyl) to map them for potential uses in optoelectronic devices. A comparison of $[\text{PhSiO}_{1.5}]_{8,10,12}$ emission properties show excimer formation and emission red shifts of 40 nm in the larger cages, showing cage size influences photophysical properties.

We also explore in detail the photophysical properties of [StilbenevinylSiO_{1.5}]_{8,10,12}, which show similar absorption and emission in solution, but decreasing fluorescence quantum efficiencies with increasing cage size, suggesting more chromophore interactions and non-radiative decay. [StilbenevinylSiO_{1.5}]₁₀ shows the highest two-photon absorption cross-section of this series (5.7 GM/chromophore), offering the best polarization and charge transfer character. Fluorescence upconversion fluorescence lifetime studies on [StilbenevinylSiO_{1.5}]_{8,10,12} find ultrafast charge transfer dynamics (<1 ps) indicative of chromophore-chromophore interactions in the excited state, unobserved for stilbenevinylSi(OEt)₃, suggesting excited state charge delocalization.

Lastly, reverse Heck cross coupling is used to link ([Ph_xvinyl₂SiO_{1.5}]_{10/12} with 1,4-dibromobenzene, 2,7-dibromo-9,9-dimethylfluorene and 4,4'-dibromostilbene to form beads on a chain (BoC) polymers. All polymers show red shifts in emission, however the 9,9-dimethylfluorene linked system shows shifts from the model bis-triethoxysilyl-divinyl-9,9-dimethylfluorene of 50 nm and 70 nm in absorption and emission respectively, suggesting ground state conjugation similar to conjugated organic polymers.

Chapter 1

Introduction

1.1 History and Background

Silicon based materials have their origins in the Stone Age, when people used quartz and other silica based stones to make tools.¹ Then in ancient Rome, sand was used to make glass bowls and vases, the beginning of silicon technologies. However, it wasn't until the 1800's that silicon (as an element) was first isolated by J.J. von Berzelius, and finally in the mid 1800's Sainte-Claire Deville developed the process carbothermal reduction to synthesize pure silicon metal¹

During the 1890's Frederick Kipping began studying the interactions of silicon and carbon, pioneering the development of organosilicon chemistry and coining the term silicone.^{2,3} In the early 1900's Kipping and others were in search of a silicon-based derivative of carboxylic acids (siloxylic acid). However, their efforts were thwarted and instead found a new class of materials that became known as silsesquioxanes $[\text{RSiO}_{1.5}]_n$.²

The real push for research in silsesquioxanes (SQs) began in the 1930's when Andrianov hydrolyzed alkyltriethoxysilanes in water; followed by the hydrolysis of phenyltrichlorosilane to make the first isolated phenylSQ derivatives as a white solid.^{4,5}

The need for natural rubber alternatives during World War II made research into silicon chemistry even more important, where such materials as silsesquioxane/silicone hybrid materials were found to offer ideal natural rubber replacement properties as well as fortunate pitfalls leading to the development of Silly Putty.^{6,7}

In the mid 1940's Scott discovered from high temperature hydrolysis polymerization of methyltrichlorosilane and silicon tetrachloride that cyclomers were formed.⁸⁻¹⁰ This then led to an early patent by Barry and Gilkey, which finally gave credence to silsesquioxanes by defining the molecular formula of polycyclic hydrolysis products as $[\text{RSiO}_{1.5}]_8$, where R = propyl, ethyl, and butyl, produced from heating

alkyltrichlorosilanes with powdered alkali salts.¹¹ However these materials were not isolated as single structures.

In 1946 Scott isolated the first SQs (low yield) with a defined structure $[\text{CH}_3\text{SiO}_{1.5}]_8$, from the hydrolysis and condensation of methyltrichlorosilane, with yields increased and reaction times decreased by employing hydroxide or amine catalysts.⁸ In the 1950's the development of new characterization techniques such as infrared analysis and advances in X-ray techniques further developed work in this area, with Sprung and Guenther in 1955 developing methods for the identification and isolation of $[\text{CH}_3\text{SiO}_{1.5}]_8$ in yields > 1%.¹²

Of particular importance to the development of this dissertation are phenylSQs, which were first synthesized in the 1950's by Barry et al,¹³ followed by Brown et al. who developed a high yield (>90%) route to $[\text{PhSiO}_{1.5}]_8$.¹⁴

These developments were the beginning of what has become a burgeoning field of scientific and engineering research. This has led to the development of high performing and novel SQs for applications as diverse as coatings for satellites,^{15,16} light emitting diodes (OLEDs),^{17,18} oil water separation,¹⁹ and polymerization catalysts.²⁰

The goal of this dissertation is to understand the synthetic methods, physical and photophysical properties and potential applications (i.e. photovoltaic materials) of T_{10} , T_{12} and oligomeric organic functionalized silsesquioxanes. The main questions we have set out to answer are as follows: 1. Can we find the optimized reaction conditions and the mechanism of converting PhT_8 to PhT_{10} by fluoride catalysis? 2. Can PhT_{10} SQs be made in high isolated yields from waste materials such as rice hull ash derived Ph-spirosiloxanes and polyphenylsilsequioxanes through TBAF (fluoride) catalyzed rearrangement? 3. Can we determine the intramolecular interactions present in chromophore functionalized SQs by two-photon absorption and fluorescence upconversion? 4. Can chromophore functionalized SQs be used as components in photovoltaic devices (i.e. replacements for electron acceptors)?

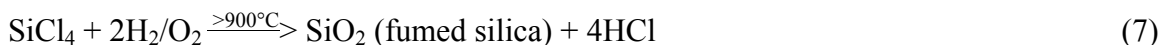
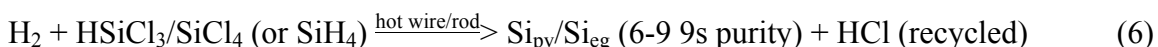
The following sections of this introduction give background into previously developed materials and their properties toward answering the questions above, and inspiration for the work of this dissertation. Section 1.2 discusses the development of functionalized alkoxysilanes with developments from biogenic silica (rice hull ash) to

silsesquioxanes. Section 1.3 gives an introduction to silsesquioxanes, what they are, how they are made, and what they are used for. Section 1.4 is an overview of the interactions of fluoride and silsesquioxanes, with emphasis on the importance of fluoride as a catalyst for making silsesquioxanes. Section 1.5 describes the synthesis, properties and applications of polymers containing silsesquioxanes. Section 1.6 gives an overview of the important optical/electronic properties of silsesquioxanes and the various advanced spectroscopic techniques used to determine their structure-property relationships. Finally, an overview of the subsequent chapters of important findings of this dissertation is given in Section 1.7.

1.2 Routes to Functionalized Alkoxysilanes

1.2.1 Commercial Methods

Alkoxysilanes and/or chlorosilanes are used as the building components for nearly all silicon containing materials, which includes solar grade silicon, silicones, and silsesquioxanes (SQs). These materials are used in applications ranging from toothpaste abrasives to photovoltaic devices for energy conversion.²¹ The most common method of making functionalized silicon is to convert silica (i.e. sand) into metallurgical grade silicon (Si_{met}) through a carbothermal reduction process (Reaction 1).



This is an expensive and energy intensive process that requires heating silica to $>1900^\circ\text{C}$ with carbon in an electric arc furnace, and generation of CO as a byproduct. Si_{met} provides the basis for most silicon-containing materials, reactions (1-7).²²⁻²⁶

The reason for such extreme conditions is the strength of the silicon-oxygen bond (534 KJ/mol), one of the strongest bonds found in nature. Silicon for photovoltaics must be further purified through the Siemens process (Reactions 5 and 6), where HCl is

recycled. Since chlorosilanes and $\text{HCl}_{(g)}$ are corrosive, and toxic, the production of these materials require expensive and extensive safeguards, which add to the overall cost of the final products.

$\text{HCl}_{(g)}$ is combined with Si_{met} over a Cu/Sn catalyst to make chlorosilanes (Reaction 2). This process makes both HSiCl_3 and SiCl_4 . SiCl_4 could then be converted to Si_{pv} and fumed silica (Reactions 6-7). One method of making hybrid organic/inorganic materials starts by taking an alkyl/aryl halide and reacting it with H_xSiCl_y in a gas phase condensation reactor.²⁷ Another method is that shown in Reaction 4, where Si_{met} is reacted directly with alkyl/aryl halides over a catalyst. The resulting products are R_xSiCl_y and HCl .

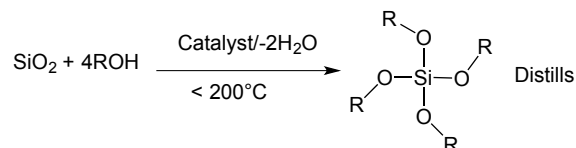
Functional materials can be made directly from R-chlorosilane derivatives (i.e. silicones, silsesquioxanes), or R-chlorosilanes are functionalized further to their alkoxy silane derivatives. This process may be achieved through refluxing R-chlorosilanes in ethanol/methanol often with an RO^-Na^+ base catalyst, which through displacement of the chloride results in R-alkoxysilanes.^{28,29} R-alkoxysilanes are then used in applications such as sol-gel synthesis, silicones, and silsesquioxanes.³⁰ R-alkoxysilanes are more desirable than their R-chlorosilane precursors due to their increased stability to hydrolysis, decreased toxicity, and decreased corrosive properties.³¹⁻³³

Another route to alkoxy silanes is through Reaction (3), where Si_{met} is combined with ethanol/methanol over a catalyst to make tetra-alkoxy silanes. These can then be further functionalized through organo-Grignard/Lithium reagents, or potentially used to make materials such as fumed silica.^{26,34}

Overall, the energy intensive and environmentally unfriendly processes involved in deriving useful silicon materials are counterintuitive. The process starts with oxidized silicon in the form of SiO_2 , which is then converted to Si_{met} , which is often converted back to fully oxidized materials such as fumed silica and alkoxy silanes. Because of this long seemingly illogical process, many researchers have looked at methods to “shortcut” the synthesis of useful silicon based materials directly from SiO_2 .

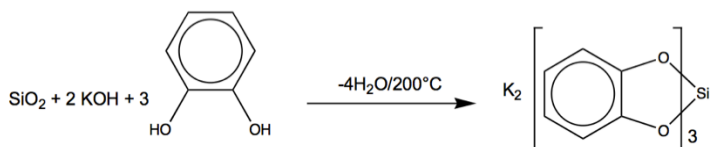
1.2.2 Other Routes to Alkoxysilanes

Researchers as early as the 1930's have sought silicon-containing materials per the low temperature depolymerization of silica. Scheme 1.1 illustrates this idea, in which catalysts are used to lower the activation energy to break open Si-O bonds, resulting in a alkoxysilane functionalized material, which by alkoxy group choice may result in distillable materials.



Scheme 1.1. Depolymerization of silica by alcohol.

Rosenheim (1931) was the first to describe silica depolymerization using catechol and stoichiometric KOH to form a hexacoordinated triscatecholato silicate (Scheme 1.2).³⁵

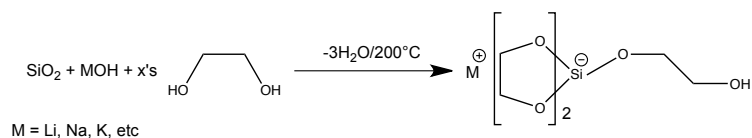


Scheme 1.2. Depolymerization of silica with catechol and KOH.

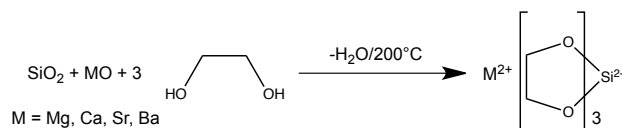
The importance of this study is evidenced by Weiss et al (1961),³⁶ Frye (1964),³⁷ Boer and Flynn (1968),^{38,39} Barnum (1970),^{40,41} and Corriu (1986)⁴² continuing to explore SiO₂ depolymerization, using Rosenheim et als methods, but with various silica feedstocks.

The success of this reaction arises because unlike carbon, SiO₂ expands its coordination sphere to form five and six bonds, so the Si-O bond strength is diminished. Though this process works well for depolymerizing silica at lower temperatures, the resulting hexacoordinated triscatecholato silicate was extremely stable and water-soluble. Also, the stoichiometry compromised the utility of this process, since equivalent base, and equivalent amounts of a diol (catechol) made its conversion to any useful products such as silica unattractive.

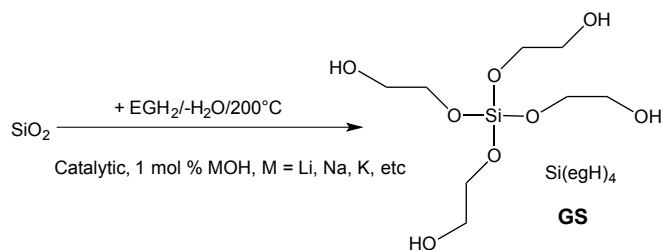
In 1991 Laine et al. published an alternative route to diolato silicates.⁴³ This method relied on depolymerizing silica with ethylene glycol rather than catechol (Scheme 1.3 and Scheme 1.4). More recently Laine et al. demonstrated that this process could be driven catalytically, and is first order in base and surface area. The activation energy is ~60 kJ/mol and the reaction works best with high surface area, amorphous silicas (Scheme 1.5).^{44,45} The product of the catalytically driven reaction could not be distilled and was not easily purified.



Scheme 1.3. Depolymerization of silica with ethylene glycol to form glycolatosilicate.



Scheme 1.4. Depolymerization of silica with ethylene glycol to form glycolatosilicate.



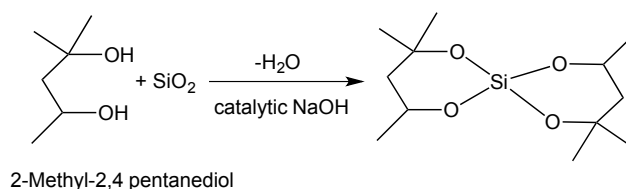
Scheme 1.5. Depolymerization of silica with ethylene glycol to form glycolatosilicate.

Later Kinrade et al. suggested that plants use similar pentacoordinated silicates to import and transport silica throughout their systems as a basis for biosilification, or the process by which plants such as Rice take up silica from the soil and store it in their stalks for structural support.⁴⁶

Most recently, Laine et al. has proposed using rice hull ash (RHA) as a starting material for silicon containing materials.^{47,48} First, it is agricultural waste product. Second, it contains >90 % silica with surface areas as high as 230 m²/g. Third, since it comes from rice husks, no heavy or toxic metals are present in the mixture since they do

not take up heavy metals from the soil, which are common in mineral sources. All of the above processes are possible using RHA as an alternative to other silica sources.

To improve upon the ethylene glycol synthetic methods, other diols were used to develop distillable spiroxiloxanes. Sterically hindered diols showed the best conversion to spiroxiloxanes.⁴⁹ Of the commercially available hindered diols, 2-methyl-2,4-pentanediol, the hydrogenated product of base catalyzed acetone condensation, is the lowest cost, sterically hindered diol available and showed the best conversions to tetrahedral alkoxy silanes (Scheme 1.6).⁵⁰



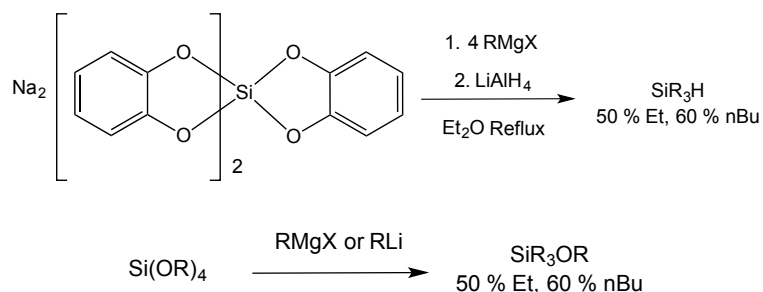
Scheme 1.6. Depolymerization of silica with 2-methyl-2,4-pentandiol and catalytic NaOH.

This diol offered >98% conversion of fumed silica and >60% conversion of high surface area RHA to Si(2-methyl-2,4-pentandiolato)₂. This product is easily distilled from the reaction pot and can be separated from residual diol by dissolving the mixture in hexanes and then washing with water to remove the diol. We have also found that this material can be easily converted to tetraethoxy or tetramethoxysilane through a trifluoroacetic acid catalyzed exchange of diol with ethanol/methanol under anhydrous conditions.^{51,52} The simple formation and purification processes led to the exploration of its applications as a starting material to R-alkoxy silane derivatives as discussed above.

1.2.3 R-alkoxy silanes from Spirosiloxanes

Efforts have also been undertaken for low temperature routes to Si-C bonds that do not require the use of Si_{met}. Thus, a first step in this direction would be to establish synthetic routes to Si-C containing compounds.

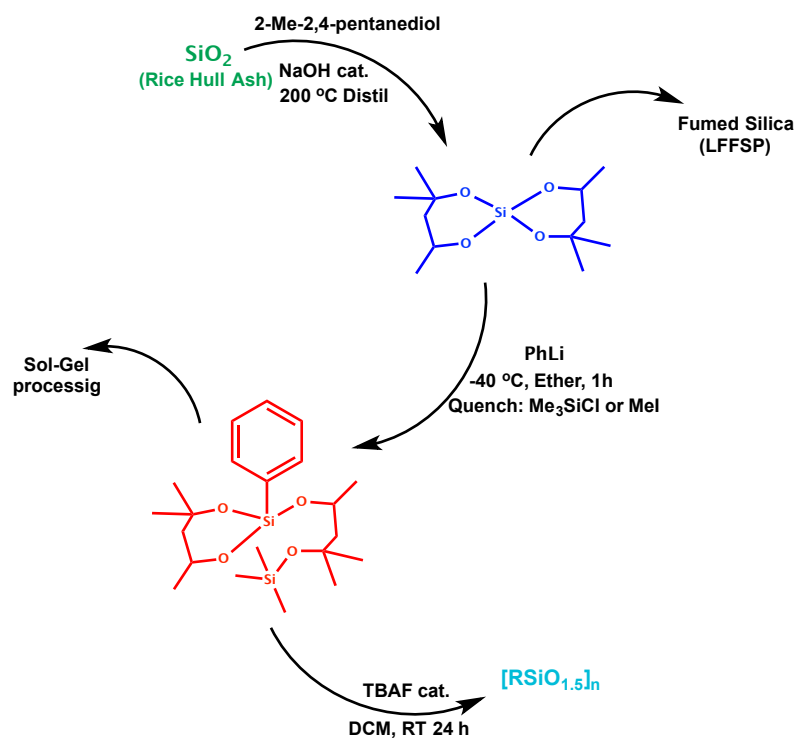
Surprisingly, very few researchers have sought out to tackle this goal. Most work in this area has been carried out by Corriu et al, who explored the potential to react alkoxy silanes (hexacoordinated triscatecholato silicate) with nucleophiles to form Si-C bonds directly. This is illustrated in Scheme 1.7.^{42,53-58}



Scheme 1.7. Typical reactions of triscatecholato silicate or tetralkoxysilanes with Grignard and lithium reagents.^{42,53–58}

Corriu et al. report reasonable yields for these types of reactions; however, the only products are tri- and tetrasubstituted silanes, as opposed to the much more useful mono- or di-substituted derivatives. The latter compounds offer potential as monomer units for the synthesis of novel siloxanes and silsesquioxanes (SQs, See Section 1.3). The Corriu group concluded from their efforts that the pentacoordinated/hexacoordinated intermediates formed are much more reactive than the tetracoordinated species, giving this as the reason tri- and tetra-substituted silanes are the products from their efforts rather than mono- and di-functionalized compounds.^{42,49,59,60}

Given our considerable interest in finding new ways to make specialty silsesquioxanes,^{29,61–63} we initiated studies using stoichiometric R-Li/Et₂O/-78 °C (R= Ph, thiophene, anthracene, 9,9-dimethylfluorene, etc.) to functionalize Si(2-methyl-2,4-pentanediolato)₂ (**I**), finding it easy to make mono-substituted products (reaction 17) if the reaction is quenched with MeI or Me₃SiCl before warming. The resulting product can be hydrolyzed in the presence of catalytic amounts of F⁻ to produce [PhSiO_{1.5}]_{8,10,12} in good yields.⁶⁴ An outline of the process of going from RHA to silsesquioxanes is shown in Scheme 1.8, and as is discussed in more detail in Chapter 3.



Scheme 1.8. Outline of a synthetic process for converting silica to silsesquioxanes.⁶⁴

1.3 Introduction to Silsesquioxanes

Polyhedral silsesquioxanes and materials based on them are of increasing research interest over the past 25 years, with nearly 400 publications in 2014 alone. There are also 18 reviews, 1 book and many book chapters.^{65,29,30,47,10,66–71,20,72–77}

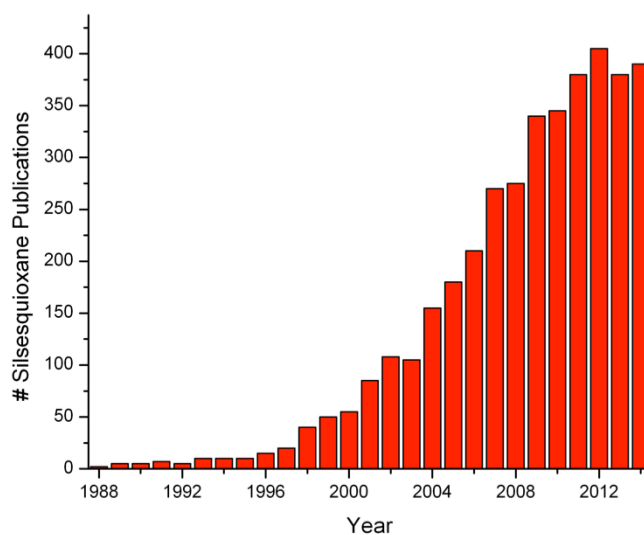
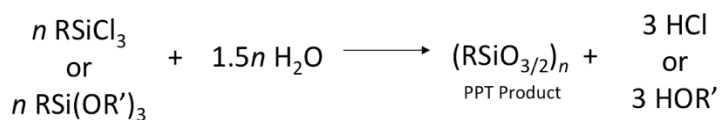


Figure 1.1. Silsesquioxane publications per year (1988-2014).⁷⁸

Silsesquioxanes (SQs) are a group of compounds with the general molecular formula $[\text{RSiO}_{1.5}]_n$, where R = H or alkyl, aryl, alkenyl, or siloxy groups. Their name stems from latin, where “sil-” (silicon), “-sesqui-” (one and a half), and “-oxane” (oxygen) refer to the 1.5 oxygen atoms shared by each silicon. They are a form of hybrid materials (organic/inorganic) with properties intermediate those of organic materials and inorganic materials due to their organic side chains and inorganic silica core.

Their popularity stems from their ease of synthesis and purification, their robust nature compared to typical organic molecules, and the ease with which their functionalities can be modified to sets of target properties in many applications. In particular, they have more silica like properties than those of silicone polymers $(\text{R}_2\text{SiO})_n$. Silsesquioxane-based materials have found use as components in polymer nanocomposites, catalysts, models for silica surfaces and heterogeneous catalysts, low-k dielectrics, antimicrobial agents, emitting layers in organic light-emitting diodes (OLEDs), and coatings.^{79–97}

Silsesquioxanes are generally synthesized through the hydrolytic cleavage and condensation of R-trichloro- or R-trialkoxysilanes (Scheme 1.9).



Scheme 1.9. Example synthetic method to R-silsesquioxanes.

Many silsesquioxane structures are known to exist. The most common of which are the fully condensed polyhedral oligomeric silsesquioxane structures, (Figure 1.2a) all of which possess unique three-dimensional orientation and symmetries; alternatively they are known as “POSS,” a trademark of Hybrid Plastics inc., but will be referred to here as SQs; incompletely condensed polyhedral cage structures (Figure 1.2b), and random structured polymeric materials (T-resins) with no long-range order, which are loosely comprised of open caged and linear chains (Figure 1.2c).^{98,99,14,100} A fourth type of structure (ladder polymer) is theorized to exist (Figure 1.2d), though examples of oligomers have been made, as of yet its existence in polymeric form remains to be proven by either characterization or isolation.⁶⁶ The formation of random structures tends to

occur preferentially at high concentrations, while the formation of polyhedral cage structures is usually favored under dilute conditions. This is generally problematic in that slow hydrolysis and condensation reactions result causing synthesis times to be relatively slow (weeks to months). Many factors influence their formation and resulting structures, including the type of starting material used (i.e. R-alkoxysilane vs. R-trichlorosilane), solvent, reaction concentration, reaction time, quantity of water, product solubility, etc.⁷⁷

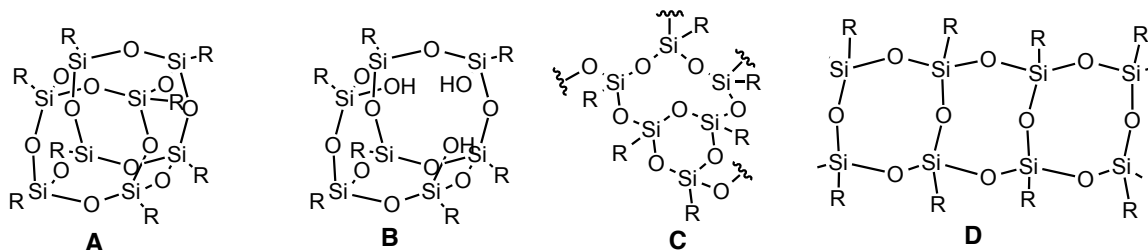


Figure 1.2. Silsesquioxane structural motifs.

There are a few naming conventions for silsesquioxanes. They are sometimes called spherosiloxanes because their polyhedral structures are considered to be topologically equivalent to a sphere.⁹ More commonly silsesquioxane structures are typically named using systematic nomenclature (similar to polymer repeat units).⁷⁴ For example, the molecular formula $[\text{PhSiO}_{1.5}]_8$ would be translated to octaphenylsilsesquioxane, which would be a completely condensed octameric cage structure with phenyl groups on each of the silicon corners. SQs may also be named by shorthand methods developed for siloxane chemistry,⁶⁶ as shown in Figure 1.3, or $M = 1O$, $D = 2O$, $T = 3O$, $Q = 4O$. For example, the octaphenylsilsesquioxane would be denoted PhT_8 , with the R-group substitution given before the description letter. In this case, each silicon is attached to phenyl and three oxygen atoms.

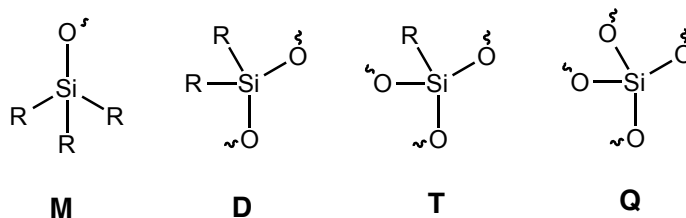


Figure 1.3. Siloxane nomenclature methodology.

1.3.1 Completely Condensed Silsesquioxanes

T_8 cubic silsesquioxanes (SQs, Figure 1.4a) are the most studied form of all of the SQs due to their high degree of symmetry (O_h) with functional groups in each octant in Cartesian space, numerous preparation routes to reasonable quantities of material, and their nanometer size.^{101–103} Though cubic SQs are extensively studied, little work has been done with any of the other sizes of condensed cages, especially SQs composed of 10 and 12 silicon atoms ($n=10, 12$). This is due mainly to the lack of synthetic routes and/or separation strategies to obtain reasonable quantities for further study/functionalization.⁷⁴ They are most often found as minimal byproducts in the synthesis of T_8 cages. Table 1.1 shows several published synthetic routes to T_{10} and T_{12} with various functionalities.

Table 1.1. Example synthetic parameters to various T_{10} and T_{12} silsesquioxanes.⁷⁴

Size	R-	Starting materials and conditions	Yield%	²⁹ Si NMR
T_{10}	-H	HSiCl ₃ + c-C ₆ H ₁₂ /PhMe + H ₂ SO ₄	3.6	-86.25
	-Cp	CpSiCl ₃ + H ₂ O, THF + (NH ₄) ₂ CO ₃ , 7 days	67	-71.50
	-CH=CH ₂	[CH ₂ =CHSi(OEt) ₂] ₂ O + H ₂ O, TBAF, THF/CH ₂ Cl ₂ , 2 days	26	-81.48
	-C ₆ H ₅	PhSiCl ₃ + H ₂ O, toluene, KOH, 9 h, then recrystallization from benzene/hexane	-	-
T_{12}	-H	HSiCl ₃ + H ₂ O, H ₂ SO ₄ , cyclohexane/toluene, 6 h	3.5	-85.78, -87.76
	-CH=CH ₂	[CH ₂ =CHSi(OEt) ₂] ₂ O + H ₂ O, TBAF, THF/CH ₂ Cl ₂ , 2 days	15	-81.34, -83.35
	-C ₆ H ₅	PhSiCl ₃ + H ₂ O, KOH, THF, reflux, 3 days	50-70	-

These structures offer further property modification over T_8 SQs since they permit greater functionalization at similar length scales and may offer increased solubility and processability.^{61,63,104} The structure of [RSiO_{1.5}]₁₀ (T_{10}) is made up of two distorted pentagonal faces, and four distorted square faces with D_{5h} symmetry (Figure 1.4b). The dodecasilsesquioxane is made up of four distorted pentagonal faces and four distorted square faces (Figure 1.4c). Multiple symmetry orientations are possible for [RSiO_{1.5}]₁₂ (T_{12}) (i.e. D_{2d} , D_{6h}), but D_{2d} appears to be the most common by crystallographic analysis.

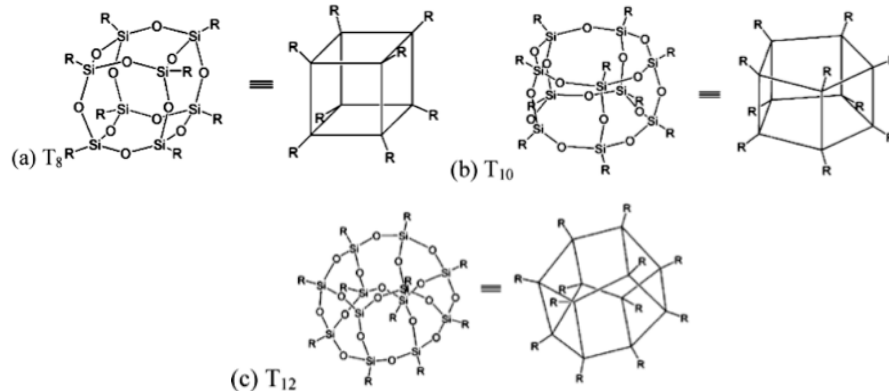


Figure 1.4. Examples of SQ cage structures and their simplified structures.

Completely condensed SQs are very useful as nanobuilding blocks due to their perfectly defined 3D structures and the ability to uniformly functionalize them at all corners, minimizing defects. SQs are also unique in that they are spherical hybrid organic/inorganic molecules with rigid silica cores, with each vertex containing an organic group. They are 1-2 nm in diameter, with volumes of $< 2 \text{ nm}^3$, and in the case of the T_8 separate each organic group into different quadrants in Cartesian space (Figure 1.5). This positioning allows access to polyfunctional nano-materials in 1-, 2-, or 3-dimensions, nanometer by nanometer (building blocks). Their rigid silica core also makes these materials more robust than conventional organic only materials.⁶⁶

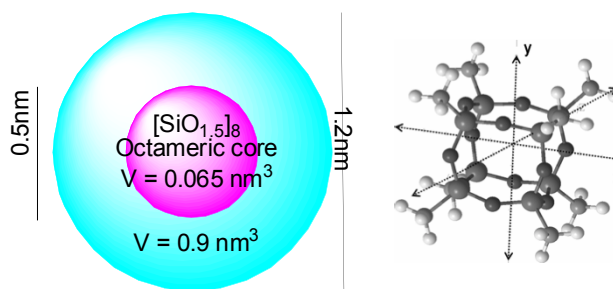


Figure 1.5. Typical sizes and volumes of silsesquioxane molecules; SQ with R-groups in different octants of Cartesian space.

Our recent work and this dissertation focus on the direct synthesis and properties of T_{10} and T_{12} cages with vinyl, phenyl and mixed vinyl/phenyl functionalities.

1.3.2 General Mechanism of Formation for Silsesquioxanes

Synthesis typically proceeds by hydrolysis and condensation of $[R-SiX_3]$, $x=Cl, OMe, OEt$ and is a complex acid or base catalyzed multi-step process. The process is very sensitive to experimental conditions due to the wide range of possible structures that may form including oligomers, polymers, gels, and partially or completely condensed cages. However, the mechanistic pathways to each of these materials are similar.

Consequently, it is difficult to develop suitable kinetic rate laws for many of the steps in this synthetic process, due to the complexity of intermediates forming under equilibrium conditions.⁷⁷ While, there are no set of universal methods to making SQs. However, many procedures permit control of the formation of specific SQs.^{66,77,105}

To this end Kudo and Gordon et al used computational methods to establish parameters for plausible mechanistic pathways for hydrolysis and condensation reactions leading to cubic SQs.¹⁰⁶⁻¹⁰⁹ The first step was to establish energies for each intermediate, transition states and final product. They find that the reaction depends very strongly on catalytic water, which lowers activation energies by ~ 10 kcal/mol in most instances. They also find that the spatial orientation of the intermediates greatly influences formation of final products, and that multiple equilibria exist between these intermediates. They also report the enthalpy difference going from the starting trisilanol $[RSi(OH)_3]$ to cubic SQ is -11.5 kcal/mol, which is only slightly favorable over the starting materials, showing why the reactions of making cubic SQs are often low yielding and result in many polymeric byproducts.

In general three major factors influence the structure and rate of SQ formation.¹¹⁰ (1) water is essential for hydrolysis and cyclization, but excess water leads to polymeric SQs; (2) higher pH also favors polymeric SQs, while lower or near neutral pH favors cyclization; (3) lower concentrations of starting materials $[R-SiX_3]$ favor intramolecular condensations (cyclization), whereas higher concentrations favor intermolecular condensation to form polymeric structures. Even though the rates of hydrolysis and condensation are controlled by varying the pH, and concentration, the mechanism is likely similar in each case (Figure 1.6).

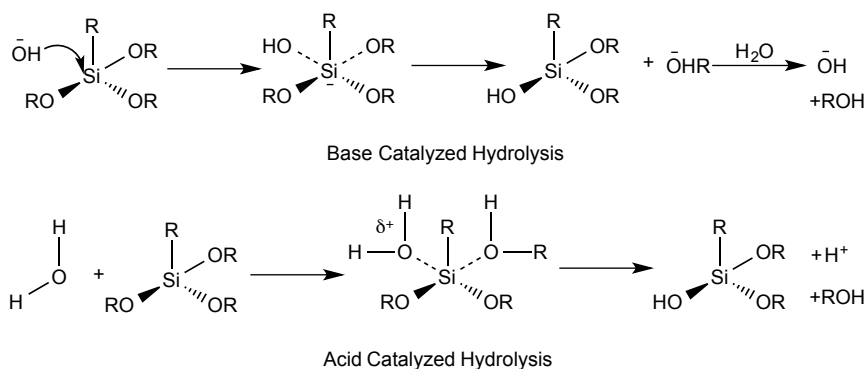
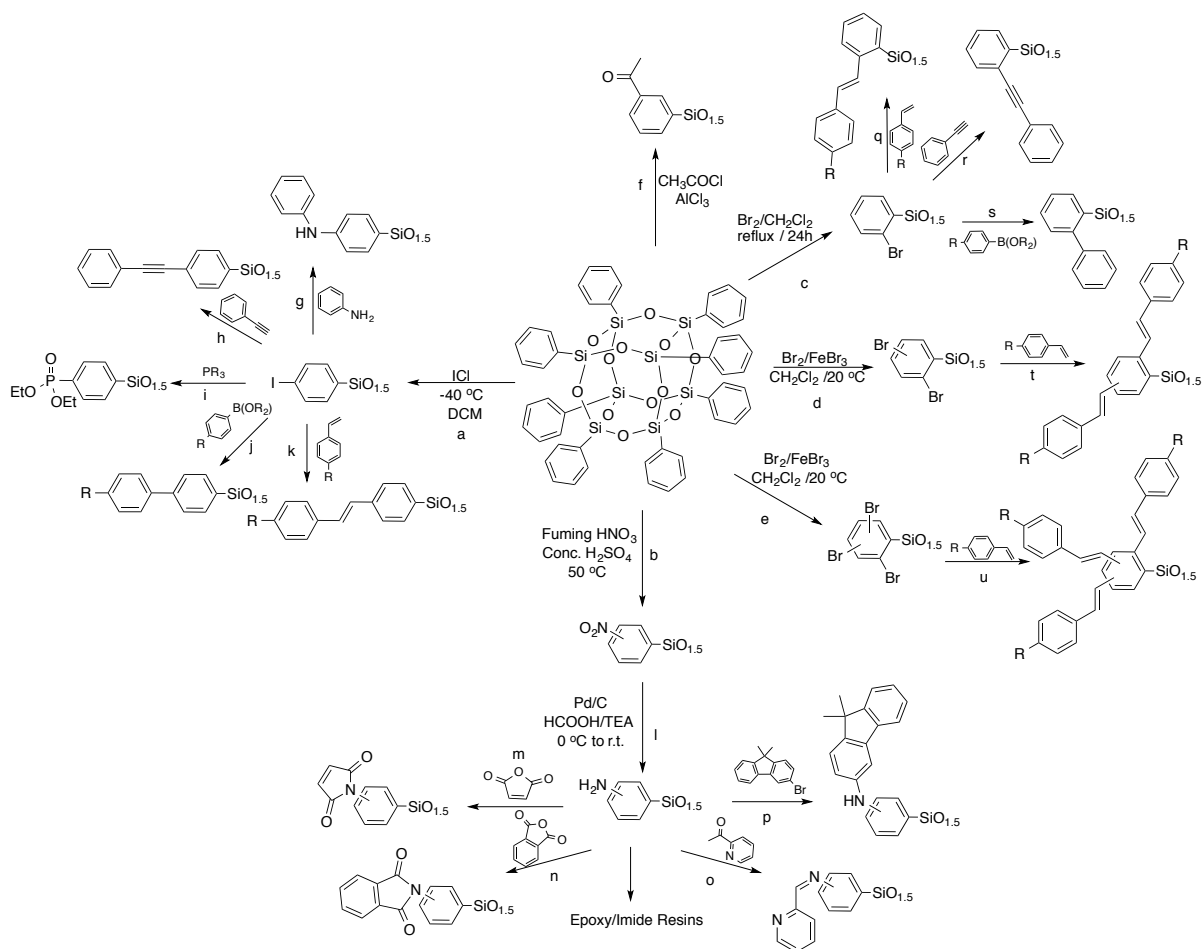


Figure 1.6. Mechanisms of acid and base catalyzed reactions to form SQs.

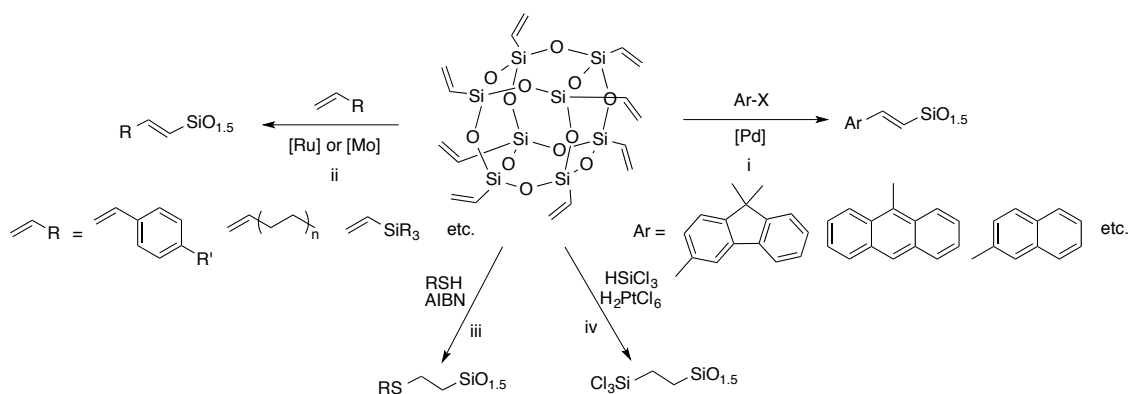
The mechanism of silsesquioxane growth from R-trialkoxysilanes by acid catalyzed hydrolysis and condensation initiates with protonation of an alkoxy, causing the silicon atom to become more electrophilic, which makes it more susceptible to nucleophilic attack by water. The first step has the fastest rate of hydrolysis as the penta-coordinated transition state is strongly stabilized by the alkoxy donating groups.¹¹⁰ Each additional hydrolysis occurs more slowly as alkoxy groups are displaced to form the trisilanol. It is also expected that condensation occurs most rapidly for the mono-hydroxylated species, which is also supported by modeling.¹⁰⁰ In the base catalyzed mechanism, the rates are reversed, with the initial attack being the slower step due to alkoxy electron density repelling hydroxide interactions with silicon. Thereafter, each subsequent hydrolysis becomes faster due to the lower electron density stabilization of the hydroxyl groups. Condensation occurs fastest for the hydrolyzed species, since they are more prone to attack.¹¹⁰

1.3.3 Examples of Post-Synthetic Functionalization

The literature offers many examples of post functionalization of silsesquioxanes, especially for T₈. Phenyl and vinyl substituted SQs are the most common SQs used in post functionalization since they can be easily modified by standard methods known for organic molecules (Scheme 1.10 and Scheme 1.11). These include electrophilic aromatic substitution (i.e. bromination, iodination, nitration, etc.),^{102,103,111–113} olefin metathesis,^{114–116} and catalytic cross-coupling reactions including Heck, Sonagashira and Suzuki.^{117,29,101,118–124}

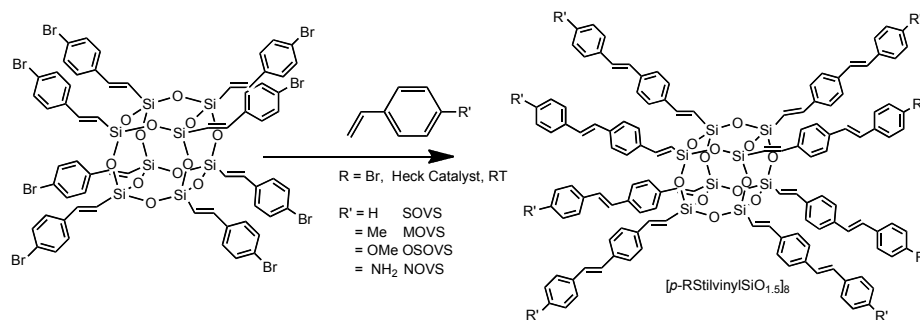


Scheme 1.10. Functionalization of phenylsilsesquioxanes (T_8): (a, b, c, d, e, and f) Electrophilic aromatic substitution (EAS), (g and p) Buchwald-Hartwig reactions, (h and r) Sonogashira, (j and s) Suzuki, (k, q, t, and u) Heck.²⁹



Scheme 1.11. Reactions of vinylsilsesquioxanes (T_8): (i) Heck cross-coupling,^{117–120} (ii) Cross-metathesis,^{114–116} (iii) Thiolene reactions,^{125–127} (iv) Hydrosilylation reactions.^{92,128,129}

Our group has focused recently on incorporating model light harvesting/light emitting chromophores onto cage corners, especially stilbene derivatives, which are models for poly(phenylenevinylene). Stilbene derivatives are easily synthesized by a combination of the above reactions making them ideal candidates as models for more complex chromophores. Scheme 1.12 provides examples of functionalizing $[p\text{-Br-Styr-SiO}_{1.5}]_8$ with various R-styrenes to synthesize $[p\text{-R-stilbenevinyl-SiO}_{1.5}]_8$. This method is also used to functionalize T₁₀ and T₁₂ vinylSQs discussed in Chapters 5 and 6.



Scheme 1.12. Heck cross-coupling to form stilbeneoctavinylSQs.

These functionalization methods are indispensable in developing SQs as advanced functional materials for applications ranging from hybrid electronics (i.e. OLEDs, photovoltaics, dielectrics) to catalyst ligands/anchors to gas storage materials.^{65,20,124,130} Since SQs are rigid 3D structures that can be functionalized with organic chromophores in all dimensions, they can be imagined as tunable highly absorbing/emitting, light harvesting materials.

Materials applications and properties are discussed in Section 1.6.

1.4 Silsesquioxanes and Fluoride

Rikowski et al, in 1997, conducted the first studies on the interactions of silsesquioxanes and the fluoride ion finding that T₁₀ and T₁₂ halo-propylSQs form by partial rearrangement of T₈ in acetonitrile using ~40 equivalents of NaF + 18-crown-6 as catalyst.¹³¹ The conversion of T₈ chloropropylSQ as determined by HPLC was 28% T₈, 61% T₁₀ and 11% T₁₂. Due to the low solubility of the catalysts in acetonitrile, the large excess of catalyst required for rearrangement to take place, and the tedious separation by HPLC this was not a viable method for making T₁₀ and T₁₂ SQs. However they did find

at this time that in polar solvents partial cage rearrangement could be achieved with nearly any weak base (i.e. acetates, cyanates, carbonates, etc.).^{132,133}

The use of F^- in SQ synthesis/rearrangement was largely ignored until 2003, when Bassindale et al explored the use of stoichiometric F^- as TBAF (tetra-*n*-butylammonium fluoride) as a method to improve yields and reaction time for the synthesis of various T_8 SQs in chloroform.¹³⁴ Yields of up to 95% were obtained for T_8 cyclopentylSQ within 24 h. Multiple groups have since explored synthesis of SQs or gels using F^- catalysts including: Mabry and Bowers et al,^{135,136} Kozelj et al,¹³⁷ Kawakami et al,^{104,138} Laine et al,^{61,62,139–142} Pope et al,¹⁴³ Bassindale et al,^{144–146} and Marsmann et al.¹³¹

Bassindale et al. and then Mabry and Bowers et al. found that F^- becomes encapsulated in the SQ cage (Figure 1.7).^{135,136,144,147} In these studies TBAF, or tetramethylammonium fluoride [Me_4NF or TMAF] were used in anhydrous solution (THF) under slightly basic conditions (pKa F^- 3.2 in water). Mabry and Bowers et al. also used F^- encapsulation to gain mass spectral ionization enhancements with an end goal of being able to ionize SQ based polymers.

Bassindale et al. found that direct encapsulation to T_8 phenylSQ ($F^-@[Ph(SiO)_{1.5}]_8$) occurred on slow solvent removal following hydrolysis-condensation of phenyltriethoxysilane with stoichiometric TBAF. They verified $F^-@[vinyl(SiO)_{1.5}]_8$ and $F^-@[p\text{-tolyl}(SiO)_{1.5}]_8$, by ^{29}Si NMR, ^{19}F NMR and single-crystal X-ray diffraction. Only small changes in Si-O bond angles and distances were observed on F^- encapsulation.^{137,140,147} The ^{19}F NMR spectrum shows a single peak at -26.4 ppm, suggesting that the encapsulated F^- behaves like a naked fluoride ion with little coordination to the silicon atoms.

Mabry and Bowers et al. synthesized $F^-@[R(SiO)_{1.5}]_8$ cubes, where R = vinyl, phenyl styrenyl, trifluoropropyl, nonafluorohexyl and tridecafluorohexyl using TMAF, starting from the $[R(SiO)_{1.5}]_8$ cage.¹³⁶ Both Bassindale et al. and Mabry and Bowers et al. found that F^- encapsulation works well for electron-withdrawing groups (aryl, vinyl, CF_3 , etc.), while the lack of electronic stabilization from electron-donating groups (ethyl, propyl, cyclohexyl, etc.) prevents encapsulation.

Lastly, Mabry and Bowers et al found by ^{29}Si NMR (Figure 1.7) that if two cages ($[\text{vinyl}(\text{SiO})_{1.5}]_8$ and $[\text{Ph}(\text{SiO})_{1.5}]_8$) are mixed together with TMAF in THF, cage scrambling occurs (See Section 1.5).¹³⁶ Figure 1.7 shows sharp peaks of the equivalent silicons on the starting F^- cages at -81.5 and -82.5 ppm become a broad peak centered between where the two sharp peaks were. This suggests the generation of multiple mixed compounds containing vinyl and phenyl substituents.

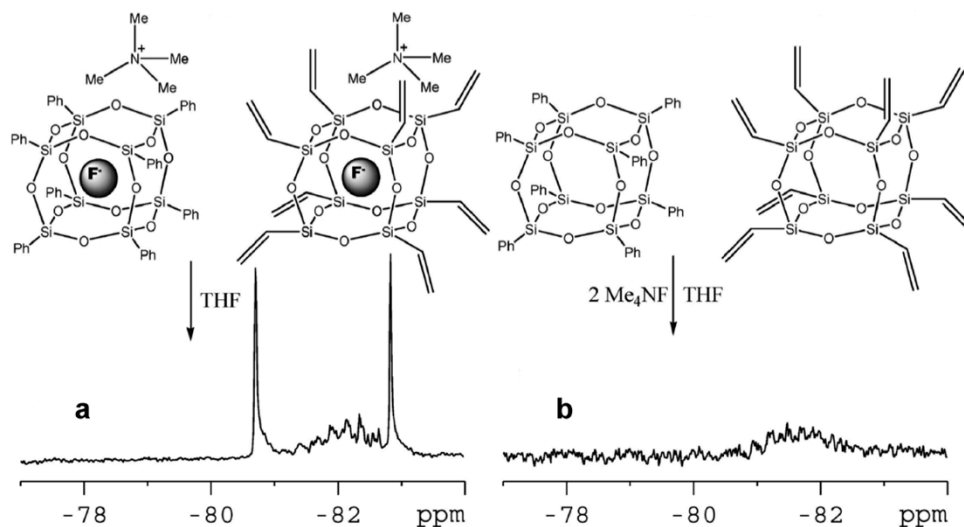


Figure 1.7. a. ^{29}Si NMR of mixed F^- @[vinyl(SiO) $_{1.5}$] $_8$ and F^- @[phenyl(SiO) $_{1.5}$] $_8$, b. ^{29}Si NMR of [phenyl(SiO) $_{1.5}$] $_8$ and [vinyl(SiO) $_{1.5}$] $_8$ equivalent Me_4NF , both in THF.^{136,140}

The mechanism of the F^- catalyzed cage formation or rearrangement processes are not reported in the literature, though multiple conjectures have been made.^{136,139,148,149} The process is thought to be strongly dependent on water, since in dry THF, cage formation and/or rearrangement is not observed.¹⁴⁸ It is suggested that F^- “activates” a molecule of water through hydrogen bonding for nucleophilic attack, which is then analogous to the Kudo mechanism discussed above. Alternatively, F^- may act as a template to assemble cages around it, but see Chapter 4.¹⁴⁹

Our group has since elaborated on F^- promoted cage scrambling methods by using catalytic TBAF (<5 mol%) to make statistical distributions of mixed functional SQ cage systems.^{62,139–141} The first example used TBAF to transform insoluble “T” resins of polyvinyl- and polymethylSQs into mixed vinyl/Me functionalized T_{10} and T_{12} cages.¹³⁹ This was followed by a series of methods to make mixed Ph/vinyl silsesquioxanes to

produce beads on a chain (BoC) polymers, as discussed in Section 1.5 and Chapter 7.^{140,150} Finally, we developed routes to mono-functionalized T_{10/12} vinylSQs, and T₁₀ phenylSQs (Chapters 4 and 5).⁶³ These are some of the first effective methods of synthesizing T₁₀ and T₁₂ with any respectable yields, in many cases >98%.

1.4.1 Theoretical Investigations of Fluoride Encapsulation/Catalysis

Modeling studies on the stabilization energies of [R(SiO)_{1.5}]₈ (R = H, F, OH, alkyl, etc.) have been done by many groups.^{151,117,152–154} These studies generally agree that the HOMO consists of the 2p lone pair on the oxygen atoms, with contributions from the R-groups and lies on the edges of the cube, while the LUMO involves the silicon atoms and oxygen atoms, is spherical and resides in the middle of the cage. Bassindale et al. suggest that the fluoride interacts with the electrophilic cage LUMO, adding stabilization to the entrapped naked F⁻ ion.¹⁴⁴

The mechanism of F⁻ entrapment is unknown experimentally, and it is likely that it is far more complicated than simple insertion through the cage face. To delineate this, Hagelberg et al modeled possible routes to F⁻ (and other ions: Cl⁻, Br⁻, Li⁺, Na⁺, etc) encapsulation and also gave inference on how cage formation occurs using F⁻.¹⁴⁹ They find that an SQ structure with fluoride encapsulated is 70 kcal/mol lower in energy than an SQ with free fluoride. They also find that the entrapped F⁻ is about 10 kcal/mol lower in energy than a pentacoordinated SQ with F⁻ attached to the cage corner (Figure 1.8). They also find that the

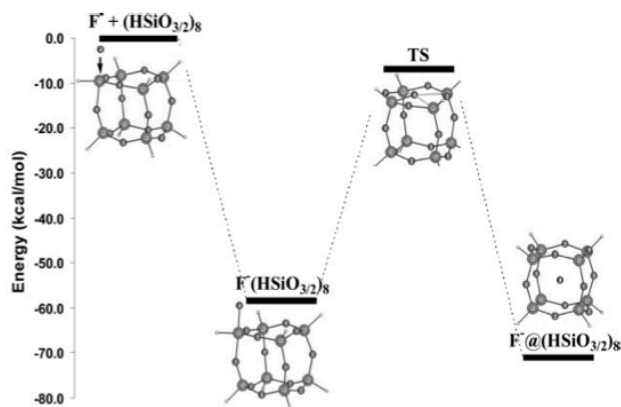


Figure 1.8. Theoretical energy diagram of fluoride encapsulation within an HSQ core.¹⁴⁹

activation energy barrier for F⁻ insertion is 51 kcal and removal is 64 kcal/mol, showing the stability of the encapsulated cage.

These results are of interest in the context of a conjecture by Bassindale et al concerning the F⁻@[vinyl(SiO)_{1.5}]₈ complex for the synthesis of SQs: “the fluoride ion must be acting as a template for formation of the cage and once inside it, it can only escape when the cage is broken down.”¹⁴⁷ This conjecture was made because refluxing the fluoride-encapsulated cage did not remove fluoride, suggesting its stability.

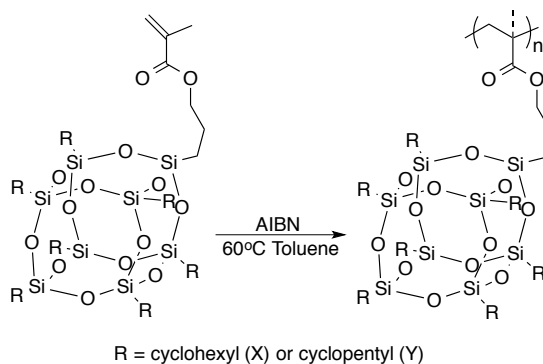
Hagelberg et al also find that F⁻ is the only ion that easily (by energy) penetrates the cage without opening the cage face, while every other ion would require breaking open the cage. No other ions were stable within the cage interior.¹⁴⁹ Further studies by Hagelberg and Saebo et al looked at encapsulation of ionic species within larger cages such as T₁₀.¹⁵⁵ They find (computationally), fluoride encapsulation within the T₁₀ HSQ is ~25 kcal/mol lower in energy than that of T₈ HSQ.

1.5 Silsesquioxane Based Polymers

Silsesquioxanes in polymers are of increasing recent interest due to their enhanced thermal stability (>200 °C), high compatibility with organic materials, and increased processability over cage molecules on their own.⁷² Hundreds of papers have been published using silsesquioxanes as pendant/end groups on organic polymers (i.e. methacrylates) because they imbue additional thermal and oxidative stabilization properties to these materials.^{69,156,157,16}

As an example, Lichtenhan et al synthesized a series of methacrylate based SQs with cyclohexyl- and cyclopentyl- R-group functionalities, and a propyl methacrylate monomer substituted on one corner (Monomers X (R=cyclohexyl) and Y (R=cyclopentyl), Scheme 1.13).^{69,157} Solubility differences were observed between the starting monomers in THF and toluene, with the cyclohexylSQ having approximately 2x the solubility of the cyclopentylSQ. Their thermal decomposition temperatures ($T_{d5\%}$) are roughly the same at ~190 °C. After polymerization, only the cyclohexylSQ based polymer remained soluble. Both polymers showed thermal decomposition ($T_{d5\%}$) improvements to ~390 °C due to the high heat capacity of the SQ core, compared to PMMA, which decomposes at

~200 °C. The SQ based polymers also showed an ~9-fold improvement in O₂ permeability over PMMA. Therefore, polymers with SQ incorporation show increased thermal stability and oxygen permeability possibly due to phase separation.



Scheme 1.13. Synthesis of propylmethacrylate silsesquioxane polymers.

There is also increasing interest in generating star polymers from SQs.^{158–163} For example, Kim et al used an octa-methacrylateSQ as an initiator in ATRP synthesis to grow methacrylate based polymers in a star fashion off of the SQ core for applications in Lithium battery separator materials.¹⁶³

However, few papers focus on using silsesquioxanes as part of the backbone in the main chain of a polymer. The first clear example was given by Lichtenhan et al,¹⁵⁶ using dihydroxy T₈ cyclohexylSQ cage (Figure 1.9) polymerized with dimethyl-dichlorosilane, to make a hybrid silsesquioxane-silicone polymer, we have designated polymers with SQs in the main chain as “beads on a chain” (BoC) polymers.

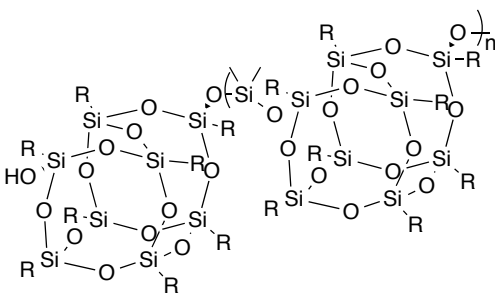
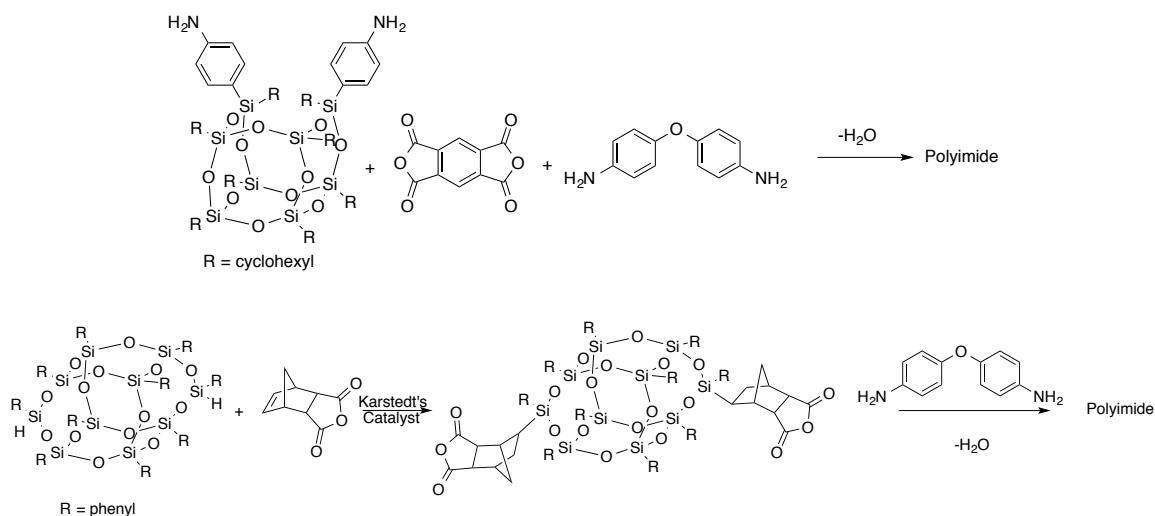


Figure 1.9. Hybrid silsesquioxane-silicone polymer, R = cyclohexyl.

A majority of these materials rely on amino-containing (-NH₂) SQs to make polyimide based polymers.^{69,72,97,16} The starting SQs are either fully aminated (i.e. octa-3-

aminopropylSQ,¹⁶⁴ or octa-aminophenylSQ^{95,102}), or partially aminated as in Scheme 1.14.¹⁶⁵ SQs with eight or more reactive groups have been examined in epoxy resins, polyimides, cyanate esters, and polyurethane thermosetting resins. SQs are mainly added to improve the thermo-oxidative stability of resin systems.

Further work by Kawakami,^{166,167} Kakimoto,^{128,168,169} and others,¹⁶ have synthesized aminated SQs with only two reactive groups. These difunctional compounds have well defined structures and stereochemistries and offer improved the properties in thermosets, but also the properties of thermoplastics as they offer limited cross-linking. Polyimides with alternating SQs in the main chain are shown in Scheme 1.14. In general polyimide based materials offer moderate increases in thermal stability ~ 50 °C, while T_g is depressed by ~ 60 °C or more. As expected, the elasticity of the materials decreases as more SQ is added. Mabry et al, have also demonstrated through ground tests and tests on the International Space Station, that SQ based polyimides show excellent resistance to erosion by atomic oxygen compared to Kapton, a commercially available material.¹⁵

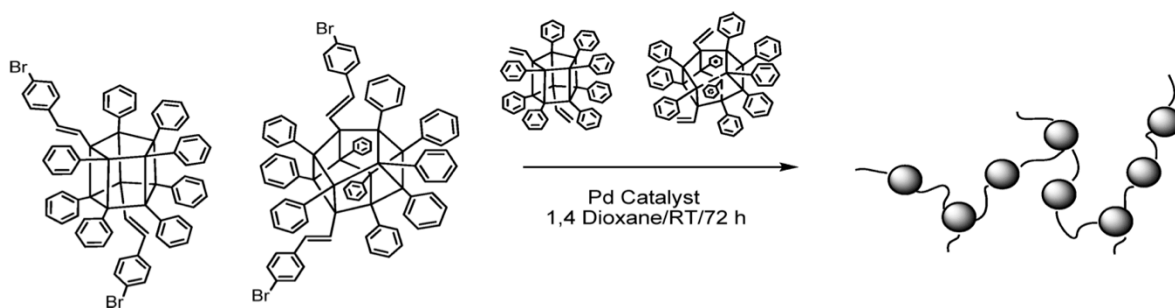


Scheme 1.14. Polymerization of difunctional SQs to form BoC polyimides.¹⁶⁵

Our group has looked at using the F^- rearrangement to “scramble” SQs into statistically mixed T_{10} and T_{12} structures to form BoC polymers.^{139,140} Our first example

used polyphenylsilsesquioxane (PPS) and polyvinylsilsesquioxane (PVS) in a stoichiometry of 4.4:1 to make mixed $T_{10/12}$ with an average of 2 vinyl groups per cage $[(\text{vinyl})_2(\text{Ph})_{x-2}\text{SQ}]_{x=10/12}$ through TBAF catalyzed rearrangement. The vinyl groups were then functionalized through a metathesis reaction with 4-bromostyrene to generate $[(4\text{-BrStyr})_2(\text{Ph})_{x-2}\text{SQ}]_{x=10/12}$, and verified by MALDI-ToF, TGA and NMR. This material was then coupled to $[(\text{vinyl})_2(\text{Ph})_{x-2}\text{SQ}]_{x=10/12}$ with 1:1 stoichiometry to generate the BOC polymer shown in Scheme 1.15.

This polymer showed thermal stabilities up to ($T_{d5\%}$) 325 °C in air, and M_w of 3716 Da by GPC suggesting ~4-5 monomer units per chain. Since this polymer (oligomer) had a conjugated organic linker between cages, absorption and emission studies were conducted offering novel properties discussed in Section 1.6 and Chapter 7.



Scheme 1.15. Heck cross-coupling reaction to form BOC polymers, (phenyl/divinylbenzene).¹⁷⁷

Our group has extended the work on polyimides by synthesizing $[(\text{NH}_2\text{Ph})_2(\text{Ph})_{x-2}\text{SQ}]_{x=10/12}$ using TBAF rearrangement with the mixed isomer (*o,m,p*) of octa-aminophenylSQ.¹⁰² $[(\text{NH}_2\text{Ph})_2(\text{Ph})_{x-2}\text{SQ}]_{x=10/12}$ was then coupled (1:1) with the diglycidyl ether of bisphenol A (DGEBA) to form an epoxy resin (Figure 1.10).¹⁶⁵ The low molecular weight portion of this material showed $T_{d5\%}$ of ~320 °C in air, M_w of 10 kDa and reasonable solubility in THF. The high molecular weights (>100 kDa for high molecular weight fraction) suggest that the coupling of the aminophenyl groups with DGEBA is very facile since the reaction times were only 24 h.

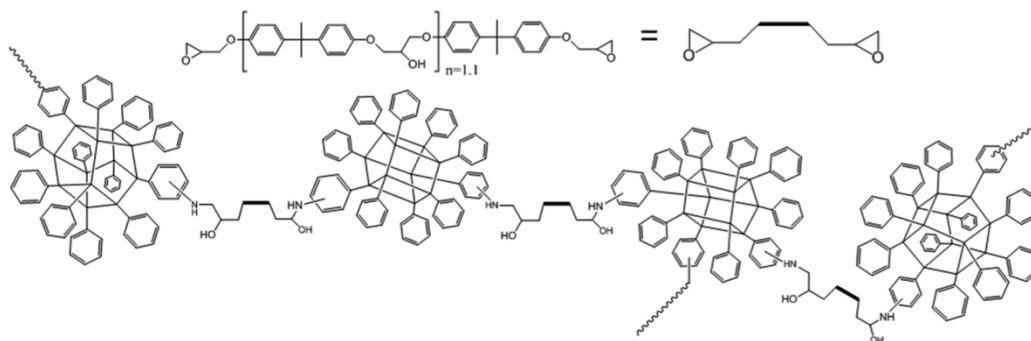


Figure 1.10. Epoxy coupling reaction to BoC polymers.¹⁶⁵

We have since extended our methodologies to include other mixed functional cages such as 4-iodophenyl/vinyl and other organic linkers including divinylbenzene (DVB), 4,4'-dibromostilbene, 1,4-dibromobenzene and 1,4-di-ethynylbenzene.^{141,170} The synthesis, characterization and the unique photophysical properties of these are discussed further in Chapter 7.

1.6 Optical/Electronic Properties of Silsesquioxanes

In general, fluorescence measurements can be used to characterize the electronic transitions, intermolecular interactions and dynamic properties of silsesquioxanes on the molecular scale; while absorption and excitation spectra give additional information about the structure of electronically excited states, minimal energy gaps between ground and excited states, and the influence of energy transfer processes.¹⁵³ Further information can be obtained about transition dipole moments, polarizability, excited state energy transfer, and fluorescence lifetimes through two photo absorption and fluorescence upconversion techniques discussed in more detail below. Many studies have used these techniques to analyze functionalized SQs for applications in photonics, photovoltaics and light emitting diodes.

The absorption and emission properties of T₈ silsesquioxane cores [R₈(SiO_{1.5})₈] and also a few [R_{10/12}(SiO_{1.5})_{10/12}] where R = H or alkyl have been studied extensively by Ossadnik et al.¹⁵² and Azinovic et al.¹⁵³ It is expected that SQs with no conjugated organic functionality would have minimal absorption and emission due to their silica-like properties.

These reports find that SQs give both absorption and emission properties in the blue spectral region for all R-groups. They also find that fluorescence intensity depends on the cage size and ligand electronegativity, with larger cage sizes and more electron rich ligands showing higher fluorescence efficiencies. Figure 1.11 compares [Cl-propyl-SiO_{1.5}]_{8,10,12}, with absorption and emission at ~4.8 eV (260 nm), and ~3.2 eV (387 nm) respectively.

Azinovic et al. proposed that photoluminescence from SQs with alkyl substituents must arise from charge transfer between the cage and ligands, a form of 3D conjugation, as previously shown in carborane cages.¹⁷¹ Lastly, they found that the optical band gaps for SQs were 1.6 eV lower than predicted, 4.4 vs 6.0 eV likely due to the negative Coulomb integral.

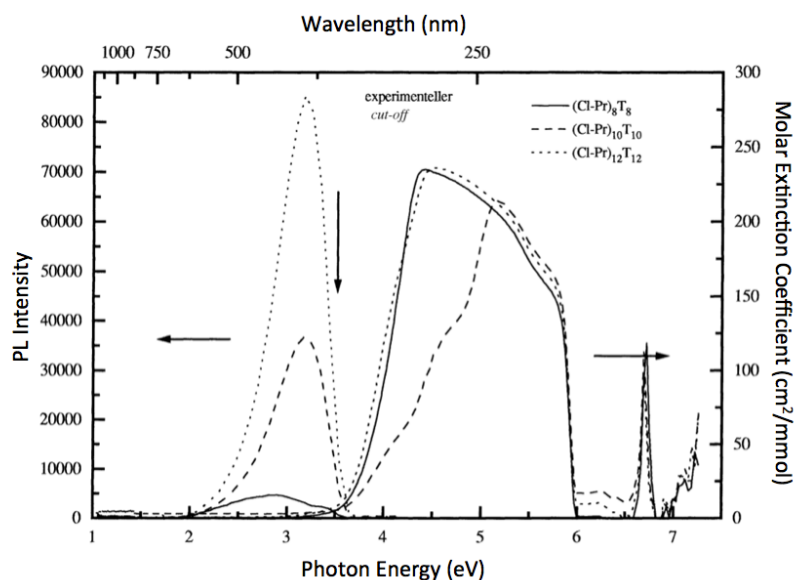


Figure 1.11. Absorption and emission of T_{8,10,12} Cl-propylSQs.¹⁵²

Silsesquioxanes with conjugated organic substituents would be expected to lower the HOMO-LUMO band-gaps even further, since their conjugation to the cage should allow for interaction between them and the SQ, extending the conjugation length. However, an alternate theory is that the cage simply acts as an anchor for the organic groups, meaning all electronic transitions would be centralized on the organics. If this were true, then the photophysical behavior should be nearly identical to the free chromophores. Numerous studies on organic substituents conjugated and anchored to the silsesquioxane core have

targeted applications such as OLEDs,⁶⁵ with varying effects on their absorption and emission properties as discussed below.^{172,173}

Extensive studies have targeted the use of SQs in OLEDs,⁶⁵ however Morgan et al report the use of octaphenylSQ as a phase separation agent in P3HT:PCBM solar devices.¹⁷⁴ Their studies show extensive aggregation of the SQ species as shown by AFM (Figure 1.12). They find that thermal annealing devices with 1 wt% phenylSQ increases power conversion efficiency (PCE) from 5.8 to 9% attributed to the phase separation and increased scattering within the films.¹⁷⁴ In our own studies we observe similar findings, in which aggregated pentafluorostilbeneSQs show PCE increases of $\sim 1\%$.¹⁷⁵

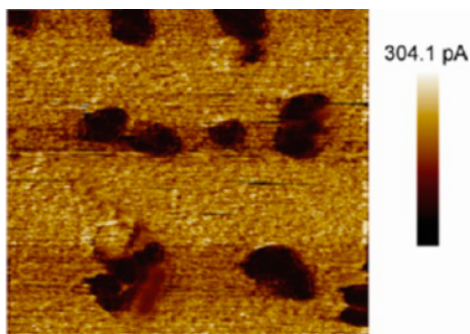


Figure 1.12. AFM image of an [PhSiO_{1.5}]₈:P3HT:PCBM film (100-150 nm aggregates).¹⁷⁴

Most work on the photophysical properties of SQs has focused on the development of solution processed SQs as hole transport materials for OLEDs, as pioneered by Canon/Laine et al starting in 2003. Canon were in search of materials that allowed for enhanced brightness and efficiencies compared to devices made with traditional hole transport materials. Heeger et al also reported using cyclopentylSQs as capping agents for conjugated organic polymers [polyfluorene (PFO) and polyphenylenevinylene (PPV)].¹⁷³ Thus devices made with MEH-PPV-POSS exhibit higher brightness (1320 cd m^{-2} at 3.5 V) and higher external quantum efficiencies ($g_{\text{ext}} = 2.2 \%$) than MEH-PPV (230 cd m^{-2} at 3.5 V and $g_{\text{ext}} = 1.5 \%$), with no effect on the absorption or emission spectra (Figure 1.13).

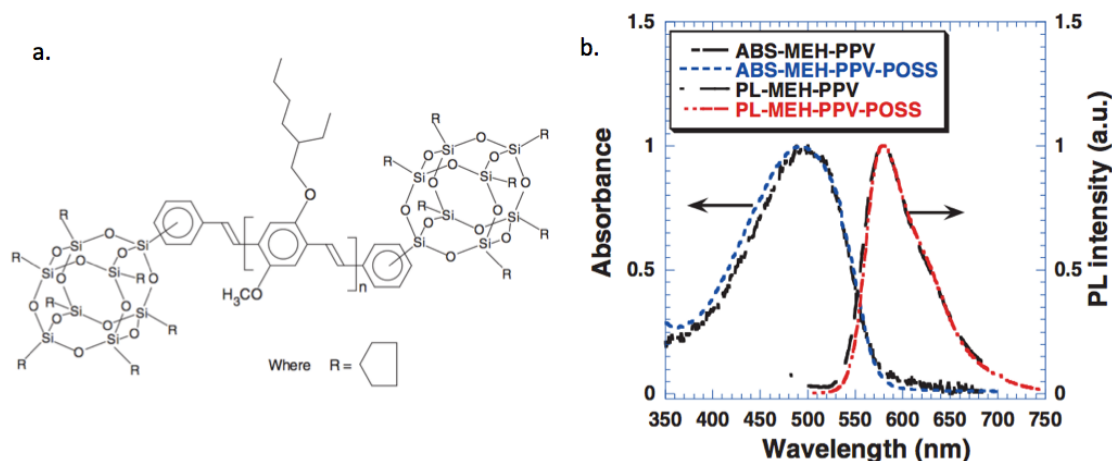


Figure 1.13. a. Structure and b. absorption and fluorescence of SQ anchored poly(2-methoxy-5-(2-ethylhexyloxy)-1,4-phenylenevinylene).¹⁷³

SQs have also been used as pendant groups (off the side chain) in common polymers such as polyfluorene derivatives because they offer increased stability and prevent aggregation of the conjugated polymers, increasing fluorescence yield.^{65,176} Shim et al synthesized a Poly-9,9'-dihexylfluorene-poly-9,9'-di-cyclopentyl₈SQ copolymer.¹⁷² They found that bulky SQs, reduced aggregation in photoluminescence spectroscopy by hindering excimer formation. They also found increased fluorescence quantum efficiency and no effect on the redox properties of the polymers by cyclic voltammetry (CV).

Since the early polymeric side chain studies, many groups have used SQs as dendritic cores for light emitting organics (i.e. $[\text{RSiO}_{1.5}]_8$) without organic polymer backbones. This is ideal since one of the main drawbacks of using conjugated polymers for light emitting applications is their propensity to π - π aggregations, thereby quenching fluorescence. Many examples of these types of materials have been studied over the years with light emitting or photovoltaic applications in mind.⁶⁵

Sellenger et al developed a strategy for attaching various conjugated organic systems (Br- phenanthrene, anthracene, dimethylfluorene, etc.) to an octavinylsilsesquioxane core using catalyzed Heck cross coupling.^{120,177} All compounds showed violet-blue emission in solution as expected for vinyl-aryl derivatives (360-380 nm emission), or blue-green emission for vinyl-anthracene/vinylphenanthrene derivatives. The fluorescence quantum yields for these materials were moderate, ~20-55%, and OLED external quantum

efficiency maxima at 2.6%. These materials also offer good-to-excellent improvements in electron and hole transport properties when used as components in OLED applications compared with simple organics.

As stated above, the addition of conjugated organic groups on SQs should lower their HOMO-LUMO band gaps. This could be by coupling of the organic groups to the SQ, making them electronically homogenous, or by centralizing electronic transitions onto the organics only. If electronic transitions were only on the organics, the photophysical properties would be expected to be similar for chromophores (light absorbing/emitting groups) on and off of the SQ cage. Many of the published studies show similar photophysical behavior for bound and unbound chromophores, with only increased quantum yields observed for the cage bound species.⁶⁵ This results from the SQ cores spreading the chromophores out in 3D thereby preventing π - π stacking (aggregates), which quench fluorescence.^{172,173}

The first studies by our group of SQs for photonic type applications were [o-Br_xPhSiO_{1.5}]₈ derived compounds, followed by the introduction of [*p*-IPhSiO_{1.5}]₈ derived compounds.¹⁰³ Section 1.3.3 discusses examples of materials made by catalytic cross-coupling reactions. Particular focus was given to R-stilbeneSQ derivatives due to their robustness, ease of synthesis, and also because phenylene-vinylene polymers are known to be excellent blue emitters, but exhibit poor solubility.¹⁷⁸ Figure 1.14 compares the absorption and emission spectra of the [Br_xPhSiO_{1.5}]₈ and [*p*-IPhSiO_{1.5}]₈ derived *o*- and *p*-methylstilbeneSQs to that of *p*-methylstilbene.

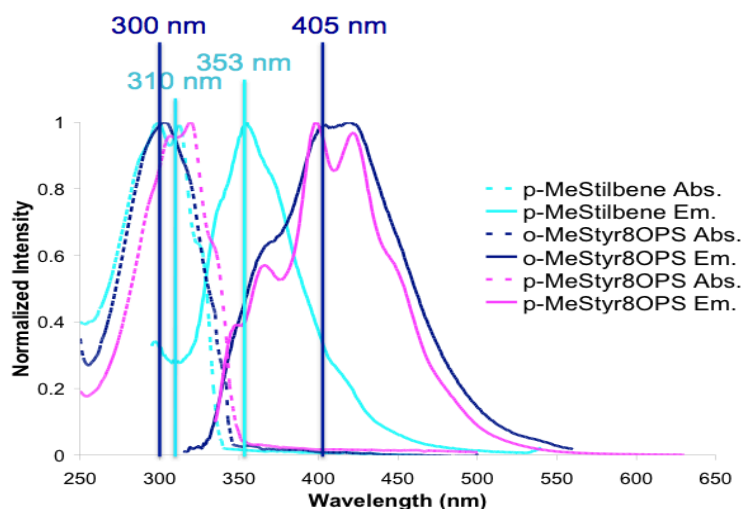


Figure 1.14. Absorption and emission comparison of ortho and para (*o/p*)-MeStilbeneSQs to *p*-MeStilbene in THF.

The key features observed are that all the stilbene derivatives absorb at wavelengths typical of both *trans*- and *para* substituted *trans*-stilbenes.¹¹⁷ Electron donating groups red shift both the absorptions and emissions equally by 10-20 nm (i.e. -OMe, -NR₂, etc). However, the most surprising discovery was that the emissions are red shifted compared to *trans*-stilbene or the model compound *p*-trimethoxysilylstilbene by 60-80 or 40-60 nm respectively.¹¹⁷ In terms of MeStilbeneSQs, the *p*-MeStilbeneSi(OEt)₃ model compound emission is red-shifted 20 nm from *trans*-stilbene and the cages are red-shifted 60-75 nm. Given the many possible explanations for this observation, our group carefully attempted to identify the true source of these red shifts.

A few other groups have also observed similar photophysical behavior.¹⁷⁹⁻¹⁸¹ Andre et al, have investigated the absorption and emission properties of various R-octa-biphenyl-vinylSQs. They find that the absorption and fluorescence spectra (Figure 1.15) of the biphenyl cage derivatives are only slightly red shifted from their small molecule analogs (~10 nm for absorption, and ~15 nm for emission). In another study, the same group looked at the photophysical behavior of 4'-vinylbiphenyl-3,5-dimethylalcohol functionalized SQs and observed a 60 nm red shift in emission when going from the free diol analog to the diolSQ (Figure 1.15), a similar observation to our studies.¹⁸⁰

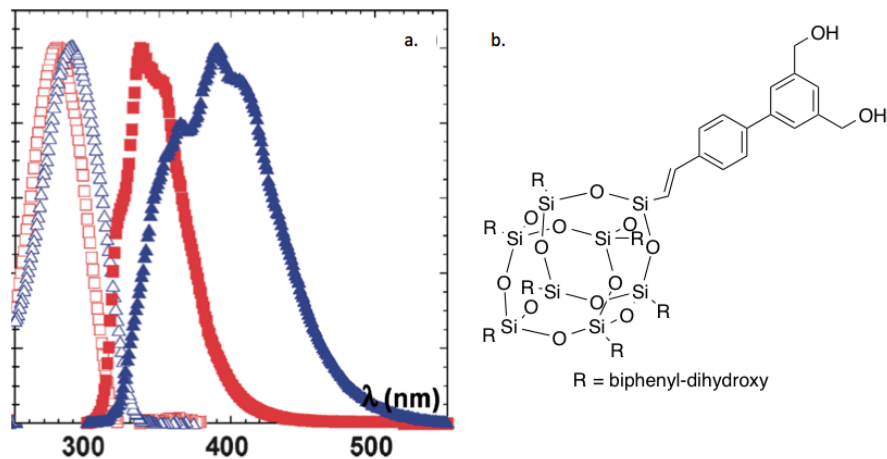


Figure 1.15. a. Normalized absorption (empty symbols) and emission (closed symbols) of 4'-vinylbiphenyl-3,5-dimethylalcohol functionalized SQ (Blue) and 4'-vinylbiphenyl-3,5-dimethylalcohol (Red).¹⁸⁰

Feher and Budzichowski suggest that the SQ core is simply an electron-withdrawing group comparable to $-\text{CF}_3$.¹⁸² If this were true, then blue shifts in absorption and emission spectra should be observed conjugated organics are attached to the SQ core, due to decreased electron density. The red shifts on the other-hand suggest the opposite; chromophores on the cage offer “longer” conjugation lengths than free chromophores. Andre et al. attributed their red shifts to some sort of electron delocalization involving the SQ,¹⁸¹ with backing from their theoretical studies on biphenyl derivatives. This theory was also explored using a new set of stilbenevinylSQ derivatives and will also be explored further throughout this dissertation.

Our group has since looked at $[\text{vinylSiO}_{1.5}]_8$ to synthesize $[p\text{-RStylSiO}_{1.5}]_8$ where $\text{R} = \text{H}, \text{Me}, \text{MeO}, \text{Br}, \text{NH}_2, \text{C}_6\text{F}_5$ and the corresponding vinylstilbenes, $[\text{RStilCH}=\text{CH}_2\text{SiO}_{1.5}]_8$.^{63,116} In general, the photophysical properties of these materials did not exhibit the same large red shifts in emission observed for the stilbeneSQs discussed above (Figure 1.16). In general, they showed similar absorption and emission to their corresponding off cage analogs. However, they did offer good two photon absorption properties, as discussed below in Section 1.6.1. The development and properties of the corresponding T_{10} and T_{12} analogs of these materials are discussed in Chapters 5 and 6.

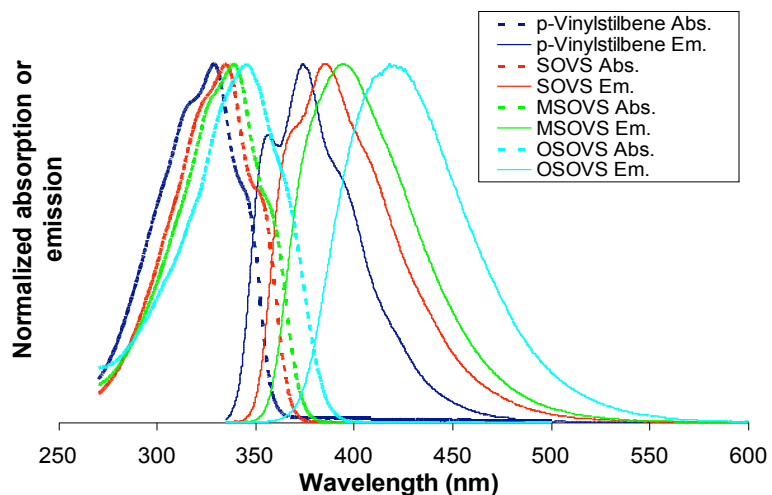


Figure 1.16. Absorption and emission of stilbeneoctavinylSQs.^{63,116}

Our group has also extensively explored the photophysical properties (steady state, two photon absorption and fluorescence upconversion lifetimes) of a set of model compounds developed by Ugo et al.^{117,183} These include dimethylaminostilbene-functionalized siloxane and cyclosiloxane molecules that are equivalent to corner units and halves of the cubic silsesquioxane molecules, respectively (Figure 1.17).¹¹⁷ These property comparisons allow us to assess the extent of conjugation between the organic tethers and different degrees of silsesquioxane units.

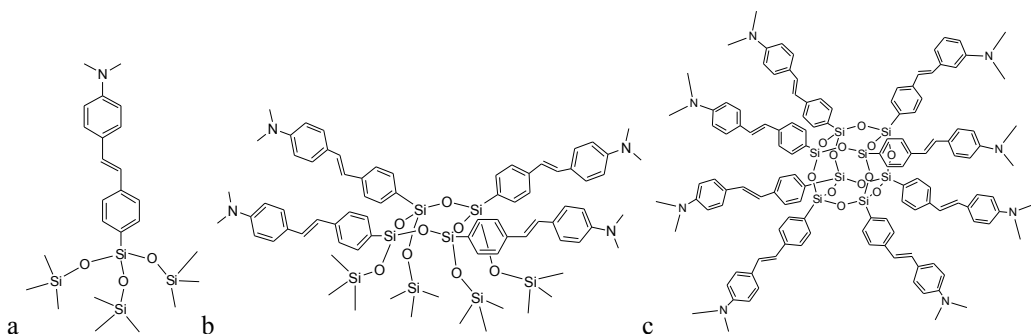


Figure 1.17. (a) Me₂NStil-corner, (b) Me₂NStil-half, and (c) Me₂NStilOS.¹¹⁷

The absorption and fluorescence spectra of the “corner” and “half” molecules are nearly identical, while those of the full cage molecules are slightly red-shifted (~5 nm for absorption and ~10 nm for emission). The low photoluminescence quantum yields and structure-less emission point to charge-transfer (CT) processes. The fluorescence

quantum yields for these molecules are 6%, 8%, and 3% for the “corner”, “half” and full cage respectively. The two-photon absorption fluorescence lifetime kinetics of these materials are discussed in detail in Section 1.6.2 and 1.6.3 respectively.

We have also developed routes to “beads on a chain” polymers (BoC) as discussed above. Comparison of the photophysical properties of 1,4-divinylbenzene linked cages vs. unlinked model compounds show emission red shifts of >50 nm, suggesting “3-D excited state conjugation” effects through the cages and conjugated bridges (Figure 1.18).¹⁴⁰

Coughlin et al. have also shown similar effects for ortho-linked carborane-polyfluorene copolymers with significant red shifts in their emission spectra from a fluorene dimer, however these shifts are unobserved in para-carborane copolymers.^{184–186} This suggests that interactions occur on the cage face, which is a potential charge transfer theory discussed above for SQs. This unique photophysical observation and the ease of synthesis of linked SQs by fluoride catalysis has opened up a whole new class of materials of which are discussed in Chapter 7.

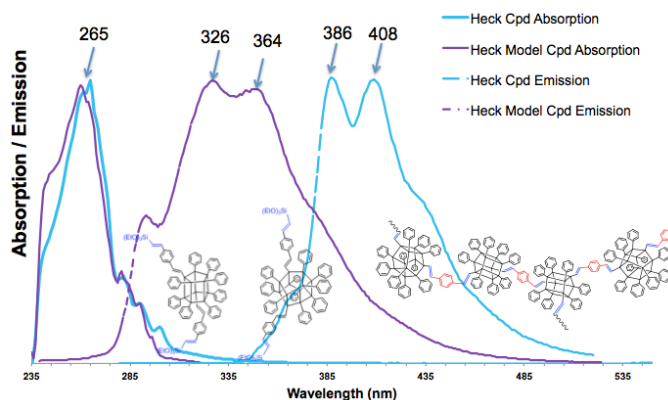


Figure 1.18. Absorption and emission of $T_{10/12}$ divinylbenzene linked oligomer (BoC).¹⁴⁰

1.6.1 Theoretical Investigations

Theoretical investigations of the stilbene-functionalized silsesquioxanes show that the HOMO of T_8 *p*-stilbeneSQ lies on the π -state of the stilbene moiety, with the LUMO made up of interactions between the silicon atoms and π^* of the stilbenes. The HOMO-LUMO band gap for *p*-stilbeneSQ is 2.6 eV, while the HOMO-SQ Core (MO) gap is 4.2 eV. If we consider the 1.6 eV difference found for T_8 HSQ between experiment and

calculation,^{151,117,152-154} then the HOMO-SQ Core (MO) gap could be reduced to 2.6 eV, allowing for the possibility of cage-chromophore interactions. Calzaferri et al also suggest similar interactions in theoretical studies with naphthyl and biphenyl groups bound to octavinylsilsesquioxanes, in which they observe SQs ranging from insulating to conducting.^{117,68,187} It was also suggested that the conjugation could be “3-D” along the edges of the cage rather than through the cage. Evidence of this is given in our studies of Förster resonance energy transfer on stilbenevinylSQs (Chapter 6). These studies offer an argument for charge delocalization throughout the cage system, which is a possible explanation for the red-shifts observed in emission.

Time-dependent density functional theoretical (TDDFT) studies were also conducted to study two possible energy transfer states, CT1 (chromophore-to-cage) and CT2 (chromophore-to-chromophore) on R-stilbenevinyl-, R-stilbene and other vinylSQs, which show variation to results in previous studies on R-stilbeneSQ (Figure 1.19).^{188,189} Phillips *et al.* similarly found that the excitations are mainly localized on the chromophores, except for vinylsilsesquioxanes, but found that emission is exclusively from the chromophore and not from a combination of cage-chromophore interactions.¹⁸⁸ Note that the calculated band gaps are overestimated by these theoretical methods, with the T₈ stilbeneSQ showing 4.0 eV theoretical and 3.1 eV measured. Zheng *et al.* suggest that the emissive state of these octahedral silsesquioxanes is ligand-to-ligand (CT2), rather than ligand- to-silsesquioxane (CT1).¹⁸⁹ However, as stated above these interactions likely depend on the distance between the chromophores (Förster resonance energy transfer), which is dependent on cage size.

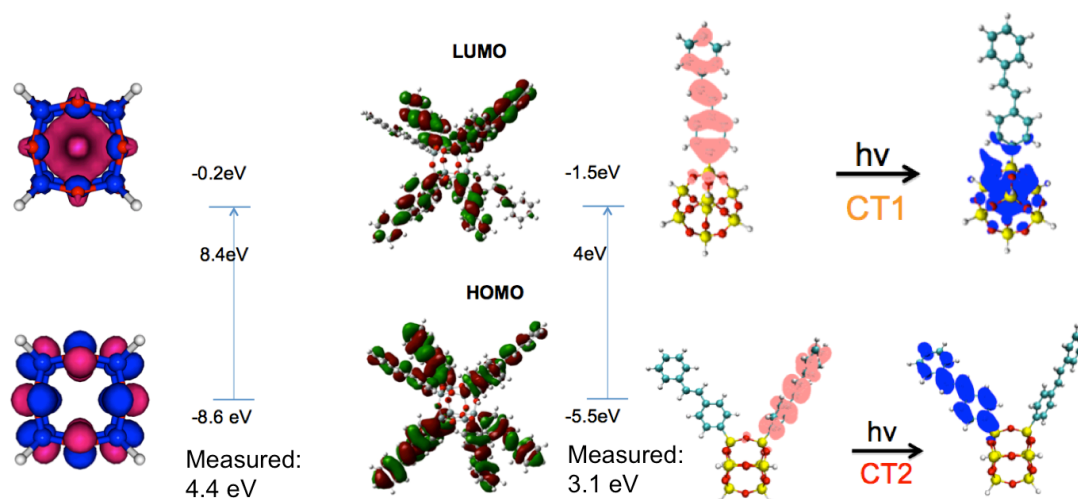


Figure 1.19. Comparison of HOMO and LUMO of silsesquioxane systems, and their charge transfer mechanisms.

1.6.2 Non-Linear Optical Properties of Silsesquioxanes

Few studies on the non-linear optical properties of SQs exist outside of our own group, however a few materials have been studied as optical limiting (OL) materials, and as performance enhancers for laser dyes.¹⁷⁶ In terms of optical limiting, which are materials that with transparency under normal conditions, but become opaque under response to high energy laser pulses, a metallophthalocyanine₁-isobutyl₇-SQ with Co (II), Cu (II) and Zn (II) were synthesized and analyzed for optical limiting by a Z-scan technique.¹⁹⁰ The Cu-phthalocyanine showed significant non-linear absorption, while the other two did not. Another example used an octastilbeneSQ derivative made by hydrosilylation of stilbene with octahydridoSQ showed similar OL to stilbene, but thermal stabilities increased by 20-60 °C.¹⁹¹ For enhancing the performance of optically pumped laser dyes, Garcia-Moreno et al. used a 1% solution of octamethylmethacrylSQ with laser dye PM567 in ethyl acetate, and found a 65% enhancement in dye efficiency and no degradation in laser output after 100,000 pump pulses.¹⁹²

Our group has been motivated by the two-photon absorption properties of various organic and inorganic materials, including functionalized silsesquioxanes.^{117,116,121,193-197} Two-photon absorption analysis is useful for understanding the underlying physical properties of materials that make them optimal performers in photovoltaics, light emitting, optical limiting and imaging applications.

1.6.2.1 Two Photon Absorption

Two-photon absorption (TPA) is a phenomenon first proposed by Maria Göppert-Mayer in 1931, in which two simultaneous photons are absorbed by a molecule and promoted into the excited state.¹⁹⁸ The first publication on the experimental use of TPA by Kaiser et al was done in 1961, soon after the invention of the first laser device, in which they found two photon-induced fluorescence of europium-doped Ca_2F crystals.¹⁹⁹ Since the development of sub-picosecond pulsed lasers (particularly the Ti:sapphire laser) and increasing commercial availability during the 1990's has led to a great increase in the studies of two-photon absorbing molecules.²⁰⁰ TPA increases with the square (quadratic dependence) of the light intensity, since it involves the simultaneous interaction of two photons (Equation 4); therefore, investigating TPA requires intense and focused laser beams, particularly from pulsed lasers, which generate very high instantaneous photon flux (~ 80 fs pulses). TPA is an efficient and less invasive method of accessing an excited state by using photons of half the energy (or twice the wavelength) of the corresponding one-photon transition (Figure 1.20).

$$\Delta I = \alpha I_0^2 \quad \text{Equation 4}$$

Two-photon absorption can be modeled theoretically as a two-step event, even though the two photons interact simultaneously. In the first step, the molecule absorbs the energy of one photon and is excited from its ground state to the virtual intermediate state, which only exists while the molecule experiences the field of the first photon (~ 5 fs).^{201–204} In the second step, the molecule absorbs the energy of another photon and completes the transition from the intermediate state to the excited state. Since the lifetime of the intermediate state is infinitely short compared to the final excited state, the two-step process of TPA is considered simultaneous.

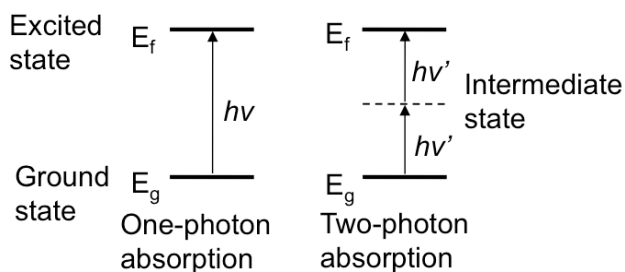


Figure 1.20. Comparison of one and two-photon excitation pathways.

The sensitivity of a molecule towards TPA is quantified by its TPA cross-section, which is reported in Göppert-Mayer (GM) units ($1 \text{ GM} \equiv 10^{-50} \text{ cm}^4 \text{ s photon}^{-1}$). The TPA cross-section is an intrinsic property as it is controlled by the molecular structure. There is a strong relationship between intramolecular charge transfer processes and two-photon absorptivity, as the absorption of photons induces polarization of the molecule. Therefore, molecules with permanent ground-state dipole moments or transitional dipole moments connected with either the ground or excited states are of great interest in two-photon spectroscopy.

Experimentally TPA cross-sections of new materials are measured by a two-photon excited fluorescence (TPEF) through a comparative process using a standard of known absolute cross-section.²⁰⁵ This process relies on the two-photon induced fluorescence from a sample, which is then compared to the fluorescence and cross-section of the standard at a given concentration. The intercept from plots of $\log(\text{photon counts})$ vs. $\log(\text{power})$ of slope = 2 (quadratic dependence from intensity squared relationship) is then compared with the standard. The relationship for finding the TPA cross-section (δ) for a sample is given by the following equation, where b are the intercepts of the sample and standard, η are the fluorescence quantum yields, $[c]$ are the concentrations, and n are the refractive indices of solutions.

$$\delta_{\text{sample}} = \frac{10^{b_{\text{sample}} - b_{\text{std}}} \eta_{\text{std}} \delta_{\text{std}} [c]_{\text{std}} n_{\text{std}}}{\eta_{\text{sample}} [c]_{\text{sample}} n_{\text{sample}}} \quad \text{Equation 5}$$

TPA studies provide information about the inherent polarizability (i.e. efficiency of charge separation) of molecules. A higher TPA cross-section signifies larger charge separation and also stronger donor/acceptor coupling. The design of high cross-section TPA chromophores is driven by concerns of intramolecular charge-transfer processes. There are three essential requirements for simple highly active conjugated organic TPA materials: a strong π -electron donor (D), a polarizable π -bridge (π), and a strong π -electron acceptor (A). Three main structural motifs exist for TPA active chromophores (Figure 1.21):^{201,206} Type I chromophores are symmetrical and consists of two terminal donor or acceptor groups separated by a π -bridge, respectively (D- π -D and A- π -A). Type II chromophores are asymmetrical and made up of an electron-rich π -bridge with a

donor part on one side and an acceptor part on the other (D- π -A). Type III chromophores consists of multi-armed or branched organic molecules with two or more Type II chromophores bound through multiple π -bridges for extended conjugation. In type three chromophores the intramolecular charge transfer/polarization can be from the molecule centers to the terminus or from terminus to center. The donor and acceptor groups in TPA chromophores can function as end groups or as part of the π -bridge.

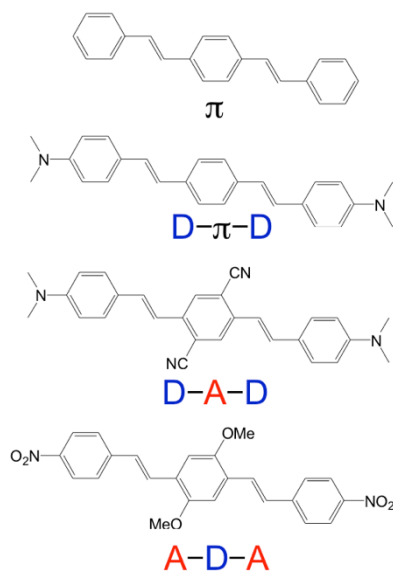


Figure 1.21. Examples of structural motifs in two-photon absorbing organic systems.

The most widely used donor groups in TPA materials are dialkyl or diaryl amino groups, because of their availability, oxidative stability and electron-donating capabilities. Hydroxy and alkoxy groups are also common and are found in many chromophores designed for biological applications. Commonly used electron-withdrawing groups include: electron-deficient heterocycles such as pyridyl,^{207,208} and quinolone,²⁰⁹ nitro,^{210,211} trifluoromethyl,^{212,213} aldehydes,^{207,209} cyano,^{212–214} and sulfonyl groups.^{208,215}

Phenylene-vinylene, 2,7-fluorenyl, and phenylene-ethynyl are common organic π – bridges due to their high efficiency in transferring charges.²⁰¹ It was found that adding electron- withdrawing groups to the center of a π -bridge in D- π -D-type chromophores leads to an increase in the TPA cross-sections.²⁰² However, adding electron deficiencies to the center destabilizes the system and makes it more susceptible to oxidation.

Increasing the conjugation length of the π -bridge extends the charge separation and often leads to a higher TPA cross-section.^{200,214,216} Electron delocalization is optimized when a π -system assumes a planar geometry, with maximum π -orbital overlap, and therefore TPA cross-section values are dependent on the conformation of the π -bridge.^{201,202} Recently however, materials without a conjugated π -bridge (meta substituted or alkyl) have shown reasonable two-photon activity by charge “hopping” from one side of the molecule to the other.^{217,218}

There are two major advantages of two-photon spectroscopy over one-photon spectroscopy: (1) the coherent laser light used in two-photon spectroscopy has much longer wavelengths (lower energy), which causes less photochemical damage to samples (important for biological samples), with a better penetration depth, and (2) since the absorption increases with the square of the light intensity at a sharp focal point and falls off rapidly away from focus, this provides much sharper resolution and prevents unwanted emission, high thermal buildup throughout sample, and photochemical conversions outside the focal area. There are many important applications/potential applications of two-photon spectroscopy including: biological probes,^{219–222} activated drug delivery,^{223,224} surface imaging and microscopy,^{225–228} microfabrication,²²⁹ optical data storage,^{193,230–232} and optical limiting.^{193,233,234}

TPA studies done previously in our group have looked at a series of functionalized silsesquioxanes with stilbene- and stilbenevinyl- functionalization.^{117,63,116,121} The two-photon cross-sections of a few of these species are compared in Table 1.2. The best overall cross-section found for any SQ species to date is for the [*p*-NH₂StilvinylSiO_{1.5}]₈, which has a total molecule cross-section of 810 GM, or 110 GM per chromophore, suggesting a large transition dipole moment (polarization) and high ability to separate charges. This is expected from a strong donor (-NH₂) component and the SQ acceptor component.

TPA studies of the “corner”, “half”, and “cube” mentioned above found cross-sections of the “corner” molecule are 12 GM/moiety, the “half” are 8 GM/moiety, and the “cube” are 26 GM/moiety.¹¹⁷ In theory, if the charge-transfer characteristics are identical for these molecules, then their TPA cross-section/moiety should also be identical.

However, since they give different cross-sections, their polarization dynamics must be different. Since the “cube” has the lowest fluorescence quantum yield and the highest TPA cross-section/moiety, it would be suggestive that this molecule has the highest charge-transfer characteristics among the “corner”, “half” and “cube” molecules. In all SQ TPA studies, it has been found that the SQ core as a whole enhances the TPA cross-section/moiety more than expected based on a sum of corner fragments.

Table 1.2. TPA properties of silsesquioxane derivatives and quantum efficiencies (Φ).^{117,63,116,121}

Sample	$\bar{\delta}$ (GM)	$\bar{\delta}$ /moiety (GM)	λ_{\max} nm	Φ_f
MeStil ₈ OS	11	1.2	735	0.06
Me ₂ NStil-corner	12	12	780	0.08
Me ₂ NStil-half	30	7.5	790	0.09
Me ₂ NStil ₈ OS	211	26	755	0.03
[StilvinylSiO _{1.5}] ₈	25	3	705	0.36
[<i>p</i> -MeOStilvinylSiO _{1.5}] ₈	110	14	705	0.12
[<i>p</i> -NH ₂ StilvinylSiO _{1.5}] ₈	810	101	720	0.05
[StilvinylSiO _{1.5}] _{10/12}	8	1	770	0.15
[<i>p</i> -MeOStilvinylSiO _{1.5}] _{10/12}	33	3	650	0.07
[<i>p</i> -NH ₂ StilvinylSiO _{1.5}] _{10/12}	750	68	770	0.07

1.6.3 Fluorescence Lifetime Kinetics

Within fluorescent molecules, many electronic processes occur on the ultrafast time-scale (fs-ps) including inter/intra-molecular interactions, fluorescence lifetimes (related to quantum efficiencies) and charge-transfer processes, thus making time-resolved fluorescence upconversion spectroscopy a very valuable technique for delineating these processes. Fluorescence upconversion takes advantage of the pulse widths of picosecond and femtosecond pulsed lasers, with femtosecond lasers usually having pulse widths <120 fs. Along with the capability to measure fs and ps fluorescence lifetimes, typical

upconversion setups provide for the ability to control the excitation beam polarization, which allows for measuring the fluorescence of analyzed molecules of the same transition dipole orientation. In solution, these dipoles would be oriented randomly and through excitation with selective polarization, only molecules oriented parallel to the field of excitation will have a distinct orientation in the excited state. Depolarization of the excited states during emission results in the measurement of fluorescence anisotropy, which results from changing the excitation beam polarization (parallel/perpendicular). Such studies can give detailed information about charge transfer and energy migration in molecules/polymers.^{235–237}

Since the excitation beam is polarized, the emission is then polarized either parallel (I_{par}) or perpendicular (I_{per}) to that beam. The observed fluorescence anisotropy is related to the relative intensities of the parallel and perpendicular signals through the following relationship,²³⁸

$$r = \frac{I_{par} - G \times I_{per}}{I_{par} + 2G \times I_{per}} \quad \text{Equation 6}$$

where r is the anisotropy value and G is the g factor, a correction factor for the sensitivity of the detection system for the two forms of polarized light. Anisotropy is a dimensionless quantity that relates the ratio of the difference in polarized intensity with that of the overall intensity.²³⁸ For one-photon processes, the maximum possible anisotropy value is 0.4, which corresponds to a molecule that shows no depolarization from excitation to emission, or an angle of 0° between the two dipoles. Multiphoton excitation may also be performed with an added benefit of having a larger dynamic range, with a maximum initial value of 0.57 in the case of two-photon excitation.²³⁹ In a sense combining the advantages of two-photon spectroscopy mentioned above with time resolved fluorescence studies.

As an example of the usefulness of fluorescence upconversion, it can be used to study resonance energy-transfer (RET) processes (i.e. Förster energy transfer).²⁴⁰ Equation 7 shows the relationship between two different molecules undergoing a Förster energy transfer,

$$k_T(r) = \frac{1}{\tau_D} \left(\frac{R_0}{r} \right)^6 \quad \text{Equation 7}$$

where k_T is the rate of energy transfer, τ_D is the fluorescence lifetime of the donor molecule on its own; R_0 is the Förster radius, the distance of separation between molecules where RET is 50% efficient; and r is the center-to-center distance between the donor and acceptor molecules. A detailed analysis of Förster energy relationships as well as fluorescence upconversion studies and their importance in silsesquioxanes will be discussed in Chapter 6, with calculations shown in Appendix C. Much of the research in the Goodson group is focused on examining energy transfer effects in macromolecular systems including functionalized silsesquioxanes.^{235,237,241–244}

Fluorescence upconversion studies were done on the “corner”, “half”, and “cube” systems by Zhang et al.^{117,245} In brief, the fluorescence lifetimes of the half and cube were nearly identical (73 and 75 ps), suggesting similar energy transfer dynamics, while the corner showed a lifetime twice as long (146 ps). This relationship is believed to be from twisting of the chromophores in a cis-trans transition, with a more rigid backbone allowing for faster isomerization. For anisotropy, the cube and half show similar dynamics with values decaying to ~ 2.5 , while the corner shows no anisotropic decay. This shows that the cube and half have polarization dependence, whereas the free chromophore does not. This is expected since the cube and half have chromophores oriented in 3D space (multiple polarizations), whereas the corner only shows a single polarization down the molecule. Charge transfer characteristics were found to be similar in all cases, suggesting chromophore-chromophore interactions.

1.7 Overview of Subsequent Chapters

The remaining chapters of this dissertation are organized as follows.

Chapter 2 describes the relevant synthetic and experimental techniques used in this dissertation including: fluoride catalyzed rearrangement of SQs, Heck cross-coupling, Grubbs metathesis; various characterization tools including: ^{29}Si and ^{19}F NMR (nuclear magnetic resonance spectroscopy), MALDI-ToF (Matrix Assisted Laser Desorption Ionization Time of Flight Mass Spectrometry), TGA (thermal gravimetric analysis), etc. Lastly, photophysical property analysis techniques will be described using steady state

absorption spectroscopy, two-photon excited fluorescence spectroscopy and time resolved fluorescence upconversion spectroscopy.

Chapter 3 describes the functionalization and characterization of alkoxy silanes (i.e. Si(2-methyl-2,4-pentanediolato)₂) using R-Li reagents, where R- is any aryl or alkynyl substituted system. Mono-functionalized R-trialkoxysilanes are then made, followed by their conversion to silsesquioxanes by fluoride catalyzed cage formation.

Chapter 4 describes the synthesis, mechanistic studies and photophysical properties of phenylsilsesquioxanes, in particular T₁₀. T₁₀ phenylSQ was made in the highest reported yield to date (~50%) by fluoride-catalyzed reactions. The fluoride catalyzed rearrangement mechanism will then be discussed in detail from a combination of experimental and computational analyses. This is followed by the functionalization of T₁₀ and T₁₂ phenylSQs by bromination and then styrene to form stilbeneSQs, and finally an analysis of photophysical properties.

Chapter 5 describes the synthesis of T_{10/12} R-stilbenevinylSQs, their unique steady state photophysical properties, and two-photon absorption properties. An extensive analysis of their solubility and fluorescence properties will be discussed. This is followed by a study of the HOMO and LUMO energy levels of these SQ systems.

Chapter 6 describes the separation of T_{10/12} H-stilbenevinylSQs and detailed photophysical property analysis of the separated T₁₀ and T₁₂ H-stilbenevinylSQs. Two-photon absorption, time resolved fluorescence upconversion, and Förster energy transfer calculations give insight into the energy transfer processes involved in SQs.

Chapter 7 describes the synthesis of beads on a chain (BoC) polymers based on mixed T_{10/12} phenyl/vinylSQ systems with 1,4-divinylbenzene and 4,4'-divinylstilbene linkers. This is followed by a discussion of the characterization and finally photophysical properties of these systems.

Chapter 8 gives the overall summary and conclusions of this work followed by a discussion of future work.

References:

1. Innovations of Silicone
<http://www.dowcorning.com/content/discover/discoverinnovate/>.
2. Asimov, I. *Asimov's Biographical Encyclopedia of Science and Technology*; Doubleday & Company: Garden City, NY, 1964; pp. 1–662.
3. Klosowski, J. M.; Wolf, A. T. The History of Sealants. In *Handbook of Sealant Technology*; Mittal, K. L.; Pizzi, A., Eds.; CRC press: Boca Raton, FL, 2009; pp. 1–22.
4. Zavin, B. G.; Muzafarov, a. M. On the 100th Anniversary of the Birth of Kuz'ma Andrianovich Andrianov. *Polym. Sci. Ser. C* **2007**, *49*, 215–218.
5. Andrianov, K. A. *Metalorganic Polymers*; Interscience: New York, 1965; pp. 1–371.
6. Rosenberg, J. The History of Silly Putty
<http://history1900s.about.com/od/1950s/a/sillyputty.htm>.
7. Colas, A.; Curtis, J. An Introduction to Materials in Medicine. *"Silicone Biomater. Hist. Chem.* **2004**, *80–85*, 698–707.
8. Scott, D. W. Thermal Rearrangement of Branched-Chain Methylpolysiloxanes I. *J. Am. Chem. Soc.* **1946**, *68*, 356–358.
9. Markovic, E.; Constantopolous, K.; Matisons, J. G. *Applications of Polyhedral Oligomeric Silsesquioxanes*; Hartmann-Thompson, C., Ed.; Advances in Silicon Science; Springer Netherlands: Dordrecht, 2011; Vol. 3, pp. 1–46.
10. Voronkov, M.; Lavrent'yev, V. Polyhedral Oligosilsesquioxanes and Their Homo Derivatives. *Top. Curr. Chem.* **1982**, *102*, 199–236.
11. Barry, Arthur, J.; Gilkey, J. W. Alkylsilsesquioxanes. 2465188, 1938.
12. Sprung, M. M.; Guenther, F. O. The Partial Hydrolysis of Ethyltriethoxysilane. *J. Am. Chem. Soc.* **1955**, *77*, 3996–4002.
13. Barry, A. J.; Daudt, W. H.; Domicone, J. J.; Gilkey, J. W. Crystalline Organosilsesquioxanes *. *J. Am. Chem. Soc.* **1955**, *77*, 4248–4252.
14. Brown, J. F.; Vogt, L. H.; Prescott, P. I. Preparation and Characterization of the Lower Equilibrated Phenylsilsesquioxanes. *J. Am. Chem. Soc.* **1964**, *86*, 1120–1125.
15. Vij, V.; Haddad, T. S.; Yandek, G. R.; Ramirez, S. M.; Mabry, J. M. Synthesis of Aromatic Polyhedral Oligomeric Silsesquioxane (POSS) Dianilines for Use in High-Temperature Polyimides. *Silicon* **2012**, *4*, 267–280.
16. Pinson, D. M.; Yandek, G. R.; Haddad, T. S.; Horstman, E. M.; Mabry, J. M. Thermosetting Poly (Imide Silsesquioxane) S Featuring Reduced Moisture A Ffi Nity and Improved Processability. *Macromolecules* **2013**.
17. Chan, K. L.; Sonar, P.; Sellinger, A. Cubic Silsesquioxanes for Use in Solution Processable Organic Light Emitting Diodes (OLED). *J. Mater. Chem.* **2009**, *19*, 9103.
18. Sonar, P.; Soh, M. S.; Cheng, Y. H.; Henssler, J. T.; Sellinger, A. Solution-Processable Materials for Application in Organic Electronics. **2010**, 4–7.

19. Kota, A. K.; Kwon, G.; Choi, W.; Mabry, J. M.; Tuteja, A. Hygro-Responsive Membranes for Effective Oil–water Separation. *Nat. Commun.* **2012**, *3*, 1025.
20. Duchateau, R. Incompletely Condensed Silsesquioxanes: Versatile Tools in Developing Silica-Supported Olefin Polymerization Catalysts. *Chem. Rev.* **2002**, *102*, 3525–3542.
21. Wright, M.; Uddin, A. Organic-Inorganic Hybrid Solar Cells: A Comparative Review. *Sol. Energy Mater. Sol. Cells* **2012**, *107*, 87–111.
22. Dosaj, V.; Kroupa, M.; Bittar, R. Silicon and Silicon Alloys, Chemical and Metallurgical. In *Kirk-Othmer Encyclopedia of Chemical Technology*; John Wiley & Sons, Inc., 2000; pp. 1–25.
23. Kawamoto, H. (Nanotechnology A. M. R. U.; Okuwada, K. Development Trend for High Purity Silicon Raw Material Technologies— Expecting Innovative Silicon Manufacturing Processes for Solar Cell Applications. *Sci. Technol. Trends* **2007**, *24*, 38.
24. Gurav, A.; Kodas, T.; Pluym, T.; Xiong, Y. Aerosol Processing of Materials. *Aerosol Science and Technology*, 1993, *19*, 411–452.
25. Okamoto, M. Reaction Pathway of Formation of Methoxysilanes in the Reaction of Silicon with Methanol Catalyzed by Copper(I) Chloride. *J. Catal.* **1994**, *145*, 537–543.
26. Falcone, J. Silicon Compounds: Anthropogenic Silicas and Silicates. In *Kirk-Othmer Encyclopedia of Chemical Tech*; John Wiley & Sons, Inc., 2007; pp. 365–547.
27. Huang, Y.; Liu, T.; Wang, C.; Wang, J. Mechanism and Kinetics of the Synthesis of Phenyltrichlorosilane from Trichlorosilane and Chlorobenzene by Gas Phase Condensation. *Chem. Eng. J.* **2013**, *226*, 255–262.
28. Bonitz, E.; Pfalz, F. Production of Organosilanes. 3.505.379, 1970.
29. Laine, R. M.; Roll, M. F. Polyhedral Phenylsilsesquioxanes. *Macromolecules* **2011**, *44*, 1073–1109.
30. Abe, Y.; Gunji, T. Oligo- and Polysiloxanes. *Prog. Polym. Sci.* **2004**, *29*, 149–182.
31. Arkles, B.; Steinmetz, J.; Zazyczny, J.; Mehta, P. Factors Contributing to the Stability of Alkoxysilanes in Aqueous Solution. *J. Adhes. Sci. Technol.* **1992**, 193.
32. Yanagisawa, T.; Yamaguchi, H.; Kobayashi, M. Absorbent of Chlorosilane Compound. 4,838,946, 1989.
33. Jean, P. A.; Gallavan, R. H.; Kolesar, G. B.; Siddiqui, W. H.; Oxley, J. A.; Meeks, R. G. Chlorosilane Acute Inhalation Toxicity and Development of an LC50 Prediction Model. *Inhal. Toxicol.* **2006**, *18*, 515–522.
34. Yi, E.; Hyde, C. E.; Laine, R. M. Fumed Silica from Sustainable, Green Sources without First Having to Make SiCl₄. *Manuscript in Prepreparation*
35. Rosenheim, A.; Raibmann, B.; Schendel, G. Über Innerkomplexe Brenzcatchinate Vierwertiger Elemente. *Z. Anorg. Chem.* **1931**, *196*, 160–176.
36. Weiss, V. A.; Reiff, G.; Weiss, A. Zur Kenntnis Wasserbestandiger Kieselsaureester. *Z. Anorg. Allg. Chem.* **1961**, *311*, 142–151.
37. Frye, C. L. Pentacoordinate Silicon Derivatives. II. 1 Salts of Bis (o-Arylenedioxy) Organosiliconic Acids. *J. Am. Chem. Soc.* **1964**, *86*, 3170–3171.

38. Boer, F. P.; Flynn, J. J.; Turley, J. W. Structural Studies of Pentacoordinate Silicon. III. Tetramethylammonium Bis(o-Phenylenedioxy)phenylsiliconate. *J. Am. Chem. Soc.* **1968**, *90*, 6973–6977.
39. Flynn, J. J.; Boer, F. P. Structural Studies of Hexacoordinate Silicon. Tris(o-Phenylenedioxy) Siliconate. *J. Am. Chem. Soc.* **1969**, *91*, 5756–5761.
40. Barnum, D. Catechol Complexes with Silicon. *Inorg. Chem.* **1970**, *9*, 1942–1943.
41. Barnum, D. Reaction of Catechol with Colloidal Silica and Silicic Acid in Aqueous Ammonia. *Inorg. Chem.* **1972**, *11*, 1424–1429.
42. Boudin, A.; Cerveau, G.; Chuit, C.; Corriu, R. J. P.; Reye, C. Reaction of Grignard Reagents with Dianionic Hexacoordinated Silicon Complexes: Organosilicon Compounds from Silica Gel. *Angew. Chemie Int. Ed. English* **1986**, *25*, 474–476.
43. Laine, R. M.; Blohowiak, K. Y.; Robinson, T. R.; Hoppe, M. L.; Nardi, P.; Kampf, J.; Uhm, J. Synthesis of Pentacoordinate Silicon Complexes from SiO₂. *Nature* **1991**, *353*, 642–644.
44. Blohowiak, K. Y.; Treadwell, D. R.; Mueller, B. L.; Hoppe, M. L.; Jouppi, S.; Pansal, P.; Chew, K. W.; Scotto, C. L. S.; Babonneau, F.; Kampf, J.; et al. SiO₂ as a Starting Material for the Synthesis of Pentacoordinate Silicon Complexes *Chem. Mater.* **1994**, *6*, 2177–2192.
45. Cheng, H.; Tamaki, R.; Laine, R. M.; Babonneau, F.; Chujo, Y.; Treadwell, D. R. Neutral Alkoxysilanes from Silica. *J. Am. Chem. Soc.* **2000**, *122*, 10063–10072.
46. Kinrade, S. D.; Del Nin, J. W.; Schach, a S.; Sloan, T. a; Wilson, K. L.; Knight, C. T. Stable Five- and Six-Coordinated Silicate Anions in Aqueous Solution. *Science* **1999**, *285*, 1542–1545.
47. Laine, R. M. Nanobuilding Blocks Based on the [OSiO_{1.5}]_x (x= 6, 8, 10) Octasilsesquioxanes. *J. Mater. Chem.* **2005**, *15*, 3725.
48. Laine, R. M.; Krug, D. J.; Marchal, J. C.; McColm, A. Low Cost Routes to High Purity Silicon and Derivatives Thereof. U.S. Patent 8475758, 2013.
49. Frye, C. L. Stable Silicon Heterocyclic Derivatives of Branched Alkane-Diols. *J. Org. Chem.* **1969**, *34*, 2496–2499.
50. Zanowiak, P.; Zanowiak, P. Ullmann's Encyclopedia of Industrial Chemistry. In *Ullmann's Encyclopedia of Industrial Chemistry*; 2000.
51. Laine, R. M.; Doan, P.; Furgal, J. C.; Pan, D.; Yi, E.; Popova, V. Distilling Silica from Biogenic, Green and Sustainable Sources. *Manuscript Submitt. to Sci.*
52. Laine, R. M.; Popova, V.; Furgal, J. C. Patent Application, 2015.
53. McBee, E. T.; Roberts, C. W.; Judd, G. F.; Chao, T. S. Reaction of Grignard Reagents with Alkoxysilanes at Elevated Temperatures. *J. Am. Chem. Soc.* **1955**, *77*, 1292–1293.
54. George, P. D.; Sommer, L. H.; Whitmore, F. C. Steric Effects in Grignard Couplings with Alkoxysilanes 1. *J. Am. Chem. Soc.* **1955**, *77*, 6647–6649.
55. Tour, J. M.; John, J. a.; Stephens, E. B. Convenient Route to Di- and Triorganosilyl Ethyl Ethers and the Corresponding Di- and Triorganosilanes. *J. Organomet. Chem.* **1992**, *429*, 301–310.

56. Silverman, G.; Rakita, P. *Handbook of Grignard Reagents*; 1996; pp. 667–675.
57. Klokov, B. a. Continuous and Batch Organomagnesium Synthesis of Ethyl-Substituted Silanes from Ethylchloride, Tetraethoxysilane, and Organotrichlorosilane for Production of Polyethylsiloxane Liquids. 2. Continuous One-Step Synthesis of Ethylethoxy- and Ethylchlorosilan. *Org. Process Res. Dev.* **2001**, *5*, 234–240.
58. Jung, K.-H.; Kim, S.-Y.; Tan, W.; Shin, D.-S.; Ahn, C. Improved Methods for the Synthesis of Aryltrialkoxysilane Derivatives via Aryllithium and ArylGrignard Bromide with Tetra-Alkoxysilane. *Bullet. Instit. Basic Sci.* **2005**, *17*, 79.
59. Boudin, a; Cerveau, G.; Chuit, C. Reactivity of Dianionic Hexacoordinated Silicon Complexes toward Nucleophiles: A New Route to Organosilanes from Silica. *Organometallics* **1988**, *7*, 1165–1171.
60. Boudin, A.; Cerveau, G.; Chuit, C.; Corriu, R. J. P.; Reye, C. Reactivity of Hypervalent Species: Reactions of Anionic Penta-Coordinated Silicon Complexes towards Nucleophiles. *Bulletin of the Chemical Society of Japan*, 1988, *61*, 101–106.
61. Furgal, J. C.; Jung, J. H.; Goodson, T.; Laine, R. M. Analyzing Structure-Photophysical Property Relationships for Isolated T₈, T₁₀, and T₁₂ Stilbenevinylsilsesquioxanes. *J. Am. Chem. Soc.* **2013**, *135*, 12259–12269.
62. Jung, J. H.; Laine, R. M. Beads on a Chain (BOC) Polymers Formed from the Reaction of NH₂PhSiO_{1.5}]_X [PhSiO_{1.5}]_{10-X} and [NH₂PhSiO_{1.5}]_X [PhSiO_{1.5}]_{12-X} Mixtures (X = 2–4) with the Diglycidyl Ether of Bisphenol A. *Macromolecules* **2011**, *44*, 7263–7272.
63. Jung, J. H.; Furgal, J.; Goodson III, T. G.; Mizumo, T.; Schwartz, M.; Chou, K.; Vonet, J.-F.; Laine, R. M. 3-D Molecular Mixtures of Catalytically Functionalized [vinylSiO_{1.5}]₁₀/ [vinylSiO_{1.5}]₁₂. Photophysical Characterization of Second Generation Derivatives. *Chem. Mater.* **2012**, *24*, 1883–1895.
64. Furgal, J. C.; Laine, R. M. Nucleophilic Attack of R-Lithium at Tetrahedral Silicon in Alkoxysilanes. An Alternate Pathway. *Manuscr. Submitt.*
65. Chan, K. L.; Sonar, P.; Sellinger, A. Cubic Silsesquioxanes for Use in Solution Processable Organic Light Emitting Diodes (OLED). *J. Mater. Chem.* **2009**, *19*, 9103.
66. Baney, R. H.; Itoh, M.; Sakakibara, A.; Suzuki, T. Silsesquioxanes. *Chem. Rev.* **1995**, *95*, 1409–1430.
67. Loy, D.; Shea, K. Bridged Polysilsesquioxanes. Highly Porous Hybrid Organic/ Inorganic Materials. *Chem. Rev.* **1995**, *95*, 1431–1442.
68. Calzaferri, G.; Corriu, R.; Jutzi, P. *Tailor-Made Silicon-Oxygen Compounds, from Molecules to Materials*; 1996; p. 149.
69. Lichtenhan, J. Silsesquioxane-Based Polymers. In *Tailor-made Silicon-Oxygen Compounds*; Salmone, J. C., Ed.; CRC Press: New York, 1996; pp. 7768–7777.
70. Provatas, A.; Matison, J. G. Synthesis and Applications of Silsesquioxanes. *Trends Polym. Sci.* **1997**, *5*, 327–333.
71. Li, G.; Wang, L.; Ni, H.; Pittman Jr, C. U. Polyhedral Oligomeric Silsesquioxane (POSS) Polymers and Copolymers: A Review. *J. Inorg. Organomet. Polym.* **2002**, *11*, 123–154.

72. Phillips, S. H.; Haddad, T. S.; Tomczak, S. J. Developments in Nanoscience: Polyhedral Oligomeric Silsesquioxane (POSS)-Polymers. *Curr. Opin. Solid State Mater. Sci.* **2004**, *8*, 21–29.
73. Kannan, R. Y.; Salacinski, H. J.; Butler, P. E.; Seifalian, A. M. Polyhedral Oligomeric Silsesquioxane Nanocomposites: The next Generation Material for Biomedical Applications. *Acc. Chem. Res.* **2005**, *38*, 879–884.
74. Lickiss, P. D.; Rataboul, F. Fully Condensed Polyhedral Oligosilsesquioxanes (POSS): From Synthesis to Application. *Adv. Organomet. Chem.* **2008**, *57*, 1–116.
75. Wu, J.; Mather, P. T. POSS Polymers: Physical Properties and Biomaterials Applications. *Polym. Rev.* **2009**, *49*, 25–63.
76. Cordes, D. B.; Lickiss, P. D.; Rataboul, F. Recent Developments in the Chemistry of Cubic Polyhedral Oligosilsesquioxanes. *Chem. Rev.* **2010**, *110*, 2081–2173.
77. Paolo P. Pescarmona, T. M. Oligomeric Silsesquioxanes: Synthesis, Characterization and Selected Applications. *Aust. J. Chem.* **2001**, *54*, 583–596.
78. Search Term “Silsesquioxanes” apps.webofknowledge.com.
79. Gromilov, S. a; Branch, S. Octakis- (Trimethylsiloxy) Octasilsesquioxane and Dodecakis- (Trimethylsiloxy) Cyclohexasiloxane. **2004**, *45*, 497–501.
80. Gromilov, S. A.; Emel, D. Y.; Kuzmin, A. V. Structural Organization of Layers In Octakis-(trimethylsiloxy) Octasilsesquioxane. *J. Struct. Chem.* **2003**, *44*, 766–768.
81. Majumdar, P.; Lee, E.; Gubbins, N.; Stafslie, S. J.; Daniels, J.; Thorson, C. J.; Chisholm, B. J. Synthesis and Antimicrobial Activity of Quaternary Ammonium-Functionalized POSS (Q-POSS) and Polysiloxane Coatings Containing Q-POSS. *Polymer (Guildf)*. **2009**, *50*, 1124–1133.
82. Chojnowski, J.; Fortuniak, W.; Rościszewski, P.; Werel, W.; Łukasiak, J.; Kamysz, W.; Hałasa, R. Polysilsesquioxanes and Oligosilsesquioxanes Substituted by Alkylammonium Salts as Antibacterial Biocides. *J. Inorg. Organomet. Polym. Mater.* **2006**, *16*, 219–230.
83. Olekhovich, N. M.; Zhabko, T. E.; Salak, a N.; Pashkovskii, O. I.; Shilin, a D.; Unyarkha, O. V. Synthesis and Dielectric Properties Of... *Inorg. Mater. (English Transl.* **1994**, *30*, 905.
84. Leu, C. M.; Chang, Y. Te; Wei, K. H. Synthesis and Dielectric Properties of Polyimide-Tethered Polyhedral Oligomeric Silsesquioxane (POSS) Nanocomposites via Poss-Diamine. *Macromolecules* **2003**, *36*, 9122–9127.
85. Solans-Monfort, X.; Filhol, J.-S.; Copret, C.; Eisenstein, O. Structure, Spectroscopic and Electronic Properties of a Well Defined Silica Supported Olefin Metathesis Catalyst, [(SiO)Re(CR)(CHR)(CH₂R)], through DFT Periodic Calculations: Silica Is Just a Large Siloxy Ligand. *New J. Chem.* **2006**, *30*, 842.
86. Duchateau, R.; Abbenhuis, H. C. L.; Van Santen, R. a; Thiele, S. K.-H.; Van Tol, M. F. H. Half-Sandwich Titanium Complexes Stabilized by a Novel Silsesquioxane Ligand: Soluble Model Systems for Silica-Grafted Olefin Polymerization Catalysts. *Organometallics* **1998**, *17*, 5222–5224.

87. Maschmeyer, T.; C. Klunduk, M.; M. Martin, C.; S. Shephard, D.; F. G. Johnson, B.; Maschmeyer, T.; Meurig Thomas, J. Modelling the Active Sites of Heterogeneous Titanium-Centred Epoxidation Catalysts with Soluble Silsesquioxane Analogues. *Chem. Commun.* **1997**, 004, 1847.
88. Contreras-Torres, F. F.; Basiuk, V. a. Imidazo[1,2-]pyrazine-3,6-Diones Derived from -Amino Acids: A Theoretical Mechanistic Study of Their Formation via Pyrolysis and Silica-Catalyzed Process. *J. Phys. Chem. A* **2006**, 110, 7431–7440.
89. Feher, F. J.; Budzichowski, T. a.; Blanski, R. L.; Weller, K. J.; Ziller, J. W. Facile Syntheses of New Incompletely Condensed Polyhedral Oligosilsesquioxanes: [(c-C₅H₉)₇Si₇O₉(OH)₃], [(c-C₇H₁₃)₇Si₇O₉(OH)₃], and [(c-C₇H₁₃)₆Si₆O₇(OH)₄]. *Organometallics* **1991**, 10, 2526–2528.
90. Feher, F. J.; Newman, D. A.; Walzer, J. F. Silsesquioxanes as Models for Silica Surfaces. *J. Am. Chem. Soc.* **1989**, 111, 1741–1748.
91. Riollet, V.; Quadrelli, E. A.; Copéret, C.; Basset, J. M.; Andersen, R. a.; Köhler, K.; Böttcher, R. M.; Herdtweck, E. Grafting of [Mn(CH₂tBu)₂(tmeda)] on Silica and Comparison with Its Reaction with a Silsesquioxane. *Chem. - A Eur. J.* **2005**, 11, 7358–7365.
92. Ropartz, L.; Morris, R. E.; Schwarz, G. P.; Foster, D. F.; Cole-Hamilton, D. J. Dendrimer-Bound Tertiary Phosphines for Alkene Hydroformylation. *Inorg. Chem. Commun.* **2000**, 3, 714–717.
93. Feher, F. J.; Budzichowski, T. a. Silasesquioxanes as Ligands in Inorganic and Organometallic Chemistry. *Polyhedron* **1995**, 14, 3239–3253.
94. Lahann, J. Vapor Based Polymer Coatings for Potential Biomedical Applications. *Polym. Int.* **2006**, 1370, 1361–1370.
95. Choi, J.; Kim, S. G.; Laine, R. M. Organic/Inorganic Hybrid Epoxy Nanocomposites from Aminophenylsilsesquioxanes. *Macromolecules* **2004**, 37, 99–109.
96. Sellinger, A.; Laine, R. M. Silsesquioxanes as Synthetic Platforms Photocurable, Liquid Epoxides as Inorganic/organic Hybrid Precursors. *Chem. Mater.* **1996**, 8, 1592–1593.
97. Asuncion, M. Z.; Laine, R. M. Silsesquioxane Barrier Materials. *Macromolecules* **2007**, 40, 555–562.
98. Frye, C. L.; Klosowski, J. M. So-Called “Ladder Structure” of Equilibrated Phenylsilsesquioxane. *J. Am. Chem. Soc.* **1971**, 93, 4599–4601.
99. Brown, J. F. Double Chain Polymers and Nonrandom Crosslinking. *J. Polym. Sci. C* **1963**, 83–97.
100. Laine, R.; Rahn, J. Synthesis and High Temperature Chemistry of Methylsilsesquioxane Polymers Produced by Titanium-Catalyzed Redistribution of Methylhydrido-oligo-and-Polysiloxanes. *Chem. Mater.* **1990**, 2, 464–472.
101. Roll, M. F.; Asuncion, M. Z.; Kampf, J.; Laine, R. M. Para-Octaiodophenylsilsesquioxane, [p-IC₆H₄SiO_{1.5}]₈, a Nearly Perfect Nano-Building Block. *ACS Nano* **2008**, 2, 320.
102. Tamaki, R.; Tanaka, Y.; Asuncion, M. Z.; Choi, J.; Laine, R. M. Octa(aminophenyl)silsesquioxane as a Nanoconstruction Site. *J. Am. Chem. Soc.* **2001**, 123, 12416.

103. Brick, C. M.; Ouchi, Y.; Chujo, Y.; Laine, R. M. Spherical, Polyfunctional Molecules Using Poly(bromophenylsilsesquioxane)s as Nanoconstruction Sites. *Macromolecules* **2005**, *38*, 4661.
104. Miyazato, A.; Pakjamsai, C.; Kawakami, Y. Octa, Deca, and dodeca(4-Nitrophenyl) Cage Silsesquioxanes via 4-Trimethylsilylphenyl Derivatives. *Dalton Trans.* **2010**, *39*, 3239–3244.
105. Pescarmona, P. P.; Raimondi, M. E.; Tetteh, J.; McKay, B.; Maschmeyer, T. Mechanistic Study of Silsesquioxane Synthesis by Mass Spectrometry and in Situ ATR FT-IR Spectroscopy. *J. Phys. Chem. A* **2003**, *107*, 8885–8892.
106. Kudo, T.; Gordon, M. S. Theoretical Studies of the Mechanism for the Synthesis of Silsesquioxanes. 1. Hydrolysis and Initial Condensation. *J. Am. Chem. Soc.* **1998**, *120*, 11432–11438.
107. Kudo, T.; Gordon, M. S. Theoretical Studies of the Mechanism for the Synthesis of Silsesquioxanes. 2. Cyclosiloxanes (D3 and D4). *J. Phys. Chem. A* **2000**, *104*, 4058–4063.
108. Kudo, T.; Gordon, M. S. Exploring the Mechanism for the Synthesis of Silsesquioxanes. 3. The Effect of Substituents and Water. *J. Phys. Chem. A* **2002**, *106*, 11347–11353.
109. Kudo, T.; Machida, K.; Gordon, M. S. Exploring the Mechanism for the Synthesis of Silsesquioxanes. 4. The Synthesis of T8. *J. Phys. Chem. A* **2005**, *109*, 5424–5429.
110. Wright, J. D.; Sommerdijk, N. A. J. M. *Sol-Gel Materials: Chemistry and Applications*; CRC press, 2000; Vol. 4.
111. Li, Z.; Yang, R. Synthesis, Characterization, and Properties of a Polyhedral Oligomeric Octadiphenylsulfonylsilsesquioxane. *J. Appl. Polym. Sci.* **2014**, *131*, 1–8.
112. Roll, M. F.; Kampf, J. W.; Kim, Y.; Yi, E.; Laine, R. M. Nano Building Blocks via Iodination of $[\text{PhSiO}_{1.5}]_n$, Forming High-Surface-Area, Thermally Stable, Microporous Materials via Thermal Elimination of I_2 . *J. Am. Chem. Soc.* **2010**, *132*, 10171–10183.
113. Chimjarn, S.; Kunthom, R.; Chancharone, P.; Sodkhomkhum, R.; Sangtrirutnugul, P.; Ervithayasuporn, V. Synthesis of Aromatic Functionalized Cage-Rearranged Silsesquioxanes (T_8 , T_{10} , and T_{12}) via Nucleophilic Substitution Reactions. *Dalt. Trans.* **2015**, *44*, 916–919.
114. Feher, F. J.; Soulivong, D.; Dklund, A. G.; Wyndham, K. . Cross-Metathesis of Alkenes with Vinyl-Substituted Silsesquioxanes and Spherosilicates: A New Method for Synthesizing Highly-Functional Si/O Frameworks. *Chem. Commun.* **1997**, 1185–1186.
115. Itami, Y.; Marciniak, B.; Kabicki, M. Functionalization of Octavinylsilsesquioxane by Ruthenium-Catalyzed Silylative Coupling versus Cross-Metathesis. *Chem. - A Eur. J.* **2004**, *10*, 1239–1248.
116. Sulaiman, S.; Bhaskar, A.; Zhang, J. Blocks for 3-D Assemblies. Elaboration of Octavinylsilsesquioxane. Unusual Luminescence Shifts May Indicate Extended Conjugation Involving the Silsesquioxane Core. *Chem. ...* **2008**, *20*, 5563–5573.
117. Laine, R. M.; Sulaiman, S.; Brick, C.; Roll, M.; Tamaki, R.; Asuncion, M. Z.; Neurock, M.; Filhol, J.-S.; Lee, C.-Y.; Zhang, J.; et al. Synthesis and

- Photophysical Properties of Stilbeneoctasilsesquioxanes. Emission Behavior Coupled with Theoretical Modeling Studies Suggest a 3-D Excited State Involving the Silica Core. *J. Am. Chem. Soc.* **2010**, *132*, 3708–3722.
118. Lo, M. Y.; Zhen, C.; Lauters, M.; Jabbour, G. E.; Sellinger, A. Organic-Inorganic Hybrids Based on Pyrene Functionalized Octavinylsilsesquioxane Cores for Application in OLEDs. *J. Am. Chem. Soc.* **2007**, *129*, 5808–5809.
 119. Lo, M. Y.; Ueno, K.; Tanabe, H.; Sellinger, A. Silsesquioxane-Based Nanocomposite Dendrimers with Photo-Luminescent and Charge Transport Properties. *Chem. Rec.* **2006**, *6*, 157–168.
 120. Sellinger, A.; Tamaki, R.; Laine, R. M.; Ueno, K.; Tanabe, H.; Williams, E.; Jabbour, G. E. Heck Coupling of Haloaromatics with Octavinylsilsesquioxane: Solution Processable Nanocomposites for Application in Electroluminescent Devices. *Chem. Commun. (Camb)*. **2005**, 3700–3702.
 121. Sulaiman, S.; Zhang, J.; Goodson, I. T.; Laine, R. M. Synthesis, Characterization and Photophysical Properties of Polyfunctional Phenylsilsesquioxanes: [o-RPhSiO_{1.5}]₈, [2,5-R₂PhSiO_{1.5}]₈, and [R₃PhSiO_{1.5}]₈. Compounds with the Highest Number of Functional Units/unit Volume. *J. Mater. Chem.* **2011**, *21*, 11177.
 122. Asuncion, M. Z.; Roll, M. F.; Laine, R. M. Octaalkynylsilsesquioxanes, Nano Sea Urchin Molecular Building Blocks for 3-D-Nanostructures. *Macromolecules* **2008**, *41*, 8047–8052.
 123. Pérez-Ojeda, M. E.; Trastoy, B.; Rol, Á.; Chiara, M. D.; García-Moreno, I.; Chiara, J. L. Controlled Click-Assembly of Well-Defined Hetero-Bifunctional Cubic Silsesquioxanes and Their Application in Targeted Bioimaging. *Chem. - A Eur. J.* **2013**, *19*, 6630–6640.
 124. Kim, Y.; Koh, K.; Roll, M. F.; Laine, R. M.; Matzger, A. J. Porous Networks Assembled from Octaphenylsilsesquioxane Building Blocks. *Macromolecules* **2010**, *43*, 6995–7000.
 125. Schreck, K. M.; Leung, D.; Bowman, C. N. Hybrid Organic/inorganic Thiol-Ene-Based Photopolymerized Networks. *Macromolecules* **2011**, *44*, 7520–7529.
 126. Li, Y.; Guo, K.; Su, H.; Li, X.; Feng, X.; Wang, Z.; Zhang, W.; Zhu, S.; Wesdemiotis, C.; Cheng, S. Z. D.; et al. Tuning “thiol-Ene” Reactions toward Controlled Symmetry Breaking in Polyhedral Oligomeric Silsesquioxanes. *Chem. Sci.* **2014**, *5*, 1046.
 127. Wang, Z.; Wang, D.; Qian, Z.; Guo, J.; Dong, H.; Zhao, N.; Xu, J. Robust Superhydrophobic Bridged Silsesquioxane Aerogels with Tunable Performances and Their Applications. *ACS Appl. Mater. Interfaces* **2015**, ASAP.
 128. Seino, M.; Hayakawa, T.; Ishida, Y.; Kakimoto, M. A.; Watanabe, K.; Oikawa, H. Hydrosilylation Polymerization of Double-Decker-Shaped Silsesquioxane Having Hydrosilane with Dienes. *Macromolecules* **2006**, *39*, 3773–3775.
 129. Purkait, T. K.; Iqbal, M.; Wahl, M. H.; Gottschling, K.; Gonzalez, C. M.; Islam, M. A.; Veinot, J. G. C. Borane-Catalyzed Room-Temperature Hydrosilylation of Alkenes/alkynes on Silicon Nanocrystal Surfaces. *J. Am. Chem. Soc.* **2014**, *136*, 17914–17917.
 130. Ventura, M.; Mosquera, M. E. G.; Cuenca, T.; Royo, B.; Jiménez, G. Cyclopentadienyl-Silsesquioxane Titanium Complexes: Highly Active Catalysts

- for Epoxidation of Alkenes with Aqueous Hydrogen Peroxide. *Inorg. Chem.* **2012**.
131. Rikowski, E.; Marsmann, H. C. Cage-Rearrangement of Silsesquioxanes. *Polyhedron* **1997**, *16*, 3357–3361.
 132. Jaroentomeechai, T.; Yingsukkamol, P.-K.; Phurat, C.; Somsook, E.; Osotchan, T.; Ervithayasuporn, V. Synthesis and Reactivity of Nitrogen Nucleophiles-Induced Cage-Rearrangement Silsesquioxanes. *Inorg. Chem.* **2012**, *51*, 12266–12272.
 133. Chimjarn, S.; Kunthom, R.; Chancharone, P.; Sodkhomkhum, R.; Sangtrirutnugul, P.; Ervithayasuporn, V. Synthesis of Aromatic Functionalized Cage-Rearranged Silsesquioxanes (T₈, T₁₀, and T₁₂) via Nucleophilic Substitution Reactions. *Dalt. Trans.* **2015**, *44*, 916–919.
 134. Bassindale, A. R.; Liu, Z.; MacKinnon, I. a.; Taylor, P. G.; Yang, Y.; Light, M. E.; Horton, P. N.; Hursthouse, M. B. A Higher Yielding Route for T₈ Silsesquioxane Cages and X-Ray Crystal Structures of Some Novel Spherosilicates. *Dalt. Trans.* **2003**, 2945.
 135. Anderson, S. E.; Somogyi, A.; Haddad, T. S.; Coughlin, E. B.; Gadodia, G.; Marten, D. F.; Ray, J.; Bowers, M. T. ESI and MALDI Mass Spectrometry of Large POSS Oligomers. *Int. J. Mass Spectrom.* **2010**, *292*, 38–47.
 136. Anderson, S. E.; Bodzin, D. J.; Haddad, T. S.; Boatz, J. a.; Mabry, J. M.; Mitchell, C.; Bowers, M. T. Structural Investigation of Encapsulated Fluoride in Polyhedral Oligomeric Silsesquioxane Cages Using Ion Mobility Mass Spectrometry and Molecular Mechanics. *Chem. Mater.* **2008**, *20*, 4299–4309.
 137. Kozelj, M.; Orel, B. Synthesis of Polyhedral Phenylsilsesquioxanes with KF as the Source of the Fluoride Ion. *Dalton Trans.* **2008**, 5072–5075.
 138. Kawakami, Y. Structural Control and Functionalization of Oligomeric Silsesquioxanes. *React. Funct. Polym.* **2007**, *67*, 1137–1147.
 139. Ronchi, M.; Sulaiman, S.; Boston, N. R.; Laine, R. M. Fluoride Catalyzed Rearrangements of Polysilsesquioxanes, Mixed Me, Vinyl T₈, Me, Vinyl T₁₀ and T₁₂ Cages. *Appl. Organomet. Chem.* **2009**, *24*, 551–557.
 140. Asuncion, M. Z.; Laine, R. M. Fluoride Rearrangement Reactions of Polyphenyl- and Polyvinylsilsesquioxanes as a Facile Route to Mixed Functional Phenyl, Vinyl T₁₀ and T₁₂ Silsesquioxanes. *J. Am. Chem. Soc.* **2010**, *132*, 3723–3736.
 141. Furgal, J. C.; Jung, J. H.; Clark, S.; Goodson, T.; Laine, R. M. Beads on a Chain (BoC) Phenylsilsesquioxane (SQ) Polymers via F- Catalyzed Rearrangements and ADMET or Reverse Heck Cross-Coupling Reactions: Through Chain, Extended Conjugation in 3-D with Potential for Dendronization. *Macromolecules* **2013**.
 142. Jung, J. H.; Furgal, J. C.; Clark, S. C.; Schwartz, M. C.; Chou, K.; Laine, R. M. “Copolymerization of [*p*-IPhSiO_{1.5}]₈, I₈OPS] with Divinyl (DVB)- and Diethynylbenzene (DEB) gives Beads on a Chain (BoC) Polymers with Functionalized Beads. The DEB Systems Exhibit through Chain, Extended 3-D Conjugation in the Excited State.” *Macromolecules*, **2013**, *46*, 7580-7590.
 143. Pope, E. J. .; Mackenzie, J. D. Sol-Gel Processing of Silica II. The Role of the Catalyst. *J. Non. Cryst. Solids* **1986**, *87*, 185–198.

144. Taylor, P. G.; Bassindale, A. R.; El Aziz, Y.; Pourny, M.; Stevenson, R.; Hursthouse, M. B.; Coles, S. J. Further Studies of Fluoride Ion Entrapment in Octasilsesquioxane Cages; X-Ray Crystal Structure Studies and Factors That Affect Their Formation. *Dalt. Trans.* **2012**, *41*, 2048–2059.
145. El Aziz, Y.; Bassindale, A. R.; Taylor, P. G.; Stephenson, R. a.; Hursthouse, M. B.; Harrington, R. W.; Clegg, W. X-Ray Crystal Structures, Packing Behavior, and Thermal Stability Studies of a Homologous Series of N -Alkyl-Substituted Polyhedral Oligomeric Silsesquioxanes. *Macromolecules* **2013**, *46*, 988–1001.
146. Zhi-hua, L.; Bassindale, A. R.; Taylor, P. G. Syn Thesis of Silsesquioxane Cages from Phenyl-Cis-Tetrol, 1,3-Divinyltetraethoxydisiloxane and Cyclopentyl Resins. *Chem. Res. Chinese. U.* **2010**, *20*, 433–436.
147. Bassindale, A. R.; Pourny, M.; Taylor, P. G.; Hursthouse, M. B.; Light, M. E. Fluoride-Ion Encapsulation within a Silsesquioxane Cage. *Angew. Chem. Int. Ed.* **2003**, *115*, 3611–3614.
148. Bassindale, A. R.; Chen, H.; Liu, Z.; MacKinnon, I. A.; Parker, D. J.; Taylor, P. G.; Yang, Y.; Light, M. E.; Horton, P. N.; Hursthouse, M. B. A Higher Yielding Route to Octasilsesquioxane Cages Using Tetrabutylammonium Fluoride, Part 2: Further Synthetic Advances, Mechanistic Investigations and X-Ray Crystal Structure Studies into the Factors That Determine Cage Geometry in the Solid State. *J. Organomet. Chem.* **2004**, *689*, 3287–3300.
149. Park, S. S.; Xiao, C.; Hagelberg, F.; Hossain, D.; Pittman, C. U.; Saebo, S. Endohedral and Exohedral Complexes of Polyhedral Double Four-Membered-Ring (D4R) Units with Atomic and Ionic Impurities. *J. Phys. Chem. A* **2004**, *108*, 11260–11272.
150. Furgal, J.C.; Jung, J.H.; Clark, S.C.; Goodson III, T.; Laine, R.M. “Beads on a Chain (BoC), Phenylsilsesquioxane (SQ), Conjugated Polymers Via F⁻ Catalyzed Rearrangements and ADMET and Reverse Heck Cross-coupling Reactions; through chain, extended conjugation in 3-D,” *Macromolecules* **2013**, *46*, 7591-7604.
151. Lin, T. T.; He, C. B.; Xiao, Y. Theoretical Studies of Monosubstituted and Higher Phenyl- Substituted Octahydrosilsesquioxanes. *J. Phys. Chem. B* **2003**, *107*, 13788–13792, and references therein.
152. Ossadnik, C.; Ā, S. V.; Marsmann, H. C.; Rikowski, E. Photolumineszenzeigenschaften von Substituierten Silsesquioxanen Der Zusammensetzung R_n/SiO_{1.5})_n. *Monatsh. für Chemie* **1999**, *130*, 55–68.
153. Azinovic, D.; Cai, J.; Eggs, C.; Konig, H.; Marsmann, H. C.; Veprek, S. Photoluminescence from Silsesquioxanes R₈(SiO_{1.5})₈. *J. Lumin.* **2002**, *97*, 40.
154. Xiang, K.-H.; Pandey, R.; Pernisz, U. C.; Freeman, C. Theoretical Study of Structural and Electronic Properties of H-Silsesquioxanes. *J. Phys. Chem. B* **1998**, *102*, 8704–8711.
155. Hossain, D.; Pittman, C. U.; Saebo, S.; Hagelberg, F. Structures , Stabilities , and Electronic Properties of Endo- and Exohedral Complexes of T₁₀ - Polyhedral Oligomeric Silsesquioxane Cages. **2007**, 6199–6206.
156. Lichtenhan, J. D.; Vu, N. Q.; Carter, J. a.; Gilman, J. W.; Feher, F. J.; Afb, E. Silsesquioxane-Siloxane Copolymers from Polyhedral Silsesquioxanes. *Macromolecules* **1993**, *26*, 2141–2142.

157. Schwab, J. J.; Lichtenhan, J. D. Polyhedral Oligomeric Silsesquioxane (POSS) -Based Polymers. *Appl. Organomet. Chem.* **1998**, *713*, 707–713.
158. Costa, R. O. R.; Vasconcelos, W. L.; Tamaki, R.; Laine, R. M. Thermoplastic Organic-Inorganic Hybrids: Star Poly (Methylmethacrylate) Via Atom Transfer Radical Polymerization Using Cubic Silsesquioxane. 692–695.
159. Lin, W.-J.; Chen, W.-C.; Wu, W.-C.; Niu, Y.-H.; Jen, A. K.-Y. Synthesis and Optoelectronic Properties of Starlike Polyfluorenes with a Silsesquioxane Core. *Macromolecules* **2004**, *37*, 2335–2341.
160. Ledin, P. a; Tkachenko, I. M.; Xu, W.; Choi, I.; Shevchenko, V. V; Tsukruk, V. V. Star-Shaped Molecules with Polyhedral Oligomeric Silsesquioxane Core and Azobenzene Dye Arms. *Langmuir* **2014**, *30*, 8856–8865.
161. Shen, J.; Zheng, S. Comparative Studies on Miscibility and Phase Behavior of Linear and Star poly(2-Methyl-2-Oxazoline) Blends with Poly(vinylidene Fluoride). *J. Polym. Sci. Part B Polym. Phys.* **2006**, *44*, 942–952.
162. Yang, Y. Y.; Wang, X.; Hu, Y.; Hu, H.; Wu, D. C.; Xu, F. J. Bioreducible POSS-Cored Star-Shaped Polycation for Efficient Gene Delivery. *ACS Appl. Mater. Interfaces* **2014**, *6*, 1044–1052.
163. Chinnam, P. R.; Wunder, S. L. Polyoctahedral Silsesquioxane-Nanoparticle Electrolytes for Lithium Batteries: POSS-Lithium Salts and POSS-PEGs. *Chem. Mater.* **2011**, *23*, 5111–5121.
164. Samthong, C.; Laine, R. M.; Somwangthanaroj, A. Synthesis and Characterization of Organic/inorganic Epoxy Nanocomposites from Poly(aminopropyl/phenyl)silsesquioxanes. *J. Appl. Polym. Sci.* **2012**, 1–8.
165. Jung, J. H.; Laine, R. M. Beads on a Chain (BOC) Polymers Formed from the Reaction of $\text{NH}_2\text{PhSiO}_{1.5} \text{X}$ [$\text{PhSiO}_{1.5} \text{X}$] 10--X and [$\text{NH}_2\text{PhSiO}_{1.5} \text{X}$] 12--X Mixtures ($\text{X} = 2\text{--}4$) with the Diglycidyl Ether of Bisphenol A. *Macromolecules* **2011**, *44*, 7263–7272.
166. Hoque, M. A.; Kakihana, Y.; Shinke, S.; Kawakami, Y. Polysiloxanes with Periodically Distributed Isomeric Double-Decker Silsesquioxane in the Main Chain. *Macromolecules* **2009**, *42*, 3309–3315.
167. Li, Z.; Kawakami, Y. Formation of Incompletely Condensed Oligosilsesquioxanes by Hydrolysis of Completely Condensed POSS via Reshuffling. *Chem. Lett.* **2008**, *37*, 804–805.
168. Wu, S.; Hayakawa, T.; Kakimoto, M. a.; Oikawa, H. Synthesis and Characterization of Organosoluble Aromatic Polyimides Containing POSS in Main Chain Derived from Double-Decker-Shaped Silsesquioxane. *Macromolecules* **2008**, *41*, 3481–3487.
169. Goseki, R.; Hirao, A.; Kakimoto, M.; Hayakawa, T. Cylindrical Nanostructure of Rigid-Rod POSS-Containing Polymethacrylate from a Star-Branched Block Copolymer. *ACS Macro Lett.* **2013**, *2*, 625–629.
170. Jung, J. H.; Furgal, J. C.; Clark, S. C.; Schwartz, M. C.; Chou, K.; Laine, R. M. “Copolymerization of [$p\text{-IPhSiO}_{1.5}$] $_8$, I $_8$ OPS] with Divinyl (DVB)- and Diethynylbenzene (DEB) gives Beads on a Chain (BoC) Polymers with Functionalized Beads. The DEB Systems Exhibit through Chain, Extended 3-D Conjugation in the Excited State.” *Macromolecules*, **2013**, *46*, 7580-7590.

171. King, R. B. Three-Dimensional Aromaticity in Polyhedral Boranes and Related Molecules. *Chem. Rev.* **2001**, *101*, 1119–1152.
172. Lee, J.; Cho, H. J.; Cho, N. S.; Hwang, D. H.; Shim, H. K. Synthesis of Polyhedral Oligomeric Silsesquioxane-Functionalized Polyfluorenes: Hybrid Organic-Inorganic-Conjugated Polymers. *Synth. Met.* **2006**, *156*, 590–596.
173. Xiao, S.; Nguyen, M.; Gong, X.; Cao, Y.; Wu, H.; Moses, D.; Heeger, a. J. Stabilization of Semiconducting Polymers with Silsesquioxane. *Adv. Funct. Mater.* **2003**, *13*, 25–29.
174. Wu, Q.; Bhattacharya, M.; Morgan, S. E. POSS-Enhanced Phase Separation in Air-Processed P3HT:PCBM Bulk Heterojunction Photovoltaic Systems. *ACS Appl. Mater. Interfaces* **2013**, *5*, 6136–6146.
175. Jung, J. H. Synthesis and Characterization of Conjugated Silsesquioxanes (SQs) and Their Beads on a Chain (BoC) Polymers, University of Michigan, 2013.
176. Hartmann-Thompson, C. Polyhedral Oligomeric Silsesquioxanes in Electronics and Energy Applications. In *Applications of Polyhedral Oligomeric Silsesquioxanes SE - 7*; Hartmann-Thompson, C., Ed.; Advances in Silicon Science; Springer Netherlands, 2011; Vol. 3, pp. 247–325 LA – English.
177. Lim, Y.; Park, Y. S.; Kang, Y.; Jang, D. Y.; Kim, J. H.; Kim, J. J.; Sellinger, A.; Yoon, D. Y. Hole Injection/transport Materials Derived from Heck and Sol-Gel Chemistry for Application in Solution-Processed Organic Electronic Devices. *J. Am. Chem. Soc.* **2011**, *133*, 1375–1382.
178. Li, G.; Wang, L.; Ni, H.; Jr, C. U. P. Polyhedral Oligomeric Silsesquioxane (POSS) Polymers and Copolymers : A Review. *J. Inorg. Organomet. Polym.* **2002**, *11*.
179. Zhen, C.-G.; Becker, U.; Kieffer, J. Tuning Electronic Properties of Functionalized Polyhedral Oligomeric Silsesquioxanes: A DFT and TDDFT Study. *J. Phys. Chem. A* **2009**, *113*, 9707–9714.
180. Vautravers, N. R.; André, P.; Cole-Hamilton, D. J. Fluorescence Activation of a Polyhedral Oligomeric Silsesquioxane in the Presence of Reducing Agents. *J. Mater. Chem.* **2009**, *19*, 4545.
181. André, P.; Cheng, G.; Ruseckas, A.; Van Mourik, T.; Früchtel, H.; Crayston, J. A.; Morris, R. E.; Cole-Hamilton, D.; Samuel, I. D. W. Hybrid Dendritic Molecules with Confined Chromophore Architecture to Tune Fluorescence Efficiency. *J. Phys. Chem. B* **2008**, *112*, 16382–16392.
182. Feher, F. J.; Budzichowski, T. A. Syntheses of Highly-Functionalized Polyhedral Oligosilsesquioxanes. *J. Organomet. Chem.* **1989**, *379*, 33.
183. Ronchi, M.; Pizzotti, M.; Orbelli Biroli, a.; Macchi, P.; Lucenti, E.; Zucchi, C. Synthesis and Structural Characterization of Functionalized Cyclotetrasiloxane Rings [4-RC₆H₄Si(O)OR]₄ (R = Cl, Br, CH=CH₂, CH₂Cl; R = Na, SiMe₃) as Scaffolds for the Synthesis of Models of a Silica Bound Monolayer of Fluorescent O. *J. Organomet. Chem.* **2007**, *692*, 1788–1798.
184. Peterson, J. J.; Werre, M.; Simon, Y. C.; Coughlin, E. B.; Carter, K. R. Carborane-Containing Polyfluorene: O- Carborane in the Main Chain. *Macromolecules* **2009**, *42*, 8594–8598.

185. Peterson, J. J.; Davis, A. R.; Werre, M.; Coughlin, E. B.; Carter, K. R. Carborane-Containing Poly(fluorene): Response to Solvent Vapors and Amines. *ACS Appl. Mater. Interfaces* **2011**, *3*, 1796–1799.
186. Peterson, J. J.; Simon, Y. C.; Coughlin, E. B.; Carter, K. R. Polyfluorene with P-Carborane in the Backbone. *Chem. Commun. (Camb)*. **2009**, 4950–4952.
187. Calzaferri, G.; Hoffman, R. The Symmetrical Octasilsesquioxanes X₈Si₈O₁₂: Electronic Structure and Reactivity. *J. Chem. Soc., Dalt. Trans.* **1991**, 917.
188. Phillips, H.; Zheng, S.; Hyla, A.; Laine, R.; Goodson, T.; Geva, E.; Dunietz, B. D. Ab Initio Calculation of the Electronic Absorption of Functionalized Octahedral Silsesquioxanes via Time-Dependent Density Functional Theory with Range-Separated Hybrid Functionals. *J. Phys. Chem. A* **2012**, *116*, 1137–1145.
189. Zheng, S.; Phillips, H.; Geva, E.; Dunietz, B. D. Ab Initio Study of the Emissive Charge-Transfer States of Solvated Chromophore-Functionalized Silsesquioxanes. *J. Am. Chem. Soc.* **2012**, *134*, 6944–6947.
190. Ceyhan, T.; Yükses, M.; Yağlıoğlu, H. G.; Salih, B.; Erbil, M. K.; Elmali, A.; Bekaroğlu, O. Synthesis, Characterization and Nonlinear Absorption of Novel Octakis-POSS Substituted Metallophthalocyanines and Strong Optical Limiting Property of CuPc. *Dalton Trans.* **2008**, 2407–2413.
191. Su, X.; Guang, S.; Li, C.; Xu, H.; Liu, X.; Wang, X.; Song, Y. Molecular Hybrid Optical Limiting Materials from Polyhedral Oligomer Silsesquioxane: Preparation and Relationship between Molecular Structure and Properties. *Macromolecules* **2010**, *43*, 2840–2845.
192. Costela, A.; Garcia-Moreno, I.; Cerdan, L.; Martin, V.; Garcia, O.; Sastre, R. Dye-Doped POSS Solutions: Random Nanomaterials for Laser Emission. *Adv. Mater.* **2009**, *21*, 4163–4166.
193. Goodson, T. G. Optical Excitations in Organic Dendrimers Investigated by Time-Resolved and Nonlinear Optical Spectroscopy. *Acc. Chem. Res.* **2005**, *38*, 99–107.
194. Wang, Y.; Xie, X.; Goodson, T. Enhanced Third-Order Nonlinear Optical Properties in Dendrimer-Metal Nanocomposites. *Nano Lett.* **2005**, *5*, 2379–2384.
195. Varnavski, O.; Yan, X.; Mongin, O.; Blanchard-Desce, M.; Goodson, T. Strongly Interacting Organic Conjugated Dendrimers with Enhanced Two-Photon Absorption. *J. Phys. Chem. C* **2006**, *111*, 149–162.
196. West, R.; Wang, Y.; Goodson III, T. G. Nonlinear Absorption Properties in Novel Gold Nanostructured Topologies. *Society* **2003**, 3419–3426.
197. Lahankar, S. A.; West, R.; Varnavski, O.; Xie, X.; Goodson, T.; Sukhomlinova, L.; Twieg, R. Electronic Interactions in a Branched Chromophore Investigated by Nonlinear Optical and Time-Resolved Spectroscopy. *J. Chem. Phys.* **2004**, *120*, 337–344.
198. Goppert-Mayer, M. Elementary Processes with Two Quantum Jumps. *Ann. Phys.* **1931**, *401*, 273–231.
199. Kaiser, W.; Garrett, C. G. . Two-Photon Excitation in CaF₂:Eu²⁺. *Phys. Rev. Lett.* **1961**, *7*, 229–231.

200. Marder, S. R. Organic Nonlinear Optical Materials: Where We Have Been and Where We Are Going. *Chem. Commun. (Camb)*. **2006**, 131–134.
201. Birge, R. R.; Pierce, B. M. Semiclassical Time-Dependent Theory of Lbo-Photon Spectroscopy . The Effect of Dephasing in the Virtual Level on the Two-Photon Excitation Spectrum of Isotach Y Sterol. *Int. J.* **1986**, *XXIX*, 639–656.
202. He, G. S.; Tan, L. S.; Zheng, Q.; Prasad, P. N. Multiphoton Absorbing Materials: Molecular Designs, Characterizations, and Applications. *Chem. Rev.* **2008**, *108*, 1245–1330.
203. Pawlicki, M.; Collins, H. a.; Denning, R. G.; Anderson, H. L. Two-Photon Absorption and the Design of Two-Photon Dyes. *Angew. Chemie - Int. Ed.* **2009**, *48*, 3244–3266.
204. Andrews, D. L.; Ghoul, W. A. Polarization Studies in Multiphoton Absorption Spectroscopy. *J. Chem. Phys.* **1981**, *75*, 530.
205. Xu, C.; Webb, W. W. Measurement of Two-Photon Excitation Cross Sections of Molecular Fluorophores with Data from 690 to 1050 Nm. *J. Opt. Soc. Am. B* **1996**, *13*, 481.
206. Reinhardt, B. a; Brott, L. L.; Clarson, S. J.; Dillard, A. G.; Bhatt, J. C.; Kannan, R.; Yuan, L.; He, G. S.; Prasad, P. N. Highly Active Two-Photon Dyes: Design, Synthesis, and Characterization toward Application. *Chem. Mater.* **1998**, *10*, 1863–1874.
207. Shao, P.; Huang, B.; Chen, L.; Liu, Z.; Qin, J.; Gong, H.; Ding, S.; Wang, Q. Synthesis and Two-Photon Absorption Properties of Novel Heterocycle-Based Organic Molecules. *J. Mater. Chem.* **2005**, *15*, 4502.
208. Lee, H. J.; Sohn, J.; Hwang, J.; Park, S. Y.; Choi, H.; Cha, M. Triphenylamine-Cored Bifunctional Organic Molecules for Two-Photon Absorption and Photorefractive. *Chem. Mater.* **2004**, *16*, 456–465.
209. Kim, O.; Lee, K.; Woo, H. Y.; Kim, K.; He, G. S.; Swiatkiewicz, J.; Prasad, P. N. New Class of Two-Photon-Absorbing Chromophores Based on Dithienothiophene Two-Photon Absorption (TPA) Offers the Advantage of High Transmission at Low Incident Intensity for Fundamental Optical Frequencies Well below the Band Gap Webb Introduced the T. *Communications* **2000**, 284–286.
210. Belfield, K.; Hagan, D. New Two-Photon Absorbing Fluorene Derivatives: Synthesis and Nonlinear Optical Characterization. *Org. ...* **1999**, 8–11.
211. Aujard, I.; Benbrahim, C.; Gouget, M.; Ruel, O.; Baudin, J. B.; Neveu, P.; Jullien, L. O-Nitrobenzyl Photolabile Protecting Groups with Red-Shifted Absorption: Syntheses and Uncaging Cross-Sections for One- And Two-Photon Excitation. *Chem. - A Eur. J.* **2006**, *12*, 6865–6879.
212. Santos-Pérez, J.; Crespo-Hernández, C. E.; Reichardt, C.; Cabrera, C. R.; Feliciano-Ramos, I.; Arroyo-Ramírez, L.; Meador, M. a. Synthesis, Optical Characterization, and Electrochemical Properties of Isomeric Tetraphenylbenzodifurans Containing Electron Acceptor Groups. *J. Phys. Chem. A* **2011**, *115*, 4157–4168.
213. Zeng, Z.; Guan, Z.; Xu, Q. H.; Wu, J. Octupolar Polycyclic Aromatic Hydrocarbons as New Two-Photon Absorption Chromophores: Synthesis and Application for Optical Power Limiting. *Chem. - A Eur. J.* **2011**, *17*, 3837–3841.

214. Albota, M.; Beljonne, D.; Bredas, J. L.; Ehrlich, J. E.; Fu, J. Y.; Heikal, a a; Hess, S. E.; Kogej, T.; Levin, M. D.; Marder, S. R.; et al. Design of Organic Molecules with Large Two-Photon Absorption Cross Sections. *Science* (80-). **1998**, *281*, 1653–1656.
215. Le Droumaguet, C.; Mongin, O.; Werts, M. H. V; Blanchard-Desce, M. Towards “Smart” Multiphoton Fluorophores: Strongly Solvatochromic Probes for Two-Photon Sensing of Micropolarity. *Chem. Commun. (Camb)*. **2005**, *2*, 2802–2804.
216. Kay, L. E.; Bax, a; Ikura, M.; Clore, G. M.; Gronenborn, a M.; Levitt, M. H.; Lett, C. P.; Dabbagh, G.; Weliky, D. P.; Tycko, R.; et al. Nonlinearities in Polarized Carotenoids. *Science*. **1997**, *276*, 1233–1236.
217. Ricks, A. B.; Solomon, G. C.; Colvin, M. T.; Scott, A. M.; Chen, K.; Ratner, M. A.; Wasielewski, M. R. Controlling Electron Transfer in Donor-Bridge-Acceptor Molecules Using Cross-Conjugated Bridges. *J. Am. Chem. Soc.* **2010**, *132*, 15427–15434.
218. Lee, S.; Thomas, K. R. J.; Thayumanavan, S.; Bardeen, C. J. Dependence of the Two-Photon Absorption Cross Section on the Conjugation of the Phenylacetylene Linker in Dipolar Donor-Bridge-Acceptor Chromophores. *J. Phys. Chem. A* **2005**, *109*, 9767–9774.
219. Clark, T. B.; Ziólkowski, M.; Schatz, G. C.; Goodson, T. Two-Photon and Time-Resolved Fluorescence Spectroscopy as Probes for Structural Determination in Amyloid-B Peptides and Aggregates. *J. Phys. Chem. B* **2014**, *118*, 2351–2359.
220. Bhaskar, A.; Ramakrishna, G.; Twieg, R. J.; Goodson, T. Zinc Sensing via Enhancement of Two-Photon Excited Fluorescence. *J. Phys. Chem. C* **2007**, *111*, 14607–14611.
221. Liu, Z. Q.; Shi, M.; Li, F. Y.; Fang, Q.; Chen, Z. H.; Yi, T.; Huang, C. H. Highly Selective Two-Photon Chemosensors for Fluoride Derived from Organic Boranes. *Org. Lett.* **2005**, *7*, 5481–5484.
222. Bozio, R.; Cecchetto, E.; Fabbrini, G.; Ferrante, C.; Maggini, M.; Menna, E.; Pedron, D.; Ricco, R.; Signorini, R.; Zerbetto, M.; et al. One- and Two-Photon Absorption and Emission Properties of a Zn (II) Chemosensor. *J. Phys. Chem. A* **2006**, *110*, 6459–6464.
223. Goodwin, A. P.; Mynar, J. L.; Ma, Y.; Fleming, G. R.; Fréchet, J. M. J. Synthetic Micelle Sensitive to IR Light via a Two-Photon Process. *J. Am. Chem. Soc.* **2005**, *127*, 9952–9953.
224. Weckler, S.; Mikhailovsky, A.; Ford, P. C. Photochemical Production of Nitric Oxide via Two-Photon Excitation with NIR Light Photochemical Production of Nitric Oxide via Two-Photon Excitation with NIR. *Nitric Oxide* **2004**, *7–9*.
225. Raymond, J. E.; Goodson, T. Single-Particle Two-Photon Absorption Imaging and Enhancement Determination for Organic Nanoparticles. *J. Phys. Chem. Lett.* **2011**, *2*, 329–333.
226. Zipfel, W. R.; Williams, R. M.; Webb, W. W. Nonlinear Magic: Multiphoton Microscopy in the Biosciences. *Nat. Biotechnol.* **2003**, *21*, 1369–1377.
227. Helmchen, F.; Denk, W. Deep Tissue Two-Photon Microscopy. *Nat. Methods* **2005**, *2*, 932–940.

228. Lin, T. C.; Chung, S. J.; S.Kim, K.; P.Wang, X.; He, G. S.; Swiatkiewicz, J.; Pudavar, H. E.; Prasad, P. N. Organics and Polymers with High Two-Photon Activities and Their Applications. *Polym. Photonics Appl. II* **2003**, *161*, 157–193.
229. LaFratta, C. N.; Fourkas, J. T.; Baldacchini, T.; Farrer, R. a. Multiphoton Fabrication. *Angew. Chemie - Int. Ed.* **2007**, *46*, 6238–6258.
230. Kawata, S.; Kawata, Y. Three-Dimensional Optical Data Storage Using Photochromic Materials. *Chem. Rev.* **2000**, *100*, 1777–1788.
231. Parthenopoulos, D. A.; Rentzepis, P. M. Three-Dimensional Optical Storage Memory. *Science.* **1989**, *245*, 843–845.
232. Walker, E.; Rentzepis, P. M. Two-Photon Technology: A New Dimension. *Nat. Photonics* **2008**, *2*, 406–408.
233. Spangler, C. W. Recent Development in the Design of Organic Materials for Optical Power Limiting. *J. Mater. Chem.* **1999**, *9*, 2013–2020.
234. Ehrlich, J. E.; Wu, X. L.; Lee, I. Y.; Hu, Z. Y.; Röckel, H.; Marder, S. R.; Perry, J. W. Two-Photon Absorption and Broadband Optical Limiting with Bis-Donor Stilbenes. *Opt. Lett.* **1997**, *22*, 1843–1845.
235. Lahankar, S. A.; West, R.; Varnavski, O.; Xie, X.; Goodson, T.; Sukhomlinova, L.; Twieg, R. Electronic Interactions in a Branched Chromophore Investigated by Nonlinear Optical and Time-Resolved Spectroscopy. *J. Chem. Phys.* **2004**, *120*, 337–344.
236. Yan, X.; Goodson, T.; Imaoka, T.; Yamamoto, K. Up-Converted Emission in a Series of Phenylazomethine Dendrimers with a Porphyrin Core. *J. Phys. Chem. B* **2005**, *109*, 9321–9329.
237. Varnavski, O. P.; Ostrowski, J. C.; Sukhomlinova, L.; Twieg, R. J.; Bazan, G. C.; Goodson, T. Coherent Effects in Energy Transport in Model Dendritic Structures Investigated by Ultrafast Fluorescence Anisotropy Spectroscopy. *J. Am. Chem. Soc.* **2002**, *124*, 1736–1743.
238. Lakowicz, J. *Principles of Fluorescence Spectroscopy*; Third.; Springer Science+Business Media: New York, 2006; pp. 47, 243, 358–359, 588.
239. Volkmer, a; Subramaniam, V.; Birch, D. J.; Jovin, T. M. One- and Two-Photon Excited Fluorescence Lifetimes and Anisotropy Decays of Green Fluorescent Proteins. *Biophys. J.* **2000**, *78*, 1589–1598.
240. Scholes, G. D. Long-Range Resonance Energy Transfer in Molecular Systems. *Annu. Rev. Phys. Chem.* **2003**, *54*, 57–87.
241. Guo, M.; Varnavski, O.; Narayanan, A.; Mongin, O.; Majoral, J. P.; Blanchard-Desce, M.; Goodson, T. Investigations of Energy Migration in an Organic Dendrimer Macromolecule for Sensory Signal Amplification. *J. Phys. Chem. A* **2009**, *113*, 4763–4771.
242. Flynn, D. C.; Ramakrishna, G.; Yang, H. B.; Northrop, B. H.; Stang, P. J.; Goodson, T. Ultrafast Optical Excitations in Supramolecular Metallacycles with Charge Transfer Properties. *J. Am. Chem. Soc.* **2010**, *132*, 1348–1358.
243. Adegoke, O. O.; Ince, M.; Mishra, A.; Green, A.; Varnavski, O.; Martínez-Díaz, M. V.; Bäuerle, P.; Torres, T.; Goodson, T. Synthesis and Ultrafast Time Resolved Spectroscopy of Peripherally Functionalized Zinc Phthalocyanine

- Bearing Oligothiénylene-Ethynylene Subunits. *J. Phys. Chem. C* **2013**, *117*, 20912–20918.
244. Varnavski, O.; Goodson, T. Femtosecond Fluorescence Dynamics and Molecular Interactions in a Water-Soluble Nonlinear Optical Polymeric Dye. *Chemical Physics Letters*, **2000**, *320*, 688–696.
245. Zhang, J. Probing Structure Function Relationships in Novel Silicon Containing Macromolecules With Nonlinear Optical and Ultra-Fast Spectroscopy, 2014.

Chapter 2

Experimental Methods

2.1 Analytical Methods

2.1.1 Standard Characterization

The following procedures were used as a standard set of characterization methods for silsesquioxane materials synthesized in this dissertation. These techniques were used to distinguish extent of reaction, structure, purity, and thermal and electronic properties. Gel permeation chromatography (GPC) gives information about the molecular weights and distributions of polymers; matrix assisted laser desorption time of flight mass spectrometry (MALDI-ToF), electron impact mass spectrometry (EI) and electrospray ionization mass spectrometry (ESI) give information about the purity, extent of functionalization and exact molecular weights of materials; nuclear magnetic resonance spectroscopy (NMR) gives information on the magnetic environments for molecular structure and atomic bonding for atoms including Si, H, C, and F; fourier transform infrared spectroscopy (FTIR) gives information on the bending, stretching and vibrational modes of molecular bonds as well as functional group analysis; differential scanning calorimetry (DSC) and thermal gravimetric analysis (TGA) are thermal analysis techniques which give information on the melting points, phase transitions and thermal stabilities of materials; cyclic voltammetry (CV) is a technique used to analyzed the redox potential and stabilities of materials.

Gel permeation chromatography (GPC). All GPC analyses were done on a Waters 440 system equipped with Waters Styragel columns (7.8 x 300, HT 0.5, 2, 3, 4) with RI detection using a Waters 2410 refractometer and THF as solvent. The system was calibrated using polystyrene standards and toluene as reference. Analyses were performed using PL Caliber 7.04 software (Polymer Labs, Shropshire UK).

Matrix-assisted laser desorption/time-of-flight mass spectrometry. MALDI-ToF was done on a Micromass ToFSpec-2E equipped with a 337 nm nitrogen laser in positive-ion reflectron mode using poly(ethylene glycol) as calibration standard, dithranol as matrix, and AgNO₃ as ion source. Sample was prepared by mixing solution of 5 parts matrix (10 mg/ml in THF), 5 parts sample (1 mg/ml in THF), and 1 part of AgNO₃ (2.5 mg/ml in methanol) and blotting the mixture on the target plate.

Electron Impact Mass Spectrometry (EI). Analyses were conducted using a VG 70-250-S magnetic sector instrument (Waters) by electron impact ionization (EI). The instrument was calibrated with perfluorokerosene-H. The samples were run in EI mode at 70 eV electron energy with an ion source temperature of 240 °C. The mass range was scanned from *m/z* 1000 to 35. Hi-Res mass spec analysis was conducted on the same instrument.

Electrospray Ionization Mass Spectrometry (ESI). Analyses were performed on an Agilent Q-TOF system with a dual ESI ion source. The mobile phase consisted of a 9:1 mixture of acetonitrile:water with 0.1% formic acid. Lockmass correction was used to obtain mass accuracy.

Nuclear Magnetic Resonance (NMR). All ¹H and ¹³C NMR were run in acetone-*d*₆ or CDCl₃ on a Varian MR400 spectrometer. ¹H-NMR spectra were collected at 500 MHz using a 7998.4 Hz spectral width, a relaxation delay of 0.5 s, a pulse width of 45°, 65k data points, and TMS (0.00ppm) as an internal reference. ¹³C-NMR spectra were collected at 100 MHz using a 25000 Hz spectral width, a relaxation delay of 1.5 s, 75k data points, a pulse width of 40°, and TMS (0.00 ppm) as the internal reference. ²⁹Si-NMR spectra were obtained on a Varian vnmrs 500 MHz and were collected at 99.35 MHz using a 4960 Hz spectral width, a relaxation delay of 20 s, 4k data points, a pulse width of 7°, and TMS (0.00 ppm) as an external reference. ¹⁹F NMR were run in methylene chloride-*d*₂ on a Varian vnmrs 500 MHz and were collected at 470.55 MHz using a 108.7 kHz spectral width, a relaxation delay of 1 s, and a pulse width of 30°.

Fourier-transform infrared spectroscopy (FTIR). Diffuse reflectance Fourier transform (DRIFT) spectra were recorded on a Nicolet 6700 Series FTIR spectrometer (Thermo Fisher Scientific, Inc., Madison, WI). Optical grade, random cuttings of KBr

(International Crystal Laboratories, Garfield, NJ) were ground, with 1.0 wt % of the sample to be analyzed. For DRIFT analyses, samples were packed firmly and leveled off at the upper edge to provide a smooth surface. The FTIR sample chamber was flushed continuously with N₂ prior to data acquisition in the range 4000-400 cm⁻¹ with a precision of ±4 cm⁻¹.

Differential scanning calorimetry (DSC). Calorimetry was performed on materials using a DSC 2910 (TA Instruments, Inc., New Castle, DE). The N₂ flow rate was 60 mL/min. Samples (10-15 mg) were placed in a pan and ramped to 400 °C (5 °C/min/N₂) without capping.

Thermal gravimetric analyses (TGA). Thermal stabilities of materials under N₂ or air were examined using a 2960 simultaneous DTA-TGA (TA Instruments, Inc., New Castle, DE). Samples (5-10 mg) were loaded in alumina pans and ramped to 1000 °C while heating at 10 °C/min. The N₂ or air-flow at 60 mL/min.

Cyclic Voltammetry (CV) was used in combination with optical absorption onset to calculate HOMO and LUMO energy levels for chromophore functionalized silsesquioxanes. Cyclic voltammograms were obtained from a CHI 600C electrochemical analyzer using a three-electrode setup. A glassy carbon working electrode was used in conjunction with a platinum wire counter electrode and a silver/silver nitrate reference electrode. All scans were taken in 0.1 M tetrabutyl ammonium hexafluorophosphate in acetonitrile at a rate of 0.1 V/s. Samples were dropcast onto the working electrode from THF for each scan polarity because reversible redox behavior was not observed. The ferrocene/ferrocenium redox pair was used as an external reference with a HOMO of -4.71 eV. Finally, the LUMO/HOMO levels were inferred from the onset of reduction/oxidation (the intercept of the two slopes slope and baseline (Figure 2.1)) for each sample (i.e. for HOMO of pentafluorophenylstilbenevinylSQ = $-[1.45 \text{ eV (intercept)} + 4.71 \text{ eV (Ag)}] = -6.2 \text{ eV}$).

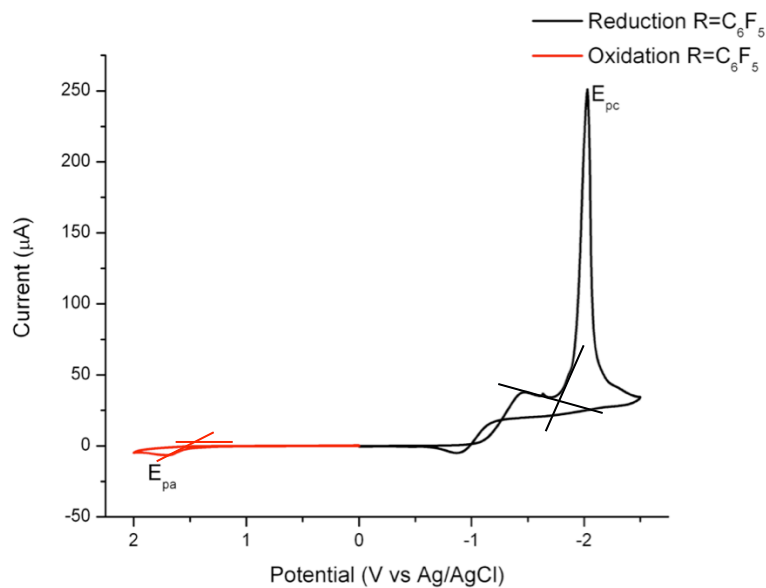


Figure 2.1. Redox example curve of pentafluorophenylstilbenevinylSQ; reduction used for calculation of LUMO, oxidation used for calculation of HOMO.

2.1.2 Photophysical Characterization

The following techniques were used to analyze the photophysical properties of chromophore-functionalized silsesquioxanes shown in this dissertation, which is important for determining the charge/energy transfer/harvesting characteristics in these materials for optoelectronic applications such as OLEDs and photovoltaics. Ultraviolet-visible spectrometry (UV-Vis) gives information about the photon absorption wavelengths and absorptivity (amount of absorption) of our materials; photoluminescence spectroscopy gives information about the fluorescence wavelength and fluorescence efficiency of materials upon excitation with a photon of specified wavelength; two photon absorption spectroscopy is an advanced laser spectroscopy technique which gives information about the intramolecular interactions present in materials, including charge separation, transition dipoles and chromophore interactions; fluorescence upconversion spectroscopy is another advanced laser spectroscopy technique which gives information about the excited state dynamics in materials, including fluorescence lifetime, charge transfer, and molecular orientational (i.e. polarization) effects on fluorescence.

UV-Vis spectrometry. UV-Vis measurements were recorded on an Agilent (model 8341) spectrophotometer in spectrophotometric grade dried THF as solvent. Concentrations were on the order of (10^{-6} - 10^{-7} M), to give absorption maximum for absorption studies to about 50% for a 0.5 cm path length. Molar extinction coefficients (ϵ $M^{-1}cm^{-1}$) were determined by plotting a standard curve with concentrations ranging from 10^{-6} to 10^{-7} M.

Photoluminescence spectrometry. Photoluminescence measurements were obtained on a Horiba Fluoromax-2 fluorimeter in THF. The R-stilbenevinylSQs were studied at their respective maximum absorption wavelengths, R= (H, 332 nm), (Me, 336 nm), (OMe 341 nm), (NH₂, 363 nm), and (C₆F₅, 316 nm). Samples from UV-vis measurements were diluted to $\sim 10^{-7}$ M, in order to reduce the likelihood of excimer formation and fluorimeter detector saturation. Photoluminescence quantum yields (Φ_{PL}). Φ_{PL} was determined by a comparison method between a standard and the sample.¹ Each sample was compared for Φ_{PL} with Bis-MSB 1,4-bis(2-methylstyryl)benzene at different wavelengths, in order to account for the most similar concentration between standard and sample. The solutions were diluted to three sets of concentrations with absorption ranging from 0.02-0.08, to reduce fluorimeter saturation and excimer formation. The total area of emission for each sample and standard was calculated by first subtracting out the background signal, and then calculating the area. The experiments were repeated at least two times, and were averaged. To obtain the best accuracy, the slope of a plot of emission versus absorption was determined and calculated according to the equation;

$$\Phi_{PL}(x) = \left(\frac{A_s}{A_x} \right) \left(\frac{F_x}{F_s} \right) \left(\frac{n_x}{n_s} \right)^2 \Phi_{PL}(s)$$

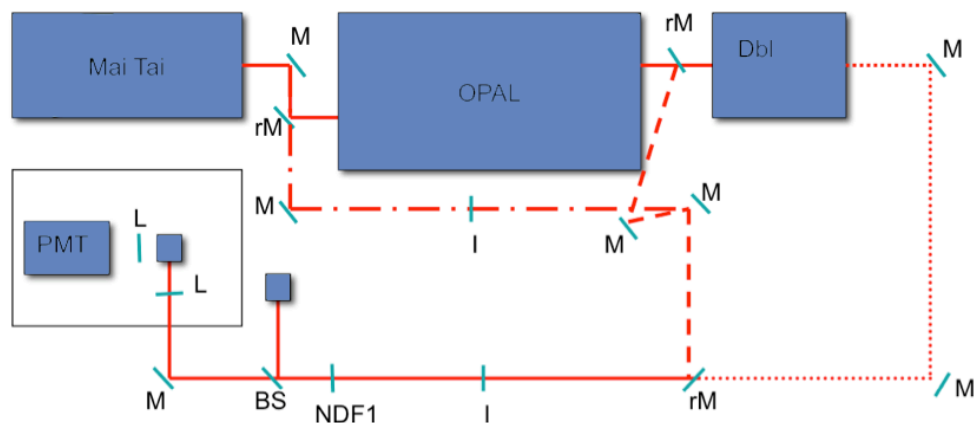
where Φ_{PL} is the quantum yield, A is the absorption at the excitation wavelength, F is the total integrated emission, and n is the refractive index of the solution, which due to low concentration, can be approximated as the refractive index of the solvent. Subscripts x and s refer to the sample and reference respectively. These measurements may have some error due to the sensitivity of the fluorescence spectrophotometer and other environmental conditions.

Solvent comparison studies. Samples of the R-stilbenevinyl SQs were prepared as concentrations of $\sim 20 \mu\text{M}$ in THF. Then 50 μL was added to 4 mL vials and diluted to 2 mL, with various ratios of either hexanes or methanol with THF to give final concentrations of $\sim 1 \mu\text{M}$. The photoluminescence was then measured for these samples and compared.

Two-Photon Excited Fluorescence Measurements. To use this technique for our SQ materials we had to develop methods of specific wavelength tuning for effective excitation and analysis as most of our materials absorb in the 300 to 350 nm region. This was challenging because the standard laser setup gives an output of 800 nm (two photon excitation), which corresponds to a 400 nm excitation wavelength. This meant we had to use a combination of down conversion (OPAL) and upconversion (Dbl) to gain access to ideal two photon excitation wavelengths (650 nm). This is extremely tricky since each time the laser beam is converted to a new wavelength it loses at least 50% of its energy. Ideally 100 mw of power would be used for an effective excitation at 800 nm, however after multiple conversions we were left with less than 20 mw for analysis at 650 nm. This meant that very careful optics tuning and focusing was necessary for successful two-photon analysis at 650 nm, our ideal wavelength. Without this careful experiment we could not have determined the full spectrum of TPA properties for our materials.

To measure the TPA cross sections, we followed the two-photon excited fluorescence (TPEF) method.² A 10^{-5} M solution of Coumarin 307 in methanol or Bis-MSB in cyclohexane were used as references. The laser used for the study was a SpectraPhysics Mai Tai diode-pumped mode-locked Ti:sapphire laser (Figure 2.2). The laser wavelength was varied from 760 nm to 820 nm, with an average band-width of ~ 30 nm, with a ~ 100 fs pulse, with 650 nm wavelengths achieved by using a SpectraPhysics OPAL and beam-doubling system pumped at 775 nm. The input power from the laser was varied using a polarizer. An iris was placed prior to the polarizer in order to ensure a circular beam. The beam from the polarizer was focused on the sample cell (quartz cuvette, 0.5 cm path length) using a lens with a focal length of 11.5 cm. The fluorescence was collected in a direction perpendicular to the incident beam. A 1-in. focal length plano-convex lens was used to direct the collected fluorescence into a monochromator.

The output from the monochromator was coupled to a photomultiplier tube. The photons were converted into counts by a photon-counting unit. A logarithmic plot between collected fluorescence photons and input intensity gave a slope of 2, ensuring a quadratic dependence between the same.³ The intercept enabled us to calculate the TPA cross-section from the action cross-section by multiplying by the fluorescence quantum yield of the sample.



rM= removable mirror

Figure 2.2. Two-photon excited fluorescence setup, dash dot line for wavelengths 720-820 nm, dashed line for wavelength of 650 nm from beam doubled system.

Fluorescence Upconversion Kinetics. To use this technique for our chromophore functionalized samples we once again had to tune the wavelengths very carefully. The fluorescence upconversion setup typically uses a 400 nm laser excitation wavelength from 2nd harmonic generation, however as mentioned above for the TPA studies our molecules absorb between 300 and 350 nm. In order to analyze our molecules we had to convert our setup to 3rd harmonic generation, which is very tricky to setup with procedure given in Appendix B. We were able to get this technique working, which gives us an laser excitation wavelength of 286 nm, much closer to the absorption bands present in chromophore functionalized SQs. Note: since the wavelength is lower (higher energy) than the main absorption of our functionalized SQs, excitation to higher energy bands is possible, whereas with 400 nm there is not sufficient energy for effective excitation to the LUMO. This technique was used for extensive analysis of stilbenevinylSQs for

comparison of their intramolecular interactions.

The fluorescence upconversion system used in our time-resolved experiments has been described previously.^{4,6} To excite our samples, a FOG-100 system (CDP, Figure 2.3) generates second harmonic light (400 nm) or third harmonic light (286 nm, described in Appendix B) from a mode-locked Ti-sapphire laser. Polarization of the excitation beam for anisotropy measurements was controlled with a Berek compensator. All samples were held in a 1 mm thick rotating sample cuvette (S). Horizontally polarized fluorescence emitted from the sample was up-converted in a nonlinear crystal of β -barium borate using a pump beam at 800 nm (NC-2), which first passed through a variable delay line. The instrument response function (IRF) was determined from the Raman signal of water for 400 nm excitation, and standards comparison (no rise time) at 286 nm. Lifetimes were obtained by convoluting the decay profile with the instrument response function. Spectral resolution was achieved by using a monochromator and photomultiplier tube. Under the experimental conditions, the stilbenevinylSQ structures investigated were relatively stable and little photodegradation observed. MATLAB and Origin 7 were used to model the fluorescence decay profile and to calculate fluorescence lifetime kinetics.

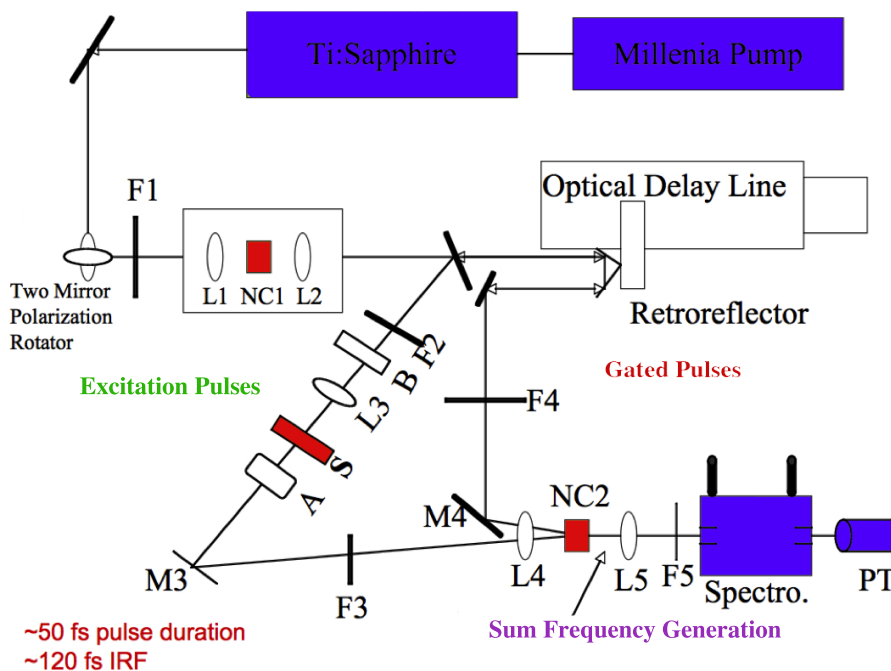


Figure 2.3. Fluorescence upconversion setup for 400 nm sample excitation.

Computational Methods. One of the many challenges in chemistry is being able to experimentally characterize materials to their full extent. This can come into play when trying to determine the reasons for photophysical/electronic properties or trying to determine reaction mechanisms. We have just started gaining experience in using the GAMESS computational software package in order to look at the energies involved in the mechanism of fluoride catalyzed rearrangement of SQs, of which we have been successful at determining reasonable reaction pathways because of it. We have also successfully looked at the orbitals involved in the HOMO and LUMO of SQs. A set of stepwise instructions for Gamess calculations is given in Appendix A.

The Gamess computational package (Build: May 2013 (R1)) was used for all modeling studies, including geometry optimization, double differenced Hessian frequency and energy calculations at the B3LYP and MP2 6-31G(d) level in both solvent and the gas phase.^{7,8} Excited state CIS calculations were also performed at the 6-31G(d,p) level.

2.2 Materials

Dichloromethane (CH_2Cl_2) and acetonitrile (CH_3CN) were purchased from Fisher and distilled from CaH_2 under N_2 prior to use. Tetrahydrofuran (THF) and 1,4-dioxane were purchased from Fisher and distilled under N_2 from Na/benzophenone prior to use. Anhydrous diethylether was purchased from Fisher and used as received. Grubbs 1st generation catalyst $[\text{RuCl}_2(=\text{ChPh})(\text{PCy}_3)_2]$, $\text{Pd}_2(\text{dba})_3$ and tetrabutylammonium fluoride (TBAF, 1 M in THF) were purchased from Sigma Aldrich and used as received. $\text{Pd}(\text{P}-\text{tBu}_3)_2$ was purchased from Acros Chemical and used as received.

Spirosiloxane **I** was synthesized as described elsewhere.⁹ Phenyllithium, n-butyllithium, thienyllithium, and lithium phenylacetylide solutions were purchased from Sigma Aldrich and used as received. 2-bromo-9,9-dimethylfluorene, 9-bromoanthacene, 2-(bromomethyl)naphthalene, and 3-bromothianaphthene were purchased from Sigma Aldrich and used as received.

Polyphenylsilsesquioxane and octaphenylsilsesquioxane were synthesized as previously described.¹⁰ Phenyltriethoxysilane was purchased from Gelest Inc.

Polyvinylsilsesquioxane (PVS) was synthesized using previously described methods.^{11,12} Decavinyl and dodecavinylsilsesquioxanes (vinylT_{10/12}) were synthesized using previously described methods or supplied by Mayaterials Inc.¹³

Octaphenylsilsesquioxane (OPS), octavinylsilsesquioxane (OVS), octaiodophenylsilsesquioxane (I₈OPS), divinyl(x-phenyl)SQ (x=8,10), and 1,4-bis-vinyltriethoxysilylbenzene were prepared using literature methods or were a gift from Mayaterials Inc.¹⁴⁻¹⁶

2.3 Synthetic Methods

The following sections describe the synthetic rational and methods for silsesquioxane precursors and functionalized silsesquioxanes. In general we set out to develop new synthetic methods to previously unknown or difficult to make functionalized silsesquioxanes (i.e. [PhenylSiO_{1.5}]₁₀), make chromophore functionalized SQs as models to determine how cage size effects the photophysical/electronic properties and the influence this may have on solar materials, and finally the development of a new class of conjugated polymers (BoC) based on silsesquioxanes.

2.3.1 Nucleophilic Substitution of Alkoxysilanes

In this section we describe the synthesis of R-spirosiloxanes, which are made from the nucleophilic substitution of R-Li at spirosiloxane. Spirosiloxanes are developed from the catalytic conversion of the agricultural waste product rice hull ash (silica), offering a new greener route to silsesquioxanes that bypasses the energy intensive carbothermal reduction processes typically used to make silsesquioxane precursors (i.e. R-SiCl₃).

Spirosiloxane:phenyllithium Reaction. To a flame dried and argon purged 100 mL Schlenk flask was added 2.5 g (0.01 mol) of spirosiloxane **I** and magnetic stir bar. The flask was then evacuated under vacuum 3 times and purged with argon. The flask was then cooled to -78 °C in a dry ice/acetone bath for 10 min under argon. Then 75 mL of dry argon purged diethyl ether was added to the reaction and allowed to cool for another 10 min. Then 10.5 mL (0.01 mol) of 1.8 M phenyl lithium solution in diethylether was

added dropwise by syringe to the reaction mixture, at which time the reaction became a yellow color. The reaction was run till the yellow color subsided and was then quenched with excess Me_3SiCl or MeI and allowed to stir cold for >30 min before warming up. The reaction was then worked up by a quick water wash (2x) to remove salts and then dried over MgSO_4 . The reaction was then filtered through Celite to remove salts and solvent removed in-vacuo. A clear semi-viscous oil was obtained. Further purification on select samples was achieved by bulb-to-bulb distillation under reduced pressure.

Tetraethoxysilane:R-Li Reaction. To a flame dried, 3x evacuated and argon purged 25 mL Schlenk flask was added 1.07 mL (0.0048 mol) of TEOS and a magnetic stir bar. The flask was then cooled to either -40 [dry ice/ethylene glycol (0.6):ethanol (0.4)] or -78 °C (dry ice/acetone bath for 10 min under argon. Then 15 mL of dry argon purged diethyl ether was added to the reaction and allowed to cool for another 10 min. Then 60 mol%, (0.0029 mol) of a Ph-Li solution was added dropwise by syringe to the reaction mixture, which became yellow in color. The reaction was run till the yellow color subsided and was then quenched with excess Me_3SiCl or MeI and allowed to stir cold for >30 min before warming up. The reaction was then worked up by a quick water wash (2x) to remove salts and then dried over MgSO_4 . The mixture was then filtered and the solvent removed in-vacuo. A clear semi-viscous oil was obtained.

Phenylsilsesquioxane synthesis. Briefly, 150 mg of oligomeric monophenyl-**I** were added to a 50 mL round bottom flask with magnetic stirrer. Then 30 mL of CH_2Cl_2 was added to the reaction, followed by 20 μL of water and 25 μL of 1 M TBAF solution in THF. The reaction was left to stir for 16 hours, and was then quenched with 50 mg of CaCl_2 to remove fluoride. The reaction was then filtered through Celite, and solvent removed in-vacuo. The product was then dissolved in a small amount of CH_2Cl_2 and precipitated into methanol to remove partial cage byproducts. The precipitate was then filtered, giving 62 mg of isolated PhSQ products in a mixture of cage sizes (T_8 , T_{10} , T_{12}).

2.3.2 Decaphenylsilsesquioxane [$\text{PhSiO}_{1.5}$] $_{10}$

T_{10} silsesquioxanes are one of the more difficult classes of silsesquioxanes to synthesize, but offer unique properties over the more prevalent T_8 class of SQs, including D_{5h} symmetry, higher solubility, and ability to achieve higher functionalization. Due to

the low yields typically achieved in the synthesis of $[\text{PhSiO}_{1.5}]_{10}$ (<15%) we developed a new method of synthesis that could easily achieve yields of >50% using fluoride catalysis as described below.

$[\text{PhSiO}_{1.5}]_{10}$ from $\text{PhSi}(\text{OEt})_3$. To an oven dried 2 L round bottom flask under N_2 was added 20 mL (0.08 mol) phenyltriethoxysilane, 1.75 L of methylene chloride, 5.2 mL (0.0052 mol) of TBAF, and 2.5 mL of H_2O and magnetic stirrer. The reaction was stirred for 2-3 days. The reaction was then worked up by one of two methods: a. Aqueous workup: 5x wash with H_2O in a separatory funnel, of which the organic layer was then dried over Na_2SO_4 , and filtered. b. The reaction was quenched with 50 g of powdered CaCl_2 and stirred for 1 day to remove the fluoride ion and then filtered through Celite. The solvent was then removed by rotary evaporation. The resulting white solid was then partially dissolved in 50 mL of a 1:1 THF:acetonitrile to selectively precipitate T_8 and T_{12} PhSQ. The resulting suspension of T_8 and T_{12} PhSQ was then filtered and reused in a subsequent synthesis. The solvent was then removed in-vacuo from the resulting solution containing T_{10} and partial cage PhSQ. It was then redissolved in a minimum amount of THF, precipitated into methanol to remove partial cages, filtered and dried under vacuum. $[\text{PhSiO}_{1.5}]_{10}$: white solid, 7.8 g, 49%. Characterization Data: ^1H NMR (400 MHz, acetone- d_6): δ 7.31 (t, Ar-H), 7.43 (t, Ar-H), 7.67 (t, Ar-H) ppm; ^{13}C NMR: δ 126.11, 126.53, 126.69, 127.29, 128.10, 128.66 ppm; ^{29}Si NMR (99 MHz, chloroform- d): 79.60 ppm; FTIR: 3066-2917 (ν C-H), 1591(ν C=C, Ar ring), 1429(ν C=C, Ar ring), 1132 (ν Si-O), 729 (ν Si-C) cm^{-1} . MALDI-TOF: m/z (Ag^+ adduct) = 1398.9 [$\text{Ag-Si}_{10}\text{O}_{15}(\text{C}_6\text{H}_5)_{10}$]. GPC (found): M_n = 1.5 kDa, M_w = 2.3 kDa, PDI = 1.06. TGA (air, 10 $^\circ\text{C}/\text{min}$ 1000 $^\circ\text{C}$): found 45.8%, calc 46.4%, $T_{d5\%}$: 420 $^\circ\text{C}$.

$[\text{PhSiO}_{1.5}]_{10}$ from $[\text{PhSiO}_{1.5}]_n$. To a 2 L round bottom flask under N_2 was added 16 g (0.12 mol) $[\text{PhSiO}_{1.5}]_n$, 1.75 L of methylene chloride, 5.2 mL (0.0052 mol) of TBAF and magnetic stirrer. The reaction was stirred for 2-3 days, or until the reaction mixture became transparent. The reaction was quenched with 50 g of powdered CaCl_2 and stirred for 1 day to remove the fluoride ion and then filtered through Celite. The solvent was then removed by rotary evaporation. The resulting white solid was then partially dissolved in 50 mL of a 1:1 THF:acetonitrile to selectively precipitate T_8 and T_{12} PhSQ.

The resulting suspension of T₈ and T₁₂ PhSQ was then filtered and reused in a subsequent synthesis. The solvent was then removed in-vacuo from the resulting solution containing T₁₀ and partial cage PhSQ. It was then redissolved in a minimum amount of THF, precipitated into methanol to remove partial cages, filtered and dried under vacuum. [PhSiO_{1.5}]₁₀: white solid, 8.2 g, 52%. Characterization Data: ¹H NMR (400 MHz, acetone-d₆): δ 7.31 (t, Ar-H), 7.43 (t, Ar-H), 7.67 (t, Ar-H) ppm; ¹³C NMR: δ 126.11, 126.53, 126.69, 127.29, 128.10, 128.66 ppm; ²⁹Si NMR (99 MHz, chloroform-d): 79.60 ppm; FTIR: 3066-2917 (ν C-H), 1591(ν C=C, Ar ring), 1429(ν C=C, Ar ring), 1132 (ν Si-O), 729 (ν Si-C) cm⁻¹. MALDI-TOF: m/z (Ag⁺ adduct) = 1399.1 [Ag-Si₁₀O₁₅(C₆H₅)₁₀]. GPC (found): Mn = 1.5 kDa, Mw = 2.4 kDa, PDI = 1.05. TGA (air, 10 °C/min 1000 °C): found 45.9%, calc 46.4%, T_{d5%}: 489 °C.

2.3.3 T_{10/12} Stilbenevinylsilsesquioxanes, [stilbenevinylSiO_{1.5}]_{10,12}

The following R-stilbenevinylSQs were developed as model systems to map the photophysical and electronic properties of silsesquioxanes for their potential use in hybrid/organic photovoltaic devices. Stilbenevinyl was the chromophore of choice due to its simplicity both in synthesis and photophysics as well as it being an analog of a reasonable photovoltaic material poly(phenylenevinylene) (PPV). Our rationale was to use the R-group on stilbenevinylSQs to try and tune their optical and electronic properties toward replacement materials for electron accepting materials in photovoltaics. This idea was based on previous experimental observations and calculations showing the electrophilic nature of the silsesquioxane core, which should act as an electronic acceptor. Though the SQ energy level as an acceptor is much too high on its own, we considered that tuning the R-groups should allow for energy level adjustment. Our synthetic procedures for making these materials are shown below.

Synthesis of Vinyl_x (x = 10, 12 and 14) T₁₀, T₁₂ and T₁₄ SQs. PVS (95 g, 1.2 mol) was placed in a 5 L round bottom flask equipped with magnetic stirrer. 4.0 L THF (4.0 L) was added to the flask. PVS was insoluble to THF at this stage. To the suspension of PVS in THF, 2.0mL of 1.0 M TBAF (2.0mmol) was added dropwise. PVS started to dissolve to THF and became a homogeneous solution in a few hours. The solution was stirred further 72 h at room temperature. To quench the reaction, CaCl₂ (100 g, 0.9 mol)

was added and stirred an additional 5 h. CaCl_2 was then filtered off and THF was removed from the filtrate under reduced pressure. The solid residue was washed with 100 mL deionized water for three times until the chloride ion was not detected by the AgNO_3 test. The product was collected and dried *in vacuo* to give a white powder (93g, 98% with respect to the initial mass of PVS). Characterization data. MALDI-TOF: m/z (Ag^+ adduct) = 829 [$\text{AgSi}_9\text{O}_{14}\text{H}_1(\text{C}_2\text{H}_3)_9$], 899 [$\text{AgSi}_{10}\text{O}_{15}(\text{C}_2\text{H}_3)_{10}$], 988 [$\text{AgSi}_{11}\text{O}_{17}\text{H}_1(\text{C}_2\text{H}_3)_{11}$], 1057 [$\text{AgSi}_{12}\text{O}_{18}(\text{C}_2\text{H}_3)_{12}$], 1216 [$\text{AgSi}_{14}\text{O}_{21}(\text{C}_2\text{H}_3)_{14}$] amu. GPC (found): $M_n = 790$; $M_w = 828$; PDI = 1.05.

General Heck reaction of vinyl_x (x = 10, 12 and 14) T₁₀, T₁₂ and T₁₄ Gen1 SQs. A dry 50 mL round bottom Schlenk flask under N_2 was charged with $\text{Pd}[\text{P}(t\text{-Bu}_3)]_2$ (194 mg, 0.38 mmol). 1,4-Dioxane (10 mL) was added and the mixture was stirred at room temperature, resulting in a homogeneous orange solution. Bromo-compounds (14.3 mmol), NCy_2Me (4.0 mL, 19.0 mmol) and vinylT₁₀/T₁₂ (1.0 g, 12.7 mmol vinyl group, solution in 2 mL of dioxane) were then added successively via syringe. The resulting solution was allowed to stir at room temperature for 72 h. The solution became light-brown in color, and white amine hydrochloride salt precipitates were observed. The solution was stirred further at 60 °C for 48 h to complete the reaction. The reaction mixture was cooled to ambient and filtered through 2 cm Celite to remove precipitates. The catalyst was quenched and product coincidentally precipitated into 200 mL of methanol. The products were isolated by filtration and dried *in vacuo* to give a powder characterized by methods described above, with the tabulated data presented in the text.

Double Heck addition reactions vinyl_{10/12}SQs. A dry 50 mL round bottom Schlenk flask under N_2 was charged with $\text{Pd}[\text{P}(t\text{-Bu}_3)]_2$ (97 mg, 0.19 mmol). 1,4-Dioxane (10 mL) was added and the mixture stirred at room temperature, resulting in a homogeneous orange solution. Bromo-compounds (14.3 mmol), NCy_2Me (4.0 mL, 19.0 mmol) and vinyl T_{10/12}-silsesquioxane (0.5 g, 6.3 mmol vinyl group, solution in 2 mL of dioxane) were then added successively via syringe. The resulting solution was allowed to stir at 90°C for 24 h. The solution turned canary-yellow, and white amine hydrochloride salt precipitates formed. The catalyst was quenched and product coincidentally precipitated into 200 mL of methanol. The products were filtered off and dried *in vacuo* to give a

powder characterized by the methods described above. Tabulated data are presented below in the text.

Gen1 via Metathesis. To a dry 25 mL Schlenk flask under N₂ was added 0.40 g (5.1 mmol of vinyl group) of vinylT_{10/12} and 21.0 mg (0.026 mmol, 0.5 mol %) of first generation Grubbs catalyst. Dry CH₂Cl₂ (6 mL) was added by syringe followed by *p*-R-styrene (7.56 mmol). The mixture was stirred at 40 °C for 72 h and then quenched in 200 mL of methanol. The solution was filtered and the powder was further purified by column chromatography (THF/hexane eluant mixtures system). Tabulated characterization data are presented in the text.

General Heck reaction of bromostyrenyl T_{10/12} SQs. To a dry 50 mL Schlenk flask under N₂ was added 0.50 g (2.1 mmol of Br) of bromostyrenylT_{10/12}, 19 mg (0.04 mmol, 2 mol %) of Pd[P(t-Bu)₃]₂, and 18 mg (0.02 mmol, 1 mol %) of Pd₂(dba)₃. Dry 1,4-dioxane (10 mL) was added by syringe, followed by NCy₂Me (2.11 mmol, 0.45 mL) and *p*-R-styrene (6.4 mmol). The resulting solution was allowed to stir at room temperature for 72 h. The reaction mixture was filtered through 2 cm Celite to remove ammonium chloride precipitate. The solution was then quenched by precipitation into 200 mL of methanol and filtered. The isolated solid was redissolved in 10 mL of THF and filtered again through a 2 cm celite to remove any remaining Pd particles and reprecipitated into 200 mL of methanol. The solution was filtered and the powder was further purified by column chromatography. The characterization data are presented in tabular form in the text.

2.3.4 Separation and Photophysical Properties of T₁₀ and T₁₂ StilbenevinylSQs

One of the big challenges in the synthesis of SQs by F⁻ catalyzed rearrangement is that the product is typically a mixture of cage sizes. Though this is not a problem for many applications, it makes characterization of individual properties difficult. Therefore we developed a technique for the effective separation of T₁₀ and T₁₂ stilbenevinylSQs so that their individual photophysical properties could be determined. This is outlined below.

General T_{10/12} cage separation procedure. The stilbenevinylSQ cage mixture (25 mg) was added to a 5 mL test tube and dissolved with 1 mL of ethyl acetate. Acetonitrile was then

added dropwise until precipitation occurred. The precipitate was then filtered using a 0.22 μm pore size syringe filter, and the solution phase was added to a new 5 mL test tube (A). The solid phase was then redissolved with THF and added to another test tube (B). To test tube (A) was added acetonitrile until precipitation occurred, and the process was repeated until the solution contained only stilbenevinylT₁₀ (3-4 iterations). Test tube (B) was dried out and redissolved in ethyl acetate, and the same procedure as that with (A) was repeated to enrich the solid in stilbenevinylT₁₂. Further purification of the T₁₂ was carried out using gel permeation chromatography (GPC) to give pure T₁₂ for spectroscopic studies. The purity was verified by MALDI-ToF spectroscopy and silicon NMR. **T₁₀ stilbenevinylSQ:** MALDI-TOF: m/z (Ag⁺ adduct) = 2681 [AgSi₁₀O₁₅(C₁₆H₁₃)₁₀]; GPC (found): M_n = 3367; M_w = 3450; PDI = 1.02; ¹H NMR (500 MHz, CDCl₃): δ 6.3-6.4 (m, -CH=CH2), 7.0-7.1 (m, -CH=CH2), 7.2-7.3 (m, Ar-H), 7.3-7.6 (m, Ar-H) ppm. ¹³C NMR (500 MHz, CDCl₃): δ 100.05, 115.00, 126.11, 126.53, 126.69, 127.29, 128.10, 128.66, 135.50, 136.63, 137.14, 138.01 ppm; ²⁹Si NMR (99.35 MHz, CDCl₃): δ -78.85 ppm. **T₁₂ stilbenevinylSQ:** 3196 [AgSi₁₂O₁₈(C₁₆H₁₃)₁₂] amu; GPC (found): M_n = 3758; M_w = 3871; PDI = 1.03; ¹H NMR (500 MHz, CDCl₃): δ 6.3-6.4 (m, -CH=CH2), 7.0-7.1 (m, -CH=CH2), 7.2-7.3 (m, Ar-H), 7.3-7.6 (m, Ar-H) ppm. ¹³C NMR (500 MHz, CDCl₃): δ 125.20, 126.54, 126.67, 127.27, 127.36, 127.70, 128.09, 128.67, 129.02, 136.68, 137.10, 137.76, 137.84 ppm; ²⁹Si NMR (99.35 MHz, CDCl₃): δ -78.69, -80.44 ppm.

2.3.5 Beads on a Chain (BoC) Polymers Based on Mixed Phenyl-vinylSQs

Silsesquioxane containing organic polymers are of increasing interest due to their increased thermal and oxidative stability. Most of these studies however have been with SQs as pendant groups on the polymer as opposed to being part of the main chain. We have set out to develop new methods of making polymers with alternating organic-silsesquioxane units (BoCs). Our goal is to use F⁻ catalyzed rearrangement techniques to make mixed functional SQs, which can be polymerized with a conjugated organic linker. The rationale is that these materials can behave in a similar manner to conjugated organic polymers typically used in organic photovoltaic and light emitting diode applications. We have observed ground and excited state charge transfer processes in these materials

suggestive of the 3D conjugation effects offered by the silsesquioxanes. The synthesis of these materials and their model compounds is described below.

Synthesis of [(vinyl)₂(*p*-IPh)_{*n-2*}SiO_{1.5}]_{*n*} (*n* = 10, 12). I₈OPS (4.76 g, 18.6 mmol) and OVS (350 mg, 4.25 mmol) were placed in a 100 mL round-bottom flask equipped with a magnetic stirrer. THF (50 mL) and 0.25 mL (1.0 M in THF, 0.25 mmol) of 95% TBAF were added via syringe under N₂. The reaction mixture was stirred at room temperature for 48 h. CaCl₂ (0.2 g, 1.8 mmol) was added to the reaction mixture and stirred an additional 6 h. Insolubles (~0.25 g) were then removed by filtration, and the solvent removed by rotary evaporation. The solid residue was dissolved in ~10 mL of THF and precipitated into 200 mL of MeOH. The precipitated products were collected and dried *in vacuo* to give a white powder (4.67 g, 90% with respect to total initial mass of reactants). ¹H NMR (400 MHz, DMSO-*d*₆): δ 5.5-6.5 (br, -CH=CH₂), 6.9-8.1 (br, Ar-*H*); ¹³C NMR: δ 130.0 (-Si-CH=CH₂), 130.7 (Ar-C), 133.8 (Ar-C), 136.3 (-CH=CH₂); FTIR: 3066-2917 (νC-H), 1591(νC=C, Ar ring), 1429(νC=C, Ar ring), 1132 (νSi-O), 729 (νSi-C) cm⁻¹. MALDI-TOF: *m/z* (Ag⁺ adduct) = 2104.3 [Si₁₂O₁₈(C₂H₃)₄(IC₆H₅)₆(C₆H₅)₂], 2230.1 [Si₁₂O₁₈(C₂H₃)₄(IC₆H₅)₇(C₆H₅)₁], 2280.1 [Si₁₂O₁₈(C₂H₃)₃(IC₆H₅)₇(C₆H₅)₂], 2355.9 [Si₁₂O₁₈(C₂H₃)₄(IC₆H₅)₈], 2405.9 [Si₁₂O₁₈(C₂H₃)₃(IC₆H₅)₈(C₆H₅)₁], 2532.7 [Si₁₂O₁₈(C₂H₃)₃(IC₆H₅)₉], amu. GPC (found): *M*_n = 2.4 kDa, *M*_w = 1.5 kDa, PDI = 1.05. TGA (air, 1000 °C): found 27.2%, calc 27.4%, T_{d5%}: 412 °C.

Metathesis polymerization of [(vinyl)₂(*p*-IPh)_{*n-2*}SiO_{1.5}]_{*n*} and [(vinyl)₂(Ph)_{*n-2*}SiO_{1.5}]_{*n*} (*n* = 10, 12) with divinylbenzene (DVB) to make polymers **A** and **B**. To a dry 100 mL Schlenk flask under N₂ was added 3.5 g (14 mmol) of [(vinyl)₂(*p*-IPh)_{*n-2*}SiO_{1.5}]_{*n*} and 100 mg (0.28 mmol) of first generation Grubbs catalyst. Dry CH₂Cl₂ (70 mL) was added by syringe followed by divinylbenzene 29.75 μL (0.21 mmol, added in equal parts over 3 days). The mixture was stirred at reflux at 40 °C for 72 h and then precipitated into 200 mL of methanol. The solution was then filtered and the solid collected. The solid was then redissolved in toluene and *n*-acetyl-L-cysteine was added to complex the catalyst for removal. The resulting solid was purified by a silica plug (1:10 CH₂Cl₂:hexanes, 5 cm diameter, 7 cm silica) and the collected sample was vacuum dried for 6 h. **Polymer A**: (3.2 g, 89%), ¹H NMR (400 MHz, CD₂Cl₂): δ 5.2-6.3 (br, -CH=CH), 6.6-8.1 (br, Ar-*H*);

FTIR: 3066-2917 (ν C-H), 1591(ν C=C, Ar ring), 1429(ν C=C, Ar ring), 1132 (ν Si-O), 729 (ν Si-C) cm^{-1} ; GPC: $M_n = 18$ kDa, $M_w = 31$ kDa, PDI = 1.7; TGA (air, 1000 °C): found 28.6 %, calc 27.7 %, $T_{d5\%} = 378$ °C. **Polymer B**: (3.4 g, 95%), ^1H NMR (400 MHz, CDCl_3): δ 5.2-6.3 (br, -CH=CH), 6.6-8.1 (br, Ar-H). FTIR: 3066-2917 (ν C-H), 1591(ν C=C, Ar ring), 1429(ν C=C, Ar ring), 1132 (ν Si-O), 729 (ν Si-C) cm^{-1} ; GPC: $M_n = 8.2$ kDa, $M_w = 13$ kDa, PDI = 1.6; TGA (air, 1000 °C): found 45.3 %, calc 44.6 %, $T_{d5\%} = 402$ °C.

Heck reaction of **Polymer A** and styrene to make (**Polymer C**). To an oven dried 10 mL Schlenk flask under N_2 was added 200 mg (0.53 mmol) of (**Polymer A**), 5 mg (0.01 mmol) of $\text{Pd}[\text{P}(t\text{-Bu})_3]_2$ and 4.75 mg (0.005 mmol) of $\text{Pd}_2(\text{dba})_3$. 1,4-dioxane (5 mL) was added by syringe, followed by 100 μL (0.50 mmol) of NCy_2Me and 54.5 mg (0.53 mmol) of styrene, and left to run to completion as monitored by GPC. The solution was then filtered and the solid collected. The solid was then redissolved in toluene and n-acetyl-L-cysteine was added to complex the catalyst for removal. The mixture was then filtered through 5 cm of Celite and then precipitated into 100 mL of methanol and filtered again. The solid was then vacuum dried for 4 h, which gave a white solid (160 mg, 67 % yield). ^1H -NMR (CHCl_3 , δ ppm): 5.3-6.4 (br, -CH=CH), 6.5-7.9 (br, Ar-H); FTIR (cm^{-1}): 3024 (ν C-H, aromatic), 1600 (ν C=C), 1130 (ν Si-O); GPC: $M_n = 9.5$ kDa, $M_w = 17$ kDa, PDI = 1.8; TGA (air, 1000 °C): found 29.5 wt %, calc 28.7 wt %, $T_{d5\%} = 348$ °C.

Heck reaction of **Polymer A** and *p*-OMe-styrene to make (**Polymer D**) To a oven dried 10 mL Schlenk flask under N_2 was added 500 mg (1.31 mmol) of **Polymer A**, 12.5 mg (0.025 mmol) of $\text{Pd}[\text{P}(t\text{-Bu})_3]_2$ and 11.9 mg (0.0125 mmol) of $\text{Pd}_2(\text{dba})_3$. 1,4-dioxane (12.5 mL) was added by syringe, followed by 250 μL (1.25 mmol) of NCy_2Me and 176 μL (1.31 mmol) of *p*-OMe-styrene, and left to run to completion as monitored by GPC. The solid was then redissolved in toluene and n-acetyl-L-cysteine was added to complex the catalyst for removal. The mixture was then filtered through 5 cm of Celite and then precipitated into 100 mL of methanol and filtered again. It was then vacuum dried for 4 h and was obtained as a white solid (0.43 g, 66 % yield). ^1H -NMR (CDCl_3 , δ ppm): 5.3-6.4 (br, -CH=CH), 6.5-7.9 (br, Ar-H), 3.84 (s, -OCH₃); FTIR (cm^{-1}): 3024 (ν C-H, aromatic), 1600 (ν C=C), 1131 (ν Si-O), 1037 (ν C-O); GPC: $M_n = 12$ kDa, $M_w = 45$ kDa, PDI = 3.7.

General Heck reaction to **Polymer E** and **Polymer F**. To a dry 50 mL Schlenk flask under N₂ was added 1 g (7.69 mmol) of divinyl(x-phenyl)SQ, (0.168 mmol) of 1,4-dibromobenzene (**E**) or 4,4'-dibromostilbene (**F**), 38 mg (0.084 mmol) of Pd[P(t-Bu)₃]₂, and 36 mg (0.04 mmol) of Pd₂(dba)₃. Dry 1,4-dioxane (20 mL) was added by syringe, followed by NCy₂Me (0.9 mL, 4.35 mmol). The resulting solution was allowed to stir at room temperature for 72 h. The reaction mixture was filtered through 5 cm of Celite to remove catalyst. The solution was then quenched by precipitation into 200 mL of methanol and filtered. The solid was then redissolved in toluene and purified by n-acetyl-L-cysteine to further remove the catalyst. Then column chromatography was used to remove the catalyst complex and unreacted starting material (CH₂Cl₂:hexanes 1:2, 3 cm diameter, 10 cm of silica). **Polymer E**: (0.86 g, 83%); ¹H-NMR (CDCl₃, δ ppm): 5.6-6.2 (br, -CH=CH), 6.7-8.0 (br, Ar-H); FTIR (cm⁻¹): 3066-2917 (νC-H), 1591(νC=C, Ar ring), 1429(νC=C, Ar ring), 1132 (νSi-O), 729 (νSi-C) cm⁻¹; GPC: M_n = 6 kDa, M_w = 11 kDa, PDI = 1.8; TGA (air, 1000 °C): found 44.7 %, calc 44.6 %, T_{d5%} = 300 °C. **Polymer F**: (0.92 g, 86%); ¹H-NMR (acetone-d₆, δ ppm): 5.6-6.2 (br, -CH=CH), 6.7-8.0 (br, Ar-H); FTIR (cm⁻¹): 3066-2917 (νC-H), 1591(νC=C, Ar ring), 1429(νC=C, Ar ring), 1132 (νSi-O), 729 (νSi-C) cm⁻¹; GPC: M_n = 5.3 kDa, M_w = 12 kDa, PDI = 2.3; TGA (air, 1000 °C): found 46.1 %, calc 42.9 %, T_{d5%} = 395 °C.

Synthesis of **4,4'-dibromostilbene**. *Metathesis*: To a dry 50 mL Schlenk flask under N₂ was added 1 g (5.5 mmol) of 4-bromostyrene and 50 mg (0.14 mmol) of first generation Grubbs catalyst. Dry CH₂Cl₂ (30 mL) was then added by syringe. The reaction was refluxed at 40 °C for 2 d. The reaction was then concentrated and precipitated into 100 mL methanol. The solid was then filtered and dried under vacuum (930 mg, 97% of **4,4'-dibromostilbene**). ¹H-NMR (acetone-d₆, δ ppm): 7.33 (s, -CH=CH), 7.56 (d, Ar-H), 7.60 (d, Ar-H); GPC: M_n = 253 Da, M_w = 256 Da, PDI = 1.01.

Heck coupling of vinyltriethoxysilane with 4,4'-dibromostilbene to make **4,4'-bis-vinyltriethoxysilylstilbene (Model 2)**: To a dry 10 mL Schlenk flask under N₂ was added 100 mg (0.295 mmol) of 4,4'-dibromostilbene, 10 mg (0.02 mmol) of Pd[P(t-Bu)₃]₂, and 8 mg (0.01 mmol) of Pd₂(dba)₃. Distilled vinyltriethoxysilane (0.5 mL, excess) was added by syringe, followed by NCy₂Me (0.3 mL, 1.4 mmol). The resulting

solution was allowed to stir at room temperature for 72 h. The reaction mixture was filtered through Celite to remove catalyst. The resulting yellow oil was then fractionally distilled to remove excess vinyltriethoxysilane (134 mg, 82%). ¹H-NMR (acetone-*d*₆, δ ppm): 1.21 (m, -O-CH₂-CH₃), 3.87 (m, -O-CH₂-CH₃), 6.28 (d, Si-CH=CH-Ar), 7.18 (d, Si-CH=CH-Ar), 7.30 (d, Ar-CH=CH-Ar), 7.57 (d, Ar-H), 7.61 (d, Ar-H); FTIR (cm⁻¹): 3066-2917 (νC-H), 1607 (νC=C, Ar ring), 1455 (νC=C, Ar ring), 1100 (νSi-O), 1080 (νSi-O) cm⁻¹; GPC: Mn = 1440 Da, Mw = 1512 Da, PDI = 1.05.

Table 2.1. Synthesized SQ materials and their chemical makeup.

Polymer	Description
A	Made from metathesis of [(vinyl) ₂ (<i>p</i> -IPh) _{<i>n-2</i>} SiO _{1.5}] _{<i>n</i>} with divinylbenzene
B	Made from metathesis of [(vinyl) ₂ (Ph) _{<i>n-2</i>} SiO _{1.5}] _{<i>n</i>} with divinylbenzene
C	Made from Heck coupling of styrene with oligomer A
D	Made from Heck coupling of <i>p</i> -OMe styrene with oligomer A
E	Made from Heck coupling of [(vinyl) ₂ (Ph) _{<i>n-2</i>} SiO _{1.5}] _{<i>n</i>} with 1,4-dibromobenzene
F	Made from Heck coupling of [(vinyl) ₂ (Ph) _{<i>n-2</i>} SiO _{1.5}] _{<i>n</i>} with 4,4'-dibromostilbene
Model 1	1,4-bis-vinyltriethoxysilylbenzene
Model 2	4,4'-bis-vinyltriethoxysilylstilbene

General Heck reaction to Phenyl-fluorene polymer. To a dry 20 mL Schlenk flask under N₂ was added 1 g (7.69 mmol) of divinyl(*x*-phenyl)SQ, (0.168 mmol) of 2,7-dibromo-

9,9-dimethylfluorene, 38 mg (0.084 mmol) of Pd[P(t-Bu)₃]₂, and 36 mg (0.04 mmol) of Pd₂(dba)₃. Dry 1,4-dioxane (15 mL) was added by syringe, followed by NCy₂Me (1.6 mL, 8.5 mmol). The resulting solution was allowed to stir at room temperature for 72 h. The reaction mixture was filtered through 5 cm of Celite to remove catalyst. The solution was then quenched by precipitation into 200 mL of methanol and filtered. The solid was then redissolved in toluene and purified by n-acetyl-L-cysteine to further remove the catalyst. Then column chromatography was used to remove the catalyst complex and unreacted starting material (CH₂Cl₂:hexanes 1:2, 3 cm diameter, 10 cm of silica). Phenylfluorene polymer: (0.67 g, 65%); ¹H-NMR (CDCl₃, δ ppm): 1.5 (s, CH₃), 5.6-6.2 (br, -CH=CH), 6.7-8.0 (br, Ar-H); FTIR (cm⁻¹): 3066-2917 (ν C-H), 1591(ν C=C, Ar ring), 1429(ν C=C, Ar ring), 1132 (ν Si-O), 729 (ν Si-C) cm⁻¹; GPC: Mn = 3.9 kDa, Mw = 6.4 kDa, PDI = 1.6; TGA (air, 1000 °C): found 38.6 %, calc 40.4 %, T_{d5%} = 210 °C.

Heck coupling of vinyltriethoxysilane with 2,7-dibromo-9,9-dimethylfluorene to make 2,7-bis-vinyltriethoxysilyl-9,9-dimethylfluorene (Fluorene Model): To a dry 10 mL Schlenk flask under N₂ was added 300 mg (0.85 mmol) of 2,7-dibromo-9,9-dimethylfluorene, 10 mg (0.02 mmol) of Pd[P(t-Bu)₃]₂, and 8 mg (0.01 mmol) of Pd₂(dba)₃. Distilled vinyltriethoxysilane (5 mL, excess) was added by syringe, followed by NCy₂Me (0.3 mL, 1.4 mmol). The resulting solution was allowed to stir at room temperature for 72 h. The reaction mixture was filtered through Celite to remove catalyst. The resulting yellow oil was then fractionally distilled to remove excess vinyltriethoxysilane (311 mg, 84%). FTIR (cm⁻¹): 3066-2917 (ν C-H), 1607 (ν C=C, Ar ring), 1455 (ν C=C, Ar ring), 1100 (ν Si-O), 1080 (ν Si-O) cm⁻¹; GPC: Mn = 771 Da, Mw = 802 Da, PDI = 1.04.

References:

1. Maciejewski, A.; Steer, R. P. "Spectral and photophysical properties of 9,10-diphenylanthracene in perfluoro-n-hexane: the influence of solute—solvent interactions," *J. Photochem.* **1986**, *35*, 59.
2. Xu, C.; Webb, W. W. "Measurement of two-photon excitation cross sections of molecular fluorophores with data from 690 to 1050 nm." *J. Opt. Soc. Am. B.* **1996**, *13*, 481.
3. Bhaskar, A.; Ramakrishna, G.; Lu, Z.; Twieg, R.; Hales, J. M.; Hagan, D. J.; Van Stryland, E.; Goodson, T. "Investigation of Two-Photon Absorption Properties in Branched Alkene and Alkyne Chromophores." *J. Am. Chem. Soc.* **2006**, *128*, 11840-11849.

4. Varnavski, O.; Goodson III, T. G. "Femtosecond fluorescence dynamics and molecular interactions in a water-soluble nonlinear optical polymeric dye." *Chem. Phys. Lett.* **2000**, 688–696.
5. Ramakrishna, G.; Bhaskar, A.; Goodson III, T. "Ultrafast excited state relaxation dynamics of branched donor-pi-acceptor chromophore: evidence of a charge-delocalized state." *J. Phys. Chem. B* **2006**, 110, 20872–8.
6. Flynn, D. C.; Ramakrishna, G.; Yang, H.; Northrop, B. H.; Stang, P. J.; Goodson III, T. G. "Ultrafast Optical Excitations In Supramolecular Metallacycles with Charge Transfer Properties." *J. Am. Chem. Soc.*, **2010**, 132, 1348–1358.
7. Schmidt, M.W.; Baldrige, K.K.; Boatz, J.A.; Elbert, S.T.; Gordon, M.S.; Jensen, J.H.; Koseki, S.; Matsunaga, N.; Nguyen, K.A.; Su, S.; Windus, T.L.; Dupius, M.; Montgomery, J.A. "General Atomic and Molecular Electronic Structure System" *J. Comput. Chem.*, **1993**, 14, 1347-1363.
8. "Advances in electronic structure theory: GAMESS a decade later" M.S.Gordon, M.W.Schmidt pp. 1167-1189, in "Theory and Applications of Computational Chemistry: the first forty years" C.E.Dykstra, G.Frenking, K.S.Kim, G.E.Scuseria (editors), Elsevier, Amsterdam, 2005.
9. R.M. Laine, P.H. Doan, J. C. Furgal, D. Pan, V. Popova, "Distilling Silica from Biogenic Silica Sources," *Manuscript in Submitted to Science*
10. Brown, J. F., Jr. "The Polycondensation of Phenylsilanetriol." *J. Am. Chem. Soc.* **1965**, 87, 4317–4324.
11. Ronchi, M.; Sulaiman, S.; Boston, N. R.; Laine, R. M.; "Fluoride catalyzed rearrangements of polysilsesquioxanes, mixed Me,Vinyl T₈, Me,Vinyl T₁₀ and T₁₂ cages," *Applied Organometallic Chemistry*, **2010**, 24, 551–557.
12. Sulaiman, S.; Brick, C.; Roll, M.; Bhaskar, A.; Goodson, T.; Zhang, J.; Laine, R. M. "Molecules with Perfect Cubic Symmetry as Nanobuilding Blocks for 3-D Assemblies. Elaboration of Octavinylsilsesquioxane. Unusual Luminescence Shifts May Indicate Extended Conjugation Involving the Silsesquioxane Core." *Chem. Mater.* **2008**, 20, 5563.
13. Abe, Y.;Gunji,T.; "Oligo- and polysiloxanes" *Prog. Poly. Sci.* **2004**, 29, 149-182.
14. Asuncion, M. Z.; Laine, R. M. Fluoride rearrangement reactions of polyphenyl- and polyvinylsilsesquioxanes as a facile route to mixed functional phenyl, vinyl T₁₀ and T₁₂ silsesquioxanes. *J. Am. Chem. Soc.* **2010**, 132, 3723–36.
15. Cornelius, M.; Hoffmann, F.; Fröba, M. Periodic Mesoporous Organosilicas with a Bifunctional Conjugated Organic Unit and Crystal-like Pore Walls. *Chem. Mater.* **2005**, 6674–6678.
16. Voronkov, M.G.; Lavrent'yev, V.I.; "Polyhedral Oligosilsesquioxanes and Their Homo Derivatives," *Top. Curr. Chem.* **1982**, 102, 199-236.

Chapter 3.

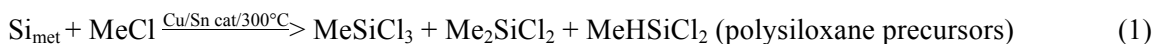
Silsesquioxanes from the Ground Up: Nucleophilic Attack of R-lithium at Tetrahedral Silicon in Alkoxysilanes

3.1 Abstract

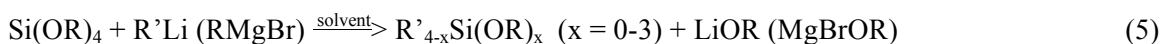
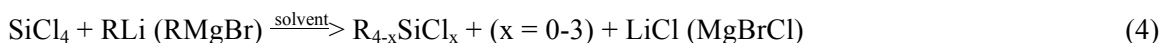
The currently accepted mechanism for nucleophilic attack at silicon in tetraalkoxysilanes, e.g. $\text{Si}(\text{OEt})_4$ is suggested to involve formation of penta- and then hexacoordinated intermediates as supported by the apparent exclusive formation of $\text{R}_3\text{SiOR}'$ and R_4Si from nucleophilic attack by RLi and RMgX . Our recent discovery of a direct route from biogenic silica to tetraalkoxy-spirosiloxanes prompted us to revisit this reaction as a potential route to diverse silicon containing species with single Si-C bonds as early studies demonstrate that spirosiloxanes form quite stable pentacoordinated alkoxysilane compounds. As anticipated, $\text{Si}(\text{2-methyl-2,4-pentane-diolato})_2$ (SP) reacts with RLi ($\text{R} = \text{Ph}$, anthracene, phenylacetylene, etc.) at $-78\text{ }^\circ\text{C}$ to form pentacoordinated Si, e.g. LiPhSP equilibrates with the starting reagents even at 3:1 ratios of $\text{PhLi}:\text{SP}$ with no evidence for formation of hexacoordinated species by mass spectral, NMR and quenching studies. Thus, quenching with MeI or Me_3SiCl allows isolation of monosubstituted products from $\text{RLi}:\text{SP}$; $\text{RSi}(\text{OR}')_3$ including some ring opened oligomers. Comparative studies of reactions of PhLi with $\text{Si}(\text{OEt})_4$ allows isolation of mono- and di-substituted products again even at 1:1 ratios of $\text{PhLi}:\text{Si}(\text{OEt})_4$. However, on standing at $-78\text{ }^\circ\text{C}$ for long periods of time or on warming to $0\text{ }^\circ\text{C}$, the primary product for both reactions is Ph_4Si *even with 0.5 equivalents of PhLi*. At reaction temperatures $\geq 0\text{ }^\circ\text{C}$ the primary product is again Ph_4Si . These results suggest that hexacoordinated intermediates are not part of the substitution mechanism and may suggest that the higher substituted compounds arise from disproportionation processes. We also briefly describe the conversion of the anthracenyl- and phenylethynylSP to silsesquioxanes.

3.2 Introduction

Silicon chemistry is dominated by compounds made starting from the products of the direct process, reaction (1).¹ Other products can be made from PhSiCl₃ available via reaction (2).² Finally, hydrosilylation as exemplified by reaction (3), provides access to other types of monofunctional silanes.^{3,4}



However, if one wants to make organosilicon compounds starting from organic compounds that do not contain an accessible double bond or compounds without phenyl or methyl groups, very few synthetic avenues remain. These typically involve reactions of nucleophiles with chloro- or alkoxy-silanes as illustrated in reactions (4) and (5).

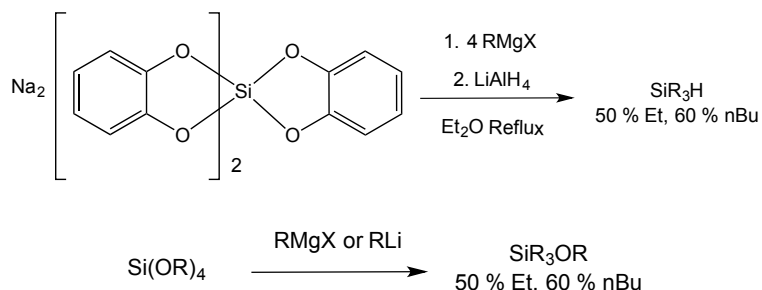


Reaction (4) proceeds reasonably well but one must contend with chlorosilanes before and after reaction and their hydrolysis products, which require extra care and often afford unwanted complications including the formation of intractable polymers. Consequently, multiple groups have explored nucleophilic attack at Si(OEt)₄ (TEOS) in particular using strong nucleophiles, however no others have targeted the synthesis of silsesquioxane precursors [RSi(OR')₃] and more importantly difunctional siloxanes [-R₂SiO- or R₁R₂SiO-] where R ≠ methyl.

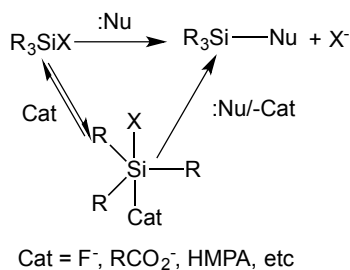
Reaction (5) also suffers from an important complication because nucleophilic substitution often does not stop at the monofunctional silane but rather commonly continues to the tri- and tetra-functional products even when the alkoxy-silane is used in excess, as suggested in Scheme 1.⁵⁻¹¹ Thus, nucleophilic *attack at tetrahedral alkoxy-silanes differs considerably from that of carbon containing compounds.*

This surprising result has prompted multiple studies on nucleophilic attack at tetrahedral silicon. Extensive studies by the Corriu group provide considerable evidence

that nucleophilic attack occurs much faster at penta- and hexacoordinated rather than tetrahedral silanes.¹²⁻¹⁶ They have proposed a general mechanism as illustrated in Scheme 2.^{15,16} Here F^- or RCO_2^- would be a catalyst for reactions not involving Grignard or Li reagents.



Scheme 3.1. Typical reactions of triscatecholatosilicate or tetralkoxysilanes with Grignard and lithium reagents.⁵⁻¹⁶



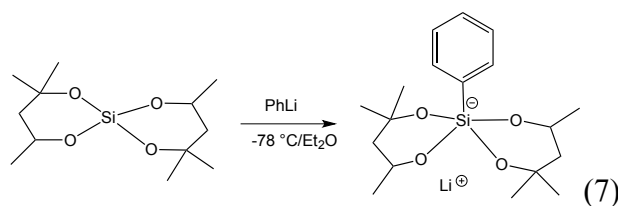
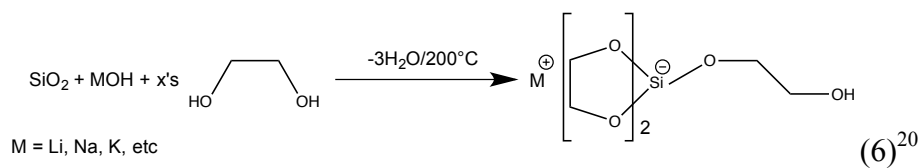
Scheme 3.2. Proposed mechanism for nucleophilic substitution at Si via pentacoordinate intermediates.^{15,16}

This mechanism seems to provide an explanation for many of the results reported to date.⁵⁻¹¹ Corriu et al argue that in the absence of catalyst, the nucleophile takes the position “Cat” in Scheme 1; thus, double and triple functionalization can be expected. Many of the Corriu et al studies were run in ether at or near reflux temperatures (≈ 30 °C).

Tour et al demonstrated that it was possible to get two of the same R groups to add to Si using alkyl/aryl lithium reagents and thereafter add a different $R'Li$ group to produce $R_2R'SiOEt$.⁷ They could never obtain $RR'Si(OR)_2$, again supporting the likelihood that pentacoordinate species react faster than tetra-coordinate ones. Although their reactions were initiated at -78 °C, they were allowed to warm to room temperature prior to quenching with water.

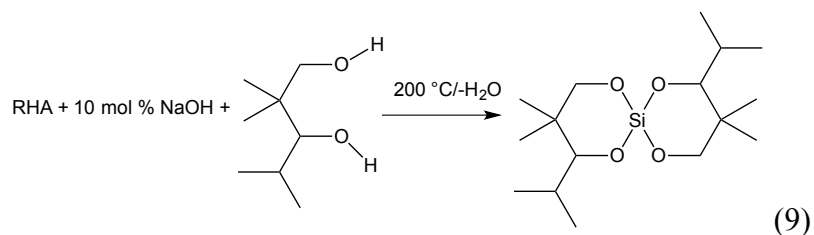
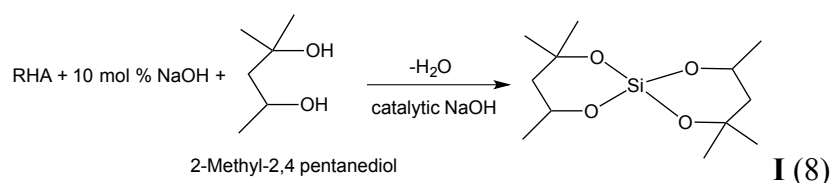
In relatively recent work, Manoso et al¹⁰ and later Jung et al¹¹ found that -78°C aryl lithium and -30°C Grignard reagents react with TEOS or $\text{Si}(\text{OMe})_4$ (TMOS) to produce monofunctional alkoxy silanes, $\text{RSi}(\text{OR})_3$. In these studies it was found that low temperature reaction conditions, excess TEOS (> 2 equiv) and low temperature quenching are key aspects in obtaining monofunctional products. Manoso et al also found that nucleophilic substitution reactions worked best with electron poor as opposed to electron rich aryl reagents, which are more reactive and tended to form R_2Si , R_3Si and R_4Si as found by Corriu.. They also reported that reaction time has little influence on reaction products and yields, regardless of temperature and $\text{RLi}(\text{MgBr})\text{:TEOS}$ stoichiometries (e.g. even at 1:3 ratios) always providing some quantities of di- and tri-alkoxy silanes. In contrast to the work of Tour, these researchers quenched with water at -78°C prior to allowing the reactions to warm to room temperature. It appears that warming before quenching makes quite a difference in the spectrum of products.

Our interest in this area is driven by the need to develop new ways to make arylsilsesquioxanes given our extensive work on their properties.¹⁷⁻²² We have previously reported the facile synthesis of pentacoordinated spiro silicates from any silica source in ethylene glycol.²³ The glycolato silicate of reaction (6) can be isolated in quantitative yield and appears to be quite stable suggesting that spiro siloxanes might be better candidates for stabilizing the mono-functionalized species as suggested by reaction (7).



Thus, our recent discovery of the direct depolymerization of biogenic silica sources such as rice hull ash (RHA) to produce spiro siloxanes per reactions (8) and (9) offered an exceptional opportunity to develop greener routes to special mono- and di-functional

silicon containing compounds. We report here our first successful efforts to develop such routes.



3.3 Experimental Methods

Synthetic methods and characterization procedures are given above in Chapter 2.

3.4 Results and Discussion

In the following sections we first discuss the substitution reactions of PhLi with **I**, and analyze the effects of temperature and quenching on the final structures. This is followed by studies on the stoichiometric reactions of various other RLi reagents (i.e. phenylacetylenyl, anthracenyl, etc.) with **I** and characterization studies. The reactions of PhLi with tetraethoxysilane (TEOS) are also discussed. Lastly, several examples are given using R-**I** to synthesize novel silsesquioxanes by fluoride catalyzed cage formation.

3.4.1 Reactions with Spirosiloxane **I**

Our first steps in these efforts were to extend the work of Manoso et al and Jung et al to our system to compare the reactions of TEOS with those of **I** produced per reaction (8).^{10,11} As such, studies were initiated using stoichiometric PhLi/Et₂O/-78 °C to arylate **I** resulting in facile formation of mono-substituted Ph**I**Li (reaction 10). Figure 3.1 presents the MALDI-ToF spectrum taken by spotting the -78 °C unquenched reaction mixture directly on a sample plate just prior to analysis.

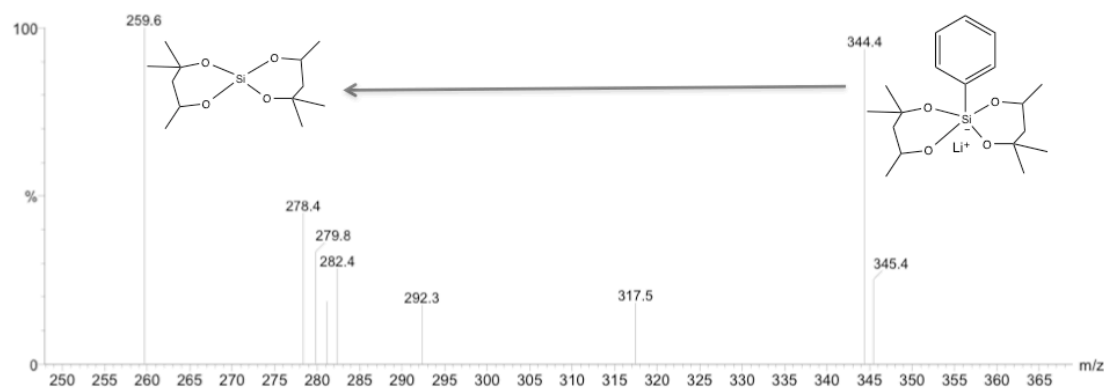
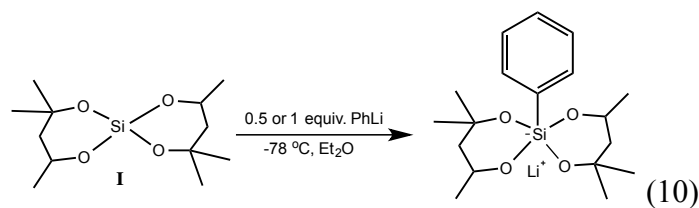


Figure 3.1. MALDI-ToF of 1:1 Spirosiloxane (**I**):PhLi (-78 °C), $m/z \approx 344.4$ is the parent ion for $\text{LiPhSi}(\text{2-methyl-2,4-diolato})_2$, which loses PhLi to give **I** at $m/z = 259$.

In contrast, if the above reaction of **I** with PhLi (1:1 ratio) is allowed to warm to ambient without quenching then a quite different product appears, which precipitates out of diethyl ether allowing easy separation from remaining **I**. The ^{29}Si NMR (Figure 3.2) of this product gives a single peak at $\delta = -14.4$ ppm, the literature value,²⁵ typical for tetraarylsilanes. The EI mass spec (Figure 3.3) provides further evidence showing the tetraphenyl product peak at 336.0 m/z . If the same reaction is run with a ratio of 0.5:1 *similar peak distributions* are observed in the EI mass spec.

This product distribution is truly unique, since it tells us something about the reaction itself. Since only monophenyl products are observed at low temperature (Figure 1), it suggests that PhLi reacts with **I** to form a stable pentacoordinated species. On warming this complex then must transfer the phenyl group perhaps by disproportionation or via a “Corriu” proposed intermediate. But this process must occur multiple times to form Ph_4Si as the final product. The sequence is easily avoided by running reactions at low temperatures and quenching with an electrophile before warming, see below.

Another aspect of these studies that seems to have been overlooked previously arises from the fact that Corriu et al. reported that hexacoordinated catecholato spiroxiloxane

reacts with PhMgBr at 35 °C (Scheme I) to give only Ph₄Si. One can envision this reaction sequence to be initiated via a 7 coordinate transition state.^{11,12,21,26,27}

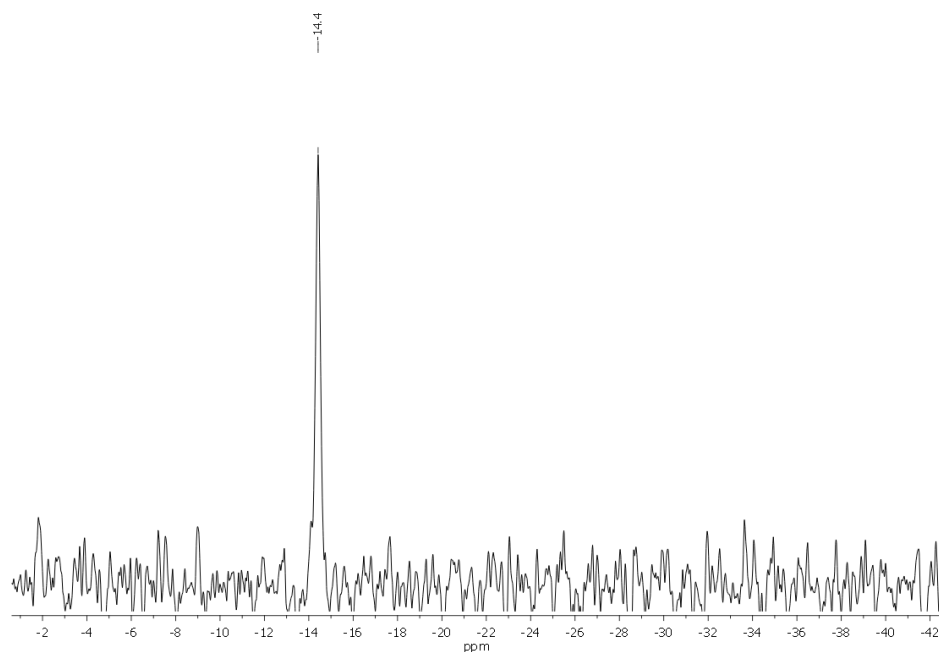


Figure 3.2. ²⁹Si NMR of synthesized tetraphenylsilane, -14.4 ppm, isolated from a 1:1 PhLi:I reaction run at -78 °C then warmed to room temperature without quenching, and then rinsed with diethyl ether to remove excess I.

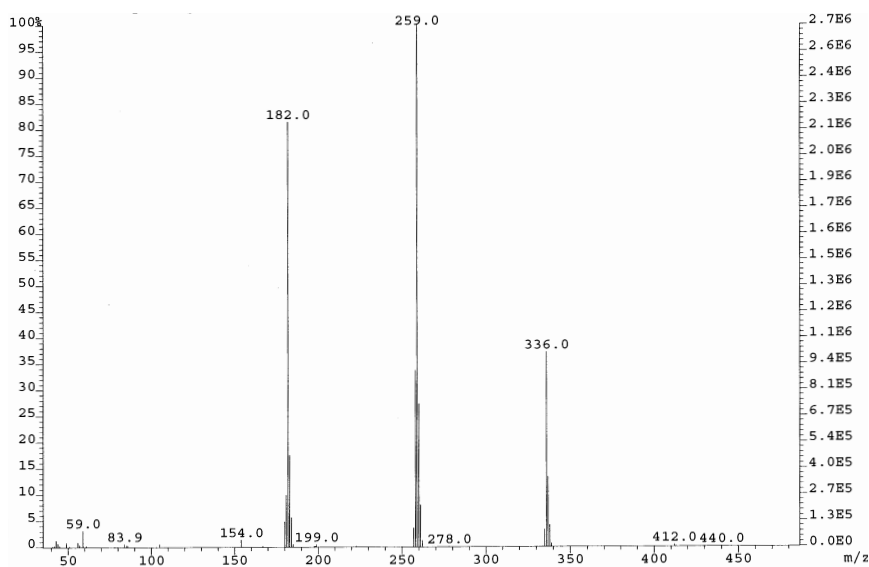


Figure 3.3. EI mass spectrum of tetraphenylsilane isolated from a 1:1 PhLi:I reaction run at -78 °C then warmed to room temperature without quenching, and then rinsed with diethyl ether to remove excess I. Tetraphenylsilane is at 336 m/z. The peak at m/z = 259 is Ph₃Si and the peak at m/z = 182 is Ph₂Si.

On quenching the 1:1 PhLi:**I** reaction with MeI at $-78\text{ }^{\circ}\text{C}$, the resulting products include ring-opened oligomers per the Figure 3.4 negative ion ESI mass spectrum. The 352.9 m/z peak is of the targeted quenched product **II** (Reaction 11), while the other peaks can be ascribed to ring-opened oligomers with structures suggested in Figure 3.4. Byproducts of the substitution reaction such as dimer **III** are also observed in EI-MS at 457.9 m/z (Figure 3.5).

The Figure 3.6 ^{29}Si NMR shows product peaks at -57 ppm likely corresponding to $\text{PhSi}(\text{OR})_3$ [see $\text{PhSi}(\text{OEt})_3$, Table 1] and at $-63\text{ to }-67\text{ ppm}$ likely peaks from

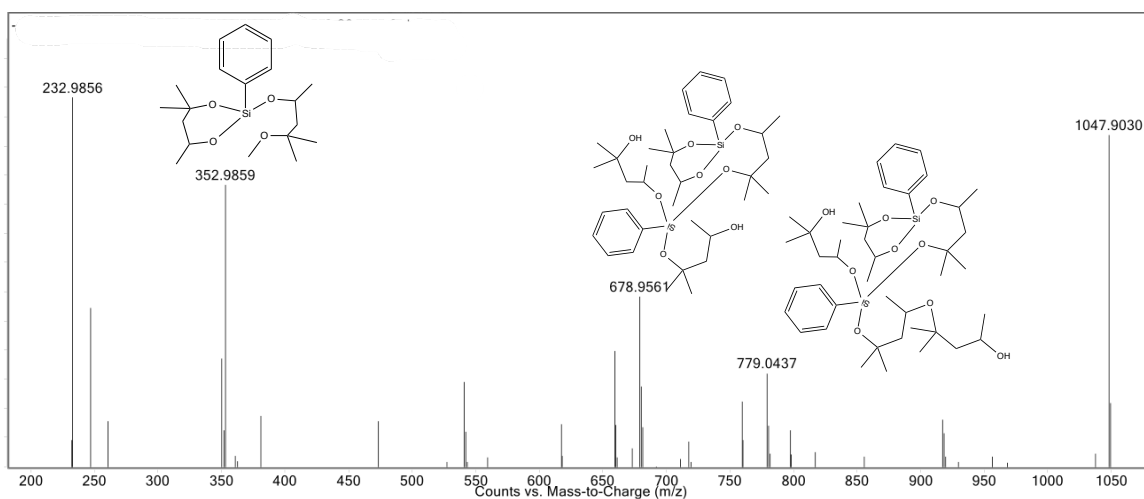
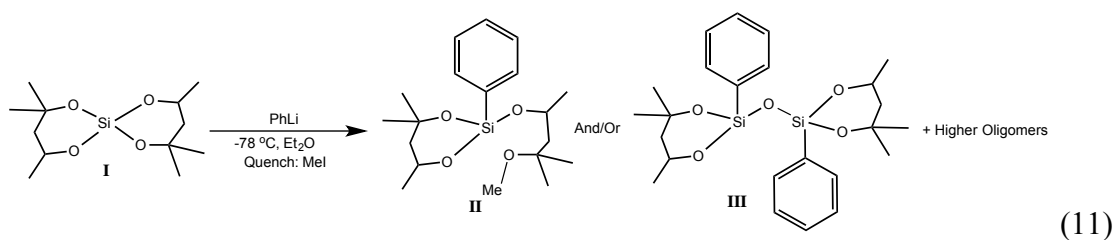


Figure 3.4. Negative ion ESI mass spectrum of 1:1 PhLi:**I** after quenching with MeI.

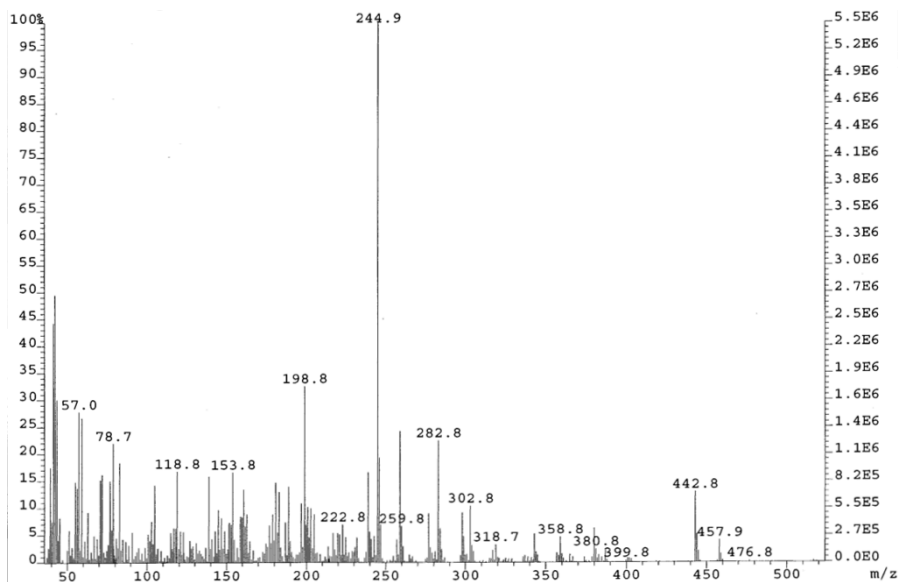


Figure 3.5. EI-MS of 1:1 PhLi:I (3 h, -78 °C) quenched with MeI, peak at 457.9 m/z is III, and peak at 442.8 m/z is III-Me.

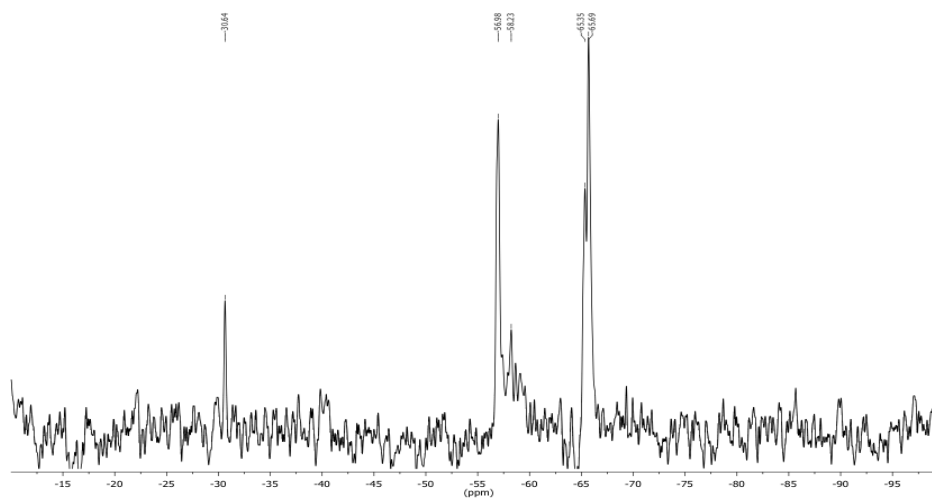


Figure 3.6. ^{29}Si NMR spectrum of the MeI quenched -78 °C 1:1 PhLi:I.

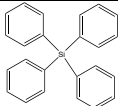
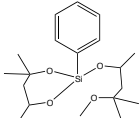
dimeric/oligomeric species containing Si-O-Si linkages (i.e. $[\text{Ph}(\text{RO})_2\text{Si}-\text{O}-\text{Si}(\text{OR})_2\text{Ph}]$) analogous to T_1 species observed in the synthesis of silsesquioxanes.^{28,29} The upfield peaks correspond to $\text{Si}(\text{OR})_4$ species, including residual **I**. Table 3.1 shows literature values for ^{29}Si NMR of various alkoxy silanes.

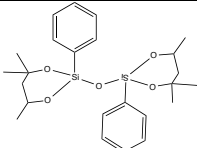
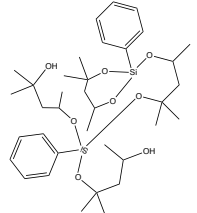
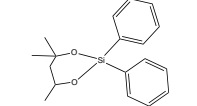
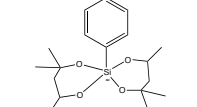
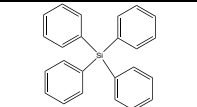
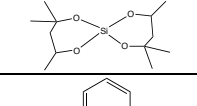
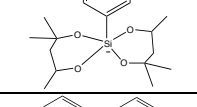
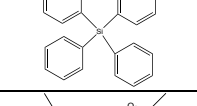
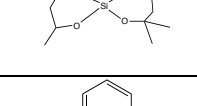
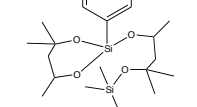
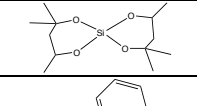
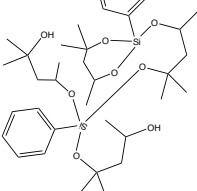
Table 3.1. Literature ^{29}Si NMR chemical shifts of selected alkoxy silanes in CDCl_3 .³⁰

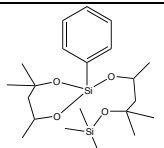
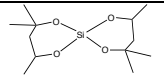
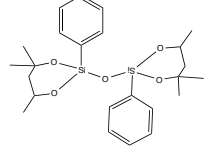
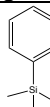
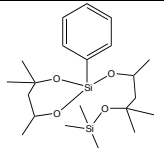
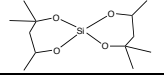
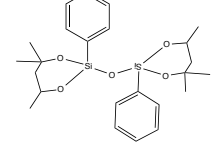
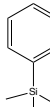
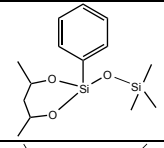
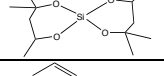
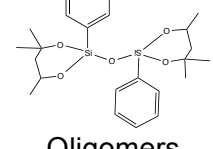
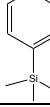
Formula	^{29}Si NMR (ppm)
$\text{Ph}_4\text{Si}^{z'}$	-14.0
Me_3SiOEt	14.5
$\text{Me}_2\text{Si}(\text{OEt})_2$	-4.3
$\text{Ph}_2\text{Si}(\text{OEt})_2$	-32.4
$\text{MeSi}(\text{OEt})_3$	-43.3
$\text{MeSi}(\text{OPr})_3$	-43.3
$\text{EtSi}(\text{OEt})_3$	-44.6
$\text{CH}_2=\text{CHSi}(\text{OEt})_3$	-58.7
$\text{CH}\equiv\text{CSi}(\text{OEt})_3$	-74.7
$\text{PhSi}(\text{OEt})_3$	-57.9
4-MePhSi(OEt) ₃	-57.2
$\text{Ph}(\text{OEt})_2\text{SiOSi}(\text{EtO})_2\text{Ph}^{z',z''}$	-64.9

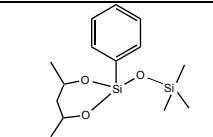
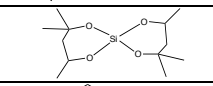
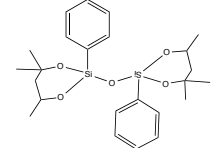
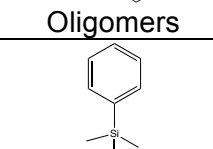
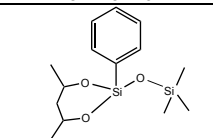
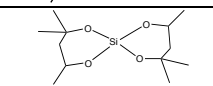
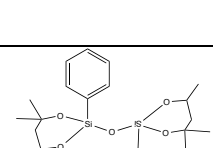
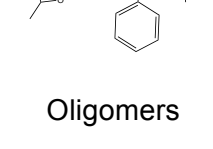
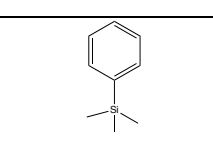
A small peak at -30 ppm likely corresponds to $\text{Ph}_2\text{Si}(\text{OR})_2$ [see $\text{Ph}_2\text{Si}(\text{OEt})_2$ in Table 1]. Note that even at a 1:1 reaction ratio, small quantities of unreacted **I** remain. This is more prevalent in the TMSCl quenched samples discussed below. Though Manoso et al and Jung et al both found good yields (>50%) by quenching the TEOS systems with water; we find that H_2O quenching gives multiple ring opened by-products. To overcome these drawbacks we switched to TMSCl and MeI, reaction (12). Table 3.2 summarizes the $\text{PhLi}:\mathbf{I}$ reaction conditions, % conversions, ^{29}Si NMR, and mass spec results.

Table 3.2. Reaction conditions and observed characterization data for PhenylLi reactions with spiro siloxane, all reactions were conducted at -78 °C for 2 h. (**I** = spiro siloxane).

Rxn ratio	Structures	Observed Mass Spec (m/z)	^{29}Si NMR (ppm)	Quenched	^{29}Si NMR Percent Conversion
1:1 $\text{PhLi}:\mathbf{I}$ (-78 °C)		336.0	-14.4	N	100
1:1 $\text{PhLi}:\mathbf{I}$ (-78 °C)		352.9	-57.0	MeI	100 $\text{Ph}_3\text{Si} + \text{PhSi}(\text{O})_x$

		457.9	-65		
		678.9	$\sim(-65)^*$		
		N/A	-30.6		
		344.4	N/A		
0.5:1 PhLi:I (-78 °C)		336.1	N/A	MeI	N/A
		260.1, 243.2 (M ⁺ -Me)			
		337.1			
0.5:1 PhLi:I (-78 °C)		336.1	N/A	N	N/A
		260.1, 243.2 (M ⁺ - Me)			
0.6:1 PhLi:I (-40 °C)		410.1	18.1, -58.9	Me ₃ SiCl	36 Ph ₁ I + PhSi(O) _x
		260.1	-82.1		
		N/A	-64 to -68		

1:1 PhLi:I (-40 °C, 30 min)		410.1	-58.9	Me ₃ SiCl	46 Ph ₁ I + PhSi(O) _x
		260.1	-82.1		
	 Oligomers	N/A	~ -64		
		N/A	-4.8		
1:1 PhLi:I (-78 °C, 3 h)		410.1	18, -57	Me ₃ SiCl	47 Ph ₁ I + PhSi(O) _x
		259.1	-82		
	 Oligomers	N/A	~ -65		
		N/A	-4.8		
1:1 PhLi:I (-78 °C, 4.5 h)		310.1	9.2, -65	Me ₃ SiCl	88 PhSi(O) _x
		245.1 (M ⁺ -Me)	-82		
	 Oligomers	N/A	-66, -69		
		N/A	-4.8		

1:1 PhLi:I (-78 °C, 6 h)		310.1	-65	Me ₃ SiCl	73 PhSi(O) _x 13 Ph ₂ I
		245.1 (M ⁺ - Me)	-82		
	 Oligomers	N/A	-66, -69		
		N/A	-4.8		
	C ₁₅ H ₂₅ O ₆ Si ₂	357.1	~ -66		
3:1 PhLi:I (-78 °C, 3 h)		310.1	-65	Me ₃ SiCl	68 PhSi(O) _x 8 Ph ₂ I
		245.1 (M ⁺ - Me)	-82		
	 Oligomers	N/A	-65, -69		
		N/A	-4.8		
	C ₁₅ H ₂₅ O ₆ Si ₂	357.1	~ -66		
		N/A	~ -32		

TMSCl quenching is complete in half the time needed for MeI (<30 min) vs MeI (>1 h). Figure 3.7 provides an EI MS for a 3 h reaction quenched with TMSCl. The desired quenched product appears at 410 m/z (**IV**) with the representative ²⁹Si NMR seen in

Figure 3.8. The peak at -58 ppm corresponds to a PhSi(OR)_3 product (**IV**) per Table 3.1, the peak at -82 ppm is remaining **I** and the peak at -4.8 ppm is TMS-benzene, from quenching PhLi. A TMS-O- signal would appear at ~18 ppm but is not seen.

To examine the influence of reaction times; we ran 1:1 PhLi:**I** reactions for 3, 4.5, and 6 h. GPC of this set of reactions show similar peak retention times and shapes for the first two samples, while the 6 h reaction shows a broader peak, perhaps indicative of more extensive ring opening polymerization.

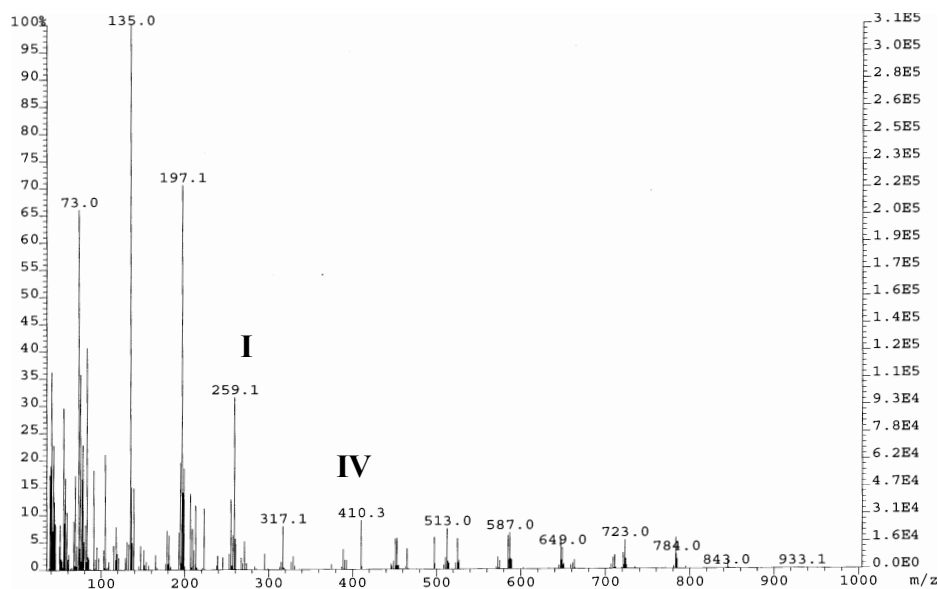
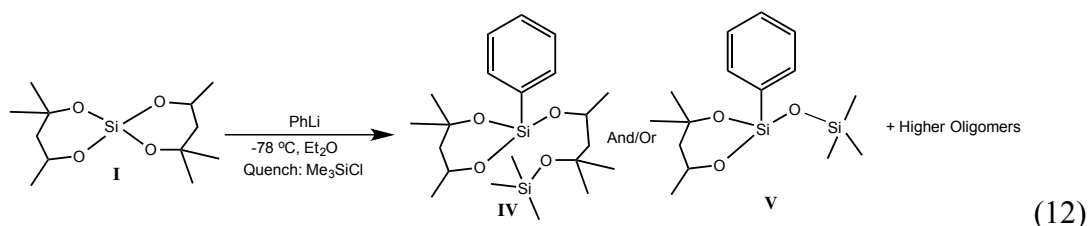


Figure 3.7. EI MS of 1:1 PhLi:**I** after quenching with TMSCl; peaks: 410.3 m/z is **IV**, 259.1 is **I**.

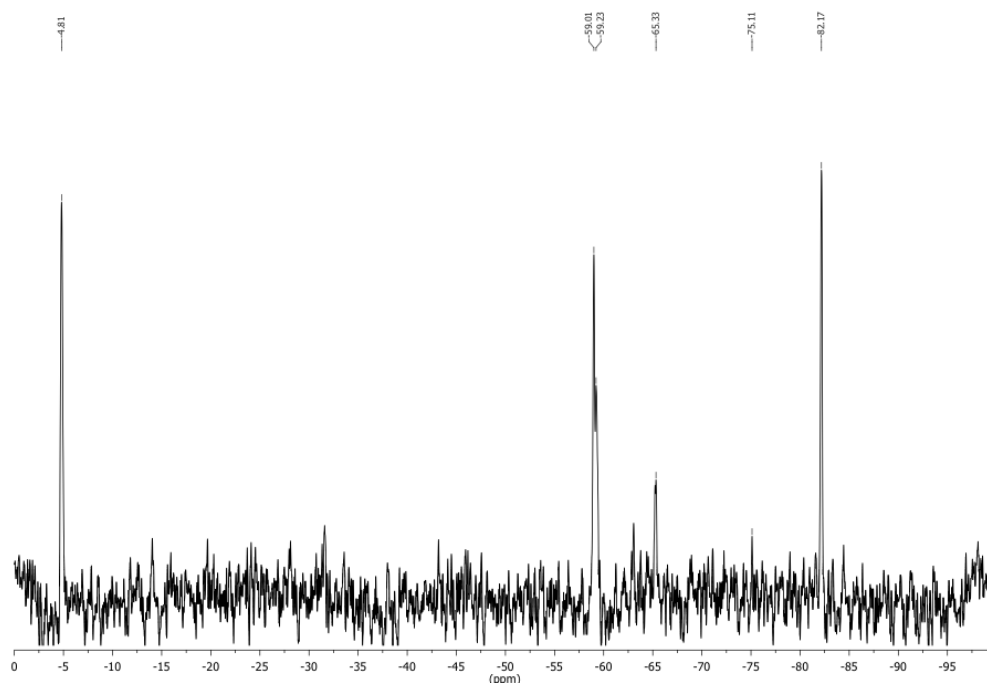


Figure 3.8. ^{29}Si NMR spectrum of the TMSCl quenched $-78\text{ }^\circ\text{C}$ 1:1 PhLi:I. Peaks: -4.8 ppm, TMS-benzene; -59 ppm $\text{PhSi}(\text{RO})_3$; -65 ppm $\text{Ph-Si-OSiMe}_3(\text{OR})_2$.

Mass spectral analysis reveals two new peaks at 310 m/z (**V**, $-\text{Me}$ peak at 295 m/z) and 357 m/z (high resolution mass spectral analysis indicates a formula of $\text{C}_{15}\text{H}_{25}\text{Si}_2\text{O}_6$, however we are unable to assign a structure for this formula). The 357 m/z peak is also more intense after 6 h vs the 4.5 h reaction. Figure 3.9 shows an exemplary EI mass spectrum of the 4.5 h sample. The Figure 3.10 ^{29}Si NMR for the 4.5 h reaction presents strong peaks in the ~ -65 ppm region, suggesting oligomers similar to those found in the MeI quenching studies.

One possible explanation for the formation of **V** and the Si-O-Si linkages in oligomeric derivatives is through cleavage of C-O bonds on the diol subunits during quenching. This would produce Si-O^- or Si-OH, which thereafter reacts with an electrophile (TMS), and a chloro-substituted alkyl (from diol) is made as a byproduct. Such reactions are observed for Michaelis-Arbuzov rearrangement reactions with phosphorus,³¹ and as suggested in the synthesis of phenylsilsesquioxane from phenyltrichlorosilane.³²

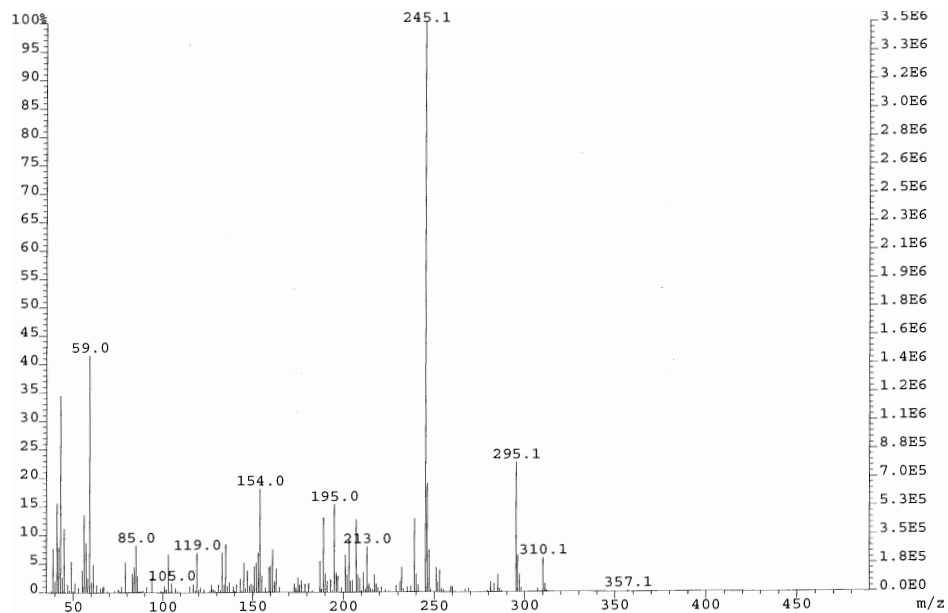


Figure 3.9. EI mass spectrum of 1:1 PhLi:I (4.5 h, -78 °C), quenched with TMSCl; **I**-Me at 245.1 m/z, **V** at 310.1 m/z, and **V**-Me at 295.1 m/z.

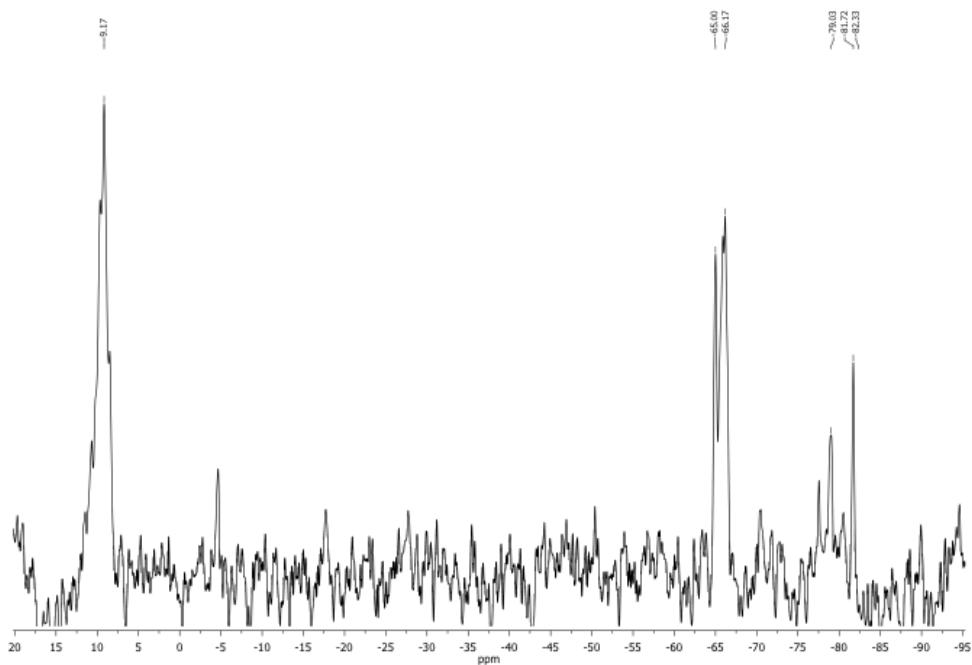


Figure 3.10. ^{29}Si NMR spectrum of 1:1 PhLi:I (4.5 h, -78 °C) quenched with TMSCl, Peaks $\approx 55\text{-}65$ ppm are $\text{PhSi}(\text{O})_x$ units, peak at 9.17 ppm is Si-O-SiMe_3 , peak at -82 ppm is **I**.

A general observation that can be made from all of our studies (see SI for more details) is that there is little change in the product distribution and starting materials no matter what the reaction conditions are chosen (see below) as long as low temperature is maintained. These results suggest equilibration between starting materials and products, contrasting greatly with the discussions present in the reports by Corriu et al, Manoso et al and Jung et al.^{10,11}

In all reaction studies done at -40 °C or below, 1:1 PhLi:I reactions always contain **I** in a nearly 1:1 PhI:I ratio by ²⁹Si NMR . This is especially evident for TMSCl quenched samples. To better understand this relationship; non-stoichiometric PhLi:I, reactions were run at 0.5 and 3.0 equivalents of PhLi. At ratios of 0.5:1 and 1:1, nearly identical product distributions are found for TMSCl quenched samples. At 3 PhLi equivalents, the main product while still only monofunctionalized is now **V**, where one diol subunit is displaced by an -OSiMe₃ unit as detailed above. Though the nature of the monosubstituted products differ, the ratio of products to starting materials changes only slightly and significant amounts of **I** and TMS-benzene are found in the ²⁹Si NMR. This further suggests that a very large excess of PhLi is needed to push the equilibrium toward monosubstituted products. The EI MS is similar to that for 1:1 samples.

Given that Corriu et al suggest that these types of reactions must take place through hexacoordinated intermediates, which may still be true at ambient; our ability to generate only monophenyl substituted products strongly suggests that the primary reaction intermediates generated at low temperatures are pentacoordinated. Reactions run at -60°, - 40°, 0° and 20 °C. Those run at ≤ -40 °C gave monophenyl products at different reaction times, whereas warmer temperatures gave, tetraphenyl or triphenylalkoxysilanes.

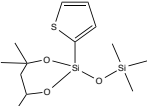
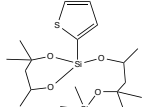
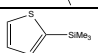
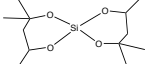
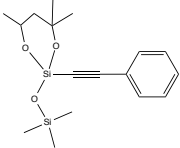
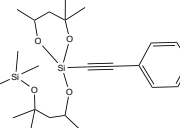
3.4.2 Other Nucleophiles

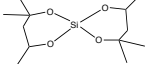
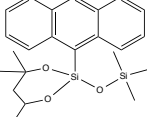
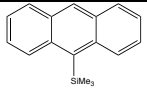
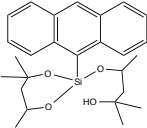
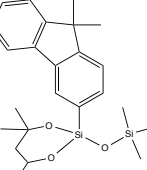
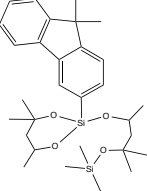
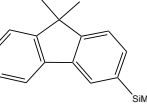
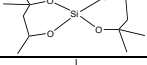
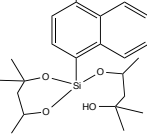
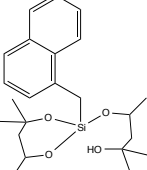
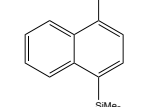
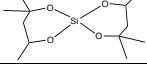
Based on our desire to generate novel silsesquioxanes, we sought to extend these mechanistic studies to other nucleophiles, including: MeLi, n-butylLi, 3-pyridinylLi, Li-TMS-acetylide, Li-acetylide (ethylene diamine complex), thianaphthenylLi, 2-thienylLi, Li-phenylacetylide, 9-anthracenylLi, 9,9-dimethylfluorenylLi and Me-naphthalenylLi. Trial reactions were run with 1.2:1 RLi:I stoichiometry, are un-optimized and are in support of the utility of these reactions. The first five [(MeLi, n-butylLi, 3-pyridinylLi,

Li-TMS-acetylide, Li-acetylide (ethylene di-amine complex)], do not provide observable/isolable monomeric products. Only starting material **I**, ROP byproducts and TMS substituted starting materials are observed by mass spectral analysis and/or ^{29}Si NMR. Grignard reagents were also explored; however either no reaction or unidentifiable products were observed likely resulting from formation of stable pentacoordinated complexes with **I**.^{33,34}

In contrast, 2-thienylli, Li-phenylacetylide, anthracenylli, 9,9-dimethylfluorenylli and Me-naphthalenylli] all gave products that could be characterized by both ^{29}Si NMR and EI mass spec (Table 3.3). Most reactions were run using methods akin to those of Monaso et al,¹⁰ Jung et al,¹¹ and those for PhLi above, in which an arylbromide is first converted to a lithium reagent via exchange with n-butylli, followed by addition of **I** (structures **VIII-X**). The ^{29}Si NMR and EI mass spec for each of these compounds are presented in Appendix C, Figures C1-C7.

Table 3.3. Reaction conditions and observed characterization data for RLi reactions with **I**, all reactions were conducted at -78 °C for 3h and quenched with Me₃SiCl unless otherwise noted.

Rxn ratio/Conditions	Structures	Observed Mass Spec (m/z)	^{29}Si NMR (ppm)	~% Conversion (^{29}Si NMR)
1.2:1 2-thienylli: I (VI) 0 °C		316.2	6.66, -62.58	18
		416.8	13.24, -62.06	
		156.3	-7.2	
		245.1 (M ⁺ -Me)	-82	
1.2:1 Li-phenylacetylide: I (VII) 25 °C		334.0	-78.8	100
		434.1	-78.3	

		245.1 (M ⁺ -Me)	-82	
1.2:1 anthracenylLi:I (VIII)		272.3	-57.9	100
		250.1	-2.9	
				
1.2:1 9,9-dimethylfluorenylLi:I (IX)		334.0	N/A	16
		434.1	-52.6	
	Dimer/Oligomers	N/A	-65.8	
		251.0 (M ⁺ -Me)	-4.8	
		245.1 (M ⁺ -Me)	-82.4	
1.2:1 Me-naphthalenylLi:I (X)		402.2	14.7, -57.5	23
		402.2	-46.1	
		-	-5.8	
		-	-82	

The nucleophilic reactions with the best conversions from **I** were (~100%) for the anthracenylLi:**I** (Reaction 13) and Li-phenylacetylde:**I** reactions; no **I** remained in either case by ^{29}Si NMR. The 2-thienylLi:**I** (**VI**) shows ~18% conversion of **I** by ^{29}Si NMR and two types of products as discussed above for Ph**I** reactions (13.2, 6.2, -62 ppm), in which the TMS quenching group is either attached to the diol, or directly attached to the central Si atom (Si-O-TMS), see Table 3.3. The Li-phenylacetylde:**I** (**VII**) reaction with **I** at room temperature gives ~100% conversion by ^{29}Si NMR (-78 ppm), with no remaining spiro-siloxane observed, and with product peaks in EI-MS at 334.0 and 434.1 m/z for the two monomeric structure types respectively (Table 3.3). The 9,9-dimethylfluorenylLi:**I** (**IX**) reaction shows ~15% conversion of **I** by ^{29}Si NMR (-52.6 and -65.0 ppm) and a clear peak in EI mass spec at 426.1 m/z for an Si-O-TMS structured monomeric product (Table 3).

Lastly, Me-naphthalenylLi:**I** (**X**) shows ~29% conversion of **I** to Me-naphthyl products by ^{29}Si NMR (-46.1, -57.5 ppm). The peak at -57.5 ppm corresponds to the expected structure formed by lithium-bromide exchange on 1-bromo-4-methylnaphthalene starting material, followed by direct attack of **I** (see Table 3.1 for examples). The peak at -46.1 ppm, is attributed to the product from deprotonation of the methyl- group by either n-butylLi or 4-methylnaphthalenylLi (due to its lower pKa), and attack by the methylenylLi group on **I**.

Alkyl-triethoxysilanes typically give ^{29}Si NMR peaks in the -45 ppm region (Table 3.1). By EI-mass spec only one product mass is observed at 402.2 m/z. This peak could correspond to both products observed by ^{29}Si NMR since they would have the same molecular formula. Note also that the observed mass is for a proton-quenched derivative, instead of being quenched with TMS (Table 3.3). This transfer may have occurred during the aqueous workup used to remove salts or is a result from incomplete quenching.

As an example, Figure 3.11 shows the EI mass spec for anthracenyl**II** (**VIII**) quenched with Me_3SiCl , with the product peak [M] at 410.2 m/z and [M-TMS] at 338.1 m/z. Figure 3.12 shows the ^{29}Si NMR of **VIII**, with the product peaks at 10.0, and -57.4 ppm, and TMS-anthracene at -2.87 ppm. Silsesquioxanes of **VIII** will be discussed in that section.

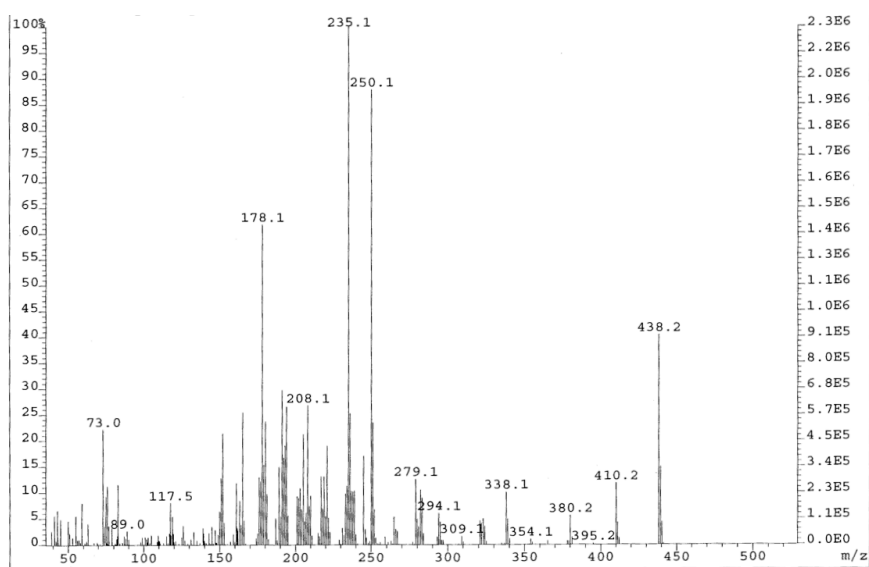
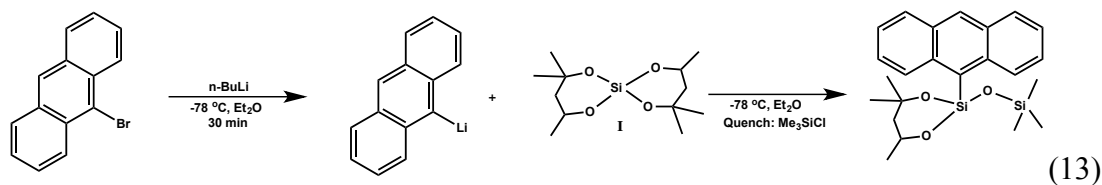


Figure 3.11. EI mass spectrum of anthracenylLi:I (3 h, -78 °C), quenched with TMSCl; VIII at 410.2 m/z, VIII-Me at 395.2 m/z, VIII-TMS at 338.1 m/z, 438.2 is VIII without TMS group.

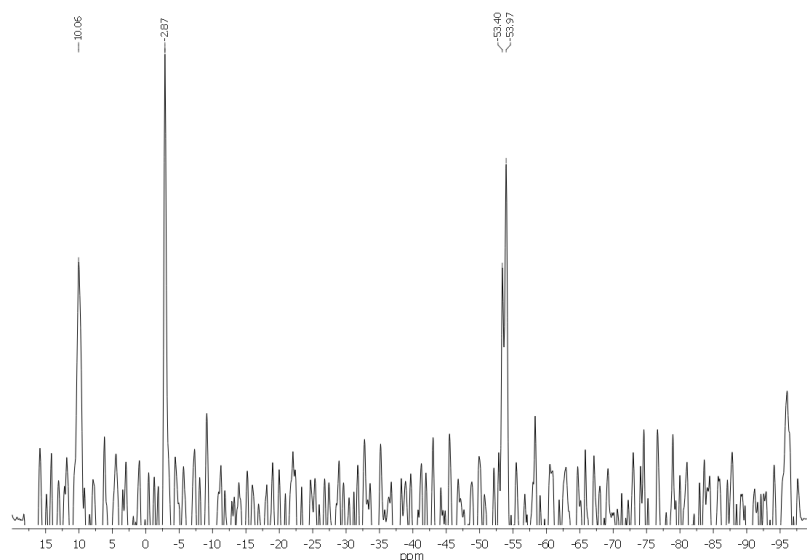


Figure 3.12. ^{29}Si NMR of 1:1 anthracenylLi:I (3 h, -78 °C, VIII) quenched with TMSCl, peak at 57.4 ppm is R-Si(OR)₃, peak at 10.0 ppm is Si-O-SiMe₃, peak at -2.8 is TMS-anthracene, I is unobserved at -82 ppm.

As with the PhI derivatives, no simple method was found to isolate monomeric products from **I**. For example bulb-to-bulb distillation led to distillation of **I** and functionalized products simultaneously. This is also similarly observed in distilling **I** from diol.²⁴ The reactions that give low conversions also tend to show TMS-R byproducts from quenching, likely due to equilibration between **I** and RLi as found with PhLi. Future work will look at developing effective separation techniques and/or optimizing reaction conditions to make separation unnecessary.

3.4.3 Nucleophilic Substitution at TEOS

For comparative purposes, we also used Si(OEt)₄ in place of **I**. These reactions gave slightly different product distributions that were also highly temperature dependent. For example, Ph:**I** reactions favor mono- or tetra-functionalization with little di- or trifunctionalization regardless of starting material ratio at temperatures below -40 °C. Ph:TEOS reactions result in a mixture of mono and difunctional products, with unreacted TEOS also remaining in 1:1 PhLi:TEOS systems at -78 °C. In general, reactions run < -40 °C favor mono- and di-functionalization, At 0 °C di- and trifunctionalization are favored, and above 0 °C Ph₄Si is favored. As with Ph:**I**, Ph:TEOS reactions were quenched with MeI or TMSCl before warming per conditions listed in Table 3.4. Thus, a -78 °C 1:1 PhLi:Si(OEt)₄ reaction quenched with MeI after 4 h gives the EI mass spectrum shown in Figure 3.13.

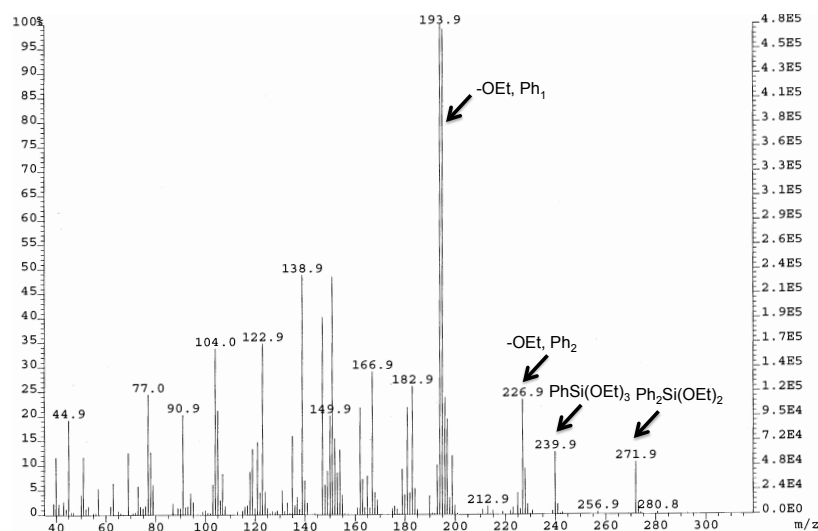


Figure 3.13. EI mass spectrum of 1:1 PhLi:TEOS after quenching with MeI at -78 °C.

As seen in Figure 3.13, the $\text{PhSi}(\text{OEt})_3$ parent ion appears at $m/z = 240$, $\text{Ph}_2\text{Si}(\text{OEt})_2$ appears at $m/z = 272.3$ and $\text{PhSi}(\text{OEt})_2$ at $m/z = 194$ after losing ethoxy and the peak at $m/z = 227$ corresponds to the diphenyl species missing an EtO group. Unfortunately, peak intensities in mass spectra do not permit quantification of the individual species. However, the ^{29}Si NMR provides a somewhat more accurate estimation of the species present. Thus, Figure 3.14 indicates that at $-78\text{ }^\circ\text{C}$, at a 1:1 ratio of $\text{Si}(\text{OEt})_4$:PhLi, the products are $\text{PhSi}(\text{OEt})_3$ (-58 ppm), $\text{Ph}_2\text{Si}(\text{OEt})_2$ (-32 ppm) and $\text{Si}(\text{OEt})_4$ (-82 ppm). The diphenyl product seems to form in smaller amounts at this temperature compared to $-40\text{ }^\circ\text{C}$. The ratio of species can be controlled to some degree. Thus, $0\text{ }^\circ\text{C}$ favors formation of Ph_3SiOEt . At $-78\text{ }^\circ\text{C}/4\text{ h}$ quenching with MeI (30 min) or TMSCl gives similar results.

One might argue based on Corriu's work that we should not see any mono or diphenyl products, yet that is all that is seen. However, Monaso et al's work suggests we might expect to see the monophenyl products. Note that Monaso et al used excess $\text{Si}(\text{OEt})_4$ at $-78\text{ }^\circ\text{C}$ as such, we also explored the use of excess alkoxysilanes discussed further below.

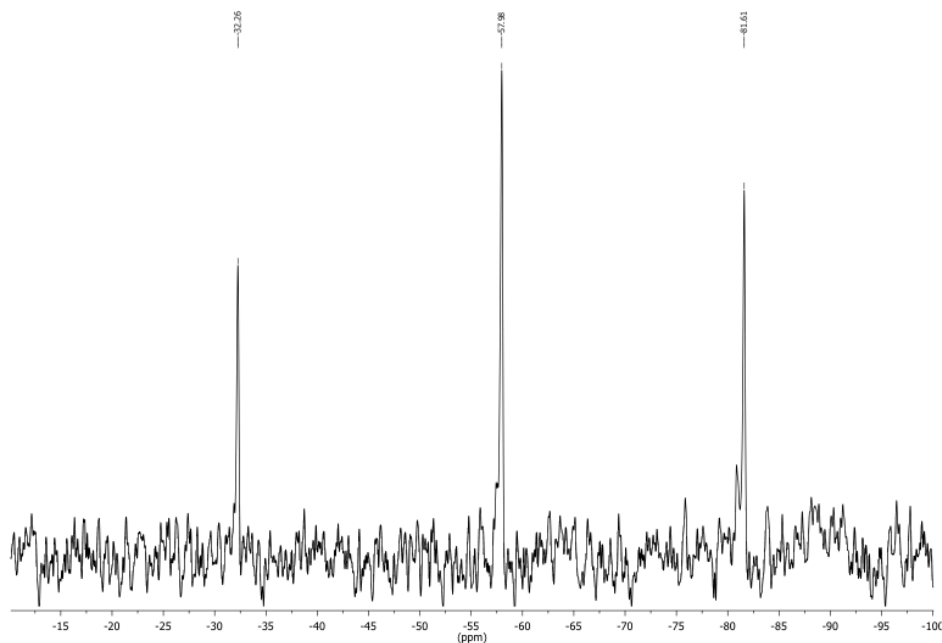
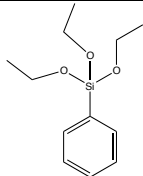
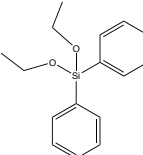
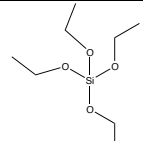
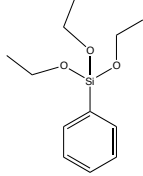
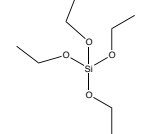
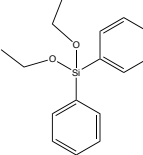
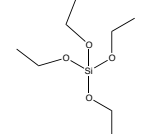
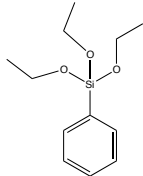
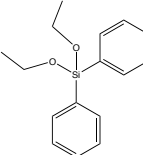


Figure 3.14. ^{29}Si NMR of 1:1 Ph:TEOS, -32.2 (18% Ph_2TE), -57.9 (Ph_1TE), -81.6 (TEOS) after quenching with MeI.

Table 3.4. Reaction conditions and observed characterization data for PhenylLi reactions with TEOS, all reactions were conducted at -78 °C or -40 °C for 30 min – 2 h. (TE = TEOS).

Rxn ratio/Conditions	Structures	Observed Mass Spec (m/z)	²⁹ Si NMR (ppm)	Quenched	~% Conversion (²⁹ Si NMR)
1:1 Ph:TE (-78 °C)		239.9	-57.9	MeI	45% Ph ₁ TE, 18% Ph ₂ TE
		271.9	-32.2		
		N/A	-81.6		
0.5:1 Ph:TE (-78 °C)		240.1	-57.9	MeI	34% Ph ₁ TE, 12% Ph ₂ TE
		208.1	-81.6		
0.5:1 Ph:TE (-78 °C)		272.3	N/A	No	N/A
		208.1			
0.6:1 Ph:TE (-40 °C)		240.1	-58.7	Me ₃ SiCl	26% Ph ₁ TE, 18% Ph ₂ TE
		N/A	-32.8		

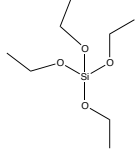
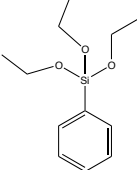
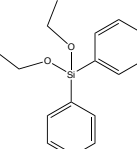
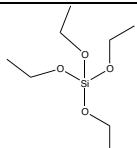
		208.1	-82.4		
1:1 Ph:TE (-78 °C)		240.1	-58.7	Me ₃ SiCl	49% Ph ₁ TE, 15% Ph ₂ TE
		N/A	-32.8		
		208.1	-82.4		

Figure 3.15 shows the EI spectrum of 0.5:1 PhLi:TEOS at -78 °C, with the peak at 240.1 m/z corresponding to PhSi(OEt)₃ and the peak at 208.1 m/z corresponding to unreacted TEOS. The peak heights suggest that the ratios are \approx 1:1, which is expected for a 0.5:1 reaction of PhLi:TEOS. Figure 3.16 shows the ²⁹Si NMR spectrum of the above reaction, in which PhSi(OEt)₃ is observed at -58 ppm, TEOS at -82 PPM, and Ph₂Si(OEt)₂ at -33 ppm. If this reaction is not quenched with MeI or TMSCl before warming up (Figure 3.16), the mass spectrum shows Ph₂Si(OEt)₂ at 272.3 m/z as the main phenyl product, as well as unreacted TEOS at 208 m/z. This shows the importance of quenching the reaction at low temperature before workup. But it also suggests a mechanism to make difunctional compounds that was not clear from previous work but was suggested by the work of Tour et al.⁷

We also explored 0.6:1 PhLi:TEOS systems at -40 °C, the results of which are similar to those at -78 °C, but at a fraction of the reaction time (30 min vs. 4 h). We see Ph₂Si(OEt)₂:PhSi(OEt)₃:TEOS distributions similar to those for the 1:1 reaction at -78 °C in the ²⁹Si NMR spectra.

Furthermore, at 0.5:1 PhLi:TEOS at 0 °C we observe Ph₃Si(OEt) as the dominant species by EI mass spec. This is expected, as higher temperatures favor further functionalization in the spiro-siloxane studies.

The most important observation is that even at low temperatures and sub-stoichiometric PhLi:TEOS ratios, the reaction products still contain Ph₂Si(OEt)₂ in considerable quantities, as found by Monaso et al.¹⁰ These results seem to at least partially support a hexacoordinated silicon mechanism of nucleophilic attack. However, PhSi(OEt)₃ is still present so there likely exists an equilibrium between the three species (Ph₂Si(OEt)₂:PhSi(OEt)₃:TEOS), involving pentacoordinated intermediates through the transfer of PhLi.

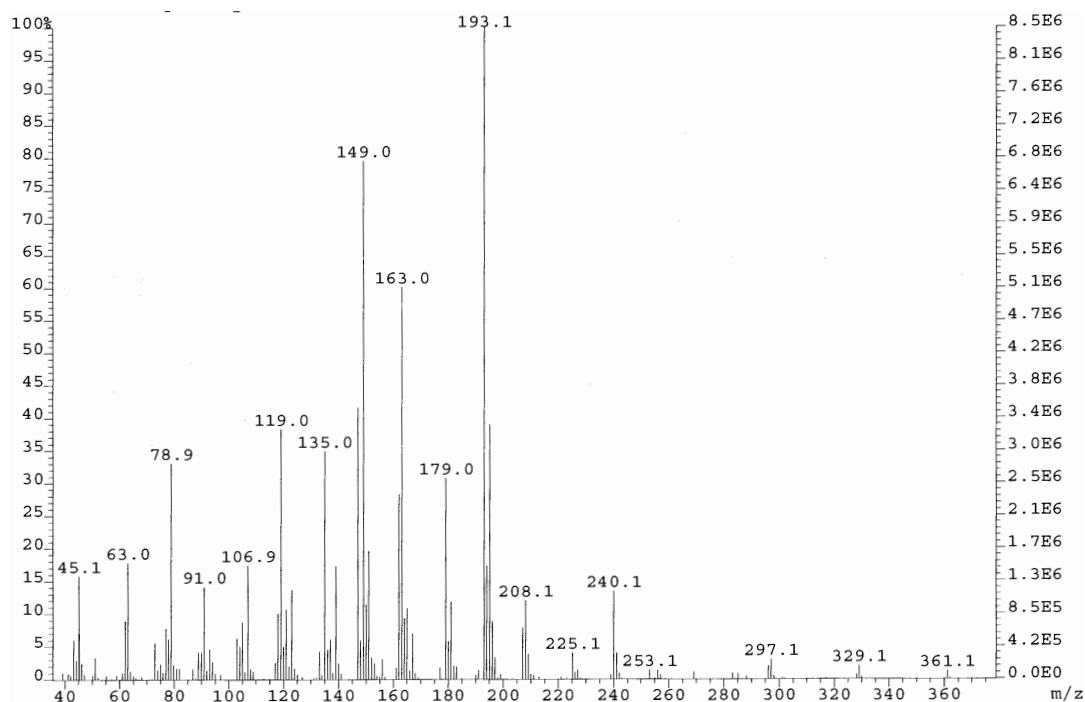


Figure 3.15. EI mass spectrum of 0.5:1 PhLi:TEOS at -78 °C (2h) after quenching with MeI. PhSi(OEt)₃ is at 240.1 m/z, TEOS is at 208.1 m/z, both of ~equal peak height.

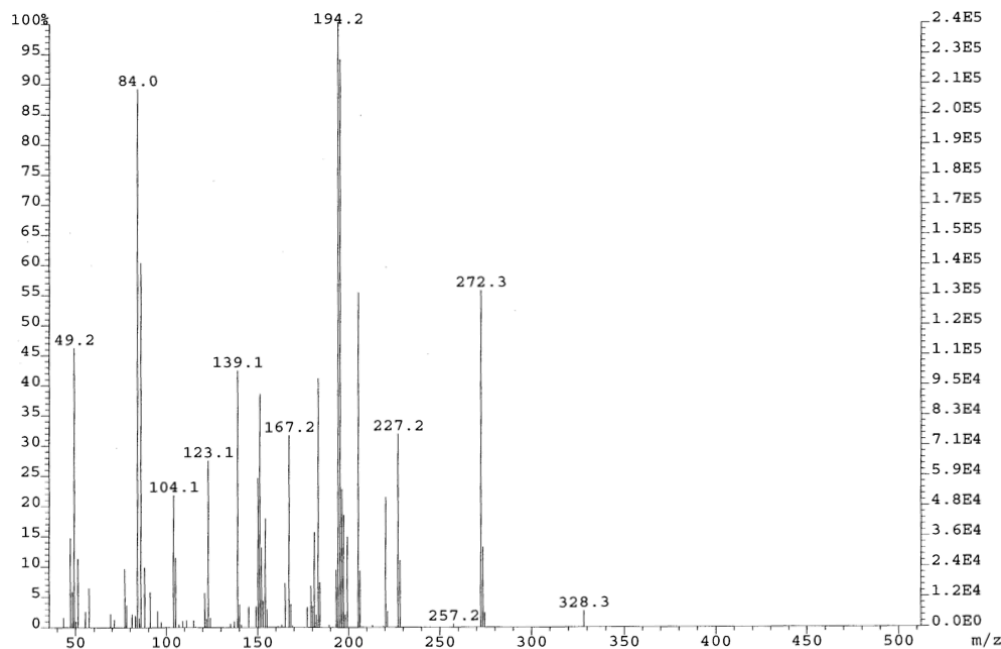


Figure 3.16. EI mass spectrum of 0.5:1 PhLi:TEOS at -78 °C (2h) without quenching, 272.3 m/z is Ph₂Si(OEt)₂.

3.4.4 Summary of Findings

In these studies on nucleophilic substitution of **I** and TEOS, we find that reaction temperature, and low temperature quenching are extremely important to achieve monosubstitution. However, contrary to previous studies, we find that **I** reacts with excess (3 equiv) of RLi still generates monofunctional products. We also find that at low temperatures, monofunctional-alkoxysilanes form exclusively, and then on warming PhLi must transfer to the other monofunctional-alkoxysilanes and then to difunctional-, etc. until only Ph₄Si and **I** remain. This suggests that temperature influences the nature of attack on **I**; at < -40 °C unsubstituted **I** is more most reactive, and at > -40 °C R-**I** is most reactive toward nucleophilic attack. A change in mechanism is likely around this point.

3.4.5 Silsesquioxane Synthesis

To verify the utility of the materials made by nucleophilic substitution of **I**, we explored the synthesis of phenylSQs and anthracenylSQs (Reaction 14). The first step was to learn to purify the products. **I** and **IV** can be recovered in a mixture after vacuum distillation, but are very difficult to separate further. However, if the 1:1 PhLi:**I** reaction is run longer than 3 h/-78 °C then oligomeric materials result that do not distill. Treating these oligomeric materials with catalytic TBAF (see experimental) provides cage

compounds.^{21,22} Thus GPC (Figure 3.17) and MALDI-ToF (Figure 3.18) analyses verify the formation of a mixture of PhT_{8,10,12} and some partial cages, which could be separated by selective solubility.

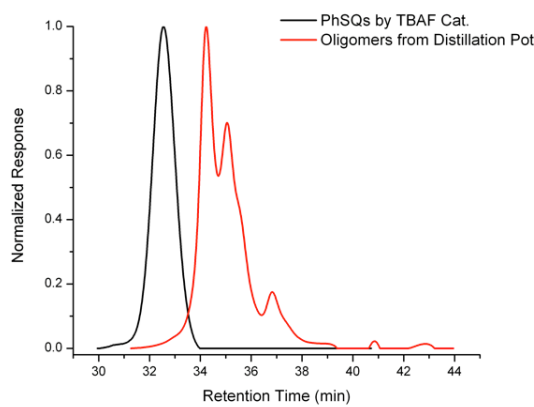
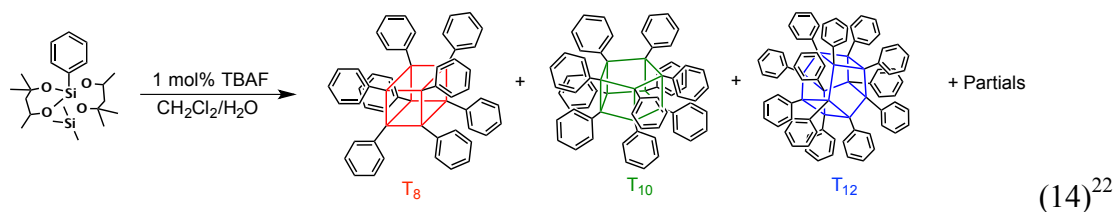


Figure 3.17. GPC trace comparison of oligomeric materials from 1:1 PhLi:I (6 h) compared with an overnight TBAF catalyzed PhSQ synthesis.

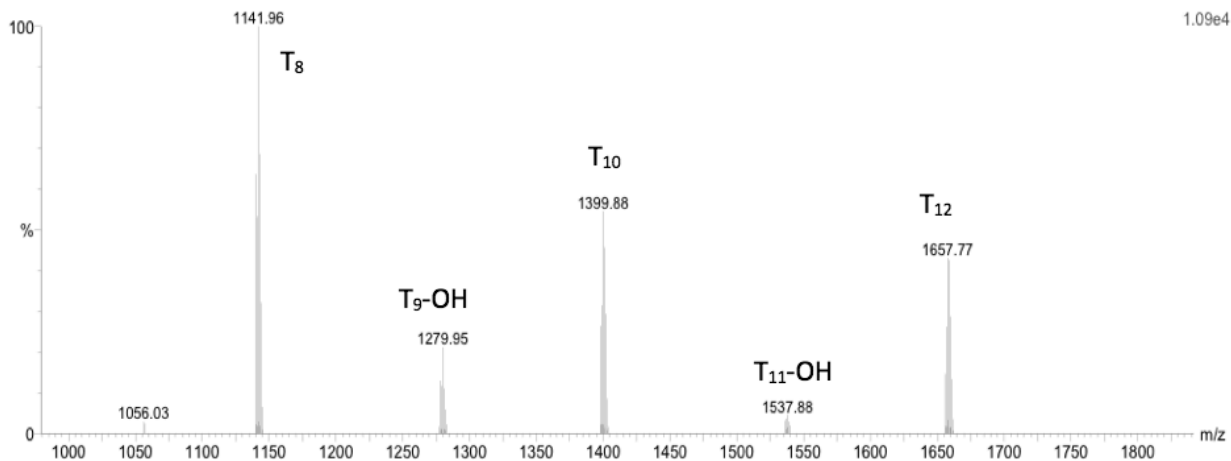


Figure 3.18. MALDI-ToF spectrum of PhSQs made by TBAF catalyzed reaction of PhI oligomers; all peaks are Ag⁺ ions.

AnthracenylSQs were made by the same method described for phenylSQs. These are exciting systems since no known anthracenylSQs have been reported. The isolated cage yield was ~58%. Figure 3.19 shows the MALDI-ToF spectrum of the anthraceneSQ cage mixture. The size of anthracene leads to formation of many partial cages, with T₇-OH as the predominant compound, with some T₈. Note the formation of the TMS derivative as a byproduct from the quenching process (1525.6 m/z); alternative-quenching methods such as MeI would prevent these byproducts.

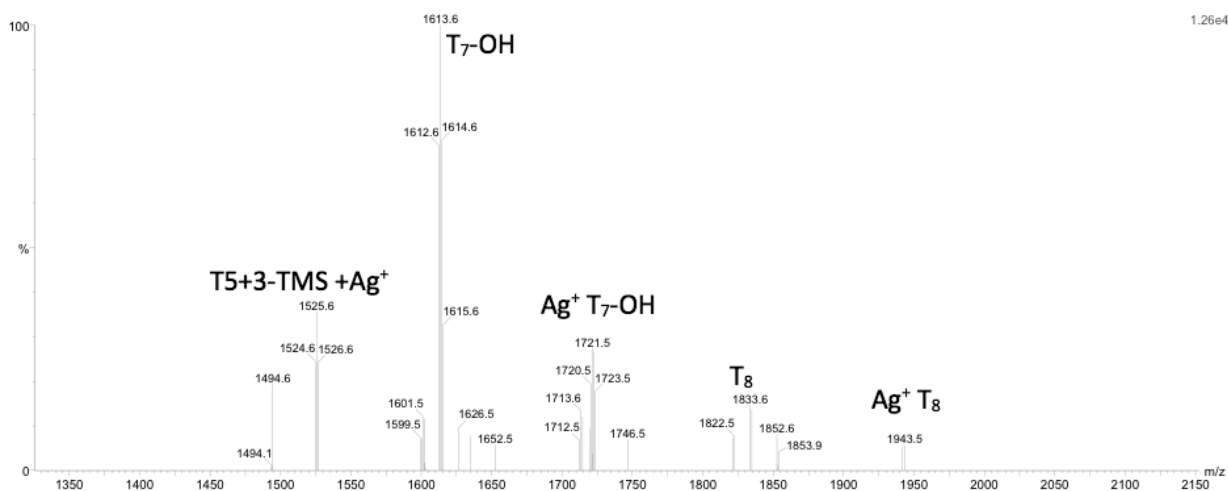


Figure 3.19. MALDI-ToF spectrum of anthraceneSQs made by TBAF catalyzed reaction of AnthraceneI (VIII).

Since anthraceneSQ is a new compound with potentially interesting photophysical properties, we explored the absorption and emission behavior, see Figure 3.20. The absorption and emission are both red-shifted from the parent anthracene by 10 and 25 nm respectively.³⁵ This and other exciting new cage systems derived from these studies will be explored in the future.

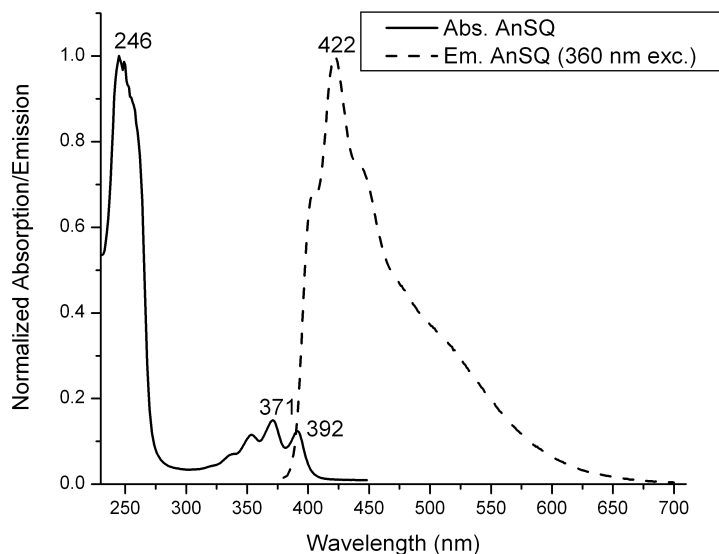


Figure 3.20. Absorption and emission spectra of anthraceneSQ.

3.5 Conclusion

We have illustrated an important development in siloxane chemistry, in which we can go from a biosourced silica (RHA) to functional alkoxy silanes. Our method uses R-Li nucleophiles at low temperatures to functionalize spiro siloxanes made from RHA, which when quenched with an electrophile such as MeI or Me₃SiCl give mono-R-alkoxy silanes; and unquenched give tetra-R-silanes with reasonable conversions. We propose that the mechanism of nucleophilic substitution takes place through a pentacoordinate intermediate below -40 °C, which if unquenched and warmed to room temperature is capable of transferring PhLi. We find that aryl halides can be easily converted to Li reagents, which can then undergo nucleophilic substitution on spiro siloxanes, while alkylLi reagents and Grignard reagents do not give clear substitution. Alkynyl derivatives such as phenylacetylene also show clean substitution with ~100% conversion of the spiro siloxane to a mono functional derivative. We have further demonstrated that silsesquioxanes can be made from mono-functional spiro siloxanes, with a never before observed anthraceneSQ.

With this class of materials, we can envision making new functionalized silsesquioxanes directly from most any aryl halide, as well as the possibility for other hybrid polymeric materials. Control to achieve di-substituted (mono and di-functional)

materials selectively can also be imagined for making new classes of siloxane polymers, all this while avoiding the use of chlorosilanes.

References:

1. E. G. Rochow, "The Direct Synthesis of Organosilicon Compounds" *J. Am. Chem. Soc.* **1945**, *67*, 963-965.
2. William H. Daudt. Production of Phenyltrichlorosilane, U.S. Patent 2,576,448, Nov. 27, 1951.
3. T. J. Barton, P. Boudjouk, "Organosilicon Chemistry. A Brief Overview," *Silicon-Based Polymer Science*, Chapter 1, *Advances in Chemistry*, **1989**, *224*, 3-46.
4. The Chemistry of Organic Silicon Compounds Z. Rappoport Y. Apeloig, eds., J. Wiley & Sons Ltd. London, 1998 Parts 1-3.
5. McBee, E. T.; Roberts, C. W.; Judd, G. F.; Chao, T. S. Reaction of Grignard Reagents with Alkoxysilanes at Elevated Temperatures. *J. Am. Chem. Soc.* **1955**, *77*, 1292-1293.
6. George, P. D.; Sommer, L. H.; Whitmore, F. C. Steric Effects in Grignard Couplings with Alkoxysilanes 1. *J. Am. Chem. Soc.* **1955**, *77*, 6647-6649.
7. Tour, J. M.; John, J. a.; Stephens, E. B. Convenient Route to Di- and Triorganosilyl Ethyl Ethers and the Corresponding Di- and Triorganosilanes. *J. Organomet. Chem.* **1992**, *429*, 301-310.
8. Silverman, G.; Rakita, P. Handbook of Grignard Reagents Marcel Dekker, 1996 pp 667-675.
9. Klokov, B. a. Continuous and Batch Organomagnesium Synthesis of Ethyl-Substituted Silanes from Ethylchloride, Tetraethoxysilane, and Organotrichlorosilane for Production of Polyethylsiloxane Liquids. 2. Continuous One-Step Synthesis of Ethylethoxy- and Ethylchlorosilan. *Org. Process Res. Dev.* **2001**, *5*, 234-240.
10. Manoso, A. S.; Ahn, C.; Soheili, A.; Handy, C. J.; Correia, R.; Seganish, W. M.; DeShong, P. Improved Synthesis of Aryltrialkoxysilanes via Treatment of Aryl Grignard or Lithium Reagents with Tetraalkyl Orthosilicates. *J. Org. Chem.* **2004**, *69*, 8305-8314.
11. Jung, K.-H.; Kim, S.-Y.; Tan, W.; Shin, D.-S.; Ahn, C. Improved Methods for the Synthesis of Aryltrialkoxysilane Derivatives via Aryllithium and Aryl Grignard Bromide with Tetra-Alkoxysilane. *Bullet. Instit. Basic Sci.* **2005**, *17*, 79.
12. Boudin, A.; Cerveau, G.; Chuit, C.; Corriu, R. J. P.; Reye, C. Reaction of Grignard Reagents with Dianionic Hexacoordinated Silicon Complexes: Organosilicon Compounds from Silica Gel. *Angew. Chemie Int. Ed. English* **1986**, *25*, 474-476.
13. Boudin, A.; Cerveau, G.; Chuit, C.; Corriu, R. J. P.; Reye, C., "Reactivity of Anionic Pentacoordinated Silicon Complexes towards Nucleophiles," *Angew. Chemie Int. Ed. English* **1986**, *25*, 4734.
14. Boudin, a; Cerveau, G.; Chuit, C. Reactivity of Dianionic Hexacoordinated Silicon Complexes toward Nucleophiles: A New Route to Organosilanes from Silica. *Organometallics* **1988**, *7*, 1165-1171.
15. Corriu, R.J. P.; Young, J.C. Chemistry of Organic Silicon Compounds, Patai, S.; Rappoport, Z. eds. Ch. 20, Wiley, Chichester, 1989.

16. Corriu, R.J. P. "Some aspects of the reactivity of hypervalent species of silicon in organic synthesis" *Pure and Appl. Chem.* **1988**, *60*, 99.
17. Laine, R. M.; Roll, M. F. Polyhedral Phenylsilsesquioxanes. *Macromolecules* **2011**, *44*, 1073–1109.
18. Furgal, J. C.; Jung, J. H.; Goodson, T.; Laine, R. M. Analyzing Structure-Photophysical Property Relationships for Isolated T₈, T₁₀, and T₁₂ Stilbenevinylsilsesquioxanes. *J. Am. Chem. Soc.* **2013**, *135*, 12259–12269.
19. Jung, J. H.; Laine, R. M. Beads on a Chain (BOC) Polymers Formed from the Reaction of NH₂ PhSiO_{1.5}] X [PhSiO_{1.5}] 10– X and [NH₂ PhSiO_{1.5}] X [PhSiO_{1.5}] 12– X Mixtures (X = 2–4) with the Diglycidyl Ether of Bisphenol A. *Macromolecules* **2011**, *44*, 7263–7272.
20. Jung, J. H.; Furgal, J.; Iii, T. G.; Mizumo, T.; Schwartz, M.; Chou, K.; Vonet, J.-F.; Laine, R. M. 3-D Molecular Mixtures of Catalytically Functionalized [vinylSiO_{1.5}]₁₀/ [vinylSiO_{1.5}]₁₂. Photophysical Characterization of Second Generation Derivatives. *Chem. Mater.* **2012**, *24*, 1883–1895.
21. Furgal, J. C.; Goodson III, T.; Laine, R. M. "Synthesis of Decaphenyl Silsesquioxane (D_{5h}-T₁₀) by Fluoride Catalyzed Rearrangement of [PhSiO_{1.5}]_n and Phenyltriethoxysilane: Steady-State Spectroscopy and Mechanism" *Manuscript in Preparation*.
22. Furgal, J. C.; Jung, J. H.; Clark, S.; Goodson, T.; Laine, R. M. Beads on a Chain (BoC) Phenylsilsesquioxane (SQ) Polymers via F- Catalyzed Rearrangements and ADMET or Reverse Heck Cross-Coupling Reactions: Through Chain, Extended Conjugation in 3-D with Potential for Dendronization. *Macromolecules* **2013**, *46*, 7591–7604.
23. Laine, R. M.; Blohowiak, K. Y.; Robinson, T. R.; Hoppe, M. L.; Nardi, P.; Kampf, J.; Uhm, J. Synthesis of Pentacoordinate Silicon Complexes from SiO₂. *Nature* **1991**, *353*, 642–644.
24. Laine, R. M.; Doan, P.; Furgal, J.C. Pan, D. Popova, V. "Distilling Silica from Biogenic Silica Sources," *Manuscript in Preparation for Submission to Science*
25. Schraml, J.; Maegi, M.; Chvalovsky, J.; Nguyen, D. C. *Collect. Czech, Chem. Commun.* **1975**, *40*, 875.
26. Carre, F.; Chuit, C.; Corriu, R. J. P.; Fanta, A.; Mehdi, A.; Rey, C. Hexacoordinate Silicon Centers . Evidence Suggestive of. *Organometallics* **1995**, *14*, 194–198.
27. Kano, N.; Nakagawa, N.; Kawashima, T. A Disilane Containing Two Heptacoordinate Silicon Atoms and Dithiocarboxylate Ligands. *Angew. Chemie - Int. Ed.* **2001**, *40*, 3450–3452.
28. Sugahara, Y.; Inoue, T.; Kuroda, K. ²⁹Si NMR Study on Co-Hydrolysis Processes in Si(OEt)₄–RSi(OEt)₃ –EtOH–water–HCl Systems (R=Me, Ph): Effect of R Groups. *J. Mater. Chem.* **1997**, *7*, 53–59.
29. Jermouni, T.; Smahi, M.; Hovnanian, N. Hydrolysis and Initial Polycondensation of Phenyltrimethoxysilane and Diphenyldimethoxysilane. *J. Mater. Chem.* **1995**, *5*, 1203.
30. Liepiņš, E.; Zicmane, I.; Lukevics, E.; A, E. S. S.; Liepiys, E.; Latvian, S. S. R.; Synthesis, O. A Multinuclear NMR Spectroscopy Study of Alkoxysilanes. *J. Organomet. Chem.* **1986**, *306*, 167–182.

31. Bhattacharya, A.; Thyagarajan, G. The Michaelis-Arbuzov Rearrangement. *Chem. Rev.* **1981**, *81*, 415–430.
32. Laine, R.M. Unpublished Work
33. Spek, A. L.; Voorbergen, P.; Schat, G.; Blomberg, C.; Bickelhaupt, F. The Structure of the Grignard Reagent. *J. Organomet. Chem.*, **1974**, *77*, 147–151.
34. Ashby, E. C.; Smith, M. B. Concerning the Structure of the Grignard Reagent. II.1 In Diethyl Ether. Relevance of Grignard Composition to the Mechanism of Addition to Ketones. *J. Am. Chem. Soc.* **1964**, *86*, 4363–4370.
35. Parker, C. a.; Rees, W. T. Correction of Fluorescence Spectra and Measurement of Fluorescence Quantum Efficiency. *Analyst* **1960**, *85*, 587.

Chapter 4

D_{5h} [PhSiO_{1.5}]₁₀ Synthesis via F⁻ catalyzed rearrangement of [PhSiO_{1.5}]_n. An Experimental/Computational Analysis of Likely Reaction Pathways, Photophysical Properties and Post Synthetic Functionalization

This chapter is based on the work of two manuscripts in preparation and one submitted manuscript with contributions from Mozhgan Bahrami.

4.1 Abstract

We describe here the synthesis and analysis of the reaction pathways leading to formation of the rare D_{5h} decaphenylsilsesquioxane (SQ) [PhSiO_{1.5}]₁₀ via F⁻ catalyzed rearrangement of [PhSiO_{1.5}]_n n = 8, 12, and oligomers initially synthesized from PhSi(OEt)₃. Isolated yields of ~50% [PhSiO_{1.5}]₁₀ are obtained via rearrangement of all starting materials. The recovered starting materials can be re-equilibrated using catalytic F⁻ to generate similar yields in second batches. These yields arise because [PhSiO_{1.5}]₁₀ exhibits higher solubility and better energy stabilization (10 kcal/mol theory) in CH₂Cl₂ compared to [PhSiO_{1.5}]₈ or [PhSiO_{1.5}]₁₂. Reaction intermediates were identified using time dependent ¹⁹F NMR and MALDI-ToF mass spectrometry eventually equilibrating to form the 8:10:12 cages in a 1:3:1.3 equilibrium in CH₂Cl₂.

Experimental results coupled with modeling using the Gamess computational package provide multiple reasonable pathways for SQ rearrangements to [RSiO_{1.5}]₁₀, starting from [RSiO_{1.5}]₈. Heats of reaction for interconversion of the model intermediates [HSiO_{1.5}]_x determined computationally, were used to select the *most reasonable reaction pathways*. The findings support a mechanism involving activation and cleavage of a T₈ cage corner by F⁻ attachment, followed by the corners stepwise removal as [i.e. RSi(OH)₃], followed thereafter by reinsertion forming [RSiO_{1.5}]₉-OH followed by, insertion of another corner to form [RSiO_{1.5}]₁₀-(OH)₂ and finally condensation to give [RSiO_{1.5}]₁₀. The most enthalpically favorable path (-24 kcal/mol) involves a hybrid mechanism.

4.2 Introduction

Silsesquioxanes (SQs) are of considerable recent interest due to their potential to offer high degrees of functionalization, high thermal stability, and simple purification. To date there have been some 18 reviews on silsesquioxane based materials, with most focusing on T_8 (O_h) compounds.¹⁻¹⁸ However, higher order SQs such as T_{10} (D_{5h}) and T_{12} (D_{2d}) are of increasing interest, since they offer new geometries, higher potential degrees of functionalization, and in many cases superior solubilities.^{13,17,19-21} They also offer similar but not identical thermal stabilities and physical properties to T_8 .

Most SQ syntheses rely on hydrolysis and condensation of R_1SiCl_3 or $R_1Si(OR')_3$.² These reactions often suffer from low yields, < 30%, can take weeks to months to reach completion, and coincidentally produce $[RSiO_{1.5}]_n$ byproducts that until recently were simply discarded. The $[PhSiO_{1.5}]_n$, $n = 8, 10, 12$, systems are particularly amenable for post synthetic modification using traditional electrophilic aromatic substitution methods.^{17,22}

$[PhSiO_{1.5}]_8$ or OPS, the most frequently studied, was first synthesized by Barry et al. in 1955.²³ Multiple synthetic routes to $[PhSiO_{1.5}]_8$ have been reported,^{13,17,24,25} whereas only a couple of reports describe the synthesis of $[PhSiO_{1.5}]_{12}$.^{21,24} A typical route to T_8 involves refluxing $PhSi(OEt)_3$ in toluene with KOH under water scarce conditions for < 48 h to give 90+ % yields.^{17,24} $[PhSiO_{1.5}]_{12}$ can be made similarly, with THF instead of toluene (~50% yield).^{13,24}

Unfortunately, there are no simple, high yield routes to pure five-fold symmetric $[PhSiO_{1.5}]_{10}$.²⁴⁻³⁷ Brown et al. first isolated $[PhSiO_{1.5}]_{10}$ in 1963 with an unreported yield, as the most soluble component after fractionation of crude $[PhSiO_{1.5}]_8$ by refluxing in benzene/hexane.²⁴ We previously synthesized $[PhSiO_{1.5}]_{10}$ using 18-crown-6/BaO to catalytically equilibrate 3 g of $[PhSiO_{1.5}]_{12}$ in m-xylene, giving only 500 mg [15% yield] after repeated recrystallization.²⁶ This method provided crystals suitable for single crystal x-ray diffraction.

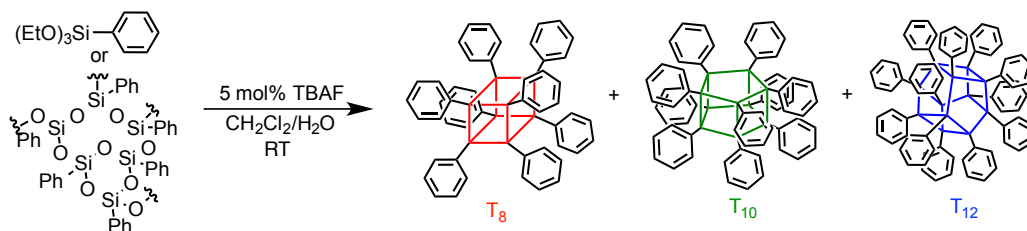
Our recent synthetic efforts have explored the utility of using fluoride as nBu_4NF (TBAF) to catalyze the synthesis of SQs containing electron withdrawing R-groups (i.e. phenyl, vinyl), with recovered yields as high as 99%.²⁷⁻³² For example we have made mixed functional SQ intermediates for “beads on a chain” (BoC) polymers; SQ cages

connected with organic linkers, with mixed $T_{10/12}$ vinyl/Me and mixed $T_{10/12}$ vinyl containing SQs.^{27,29,31-32} Motivation for our initial work comes from studies by Bassindale et al. and Mabry and Bowers et al. who found that SQs will react with stoichiometric TBAF (or Me_4NF , TMAF) forming cages that encapsulate F^- ($\text{F}^- @[\text{RSiO}_{1.5}]_8$) on slow evaporation of dry THF solution.³⁸⁻⁴²

Bassindale et al. also explored F^- catalyzed syntheses of T_8 cages from $\text{RSi}(\text{OR}')_3$.³⁹ They compared the activity of anhydrous F^- with $\text{F}^- + ^{18}\text{O}$ labeled water, finding that cage formation depends strongly on water concentration, similar to what is observed in standard hydrolysis/condensation conditions using strong acids/bases. This is expected since $\text{RSi}(\text{OR}')_3$ hydrolysis is a necessary first step before condensation.

Further motivation comes from Kawakami et al. who used TBAF to catalyze formation of $4\text{-TMS-PhSiO}_{1.5}]_{8,10,12}$ derivatives from $4\text{-TMS-PhSi}(\text{OEt})_3$.³³ The $[4\text{-TMS-PhSiO}_{1.5}]_{8,10,12}$ cages were then nitrated forming $[4\text{-NO}_2\text{-PhSiO}_{1.5}]_{8,10,12}$ and the individual cages isolated by selective crystallization.

Our objectives in the studies reported here are to develop a mechanistic picture of the processes that occur in F^- catalyzed rearrangement of $[\text{PhSiO}_{1.5}]_{8/12}$, $\text{PhSi}(\text{OEt})_3$, and the $[\text{PhSiO}_{1.5}]_n$ by-products with the goal of optimizing the synthesis of $[\text{PhSiO}_{1.5}]_{10}$. Optimization was necessary to generate $[\text{PhSiO}_{1.5}]_{10}$ in sufficient quantities to permit further functionalization e.g. bromination, iodination, acylation, sulfonylation, alkylation, etc.^{17,26,34,43} Scheme 4.1 depicts the general conditions for F^- catalyzed synthesis of $[\text{PhSiO}_{1.5}]_{8,10,12}$.



Scheme 4.1. Synthesis of $[\text{PhSiO}_{1.5}]_{8,10,12}$ by fluoride catalyzed rearrangement.

The mechanism(s) of SQ cage formation even for the widely studied $[\text{RSiO}_{1.5}]_8$ compounds is(are) largely unknown, however Kudo and Gordon in a comprehensive modeling study developed a detailed picture of “reasonable” routes to T_8 cage formation via hydrolysis/condensation reactions of $\text{HSiO}(\text{OH})_3$. Their studies suggest a very

complex set of equilibria including more than 25 possible intermediates.⁴⁴⁻⁴⁷ In short, cage formation is initiated by formation of D₄ rings that then self-condense. Experimental support for this path finds that all cis [PhSi(O)OH]₄ rings form easily from PhSi(OH)₃. On standing at ambient, these rings self-condense to form OPS.^{48,49}

Kudo and Gordon find that the presence of water promotes condensation of HSi(OH)₃ to [HSiO_{1.5}]₈ with a net heat of formation of -11.5 kcal/mol. In complementary work, Mashmeyer et al. also explored the cage formation mechanisms with the synthesis of incompletely condensed [(c-C₅H₉)SiO_{1.5}]₇-(OH)₃.⁵⁰ Reaction progress monitored via ESI mass spec and time dependent ATR-FTIR studies also suggest condensation mechanisms similar to those of Kudo and Gordon suggesting that [(c-C₅H₉)SiO_{1.5}]₇-(OH)₃ is a kinetic product. These studies provide the background for the work presented here.

The following sections discuss optimization of [PhSiO_{1.5}]₁₀ synthesis via a detailed analysis of the effects of variations in reaction conditions (i.e. concentration, solvent, catalyst, etc.), intermediates involved, and kinetic analyses of the synthetic process. This is followed by computational enthalpic/energy analysis of analogous [HSiO_{1.5}] intermediates for the development of a potential mechanism for fluoride-catalyzed rearrangement of SQs.

4.3 Experimental

Synthetic methods and characterization procedures are given above in Chapter 2.

4.4 Results and Discussion

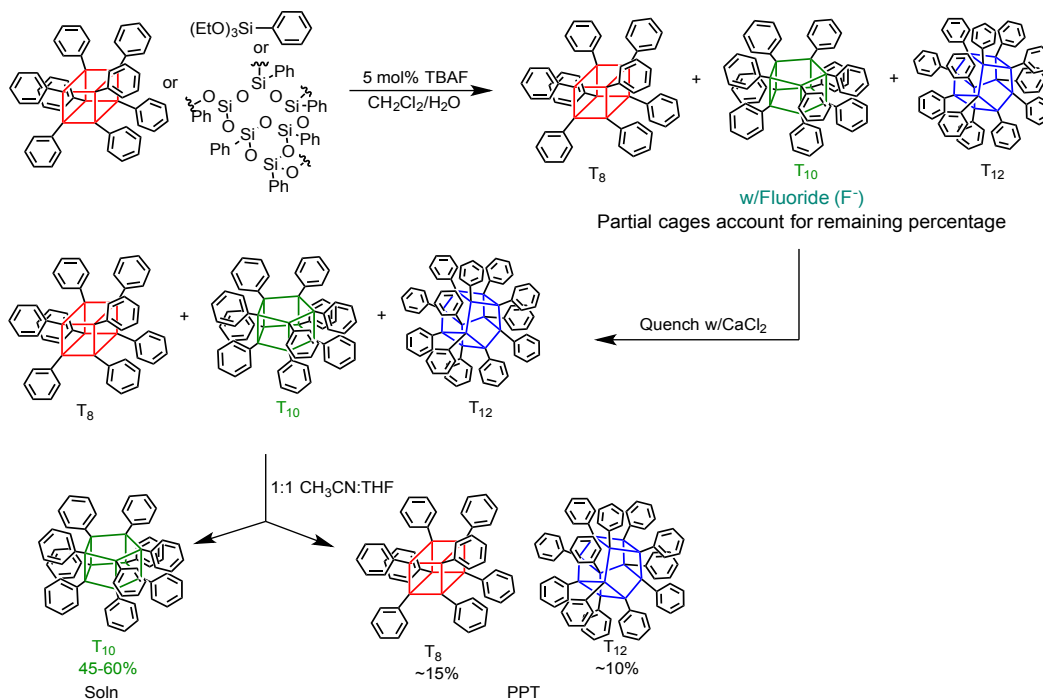
In the following sections, we first discuss optimization of [PhSiO_{1.5}]₁₀ synthesis by F⁻ catalyzed rearrangement of [PhSiO_{1.5}]_n via variations in experimental conditions and its characterization by MALDI-ToF, NMR, and TGA. This is followed by computational analyses of reaction intermediates (enthalpies). Lastly, we identify the multiple potential mechanistic pathways for the F⁻ catalyzed rearrangement of SQs and suggest the most likely reaction paths.

4.4.1 Optimized Synthesis of [PhSiO_{1.5}]₁₀

[PhSiO_{1.5}]₁₀ can be synthesized in high yield by F⁻ rearrangement of [PhSiO_{1.5}]_n in dilute (~60 mM) CH₂Cl₂. This solvent system and concentration provides the highest

selectivities/solubility for $[\text{PhSiO}_{1.5}]_{10}$ in the mixture of $[\text{PhSiO}_{1.5}]_{8,10,12}$ formed under these conditions. Reactions were typically run for 48 h to ensure full conversion of partial cages to completely condensed cages, starting from $\text{PhSi}(\text{OEt})_3$, $[\text{PhSiO}_{1.5}]_n$, $[\text{PhSiO}_{1.5}]_{12}$ or $[\text{PhSiO}_{1.5}]_8$. Since this reaction results in a mixture of products, several steps are necessary to isolate pure $[\text{PhSiO}_{1.5}]_{10}$.

First, F^- must be removed as CaF_2 by treating the reaction solution with CaCl_2 or by washing with water as it will re-equilibrate all the cages if the isolated products are re-dissolved. Reactions were worked up using two methods. Aqueous extraction does work, but produces a higher proportion of hydroxyl containing partial cages that complicate further purification.^{8,54} CaCl_2 quenching requires 24 h of stirring, but insoluble CaF_2 is removed easily by filtering and partial cage byproducts are minimal. This workup is the method of choice (Scheme 4.2). The crude product mixture (before isolation) has a cage ratio: $T_8:T_{10}:T_{12}$ of $\sim 1:3:1.3$ by MALDI-ToF analysis (Figure 4.1). $T_{18,20,22}$ cage sizes were also observed and isolated as discussed below.



Scheme 4.2. Synthesis and separation of phenylSQs by the CaCl_2 quenching method.

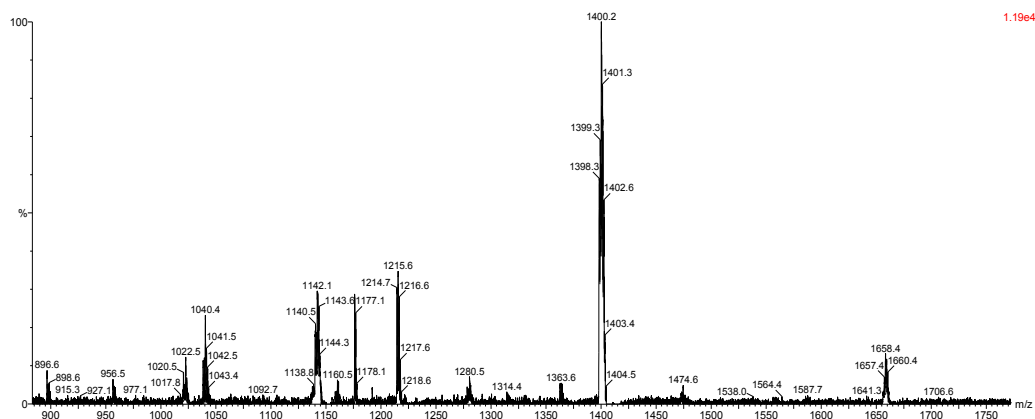


Figure 4.1. MALDI-ToF of crude phenylSQ reaction product mixture, $[\text{PhSiO}_{1.5}]_{10}$ at 1400.2 m/z.

Kawakami et al. reported that the individual cages could be separated from the mixture $[4\text{-TMS-PhSiO}_{1.5}]_{8,10,12}$ using selective solubility/crystallization providing the point of entrée for our studies. We explored single and double component solvent systems (i.e. acetonitrile, ethyl-acetate, etc) finding that mixtures of THF/acetonitrile or ethyl-acetate/acetonitrile permit effective separation.^{33,55} A 1:1 or 1:1.2 mixture of THF:acetonitrile solubilizes the T_{10} cage to the exclusion of the T_8 and T_{12} cages, which can be filtered off as white powder. The 1:1.2 solvent mixture gives purer T_{10} , but at a lower yield (~40 %). Note that the T_8 and T_{12} mixture can be recycled through re-equilibration to give more $[\text{PhSiO}_{1.5}]_{10}$.

The dissolved T_{10} is then concentrated, precipitated into methanol and isolated by filtration. This reaction system typically gives T_{10} yields of 45-60%, with the remaining products made up of partial cages, T_8 , T_{12} , and <1% larger cage, at scales achieving 8.2 g (see experimental). A short silica column (2:1 hexanes:methylene chloride) allows removal of small amounts of partial cage byproducts (~2-5%).

Figure 4.2 shows the MALDI-ToF of $[\text{PhSiO}_{1.5}]_{10}$ after purification [1398.9 m/z $\text{Ag}^+\text{-Si}_{10}\text{O}_{15}(\text{C}_6\text{H}_5)_{10}$]. Figure 4.3 provides the ^{29}Si NMR showing a single peak at -79.61 ppm. TGA of $[\text{PhSiO}_{1.5}]_{10}$ gives a ceramic yield of 45.9%, vs. 46.1% (theory) per Figure 4.4 and a $T_{d5\%}$ of 490 °C.

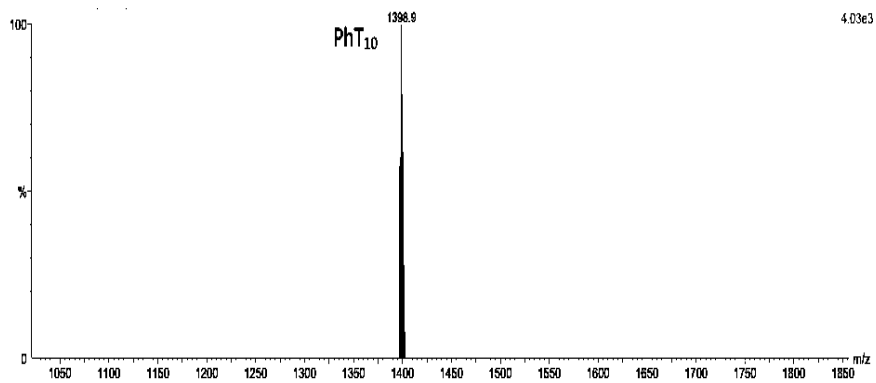


Figure 4.2. MALDI-ToF spectrum of $[\text{PhSiO}_{1.5}]_{10}$ (Phenyl T_{10}), Ag^+ peak at 1398.9 m/z $[\text{Ag-Si}_{10}\text{O}_{15}(\text{C}_6\text{H}_5)_{10}]$.

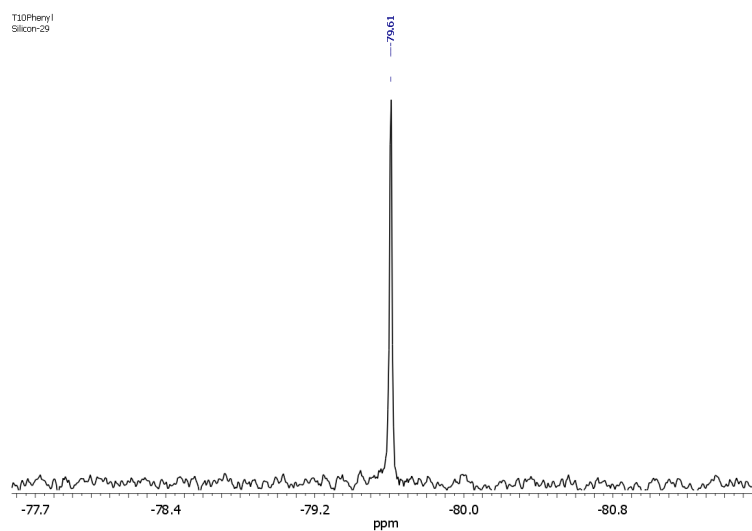


Figure 4.3. ^{29}Si NMR of $[\text{PhSiO}_{1.5}]_{10}$, peak at -79.61 ppm corresponding to a T_{10} compound.

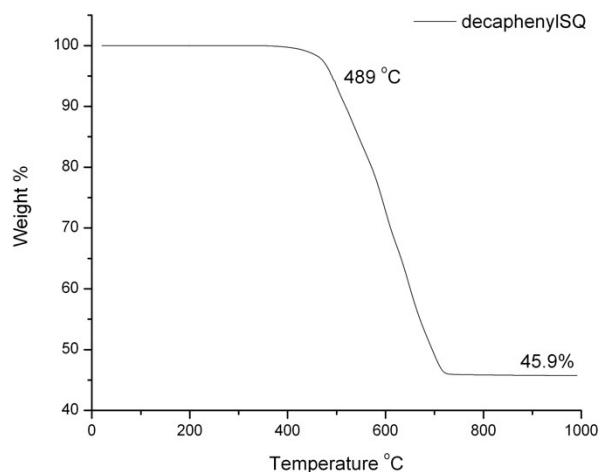


Figure 4.4. TGA of $[\text{PhSiO}_{1.5}]_{10}$ in air ($10^\circ\text{C}/\text{min}$), actual and theoretical ceramic yields are 45.9% and 46.4%, with $T_{d5\%}$ of 490°C .

The larger cages $[\text{PhSiO}_{1.5}]_{18,20,22}$, also likely equilibration products, can be separated in small quantities from $[\text{PhSiO}_{1.5}]_{10}$ using a 2:1 hexane:methylene chloride solvent system eluted through a silica column. Thus, 1 g of T_{10} provides 30 – 50 mg of the larger cages (~4%). Figure 4.5 shows the MALDI-ToF of the isolated $[\text{PhSiO}_{1.5}]_{18,20,22}$ mixture.

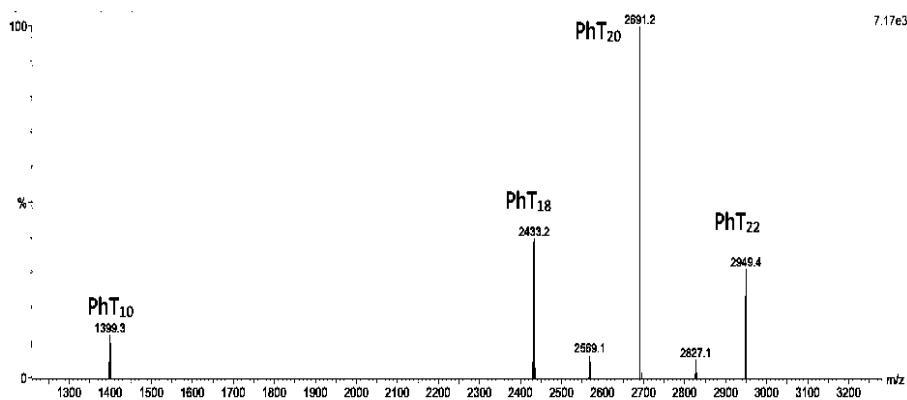


Figure 4.5. MALDI-ToF of $[\text{PhSiO}_{1.5}]_{18,20,22}$ mixture.

4.4.2 Reaction Mechanism Studies

As noted above, one objective of these studies was to decipher, at least qualitatively, the equilibria involved in F^- promoted rearrangement reactions. The PhSQ system is used for this analysis due to its facile rearrangement with F^- , isolable products, and ease of ionization in MALDI-ToF of full and partial cages.

$[\text{PhSiO}_{1.5}]_8$, octaphenylsilsesquioxane (OPS) was chosen as the model starting material as it is a well defined structure. Note $[\text{PhSiO}_{1.5}]_{10}$ or $[\text{PhSiO}_{1.5}]_{12}$ could also have been used since equilibration of these cages results in similar product ratios (Figures 4.6 and 4.7), but since we are interested in forming $[\text{PhSiO}_{1.5}]_{10}$ it makes more sense to study the equilibria involved starting from readily available $[\text{PhSiO}_{1.5}]_8$.

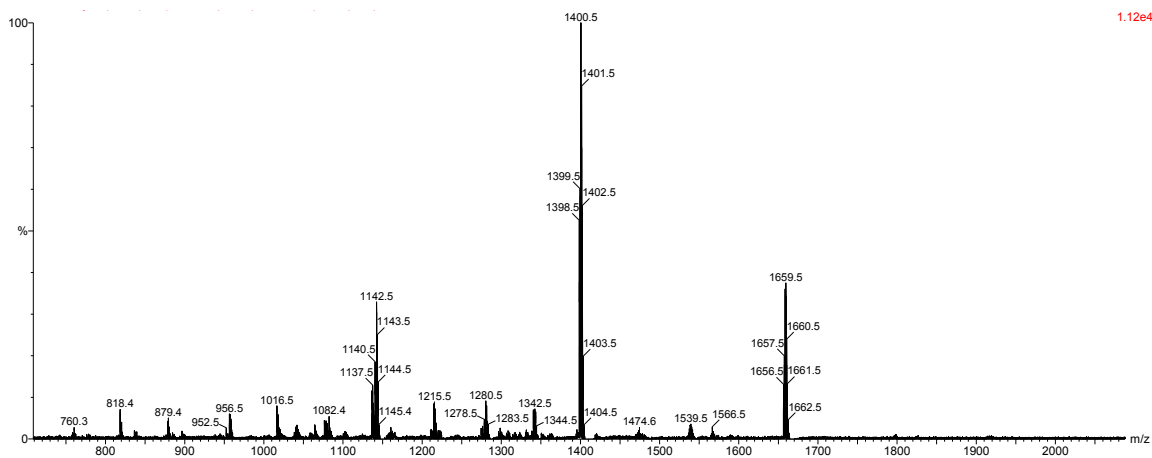


Figure 4.6. MALDI-ToF analysis of $[\text{PhSiO}_{1.5}]_{10}$ equilibration with F^- after 3 days, ratio 8:10:12 of 1:3:1.3.

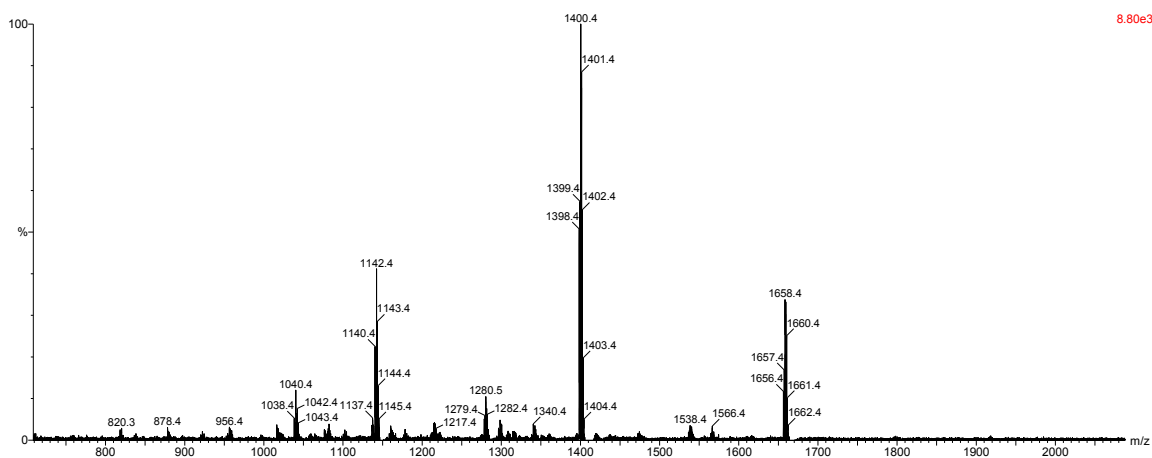


Figure 4.7. MALDI-ToF analysis of $[\text{PhSiO}_{1.5}]_{12}$ equilibration with F^- after 3 days, ratio 8:10:12 of 1:3:1.3.

Reaction progress was monitored using MALDI-ToF and ^{19}F NMR. MALDI-ToF allows rapid identification of reaction intermediates and relative compositions (assuming intensities are close to quantitative), because it gives a clear indication by the mass of each species present, with intensities being proportional to its solution concentration.³² MALDI-ToF is particularly useful for time dependent studies, since the rearrangement reactions cease in the solid state after spotting on a MALDI analysis plate. Our data

suggests that similarly functionalized species exhibit similar degrees of ionization; thus the peak intensities permit qualitatively if not quantitative characterization of the ratios of individual species.³² ^{19}F NMR permits observation of Si-F species in the reaction mixture.

In the Figure 4.8 ^{19}F NMR study at 0 °C (standard 60 mM OPS in DCM/5 mol% F^-) only one peak, at -130 ppm, changes intensity. We suggest that this peak corresponds to a free corner possibly $\text{Ph-O}_2\text{Si-F}$, or PhSiF_3 both of which are observed at -135 to -140 ppm (Table 4.1).⁵⁶⁻⁶⁰ Slight shifts of ≤ 10 ppm arise as a function of solvent and/or the exchange of F with O atoms. The peak at -111 ppm is one of several possible species, including pentacoordinate silicates (e.g. PhSiF_4^- literature at -118.7 ppm) or fluorobenzene arising via cleavage of the Si-C bond (-113.15 ppm),⁶¹ or possibly $\text{F}^-@[\text{PhSiO}_{1.5}]_{10}$. $\text{F}^-@[\text{RSiO}_{1.5}]_{10}$ has never been observed experimentally, but the computationally determined chemical shift is -112.6 ppm.⁶² This value is close to the -111 ppm peak observed, however the calculated value for $\text{F}^-@[\text{PhSiO}_{1.5}]_8$ is -26 vs -38 ppm found, thus, we must be cautious in assigning this value as suggested (Figure 4.9). The -123 ppm peak is from the TBAF (F^-). The peak at -155 ppm is attributed to HF_2^- (-149.5 ppm literature),⁶⁰ known to exist in TBAF mixtures due to deprotonation of water, coincidentally forming ^-OH . This species is in relatively small quantity to the TBAF F^- ion at -123.11 ppm.⁶³

In another ^{19}F NMR study we looked at the reaction mixture 5 min after F^- introduction at -20 °C. Two additional peaks are observed at -145.1 and -64.8 ppm likely corresponding to a PhSiO_2F derivative (Table 4.1) and $[\text{PhSiO}_{1.5}]_{10}[\text{F}^-]$ or $[\text{PhSiO}_{1.5}]_8[\text{F}^-]$ derivatives respectively, as suggested from MALDI results discussed below. Though this technique seemed promising, the absence of definitive changes in the reaction over time limit the utility of ^{19}F NMR.

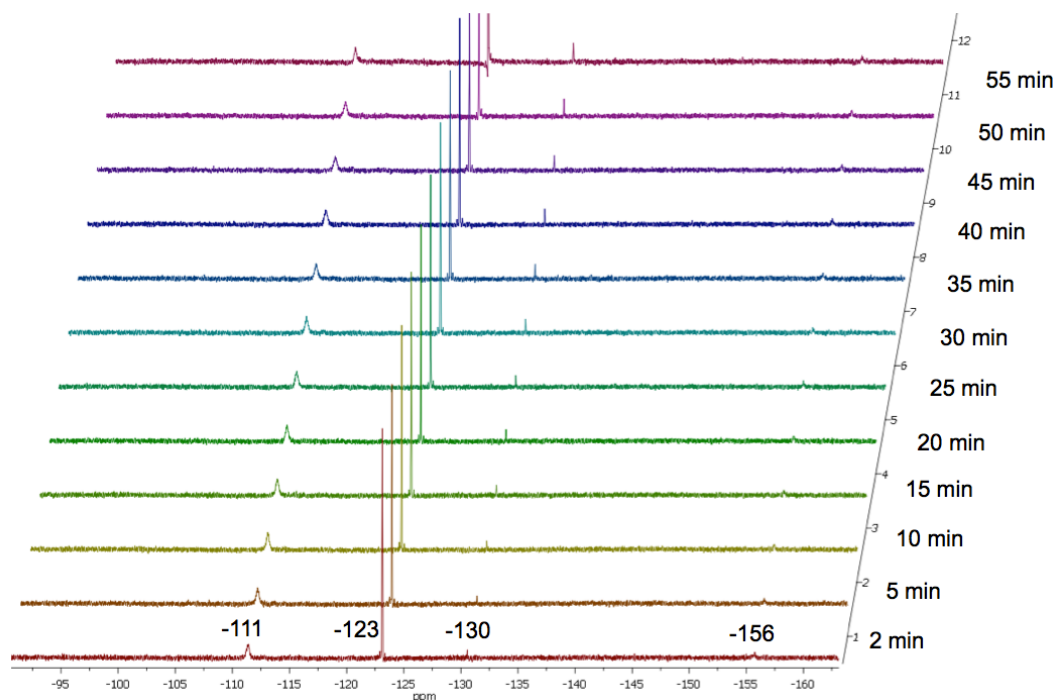


Figure 4.8. ^{19}F NMR reaction analysis of Reaction 3 conditions (OPS F^- rearrangement) over a 55 min time frame at $0\text{ }^\circ\text{C}$.

Table 4.1. Literature ^{19}F NMR data for select Si-F species.

Structure	^{19}F NMR (ppm)
PhSiF_3 ⁵⁴	-140.94
$(\text{PhSiF}_2)\text{O}_2$ ⁵⁴	-136.9
$\text{PhSi}(\text{OEt})\text{F}_2$ ⁵⁴	-140.90
$\text{PhSi}(\text{OEt})_2\text{F}$ ⁵⁴	-142.36
PhSiF_4 ⁵¹	-118.7
HF_2^- ⁵⁴	-149.4
TBAF ⁵⁷	-125.3
Fluorobenzene ⁵⁶	-113.15
$\text{F}^- @[\text{HSiO}_{1.5}]_{10}$ (calc) ⁵⁵	-112.6
$\text{F}^- @[\text{PhSiO}_{1.5}]_8$ ⁵⁵	-26, -38 (calc)
$\text{F}^- @[\text{HSiO}_{1.5}]_{12}$ (calc) ⁵⁵	-170.8
$[\text{HSiO}_{1.5}]_{10}[\text{F}^-]$ (calc) ⁵⁵	-54.2
$[\text{HSiO}_{1.5}]_{12}[\text{F}^-]$ (calc) ⁵⁵	-68.7

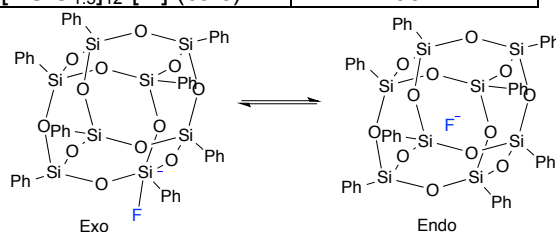


Figure 4.9. Structures of exo and endo fluoro T_8 , $[\text{PhSiO}_{1.5}]_8[\text{F}^-]$ and $\text{F}^- @[\text{PhSiO}_{1.5}]_8$ respectively.

A ^{29}Si NMR study at $-20\text{ }^{\circ}\text{C}$ (12 h collection time) shows two silicon environments at -72.6 and -80.5 ppm (Figure 4.10) that could correspond to PhSiF_3 and $[\text{PhSiO}_{1.5}]_{10}$ respectively. The breadth and side bands of the peak at -80 ppm suggest that multiple species could be present. The literature value for PhSiF_3 in DCM is -72.6 ppm.⁵⁴ Attempts to use ^{29}Si NMR as an analytical tool for kinetics were thwarted by the low concentrations needed to maintain complete solution as the rearrangement reactions take place (~ 60 mM), resulting in long acquisition times. Therefore, MALDI-ToF remains the most reliable analytical tool. Appendix E shows all the masses found in the MALDI studies and their proposed formulas.

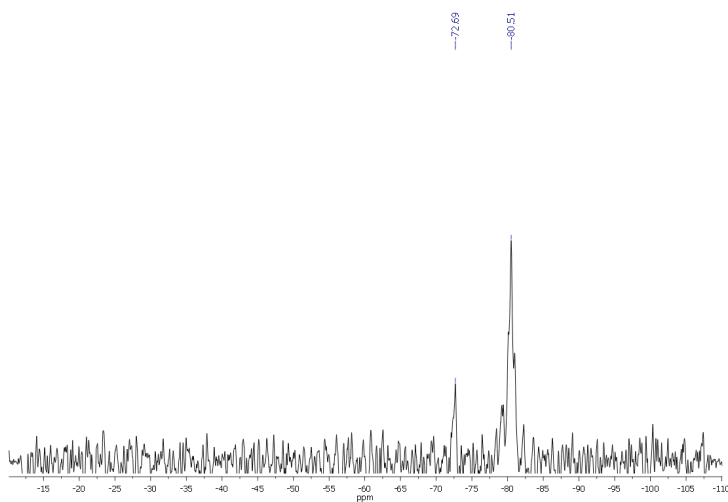


Figure 4.10. ^{29}Si NMR of OPS+5 mol% TBAF in DCM at $-20\text{ }^{\circ}\text{C}$ after 12 h acquisition time.

Table 4.2 shows the set of conditions used to study $[\text{PhSiO}_{1.5}]_8$ rearrangements via MALDI-ToF analysis in dichloromethane (DCM). Reaction (3) offers the best overall conditions, with MALDI-ToF yields of 68% T_{10} and isolated yields of 52% T_{10} after 48 h.

Table 4.2. Reaction condition studies in DCM MALDI taken at 5 min intervals up to 25 min, and then taken at 24 h for final relative %T₁₀ (108 mg OPS).

Rxn	[OPS] (mM)	TBAF (mol%)	Temp. (°C)	MALDI ~%T ₁₀
1	60	10	20	<1
2	60	2.5	20	32
3	60	5	20	54
4	60	1	20	21
5	120	5	20	43
6	30	5	20	25
7	15	5	20	<1
8	60	7	20	21
9	180	5	20	5
10	60	5	35	4
11	60	5	0	10
12	60	5	-35	N/A
13	60	5	-78	N/A

* Fluoride becomes nearly unreactive below 0 °C due to insolubility.

Figures 4.11 and 4.12 show MALDI-ToF spectra for reaction (3) at 2 and 45 min. Table 4.3 shows the predominant species and their proposed formulae. T₁₀ is observed in small amounts with various partial and fluoride intermediate cages within 2 min after initiation at RT. These intermediates appear and show reasonable intensities at the start of the reaction, followed by further distribution into more partial cages. At 45 min, T₁₀ is already the dominant product at 42% relative composition by MALDI Intensities, with the next most abundant species being [PhSiO_{1.5}]₉(OH), T₁₀ missing a corner (Table 4.2).

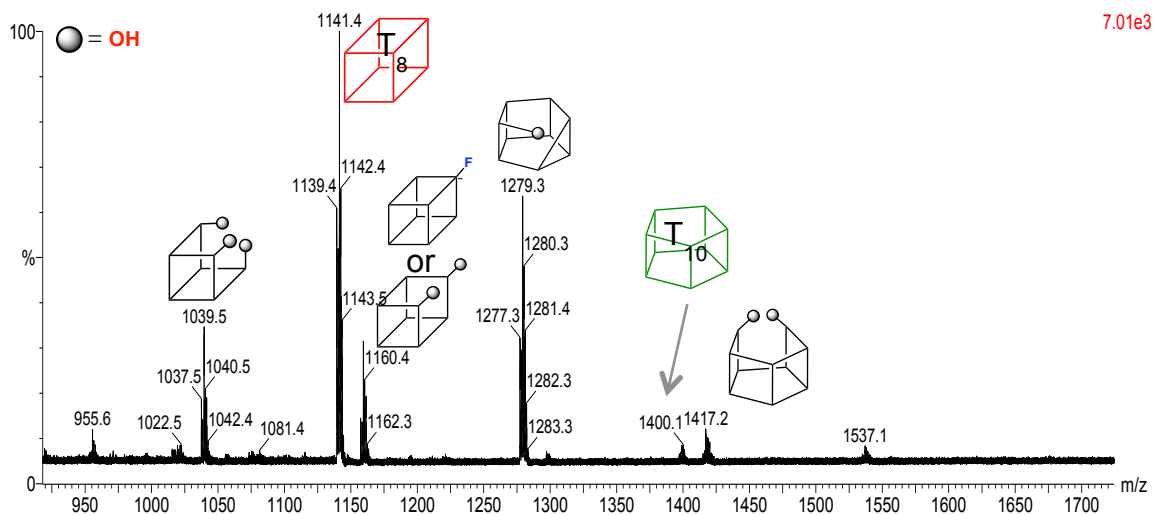


Figure 4.11. MALDI-ToF showing T₈ to T₁₀ rearrangement reaction taken after 2 min at RT, with 1141.4 m/z T₈ and 1400.1 m/z T₁₀, Ag⁺ ion peaks.

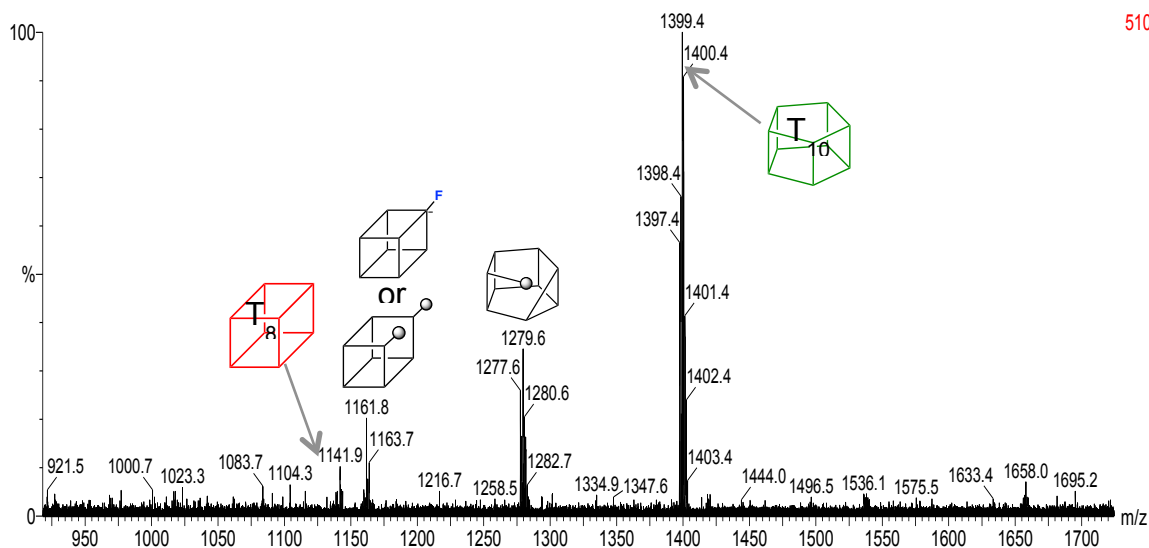


Figure 4.12. MALDI-ToF showing T_8 to T_{10} rearrangement reaction taken after 45 min at RT, with 1141.9 m/z T_8 , 1399.4 T_{10} , and 1658 T_{12} all of which are Ag^+ ion peaks.

Table 4.3. Observed MALDI-ToF peaks from Reaction (3), predicted formulae and relative peak intensities.

Peak Ag^+ (m/z)	Predicted formula	Proposed Structure(s)	Relative Intensity % (2 min)	Relative Intensity % (45 min)
1039.5	$[PhSiO_{1.5}]_7(OH)_3$		13	-
1141.4	$[PhSiO_{1.5}]_8$		44	3
1160.4	$[PhSiO_{1.5}]_8F$ (exo) or $[PhSiO_{1.5}]_8(OH)_2$		11	12
1279.3	$[PhSiO_{1.5}]_9(OH)$		27	21

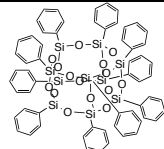
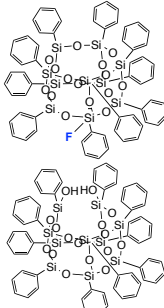
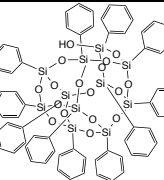
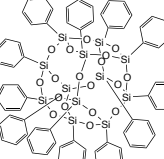
1400.1	$[\text{PhSiO}_{1.5}]_{10}$		1	42
1417.2	$[\text{PhSiO}_{1.5}]_{10}\text{F}$ (exo) or $[\text{PhSiO}_{1.5}]_{10}(\text{OH})_2$		2	-
1537.1	$[\text{PhSiO}_{1.5}]_{11}(\text{OH})$		1	2
1658.0	$[\text{PhSiO}_{1.5}]_{12}$		-	3

Figure 4.13 plots the relative composition of T_{10} from MALDI peak intensities over 36 h per Reaction (3) conditions. After 45 min, the relative composition of T_{10} compared to other species remains fairly constant at ~42%, increasing slightly to 46% at 36 h suggesting the reaction to form T_{10} is actually complete within 45 min; however, during this 36 h period, the partial cages keep equilibrating until they are converted to full cages, giving a final ~1:3:1.3, ratio of T_8 , T_{10} , T_{12} , with ~2-5% partials remaining.

Given that MALDI-ToF provides effective analysis of intermediate formation and products, we ran time dependent studies using Table 4.2 reaction conditions. Note that reactions (1) and (7) give less than 1% T_{10} by MALDI-ToF even after 24 h. Figure 14 compares T_{10} composition vs time in the first 1500 seconds of reactions (2-6 and 9, in Table 4.2).

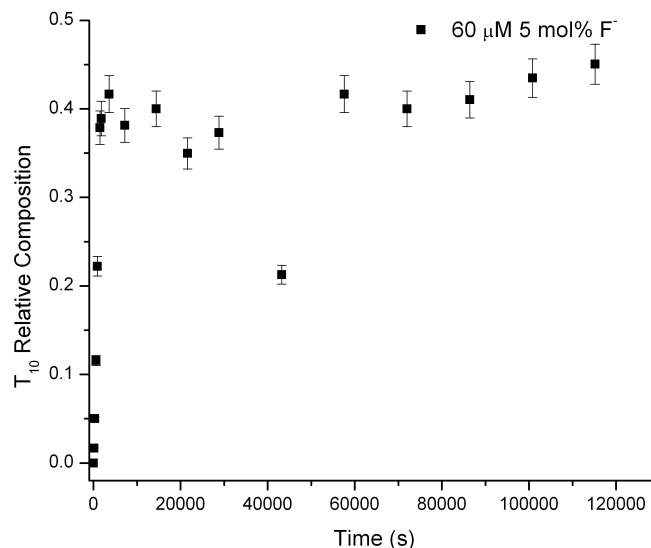


Figure 4.13. $[\text{PhSiO}_{1.5}]_{10}$ (1400 m/z) composition (relative intensity vs. time) over 36 h under Reaction (3) conditions (60 mM OPS in DCM, 5 mol% F^-).

Though the peak intensities from MALDI-ToF are not ideal, clear trends are observed. First, reactions at concentrations above 120 mM or below 30 mM show decreases in T_{10} formation. Literature suggests that higher concentrations of starting materials in SQ cage formation reactions typically result in polymeric/open cages,¹⁻⁴ while lower concentrations slow intermolecular interactions decreasing reaction rates.

An alternate explanation is that increased solvation stabilizes OPS against rearrangement. Second, the addition of F^- above 10 mol% significantly hinders the rearrangement efficiency, likely due to increase in water concentration from added TBAF, favoring partial over fully condensed cages (see below). From this analysis, the best reaction concentrations to form T_{10} range from 30 to 120 mM, with F^- catalyst in the range of 1.5 – 7 mol%.

Figure 15 plots T_{10} formation at 0°, 20° and 35 °C over the first 1500 sec. T_{10} forms faster at 35 °C; however, the T_{10} composition falls from ~11% at 120 sec to ~1% by 1500 sec. Two explanations are possible; one is that higher temperatures stabilize partial cage intermediates, supported by the predominance of partial cages in MALDI-ToF after 10 min (Figure 16). Alternately, F^- is known to cleave Si-C bonds at ≥ 50 °C resulting in loss of R-groups.^{60,64}

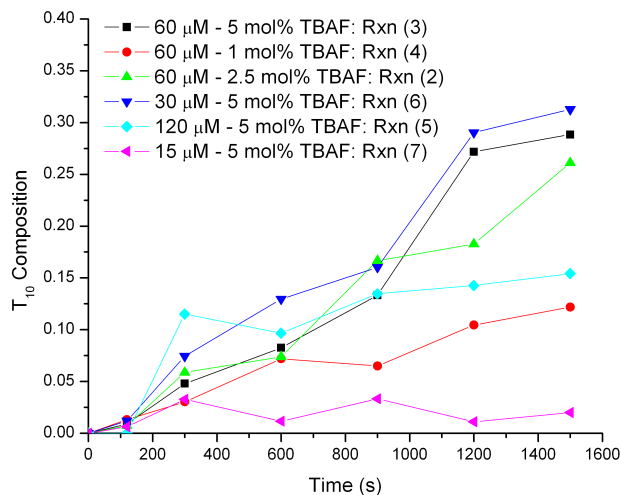


Figure 4.14. Comparison of $[\text{PhSiO}_{1.5}]_{10}$ composition within the first 25 min of reactions (2-6 and 9).

At $\leq 0^\circ\text{C}$, TBAF solubility drops and ice forms on the reaction surface reducing the solution water content and coincidentally rates of reaction. This results in less than 1% conversion to T_{10} within 1500 sec, and only 10% conversion after 24 h. It is likely that water solvation of F^- contributes to its catalytic activity.

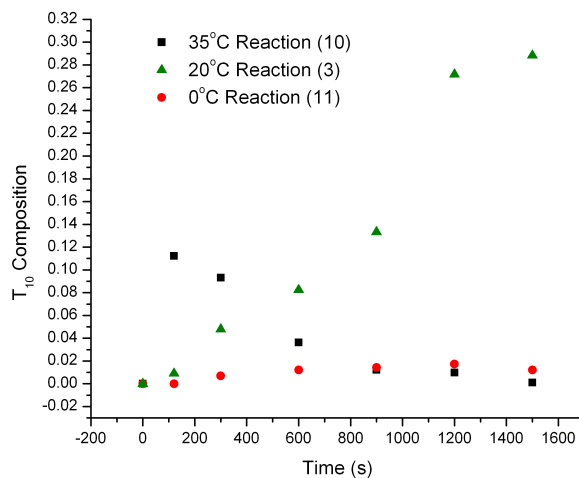


Figure 4.15. T_{10} composition at 0, 20 and 35°C for F^- catalyzed rearrangement of OPS over the first 25 min of reaction.

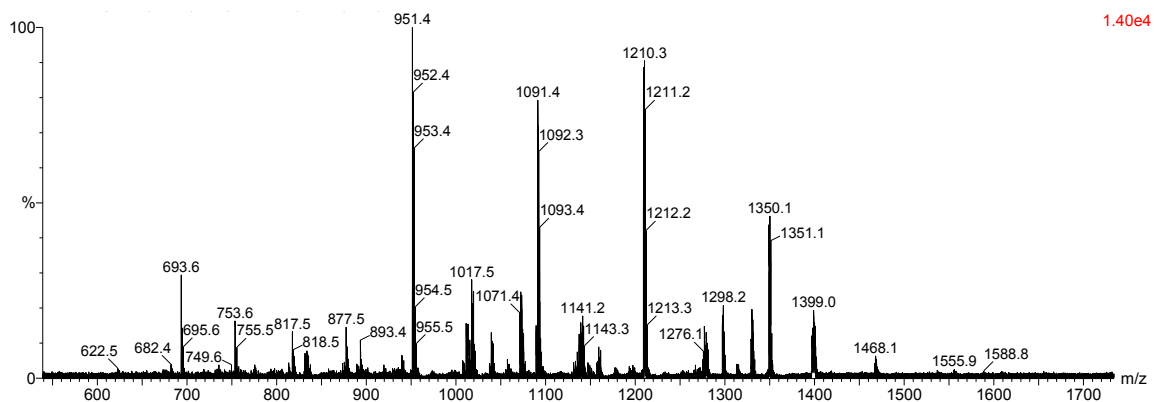


Figure 4.16. MALDI-ToF of 35 °C OPS rearrangement Reaction 10.

We also examined solvent effects on OPS-F⁻ rearrangement reactions (Table 4.4). Likewise, reactions (14-17) explore the influence of water. In contrast, reactions (14) and (15) were run under anhydrous conditions (dry DCM, dry TBAF). The reaction (14) solution without OPS was dried for 3 h with molecular sieves to remove water from TBAF before adding OPS. After 24 h, the predominant product was unexpectedly [PhSiO_{1.5}]₁₀. This is surprising since both Bassindale et al.³⁸ and Mabry and Bowers et al.⁴² suggest water is necessary for rearrangement. Reaction (15) used drying conditions analogous to Bassindale et al.,³⁸ with TBAF and distilled DCM stirred over molecular sieves/N₂/3 d, before adding oven dried OPS. The Figure 4.17 MALDI-ToF of this reaction shows only unreacted OPS as the predominant peak (1142.1 m/z) indicating that extensive drying is needed to remove most of the water. At this point TBAF is no longer solvated and precipitates out of solution.

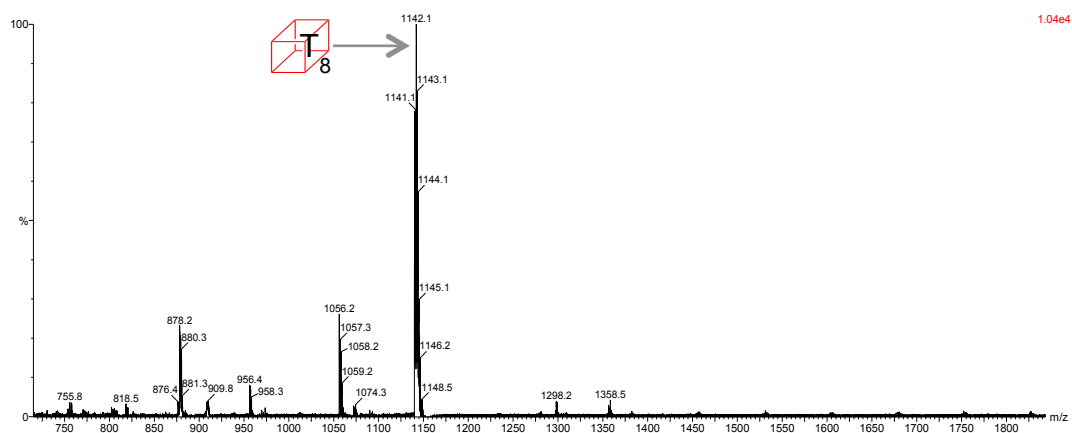


Figure 4.17. MALDI-ToF OPS + TBAF in DCM under anhydrous Reaction (3) conditions (3 days drying with 4Å molecular sieves), showing OPS Ag⁺ ion at 1142.1 m/z.

Reaction (15) with the 5 vol % water present in commercial 1M TBAF solutions gave the best isolated yields of $[\text{PhSiO}_{1.5}]_{10}$ of 54% (Table 4.2, Reaction 3). Reaction (16), with 1 equivalent of water per cage oxygen also provided $[\text{PhSiO}_{1.5}]_{10}$ as the predominant species. Excess water [1 mL, Reaction (17)], favors partial cages, with $[\text{PhSiO}_{1.5}]_9\text{-[OH]}_1\text{-[F]}_1$ or $[\text{PhSiO}_{1.5}]_9\text{-[OH]}_3$ as the predominant species by MALDI at 1297.6 m/z. Both possible intermediates are within 1 amu of each other.

Table 4.4. OPS rearrangement studies in selected solvents without F^- removal. [60 mM concentration (108 mg of OPS in 15 mL of solvent), 20 °C/45 μL -1M TBAF DCM/24 h.

Rxn	Solvent	Water	Predominant Species by MALDI 24 h (m/z)
14	DCM	$\sim 0^{\text{a}}$	$[\text{PhSiO}_{1.5}]_{10}$ (1400.2 m/z)
15	DCM	0^{b}	$[\text{PhSiO}_{1.5}]_8$ (1142.2 m/z)
15	DCM	$\sim 2.25 \mu\text{L}^{\text{c}}$	$[\text{PhSiO}_{1.5}]_{10}$ (1400.2 m/z)
16	DCM	36 μL (~ 1 equiv)	$[\text{PhSiO}_{1.5}]_{10}$ (1400.4 m/z)
17	DCM	1 mL (excess)	$[\text{PhSiO}_{1.5}]_9\text{-[OH]}_1\text{-[F]}_1$ (1297.6 m/z)
18	DCM	2.25 μL H_2^{18}O	$[\text{PhSiO}_{1.5}]_8$ (1142.2 m/z)
19	Acetone	$\sim 2.25 \mu\text{L}$	$[\text{PhSiO}_{1.5}]_8\text{-[F]}$ or $[\text{PhSiO}_{1.5}]_8\text{-[OH]}_2$ (1160.6 m/z)
20	Acetonitrile	$\sim 2.25 \mu\text{L}$	$[\text{PhSiO}_{1.5}]_9\text{-[OH]}_1$ (1280.2 m/z)
21	DMF	$\sim 2.25 \mu\text{L}$	$[\text{PhSiO}_{1.5}]_{10}\text{-[F]}$ or $[\text{PhSiO}_{1.5}]_{10}\text{-[OH]}_2$ (1418.0 m/z)
22	Methanol	$\sim 2.25 \mu\text{L}$	$[\text{PhSiO}_{1.5}]_8$ (1142.4 m/z)
23	THF	$\sim 2.25 \mu\text{L}$	$[\text{PhSiO}_{1.5}]_9\text{-[OH]}_1$ (1280.2 m/z)
24	Toluene	$\sim 2.25 \mu\text{L}$	$[\text{PhSiO}_{1.5}]_8\text{-[F]}$ or $[\text{PhSiO}_{1.5}]_8\text{-[OH]}_2$ (1160.6 m/z)
25	1:1 THF:Acetonitrile	$\sim 2.25 \mu\text{L}$	$[\text{PhSiO}_{1.5}]_9\text{-[OH]}_1$ (1280.2 m/z)

^aReaction mixture dried over 4Å molecular sieves and Na_2SO_4 for 3 h to remove water from TBAF, which was then filtered and added to a mixture of 4Å molecular sieves and OPS. ^bReaction mixture dried over 4Å molecular sieves for 3 days under N_2 to remove water from TBAF before adding vacuum oven dried OPS. ^c1M TBAF solution contains $\sim 5\%$ water

To fully understand the influence of water, H_2^{18}O was added in place of the $\sim 2.25 \mu\text{L}$ H_2O in TBAF [Reaction (18)] by drying the solution for 3 days as above then adding 2.25 μL of H_2^{18}O . The MALDI-ToF was taken after 24 h, finding that ^{18}O was incorporated into T_{10} and partial cage intermediates by their isotope patterns (1 to 14 ^{18}O atoms are observed for T_{10} , Figure 4.18). The use of H_2^{18}O slowed reaction rates, with T_8 still predominating after 24 h, however incorporation of ^{18}O into T_{10} shows that water is

involved in the reaction mechanism, even though all required Si-O bonds are already present.

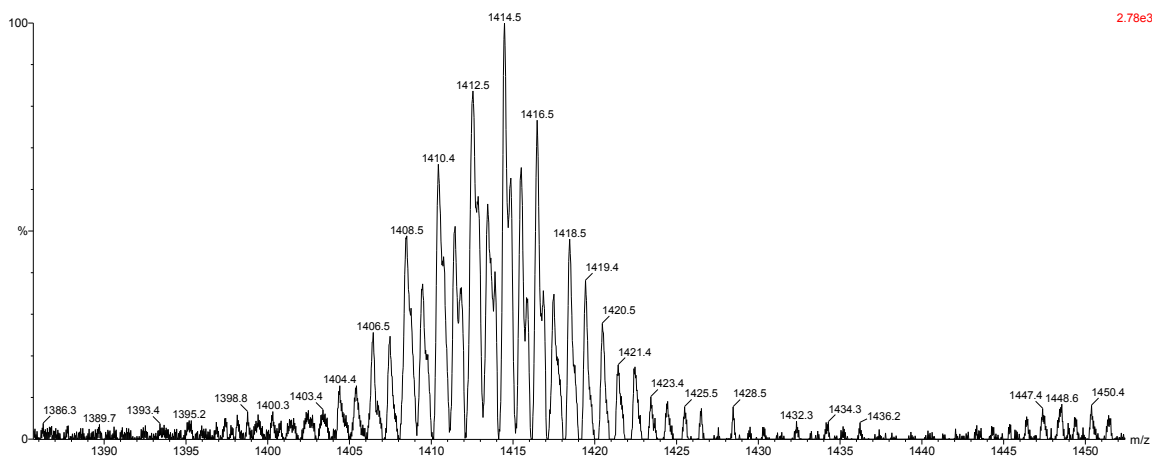


Figure 4.18. MALDI-ToF of H_2^{18}O isotope study under pseudo reaction (3) conditions; T_{10} region shown at 1414.5 m/z, suggesting seven ^{18}O are incorporated on average.

Reactions 19-25 (Table 4.4) reveal solvent effects that are likely a consequence of poor OPS solubility and only soluble species are observed by MALDI-ToF.

Similar peaks are observed in most of the reactions regardless of solvent. Reaction (19) in acetone generates either $[\text{PhSiO}_{1.5}]_8\text{-[F]}$ or $[\text{PhSiO}_{1.5}]_8\text{-[OH]}_2$ (1160.6 m/z) as the major species. $[\text{PhSiO}_{1.5}]_7\text{-[OH]-[F]}$ or $[\text{PhSiO}_{1.5}]_9\text{-[OH]}_3$, $[\text{PhSiO}_{1.5}]_9\text{-[OH]}_1$ and $[\text{PhSiO}_{1.5}]_{10}\text{-[F]}$ or $[\text{PhSiO}_{1.5}]_{10}\text{-[OH]}_2$ are also observed at m/z = 1040.4, 1280.2 and 1418.6 respectively. Multiple cage structures are possible for each peak as the difference between F and OH containing structures is one proton (see Table 3). Similar peaks are also observed in toluene and acetonitrile.

In THF, $[\text{PhSiO}_{1.5}]_9\text{-[OH]}_1$ (1280.2 m/z) is the major species (see Table 4.3 for structures), with $[\text{PhSiO}_{1.5}]_{10}$ (1400.2 m/z) as the second most predominant species. In DMF, $[\text{PhSiO}_{1.5}]_{10}\text{[F]}/[\text{PhSiO}_{1.5}]_{10}\text{-[OH]}_2$ are the predominant species and the only solvent to show $[\text{PhSiO}_{1.5}]_{12}\text{[F]}/[\text{PhSiO}_{1.5}]_{12}\text{-[OH]}_2$ (Figure 4.19). OPS dissolves completely in 2 min in DMF, the fastest of any solvent. In methanol, no F^- interactions were observed, and only starting OPS was seen by MALDI-ToF due to the insolubility of OPS. However, as mentioned above, no fluoride-encapsulated T_8 species were observed in the ^{19}F NMR analysis (-26 ppm). Therefore, we propose that fluoride would have to form bonds exo to the cage, initially as a pentacoordinated corner (Figure 4.9). The

solvent studies did not reveal any special solvent effects that could not be attributed to poor solubility.

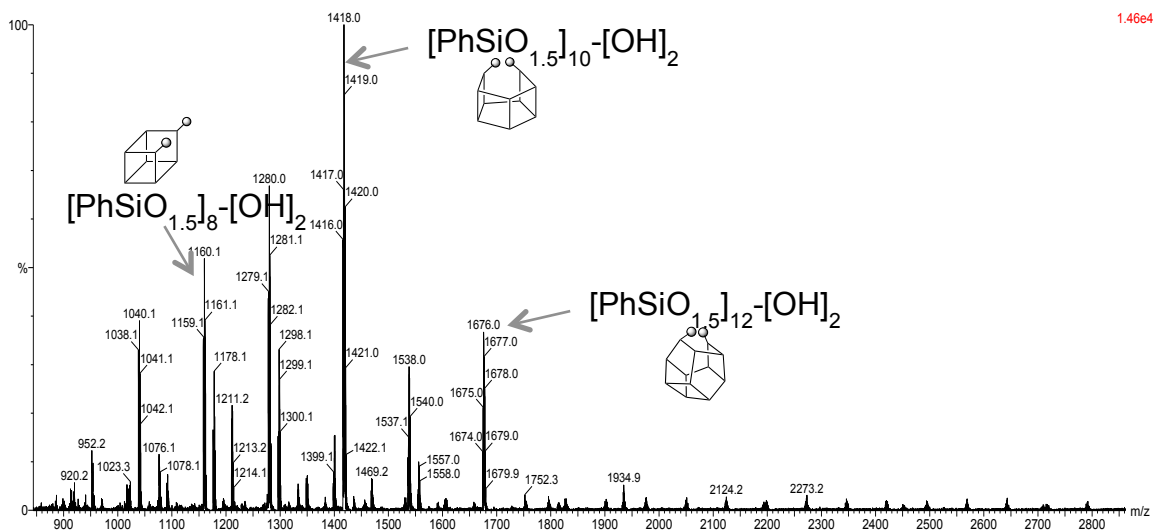


Figure 4.19. MALDI-ToF spectrum of OPS + TBAF in DMF after 24 h (Reaction 20).

As part of our studies, we also attempted to characterize cage fragments to gain insight into the reaction mechanism(s). EI mass spec was taken of Reaction (3) at 2 and 5 min. Figure 4.20a shows an EI mass spectrum 2 min after initiation. Both $\text{PhSi}(\text{OH})_3$ and PhSiF_3 (free corners) are observed at 156.1 and 161.9 m/z respectively. Free corners $[\text{Ag}^+\text{PhSi}(\text{OH})_2\text{F}]$, 266.2 m/z were also observed in MALDI-ToF 60 sec after adding F^- (Figure 4.20b). This peak is consistent across solvent studies and has been compared to the MALDI-ToF of TBAF to verify that it is not a component of the catalyst mixture. This supports the likelihood of free cage corner transfer mechanisms theorized by Mabry and Bowers et al.⁴²

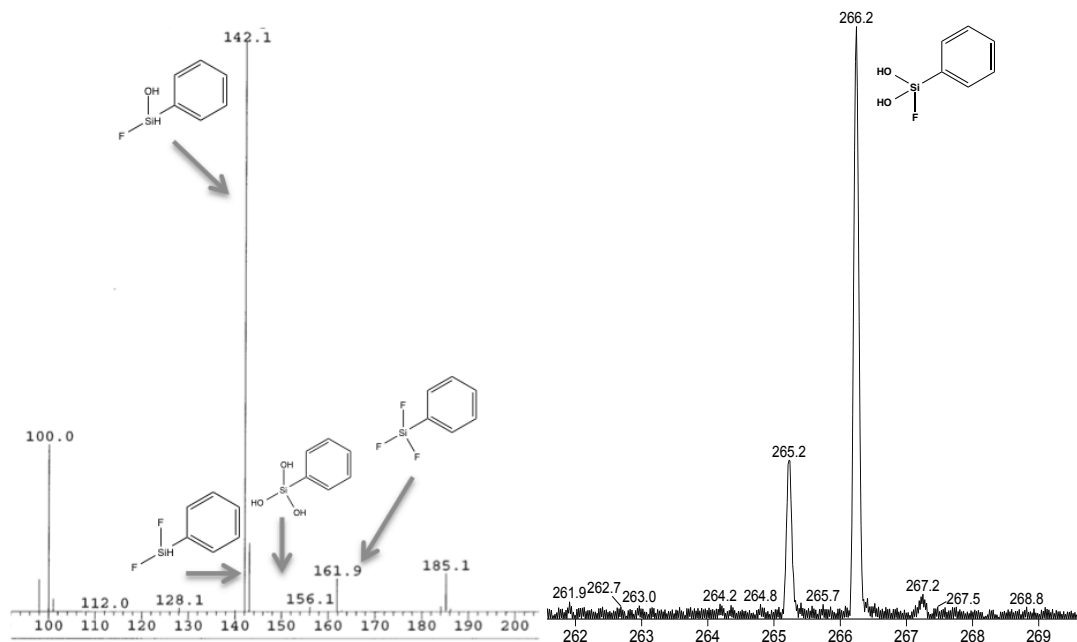


Figure 4.20. EI mass spectrum showing fluoride functionalized free corners ($185.1\text{ m/z} =$ tributylammonium), Reaction (3) after 2 min. b. MALDI-ToF showing $\text{Ag}^+ \text{PhSi}(\text{OH})_2\text{F}$ at 266.2 m/z , Reaction (3) after 1 min.

Mabry and Bowers et al. previously demonstrated the efficacy of TMAF (tetramethylammonium fluoride) in rearrangement.⁴² Efforts to use $n\text{Bu}_4\text{NX}$ ($\text{X} = \text{Cl}^-$, Br^-) gave no reaction.^{42,65} However, the introduction of 5 mol% TBAOH w/5 vol% water using Reaction (3) conditions, promoted rearrangements forming partial cages but little T_{10} (1400 m/z) (Figure 4.21), These partial cages are similar to those seen with F^- and in polar solvent studies.

The primary products observed are $[\text{PhSiO}_{1.5}]_8\text{-}[\text{OH}]_2$ and $[\text{PhSiO}_{1.5}]_{10}\text{-}[\text{OH}]_2$ 1160 and 1418 m/z respectively, which show edge opening of both the T_8 and T_{10} cages as also seen in TBAF studies, *suggesting that partial cages with -OH are more likely than -F functionalized cages in those studies.* Other previously observed partial cage peaks present include $[\text{PhSiO}_{1.5}]_7\text{-}[\text{OH}]_3$ at 1040 m/z and $[\text{PhSiO}_{1.5}]_9\text{-}[\text{OH}]$ at 1280 m/z . The peak at 1175 m/z is $[\text{PhSiO}_{1.5}]_8\text{-}[\text{OH}]_4$, a likely intermediate just prior to loss of a corner in the rearrangement process.

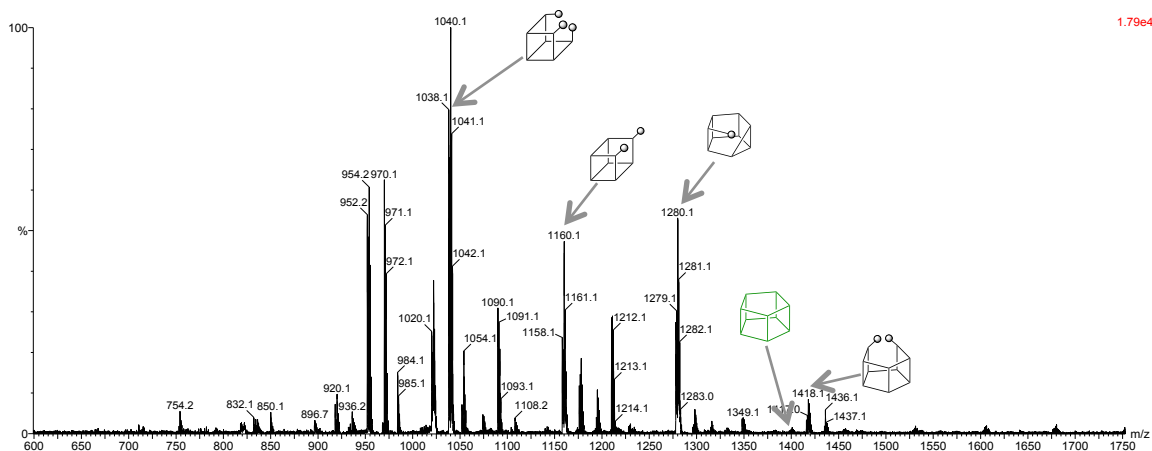


Figure 4.21. MALDI-ToF spectrum of OPS + TBAOH in DCM under pseudo Reaction (3) conditions.

We also followed changes in concentration of various reaction intermediates over time using Reaction (3) conditions (20 °C) plotting time vs intensities for T_{10} , T_8 and reaction intermediates per Figures 4.22 and 4.23.

Figure 4.22 plots $[T_8]$ over the first 50 min of reaction revealing an exponential decay suggesting a first order dependence in $[T_8]$.^{66,67} Assuming that T_8 is the sole monomer, a plot of $\ln[T_8]$ vs. time (Figure 4.23a), gives a slope of $(5.2 \times 10^{-3} \text{ s}^{-1})$ equal to the rate of T_8 consumption.

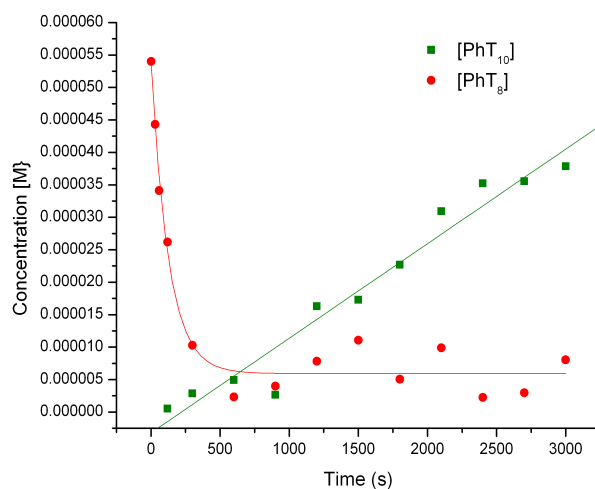


Figure 4.22. T_8 and T_{10} concentration vs time for Reaction (3) monitored by MALDI-ToF over the first 50 min of reaction.

The most likely first step as suggested above is attack of F^- on the T_8 cage and is supported by this plot. T_8 consumption at 35° , 0° and $-35^\circ C$ can be plotted to give an activation energy (Figure 4.23b, Table 4.5) of $\sim 5 \pm 1$ kcal/mol for this presumed first step. The formation of pentacoordinate intermediates for both F^- and OH^- at silicon are reported in the literature to be $\sim 5-6$ kcal/mol.⁶⁸⁻⁷⁰ The Figure 4.22 plot of $[T_{10}]$ concentration over the first 50 min is linear, suggesting the reaction is not influenced by the T_{10} concentration and T_{10} formation is not directly proportional to the consumption of T_8 . This is not unreasonable if the E_a found is similar to that for formation of a pentacoordinated intermediate as a first and slow step in the rearrangement process.

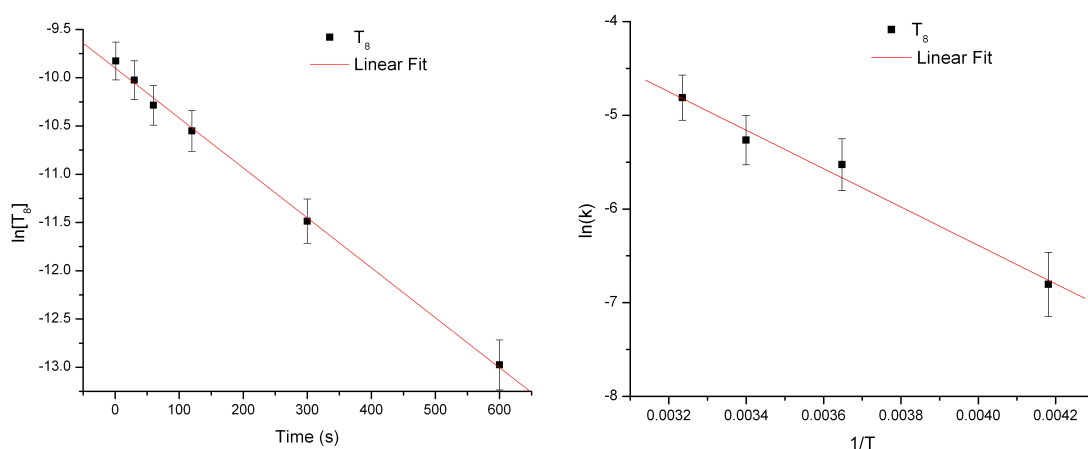


Figure 4.23. a. Natural log plot of T_8 concentration over the first 600 sec giving a slope of $-5.2 \times 10^{-3} \text{ s}^{-1}$. b. Arrhenius plot from T_8 concentrations at 35° , 20° , 0° , and $-35^\circ C$, $E_a \sim 5 \pm 1$ kcal/mol.

Table 4.5. Rate constants from T_8 consumption at different temperatures.

Temperature $^\circ C$	k (s^{-1})
35	6.7×10^{-3}
20	5.2×10^{-3}
0	1.8×10^{-3}
-35	$7 \times 10^{-4*}$

*After 25 min induction period.

Partial cage intermediates predominate after the first 600 sec of reaction. Figure 4.24 uses MALDI-ToF to plot four dominant intermediates throughout the reaction. The intermediates tracked over time were inconsistent and do not permit kinetics analyses.

These studies provide a critical analysis of the rearrangement mechanism(s). First, fluoride encapsulation is not observed in ^{19}F NMR. Second, large cages (T_{16+}) do not appear early, thus they must form late in the process perhaps because of their higher energies ($5 \text{ hartrees/Si} > T_8$). Third, cage fragments of 2 - 5 Si units are not seen in MALDI-ToF or EI-MS studies. Fourth, free cage corners containing both F and OH were observed early on in EI and MALDI-ToF MS, suggesting their mechanistic involvement. Fifth, TBAF solutions are known to contain four main species: OH^- , HF_2^- , and H_2O , each

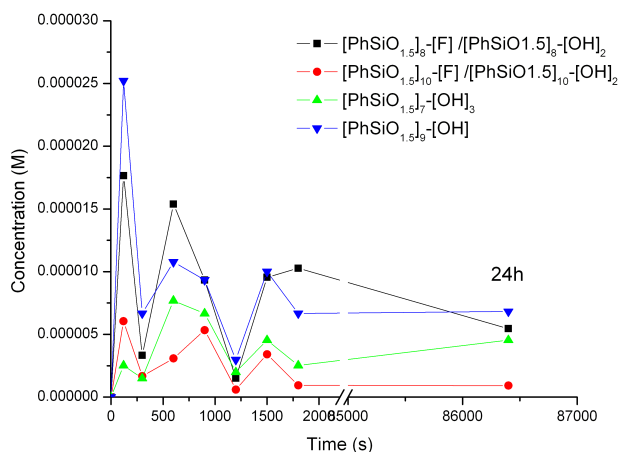


Figure 4.24. Reaction (3) intermediate concentrations by MALDI-ToF over the first 25 min and then after 24 h.

of these components or a combination of them could contribute to the reaction mechanism(s). Sixth, H_2^{18}O studies show that ^{18}O readily incorporates into the T_{10} and partial cages, indicating at a minimum that free Si-OH forms and readily exchanges with water present. Given the results with TBAOH, hydroxyl groups may also participate in cage/ring-opening processes. Seventh, solvent choice greatly influences the final product ratio and composition, likely due to the difference in solubilities and stabilities of reaction intermediates. We find that dichloromethane gives the highest ratio of T_{10} and the fewest partial cages after equilibration. Eighth, $[\text{MeSiO}_{1.5}]_n$ and $[\text{PhSiO}_{1.5}]_n$ scramble with F^- to form mixed functional cages, but $[\text{MeSiO}_{1.5}]_n$ does not rearrange on its own, suggesting units from $[\text{PhSiO}_{1.5}]_n$, such as a free corner, must attack $[\text{MeSiO}_{1.5}]_n$ to insert $\text{PhSiO}_{1.5}$ to make mixed functional cages.²⁸ Lastly, the quenching step with CaCl_2 serves to remove fluoride ions to halt equilibration.

From the mass spec and NMR studies above we have proposed the structures of reaction intermediates, but we were not able to follow the changes in concentration of reaction intermediates to determine a proposed mechanism based solely on experiment. In order to determine the most likely pathways we now turn to computational analysis.

4.4.3 Modeling Studies

$[\text{HSiO}_{1.5}]_n$ was used to model the $[\text{PhSiO}_{1.5}]_n$ systems within the Gamess computational package.⁵²⁻⁵³ We determine the energies of the analogous $[\text{HSiO}_{1.5}]_n$ intermediates proposed above from mass spec by adapting the methods of Kudo et al who modeled T_8 cage formation from $\text{HSi}(\text{OH})_3$.⁴⁴

The gas phase B3LYP-6-31G(d) method was used to generate: 1. geometry optimized structures (Figure 4.25); 2. thermal analysis using a double difference Hessian frequency calculations; and 3. single point energy calculations, for formation of T_8 from T_{10} . MP2 energy calculations were also performed on select systems. Table 4.6 compiles energy calculations for several cage/partial cage species. In gas phase computation, T_{10} and T_{12} are both lower in total energy than T_8 by 1 and 1.5 kcal/mol/Si unit respectively, which is reasonable when compared to literature (-0.3 and -0.5 kcal/mol respectively by Hartree Fock (HF) methods^{47,71-73}). These energy values, combined with the thermal analyses were used to determine heats of reaction for conversions between intermediates (Figure 26).

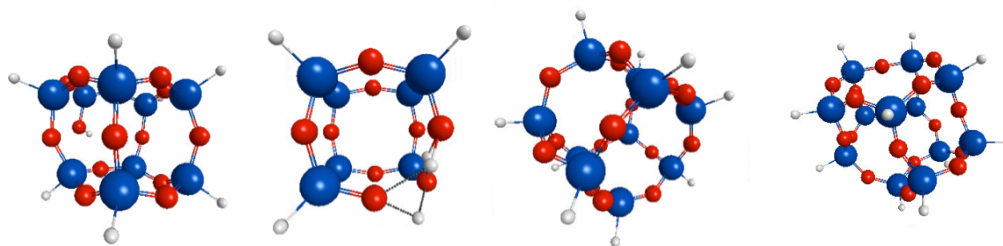


Figure 4.25a-d. B3LYP optimized structures: a) $T_9\text{-OH}_1$ b) $T_7\text{-OH}_3$, c) T_{10} , d) T_{12} .

Table 4.6. MP2 and B3LYP (6-31G(d)) total energies in Hartrees (gas and DCM), solvent stabilization energies in kcal/mol and ZPC corrected electronic+thermal enthalpies (Hartrees) of some HSQ structures.

SQ	MP2 Energy (Hartrees)	B3LYP Energy (Hartrees)	ΔE [gas phase to solvent] (kcal/mol)	B3LYP ZPC corrected Electronic + Thermal Enthalpy (Hartrees)
T ₉ -OH ₃	-3734.982	-3741.369	-5.62	N/A
T ₉ -OH ₁	-3658.839	-3664.958	-3.87	-3664.573
T ₇ -OH ₃	-2930.217	-2935.274	-5.81	-2935.037
T ₈ -OH ₄	N/A	-3376.601	-10.87	-3376.124
T ₉ -OH ₅	N/A	-3817.765	-10.21	N/A
T ₁₀ -OH ₄	N/A	-4182.537	-10.35	N/A
T ₁₁ -OH ₁	N/A	-4470.896	-4.80	N/A
T ₁₀	-4022.793	-4009.551	-9.71	-4009.139
T ₁₂	-4827.580	-4811.468	-2.71	-4810.983
T ₆	-2413.816	-2417.839	-3.20	N/A
T ₈	-3215.6	-3207.6204	-1.71	-3207.299
T ₁₆	-6447.571	-6447.578	-4.60	N/A
T ₁₈	-7253.547	-7253.547	-4.70	N/A
T ₂₀	-8059.500	-8059.500	-4.96	N/A
T ₈ F ⁻ exo	N/A	-3323.522	-33.58	-3323.301
T ₈ F ⁻ endo	N/A	-3323.728	-33.73	
T ₈ -(OH) ₁₀ Linear	N/A	-3605.73	-17.22	N/A

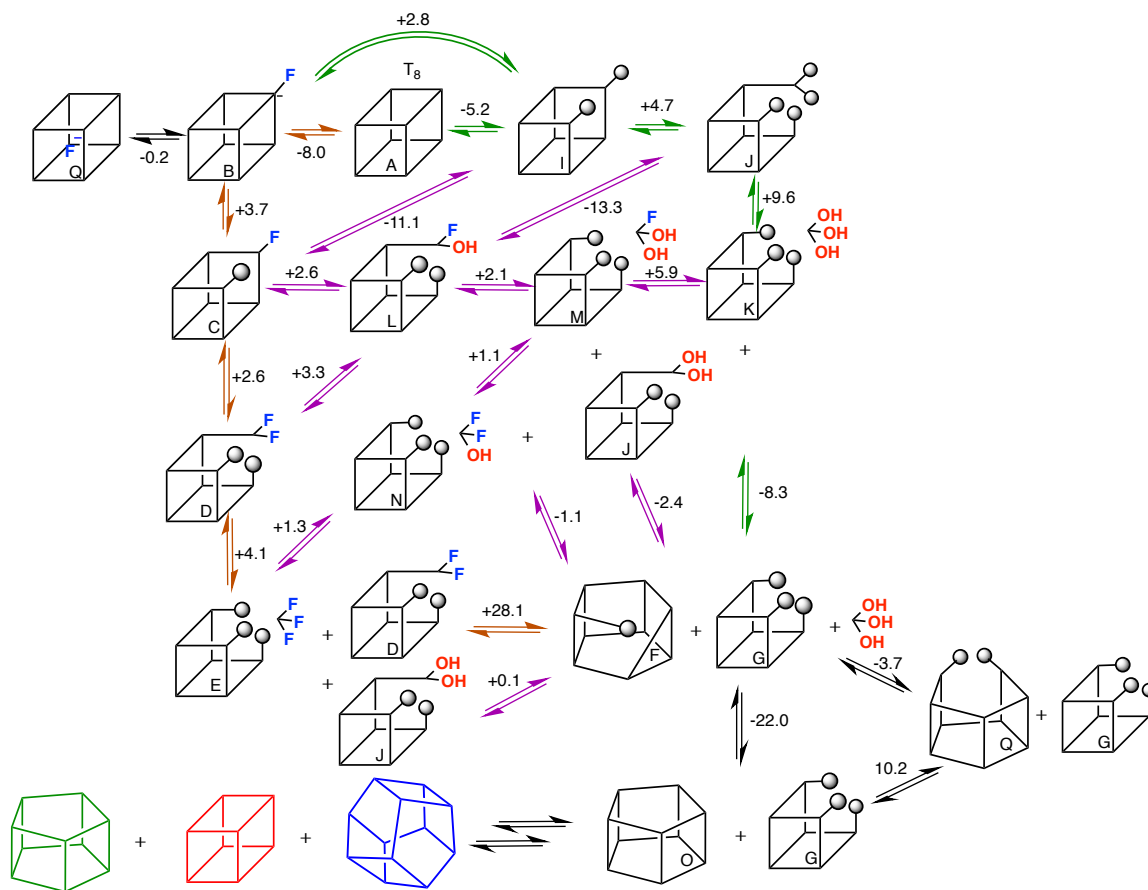


Figure 4.26. Potential mechanism from observed reaction intermediates and their model $[\text{HSiO}_{1.5}]_n$ heats of reaction, ΔH (kcal/mol).*

ΔH are given on the side of the forward reaction arrow, spheres represent hydroxide capped corners, corners represent H-Si units, and lines represent oxygen bridges. Orange corresponds to F^- catalyzed pathway with net energy of 8.5 kcal/mol; Green corresponds to an OH^- -catalyzed pathway with net energy -21.2 kcal/mol; Purple corresponds to a hybrid system $\text{F}^-/(\text{OH}/\text{H}_2\text{O})$ with net energy of -24 kcal/mol.

*Enthalpies were used to ensure the most precise analysis, since free energies, which depend on entropies can be inconsistent due to the many vibrational modes present in these molecules.

Figure 4.26 depicts a non-exhaustive set of potential intermediates and reaction pathways for rearrangements of T_8 to T_{10} , with formation of T_{12} likely being similar. The formation and rearrangements of SQs most certainly involve complex multiple step and multiple intermediate processes leading to complex equilibria. We describe here three reasonable pathways based on experimental analysis. The first, shown in orange, is the pure F^- catalyzed system, with minimal involvement of water. The first step involving the formation of F-pentacoordinated T_8 [T_8 (A) to (B)] is favored enthalpically by 8 kcal/mol.

Thereafter three endothermic processes are observed in reactions (B-E), in which multiple F^- react to remove a cage corner. The biggest barrier (28 kcal/mol) is found for reaction (E+D to F+G); considerable energy is needed to remove F^- followed by replacement with ^-OH before condensation occurs. The net reaction enthalpy for the orange pathway is 8.5 kcal/mol. If we assume structure J instead of D for this conversion, the net reaction enthalpy drops dramatically to -19.5 kcal/mol.

The green pathway depends on strong ^-OH and H_2O interactions. The first step could consist of two possible reactions; 1. (A to B) activation of the cage by F^- coordination (-8.0 kcal/mol) or 2. direct attack of hydroxide (A to I). Surprisingly, both pathways are favored by the same -5.2 kcal/mol, so both are plausible. In going from (J+K to F+G to O+A) multiple intermediate steps and potential structures are possible, however few of these were repeatedly observed in our experimental studies. The net enthalpic contribution is -21.2 kcal/mol for the green pathway, which is ~ 30 kcal/mol lower than the orange pathway. The TBAOH catalyzed reaction studies support this pathway.

A hybrid mechanism using F^- with water can be proposed starting with the orange pathway (A to B to C), then following the purple arrows across (L to M) for corner removal, and then M+J through F+G to T_{10} (O). This pathway is favored by -24 kcal/mol. If the F to Q to T_{10} (O) transition is considered, the net reaction enthalpy rises to 4.5 kcal/mol. Our experimental analysis with TBAF supports the hybrid theory, since we observe mixed fluoro and hydroxyl species and ^{18}O incorporation by mass spectrum analysis, and Si-F bonds in ^{19}F and ^{29}Si NMR. Therefore we consider this (-24 kcal/mol) one of the most reasonable pathways.

Other possible but less likely mechanisms may also be considered. For example HF_2^- may act as a transient catalyst in these systems, even though it is not observed by MALDI-ToF. As mentioned above, large cage structures (T_{16} and larger) may act as intermediates in these reactions so that T_{20} would disproportionate to two T_{10} 's. However, they are only observed late in the reaction and seem to be end products rather than intermediates.

One factor not accounted for above is the influence of solvent; in that we find that using two different solvents (THF and DCM) for Reaction (3) conditions give different equilibrium product distributions of T_8 , T_{10} and T_{12} after 3 days. The explanation for

changes in equilibrium may simply be attributed to the difference in solubilities of the products in different solvents. Alternately this can be thought of in terms of solvent stabilization energies. Table 4.7 compares the computationally modeled solvent stabilization energies for T₈, T₁₀ and T₁₂ and the corresponding experimental MALDI-ToF ratios for each solvent. Though speculative, the solvent stabilization energies trend with the peak intensity ratios observed in MALDI-ToF for T₈, T₁₀ and T₁₂, showing that solvent would likely influence the mechanistic pathway, stabilizing some intermediates, while destabilizing others. Verification of this will be considered in future studies.

Table 4.7. Comparison of cage solvent stabilization energy and their corresponding MALDI ratios.

	T ₈	T ₁₀	T ₁₂
Comp E _{stab} (kcal/mol) THF	-1.6 (-0.2/Si)	-2.7 (-0.3/Si)	-2.6 (-0.2/Si)
~MALDI ratio THF	1	1	1
Comp E _{stab} (kcal/mol) DCM	-1.7 (-0.2/Si)	-9.7 (-1.0/Si)	-2.7 (-0.2/Si)
~MALDI ratio DCM	1	3	1.3

4.4.4 Photophysical Properties of [PhenylSiO_{1.5}]_x

We have previously reported on the novel photophysical properties offered by stilbene functionalized SQs. We recently realized that we had not characterized the same properties for the base systems, the phenyl cages [PhSiO_{1.5}]_{8,10,12}.⁷⁴⁻⁷⁵ While these cages all exhibit the same absorption properties; to our surprise they exhibit quite different emission behavior. Thus, Figure 4.27 compares the UV/vis and PL properties of the T_{8,10,12} and larger cage phenylSQ systems isolated in small quantities from the synthesis of PhT₁₀.

Thus, all of the cages exhibit absorption λ_{\max} at 223 and 264 nm typical of simply phenyl compounds (see Table 4.8). However, with increasing cage sizes up to T₁₂, the emission λ_{\max} shifts to red (lower energy). The PhT₈ λ_{\max} = 285 nm, which is also typical of simple phenyl compounds; however, for all the larger cages two emission are seen with λ_{\max} at 287 nm as a shoulder on a new λ_{\max} at 324-328 nm.

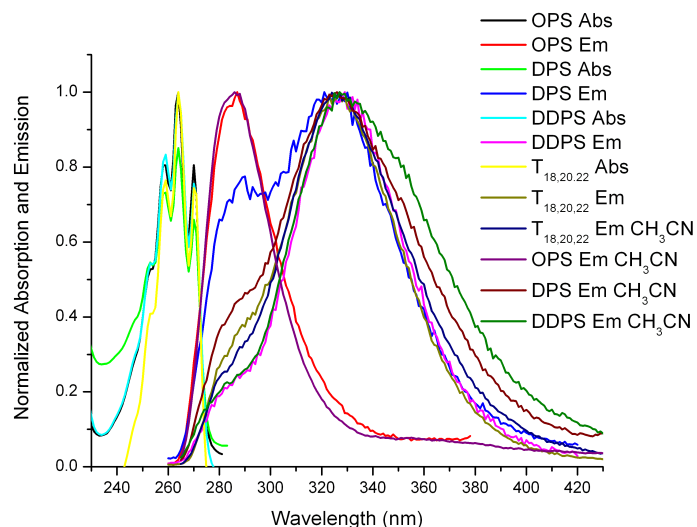


Figure 4.27. Absorption and emission spectra for $[\text{PhSiO}_{1.5}]_{8,10,12,[18,20,22]}$ in THF and acetonitrile.

It is important to note that the larger cages ($T_{18,20,22}$) show similar spectra to those observed for the T_{10} and T_{12} cages, suggesting they are likely combinations of the smaller cages. The absorption spectra of all cages are nearly identical with $\lambda_{\text{max}} = 223, 264$ nm. Table 4.8 shows the absorption and emission maxima for all the $[\text{PhSiO}_{1.5}]_x$ systems.

Table 4.8. Absorption and emission λ_{max} for $[\text{PhSiO}_{1.5}]_{8,10,12}$ and $T_{18,20,22}$ in THF.

	Cage Abs. (nm)	Abs. λ_{max} (nm)	Em. λ_{max} (nm)
$[\text{PhSiO}_{1.5}]_8$	223	264	287
$[\text{PhSiO}_{1.5}]_{10}$	223	264	324
$[\text{PhSiO}_{1.5}]_{12}$	223	264	328
$[\text{PhSiO}_{1.5}]_{18,20,22}$	223	264	327

Given that phenyl excimers typically emit at ~ 328 nm, as found in cyclic polystyrene and phenylsiloxane absorption and emission studies;⁷⁶⁻⁷⁸ we can suggest that the observed emission λ_{max} arises from formation of phenyl excimers.

Perhaps one of the more important observations is that the extent of excimer formation can be directly related to the centroid distance between adjacent phenyl rings on the cages. Thus, Figure 4.28 and Table 4.9 relate the effects centroid distance and “bite angle” or angle between phenyl groups.³⁰ The distance between phenyl groups was

found by analysis of previously determined crystal structures.²⁶ As might be expected from the cage structures, the centroid distances and angles between the phenyl groups decrease with increasing cage size.

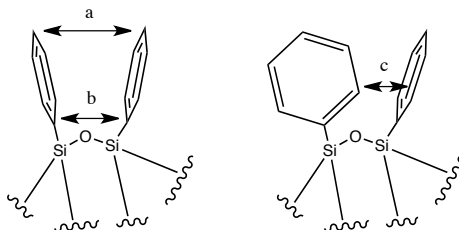


Figure 4.28. Proposed interaction orientations between phenyl groups.

This suggests that the phenyl groups' Förster radius for energy transfer is met when going to the T₁₀ cage size and gives even more orbital overlap in the larger cages. Though we have not calculated the Förster radius for the phenyl compounds, our previous calculations for stilbene

Table 4.9. Phenyl-phenyl distances for different cage sizes.

	a (Å)	b (Å)	c (Å)	Centroid (Å)
[PhSiO _{1.5}] ₈	8.20	5.15	4.74	6.76
[PhSiO _{1.5}] ₁₀	7.43	4.94	4.68	6.21
[PhSiO _{1.5}] ₁₂	7.14	4.90	4.42	6.02

systems suggest that the radius for energy transfer to be ≈ 7 Å, which is on the same order for what we observe here.⁵⁵ If we assume using the average centroid distance for comparison, the Förster radius for the phenyl systems would be on the order of ~ 6.5 Å, allowing for orbital overlap in the T₁₀ and larger cages, but not in the T₈. This supports the spectral observations. An alternative explanation from theoretical calculations suggest that this may also result from phenyl-cage interactions through overlapping orbitals with the cage face as discussed further below.⁷⁹

One of the more interesting set of conclusions that might be drawn from the data begins with the fact that the λ_{max} emission at 287 nm in T₈ must be exclusively from the individual phenyl groups. In contrast, two λ_{max} are observed in T₁₀ at 287 and 324 nm. This means that an excited state must be partitioning between two emitting states. Thus,

some phenyls can emit without the formation of an excimer despite the obvious lower energy of the 324 nm emitting state.

Finally for the T₁₂ system, there is a very slight shoulder at 287 nm with the major emission at $\lambda_{\text{max}} = 327$. Despite the larger cage size and extra numbers of phenyl groups, emission is almost completely from the excimer. The same observations can be made for the larger cages. *One possible conclusion from these observations is that the excimer is actually delocalized over the cage surface* basically overcoming any emission from individual phenyls.

If this were true, then one might argue that all of the shifts seen to date in the stilbene functionalized cages are from delocalized states over cage faces rather than from interactions with the cage LUMOS as proposed in several papers. However, the bromination studies described in the manuscript and reported previously strongly support LUMO interactions. Thus, at this time, it may be fair to state that both types of processes may occur. But one final study was done wherein the solvent was changed from THF to acetonitrile.

Basically, the introduction of a more polar solvent was used to ascertain if there were a polarized state formed with the excimer that would lead to red shifts in emission. As can be seen, this is not the case and as such the excimer does not exhibit CT behavior as expected for a traditional Förster energy transfer process. Consequently, the basic [PhSiO_{1.5}]_{8,10,12} photophysical property analyses provides partial support for the claims of internal excimers in these cage systems.

Further computational studies were conducted within our lab using the Gamess computational package with Configuration Interactions (CI) singles in order to determine the electronic interactions between the chromophore and the cage. Below in Figure 4.29, Figure 4.30 and Figure 4.31 we show the calculated HOMO and LUMO orbitals of the [PhSiO_{1.5}]_{8,10,12} cage systems, with HOMO and LUMO energies ± 1 given in Table 7. The energy values given are much smaller than would be realistically possible, but are given here for comparison between the cage sizes and their properties.

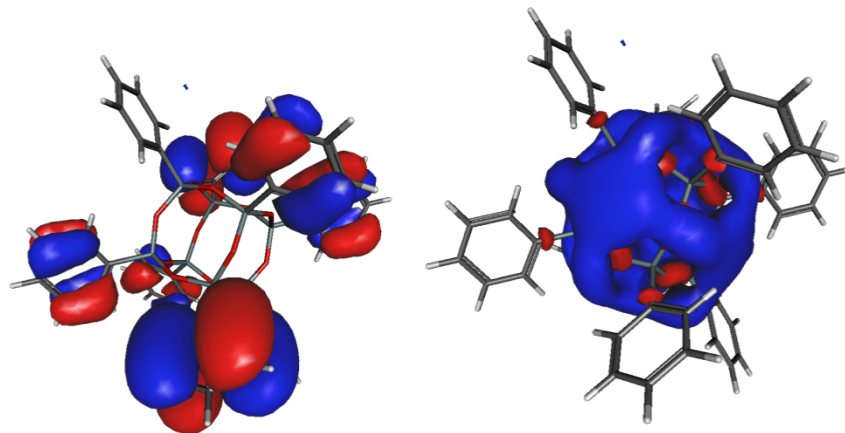


Figure 4.29. CIS-6-31G(d,p) calculated a. HOMO (-0.3272 eV) and b. LUMO (0.1062 eV) of $[\text{PhSiO}_{1.5}]_8$.

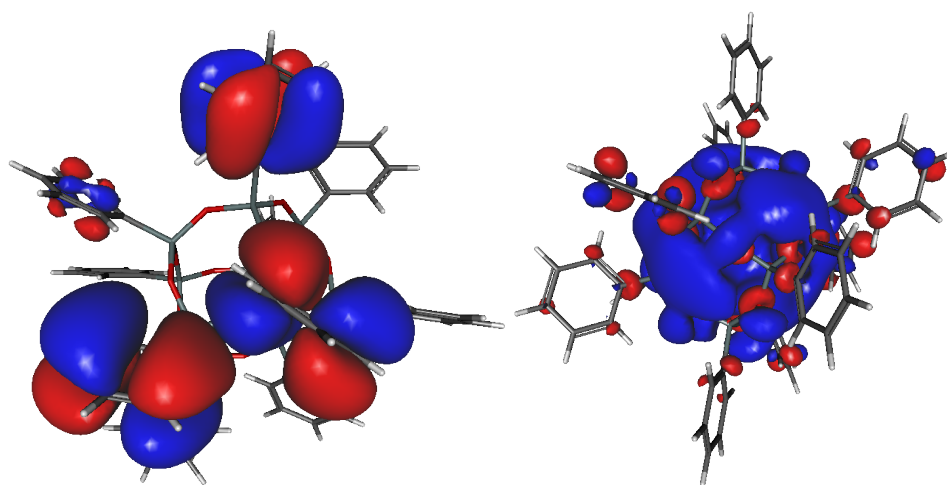


Figure 4.30. CIS-6-31G(d,p) calculated a. HOMO (-0.3221 eV) and b. LUMO (0.1087 eV) of $[\text{PhSiO}_{1.5}]_{10}$.

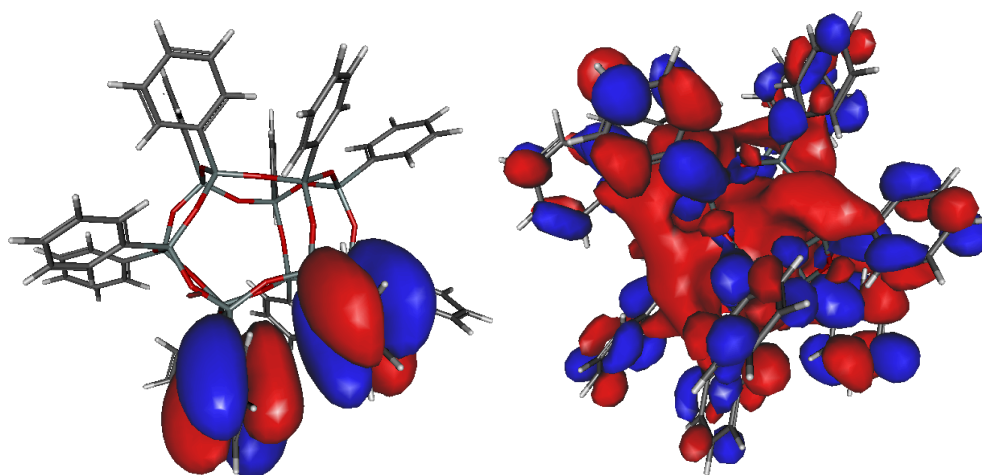


Figure 4.31. CIS-6-31G(d,p) calculated a. HOMO (-0.3174 eV) and b. LUMO (0.1180 eV) of [PhSiO_{1.5}]₁₂.

Table 4.10. CIS-6-31G(d,p) calculated HOMO and LUMO energy levels for [PhSiO_{1.5}]_x.

	[PhSiO _{1.5}] ₈	[PhSiO _{1.5}] ₈	[PhSiO _{1.5}] ₁₂
HOMO-1 (eV)	-0.3272	-0.3228	-0.3174
HOMO (eV)	-0.3272	-0.3221	-0.3173
LUMO (eV)	0.1062	0.1087	0.1180
LUMO+1 (eV)	0.1237*	0.1218*	0.1207*

*Note: LUMO+1 orbitals oriented on the phenyls and the relative distance between LUMO and LUMO+1 gets smaller with larger cages.

The above calculations may also give a reasonable explanation for why we observe changes in the emission spectra for the various cage sizes. If we compare the LUMO orbital interactions for each cage size, we see for the T₈, the LUMO is near completely centered on the cage core and cage faces, with little to no interaction with the phenyl substituents. This would likely give rise to a single peak emission on returning to the ground state. In the T₁₀ LUMO, we observe slightly more interaction between the cage and phenyl orbitals, which may give rise to a slight 3D excimer involving the cage and phenyls resulting in the combined emission observed in Figure 4.27. The T₁₂ LUMO on the other hand completely involves both the phenyls and the cage. This suggests a strong ability to delocalize the charge over the whole molecule in the excited state, giving rise to a strong excimer emission upon relaxation.

The HOMO calculations are also quite interesting. For the T₈ there is a degenerate HOMO, involving a symmetric set of phenyls, which may be expected for such a symmetric molecule. The other HOMO orbital set involves the orbitals not shown in Figure 4. When going to larger cages this degeneracy is lost. A further interesting observation is the number of orbitals contributing to the HOMO in each cage size. In the T₈, T₁₀ and T₁₂ there are 6, 4, and 2 sets of orbitals respectively contributing to the HOMO, which may have some bearing on the previously observed quantum yields for different cage sizes, in which we observe a strong decrease in quantum yields on going to larger cages. If there are fewer electrons contributing to the HOMO-LUMO transition, then we would expect lower quantum efficiencies.

4.4.5 Functionalization of [PhenylSiO_{1.5}]_{10,12}

We have also explored the synthesis and properties of [*o*-4-RstilbeneSiO_{1.5}]_{10,12}, [*o*-4-RstilbeneSiO_{1.5}]₃-[PhSiO_{1.5}]₇ and [*o*-4-RstilbeneSiO_{1.5}]₆[PhSiO_{1.5}]₆ for cage size, geometry and partial substitution effects on photophysical properties.⁸⁰ All compounds were characterized by traditional methods including solution spectroscopy and two photon absorption (TPA) cross-sections and except R = NBoc offer T_{d5%} ≥ 400°C/air. All exhibit absorption and emission spectra similar to the T₈ cages, but with some important differences. The R-stilbenes appear to interact in the excited state through the cage, exhibiting emissions spectra red-shifted from the parent stilbenes. TPA studies show novel behavior that is functional group, geometry and substitution number dependant. Thus NBoc TPA *cross-sections/moiety increase, with decreasing numbers* of functional groups from 8 to 3 for PhT₁₀ and 10 to 6 for PhT₁₂ where [NBocstilbeneSiO_{1.5}]₈ TPA/moiety ≈ 0. In contrast, CN cages offer TPA/moiety values slightly greater on going from 3 to 8 (PhT₁₀) and 6 to 10 (PhT₁₂).

NBoc TPA data are best explained if bromination occurs asymmetrically leading to asymmetric functionalization and exceptional polarization in partially substituted cages as symmetrically substituted cages exhibit opposing polarizations. *The molecular sum of the individual induced transition dipoles on excitation self-cancel.* In contrast both the cage and CN are strongly electron withdrawing such that no significant polarization is observed/expected when asymmetrically functionalized. Both NBoc and CN substituents offer red shifts greater than Me and MeO T_{10,12} suggesting extended conjugation without polarization. Asymmetric bromination is supported by DFT modelling studies where initial *o*-Br/*o*-H bonding stabilize incoming Br₂ by 300 mEv.

4.5 Conclusions

We have developed a simple F⁻ catalyzed synthetic method to [PhSiO_{1.5}]₁₀, a molecule with the rarely observed D_{5h} structural motif. [PhSiO_{1.5}]₁₀ can be synthesized from any [PhSiO_{1.5}]_n or PhSi(OR)₃ in yields up to 50% on multigram scales in CH₂Cl₂. [PhSiO_{1.5}]₁₀ offers a highly soluble, easily functionalized and stable 5-fold symmetric building block. We have shown in previous publications that the unique structure of stilbene/stilbenevinyl functionalized T₁₀ cages offer enhanced photophysical properties

such as two-photon absorption over T_8 and T_{12} . A property directly related to the polarization and charge separating ability of a system.

We have used F^- catalyzed rearrangement to make many SQ systems over the years, including vinyl and mixed phenyl/vinylSQs, however the process by which this occurs has eluded us. In this report we set out to solve at least qualitatively the processes involved in this rearrangement process, specifically for the conversion of $[PhSiO_{1.5}]_8$ to $[PhSiO_{1.5}]_{10}$. We have shown that the mechanism by which F^- catalyzed rearrangement occurs is highly complicated and involves the equilibration of many intermediates. MALDI-ToF was the most effective method for experimentally analyzing reaction progress and kinetics. We find that the activation energy for the formation of pentacoordinated F^- - $[PhSiO_{1.5}]_8$ is 5 ± 1 kcal/mol, a barrier readily overcome at room temperature, and that trace water is necessary for rearrangement to occur. With the assistance of computational modeling we proposed the three most plausible reaction pathways, finding that F^- catalyzed rearrangement most likely follows a hybrid mechanism involving F^- and water with a net enthalpic favorability of -24 kcal/mol. The mechanistic studies described here will help in the design of F^- catalyzed reaction conditions for favoring specific cage sizes and synthesizing other $[RSiO_{1.5}]_{10}$ derivatives.

Photophysical property analysis of $[PhSiO_{1.5}]_{8,10,12}$ show that with increasing cage size the extent of excimer formation in fluorescence also increases from 287 nm for $[PhSiO_{1.5}]_8$ to 328 nm for $[PhSiO_{1.5}]_{12}$. This is indicative of greater charge delocalization in the larger cages.

References:

1. Voronkov, M.; Lavrent'yev, V. Polyhedral Oligosilsesquioxanes and Their Homo Derivatives. *Top. Curr. Chem.* **1982**, *102*, 199–236.
2. Baney, R. H.; Itoh, M.; Sakakibara, A.; Suzuki, T. Silsesquioxanes. *Chem. Rev.* **1995**, *95*, 1409–1430.
3. Loy, D.; Shea, K. Bridged Polysilsesquioxanes. Highly Porous Hybrid Organic-Inorganic Materials. *Chem. Rev.* **1995**, *95*, 1431–1442.
4. Calzaferri, G.; “Silsesquioxanes,” in Tailor-made Silicon-Oxygen Compounds, from molecules to materials, R. Corriu and P. Jutzi eds. Publ. Friedr. Vieweg&Sohn GmbH, Braunschweig/Weisbaden, Germany 1996, 149-169.
5. Lichtenhan, J.; “Silsesquioxane-based Polymers,” in Polymeric Materials Encyc., J.C. Salamone Ed. Vol. 10, CRC Press, N.Y., 1996, 7768-77.
6. Provatas, A.; Matison, J.G.; Synthesis and Applications of Silsesquioxanes *Trends Polym. Sci.* **1997**, *5*, 327-33.

7. Wang, L.; Ni, H.; Pittman Jr, C. U. Polyhedral Oligomeric Silsesquioxane (POSS) Polymers and Copolymers: A Review. *J. Inorg. Organomet. Polym.* **2002**, *11*, 123–154.
8. Duchateau, R. Incompletely Condensed Silsesquioxanes: Versatile Tools in Developing Silica-Supported Olefin Polymerization Catalysts. *Chem. Rev.* **2002**, *102*, 3525–3542.
9. Abe, Y.; Gunji, T. Oligo- and Polysiloxanes. *Prog. Polym. Sci.* **2004**, *29*, 149–182.
10. Phillips, S. H.; Haddad, T. S.; Tomczak, S. J. Developments in Nanoscience: Polyhedral Oligomeric Silsesquioxane (POSS)-Polymers. *Curr. Opin. Solid State Mater. Sci.* **2004**, *8*, 21–29.
11. Kannan, R. Y.; Salacinski, H. J.; Butler, P. E.; Seifalian, A. M. Polyhedral Oligomeric Silsesquioxane Nanocomposites: The next Generation Material for Biomedical Applications. *Acc. Chem. Res.* **2005**, *38*, 879–884.
12. Laine, R. M. Nanobuilding Blocks Based on the $[\text{OSiO}_{1.5}]_x$ ($x = 6, 8, 10$) Octasilsesquioxanes. *J. Mater. Chem.* **2005**, *15*, 3725.
13. Lickiss, P. D.; Rataboul, F. Fully Condensed Polyhedral Oligosilsesquioxanes (POSS): From Synthesis to Application. *Adv. Organomet. Chem.* **2008**, *57*, 1–116.
14. Chan, K. L.; Sonar, P.; Sellinger, A. Cubic Silsesquioxanes for Use in Solution Processable Organic Light Emitting Diodes (OLED). *J. Mater. Chem.* **2009**, *19*, 9103.
15. Wu, J.; Mather, P. T. POSS Polymers: Physical Properties and Biomaterials Applications. *Polym. Rev.* **2009**, *49*, 25–63.
16. Cordes, D. B.; Lickiss, P. D.; Rataboul, F. Recent Developments in the Chemistry of Cubic Polyhedral Oligosilsesquioxanes. *Chem. Rev.* **2010**, *110*, 2081–2173.
17. Laine, R. M.; Roll, M. F. Polyhedral Phenylsilsesquioxanes. *Macromolecules* **2011**, *44*, 1073–1109.
18. Pescarmona, P.; Maschmeyer, T. Oligomeric Silsesquioxanes: Synthesis, Characterization and Selected Applications. *Aust. J. Chem.* **2001**, *54*, 583–596.
19. Chimjarn, S.; Kunthom, R.; Chancharone, P.; Sodkhomkhum, R.; Sangtrirutnugul, P.; Ervithayasuporn, V. Synthesis of Aromatic Functionalized Cage-Rearranged Silsesquioxanes (T8, T10, and T12) via Nucleophilic Substitution Reactions. *Dalt. Trans.* **2015**, *44*, 916–919.
20. Ervithayasuporn, V.; Chimjarn, S. Synthesis and Isolation of Methacrylate- and Acrylate-Functionalized Polyhedral Oligomeric Silsesquioxanes (T8, T10, and T12) and Characterization of the Relationship between Their Chemical Structures and Physical Properties. *Inorg. Chem.* **2013**, *52*, 13108–13112.
21. Lee, A. S.; Choi, S.-S.; Lee, H. S.; Baek, K.-Y.; Hwang, S. S. A New, Higher Yielding Synthetic Route towards Dodecaphenyl Cage Silsesquioxanes: Synthesis and Mechanistic Insights. *Dalt. Trans.* **2012**, *41*, 10585.
22. Kawakami, Y.; Kabe, Y. Novel Meta-Selective Friedel–Crafts Acylation of Phenylsilsesquioxane. *Chem. Lett.* **2010**, *39*, 1082–1083.
23. Barry, A. J.; Daudt, W. H.; Domicone, J. J.; Gilkey, J. W. Crystalline Organosilsesquioxanes. *J. Am. Chem. Soc.* **1955**, *77*, 4248–4252.

24. Brown, J. F.; Vogt, L. H.; Prescott, P. I. Preparation and Characterization of the Lower Equilibrated Phenylsilsesquioxanes. *J. Am. Chem. Soc.* **1964**, *86*, 1120–1125.
25. Bassindale, A. R.; Liu, Z.; MacKinnon, I. A.; Taylor, P. G.; Yang, Y.; Light, M. E.; Horton, P. N.; Hursthouse, M. B. A Higher Yielding Route for T8 Silsesquioxane Cages and X-Ray Crystal Structures of Some Novel Spherosilicates. *Dalt. Trans.* **2003**, 2945–2949.
26. Roll, M. F.; Kampf, J. W.; Kim, Y.; Yi, E.; Laine, R. M. Nano Building Blocks via Iodination of $[\text{PhSiO}_{1.5}]_n$, Forming High-Surface-Area, Thermally Stable, Microporous Materials via Thermal Elimination of I_2 . *J. Am. Chem. Soc.* **2010**, *132*, 10171–10183.
27. Asuncion, M. Z.; Laine, R. M. Fluoride Rearrangement Reactions of Polyphenyl- and Polyvinylsilsesquioxanes as a Facile Route to Mixed Functional Phenyl, Vinyl T10 and T12 Silsesquioxanes. *J. Am. Chem. Soc.* **2010**, *132*, 3723–3736.
28. Ronchi, M.; Sulaiman, S.; Boston, N. R.; Laine, R. M. Fluoride Catalyzed Rearrangements of Polysilsesquioxanes, Mixed Me, Vinyl T8, Me, Vinyl T10 and T12 Cages. *Appl. Organomet. Chem.* **2009**, *24*, 551–557.
29. Jung, J. H.; Laine, R. M. Beads on a Chain (BOC) Polymers Formed from the Reaction of $\text{NH}_2\text{PhSiO}_{1.5}]_X$ $[\text{PhSiO}_{1.5}]_{10-X}$ and $[\text{NH}_2\text{PhSiO}_{1.5}]_X$ $[\text{PhSiO}_{1.5}]_{12-X}$ Mixtures ($X = 2-4$) with the Diglycidyl Ether of Bisphenol A. *Macromolecules* **2011**, *44*, 7263–7272.
30. Jung, J. H.; Furgal, J.; Goodson III, T. G.; Mizumo, T.; Schwartz, M.; Chou, K.; Vonnet, J.-F.; Laine, R. M. 3-D Molecular Mixtures of Catalytically Functionalized $[\text{vinylSiO}_{1.5}]_{10}$ / $[\text{vinylSiO}_{1.5}]_{12}$. Photophysical Characterization of Second Generation Derivatives. *Chem. Mater.* **2012**, *24*, 1883–1895.
31. Jung, J. H.; Furgal, J. C.; Clark, S. C.; Schwartz, M. C.; Chou, K.; Laine, R. M. “Copolymerization of $[p\text{-IPhSiO}_{1.5}]_8$, I_8OPS] with Divinyl (DVB)- and Diethynylbenzene (DEB) gives Beads on a Chain (BoC) Polymers with Functionalized Beads. The DEB Systems Exhibit through Chain, Extended 3-D Conjugation in the Excited State.” *Macromolecules*, **2013**, *46*, 7580-7590.
32. Furgal, J.C.; Jung, J.H.; Clark, S.C.; Goodson III, T.; Laine, R.M. “Beads on a Chain (BoC), Phenylsilsesquioxane (SQ), Conjugated Polymers Via F^- Catalyzed Rearrangements and ADMET and Reverse Heck Cross-coupling Reactions; through chain, extended conjugation in 3-D,” *Macromolecules* **2013**, *46*, 7591-7604.
33. Miyazato, A.; Pakjamsai, C.; Kawakami, Y. Octa, Deca, and dodeca(4-Nitrophenyl) Cage Silsesquioxanes via 4-Trimethylsilylphenyl Derivatives. *Dalton Trans.* **2010**, *39*, 3239–3244.
34. Roll, M. F.; Kampf, J. W.; Laine, R. M. Halogen Bonding Motifs in Polyhedral Phenylsilsesquioxanes: Effects of Systematic Variations in Geometry or Substitution. *Cryst. Growth Des.* **2011**, *11*, 4360–4367.
35. Feng, X.; Zhu, S.; Yue, K.; Su, H.; Guo, K.; Wesdemiotis, C.; Zhang, W.-B.; Cheng, S. Z. D.; Li, Y. T_{10} Polyhedral Oligomeric Silsesquioxane-Based Shape Amphiphiles with Diverse Head Functionalities via “Click” Chemistry. *ACS Macro Lett.* **2014**, *3*, 900–905.

36. Bauert, T.; Merz, L.; Bandera, D.; Parschau, M.; Siegel, J. S.; Ernst, K.-H. Building 2D Crystals from 5-Fold-Symmetric Molecules. *J. Am. Chem. Soc.* **2009**, *131*, 3460–3461.
37. Ayme, J.-F.; Beves, J. E.; Leigh, D. A.; McBurney, R. T.; Rissanen, K.; Schultz, D. Pentameric Circular Iron(II) Double Helicates and a Molecular Pentafoil Knot. *J. Am. Chem. Soc.* **2012**, *134*, 9488–9497.
38. Bassindale, A. R.; Chen, H.; Liu, Z.; MacKinnon, I. A.; Parker, D. J.; Taylor, P. G.; Yang, Y.; Light, M. E.; Horton, P. N.; Hursthouse, M. B. A Higher Yielding Route to Octasilsesquioxane Cages Using Tetrabutylammonium Fluoride, Part 2: Further Synthetic Advances, Mechanistic Investigations and X-Ray Crystal Structure Studies into the Factors That Determine Cage Geometry in the Solid State. *J. Organomet. Chem.* **2004**, *689*, 3287–3300.
39. Bassindale, A. R.; Pourny, M.; Taylor, P. G.; Hursthouse, M. B.; Light, M. E. Fluoride-Ion Encapsulation within a Silsesquioxane Cage. *Angew. Chem. Int. Ed.* **2003**, *115*, 3611–3614.
40. El Aziz, Y.; Bassindale, A. R.; Taylor, P. G.; Horton, P. N.; Stephenson, R. A.; Hursthouse, M. B. Facile Synthesis of Novel Functionalized Silsesquioxane Nanostructures Containing an Encapsulated Fluoride Anion. *Organometallics* **2012**, *31*, 6032–6040.
41. Rikowski, E.; Marsmann, H. C. Cage-Rearrangement of Silsesquioxanes. *Polyhedron* **1997**, *16*, 3357–3361.
42. Anderson, S. E.; Bodzin, D. J.; Haddad, T. S.; Boatz, J. a.; Mabry, J. M.; Mitchell, C.; Bowers, M. T. Structural Investigation of Encapsulated Fluoride in Polyhedral Oligomeric Silsesquioxane Cages Using Ion Mobility Mass Spectrometry and Molecular Mechanics. *Chem. Mater.* **2008**, *20*, 4299–4309.
43. Bahrami, M.; Hashemi, H.; Ma, X.; Kieffer, J.; Laine, R. M. Why Do the [PhSiO(1.5)](8,10,12) Cages Self-Brominate Primarily in the Ortho Position? Modeling Reveals a Strong Cage Influence on the Mechanism. *Phys. Chem. Chem. Phys.* **2014**, *16*, 25760–25764.
44. Kudo, T.; Gordon, M. S. Theoretical Studies of the Mechanism for the Synthesis of Silsesquioxanes. 1. Hydrolysis and Initial Condensation. *J. Am. Chem. Soc.* **1998**, *120*, 11432–11438.
45. Kudo, T.; Gordon, M. S. Theoretical Studies of the Mechanism for the Synthesis of Silsesquioxanes. 2. Cyclosiloxanes (D3 and D4). *J. Phys. Chem. A* **2000**, *104*, 4058–4063.
46. Kudo, T.; Gordon, M. S. Exploring the Mechanism for the Synthesis of Silsesquioxanes. 3. The Effect of Substituents and Water. *J. Phys. Chem. A* **2002**, *106*, 11347–1135.
47. Kudo, T.; Machida, K.; Gordon, M. S. Exploring the Mechanism for the Synthesis of Silsesquioxanes. 4. The Synthesis of T8. *J. Phys. Chem. A* **2005**, *109*, 5424–5429.
48. Yamamoto, S.; Yasuda, N.; Ueyama, A.; Adachi, H.; Ishikawa, M. Mechanism for the Formation of Poly(phenylsilsesquioxane), *Macromolecules* **2004**, *37*, 2775–2778.
49. Feher, F.; Schwab, J. J.; Soulivong, D.; Ziller, J. W. Synthesis, Characterization and Reactivity of cis-cis-cis [(C₆H₅)₄Si₄O₄-(OH)₄], *Main Group Chem.* **1997**, *2*,

- 123–32.
50. Pescarmona, P. P.; Raimondi, M. E.; Tetteh, J.; McKay, B.; Maschmeyer, T. Mechanistic Study of Silsesquioxane Synthesis by Mass Spectrometry and in Situ ATR FT-IR Spectroscopy. *J. Phys. Chem. A* **2003**, *107*, 8885–8892.
 51. Brown, J. F., Jr. The Polycondensation of Phenylsilanetriol. *J. Am. Chem. Soc.* **1965**, *87*, 4317–4324.
 52. Schmidt, M.W.; Baldrige, K.K.; Boatz, J.A.; Elbert, S.T.; Gordon, M.S.; Jensen, J.H.; Koseki, S.; Matsunaga, N.; Nguyen, K.A.; Su, S.; Windus, T.L.; Dupius, M.; Montgomery, J.A. "General Atomic and Molecular Electronic Structure System" *J. Comput. Chem.*, **1993**, *14*, 1347-1363.
 53. "Advances in electronic structure theory: GAMESS a decade later" M.S. Gordon, M.W. Schmidt pp. 1167-1189, in "Theory and Applications of Computational Chemistry: the first forty years" C.E. Dykstra, G. Frenking, K.S. Kim, G.E. Scuseria (editors), Elsevier, Amsterdam, 2005.
 54. Li, Z.; Kawakami, Y. Formation of Incompletely Condensed Oligosilsesquioxanes by Hydrolysis of Completely Condensed POSS via Reshuffling. *Chem. Lett.* **2008**, *37*, 804–805.
 55. Furgal, J.C.; Jung, J.H.; Goodson, T.; Laine, R.M. Analyzing Structure-Photophysical Property Relationships of Isolated T₈, T₁₀, and T₁₂ Stilbenevinyl Silsesquioxanes, *J. Am. Chem. Soc.*, **2013**, *135*, 12259-12269.
 56. Lenormand, H.; Goddard, J. P.; Fensterbank, L. Spirosilane Derivatives as Fluoride Sensors. *Org. Lett.* **2013**, *15*, 748–751.
 57. Klanberg, F.; Muetterties, E. L. Nuclear Magnetic Resonance Studies On Pentacoordinate Silicon Silicon Fluorides. *Inorg. Chem* **1968**, *7*, 155.
 58. Farnham, W. B.; Harlow, R. L. Stereomutation at Pentacoordinate Silicon by Intramolecular Ligand Exchange. *J. Am. Chem. Soc.* **1981**, *15*, 4608–4610.
 59. Day, R. O.; Sreelatha, C.; Deiters, J. a.; Johnson, S. E.; Holmes, J. M.; Howe, L.; Holmes, R. R. Anionic Five-Coordinated Cyclic Organofluorosilicates Varying in Ring Size From Five- To Seven-Membered. *Phosphorus. Sulfur. Silicon Relat. Elem.* **1995**, *100*, 87–105.
 60. Voronkov, M. G.; Boyarkina, E. V; Gebel, I. a; Albanov, a I.; Basenko, S. V. Cleavage of the C-Si Bond in Trifluoro (Phenyl) Silane with Aliphatic Alcohols. *Russ. J. Gen. Chem.* **2005**, *75*, 1927–1929.
 61. Aguilar, J. A.; Morris, G. A.; Kenwright, A. M. "Pure Shift" ¹H NMR, a Robust Method for Revealing Heteronuclear Couplings in Complex Spectra. *RSC Adv.* **2014**, *4*, 8278.
 62. Tossell, J. Calculation of ¹⁹F and ²⁹Si NMR Shifts and Stabilities of F-Encapsulating Silsesquioxanes. *J. Phys. Chem. C* **2007**, *111*, 3584–3590.
 63. Yu, G.; Zhang, Z.; Han, C.; Xue, M.; Zhou, Q.; Huang, F. A Non-Symmetric pillar[5]arene-Based Selective Anion Receptor for Fluoride. *Chem. Commun.* **2012**, *48*, 2958.
 64. Laine, R.M.; Bahrami, M.; Zhang, X. *Manuscript in Preparation.*
 65. Ronchi, M.; Laine, R.M. *Unpublished Results*
 66. Cheng, H.; Tamaki, R.; Laine, R. M.; Babonneau, F.; Chujo, Y.; Treadwell, D. R. Neutral Alkoxysilanes from Silica. *J. Am. Chem. Soc.* **2000**, *122*, 10063–10072.

67. Anslyn, E. V.; Dougherty, D. A. *Modern Physical Organic Chemistry*; Murdzek, J., Ed.; University Science Books: Sausalito, CA, 2006; pp. 355–406.
68. Asuncion, M. Z.; Hasegawa, I.; Kampf, J. W.; Laine, R. M. The Selective Dissolution of Rice Hull Ash to Form $[\text{OSiO}_{1.5}]_8[\text{R}_4\text{N}]_8$ (R = Me, $\text{CH}_2\text{CH}_2\text{OH}$) Octasilicates. Basic Nanobuilding Blocks and Possible Models of Intermediates Formed during Biosilicification Processes. *J. Mater. Chem.* **2005**, *15*, 2114.
69. Day, R. O.; Sreelatha, C.; Deiters, J. A.; Johnson, S. E.; Holmes, J. M.; Howe, L.; Holmes, R. R. Anionic Five-Coordinated Cyclic Organofluorosilicates Varying in Ring Size From Five- To Seven-Membered. *Phosphorus. Sulfur. Silicon Relat. Elem.* **1995**, *100*, 87–105.
70. Marat, R. K.; Janzen, A. F. Fluorine Exchange between Four-, Five-, and Six-Coordinate Silicon Compounds. *Can. J. Chem.* **1977**, *55*, 3845–3849.
71. Xiang, K.-H.; Pandey, R.; Pernisz, U. C.; Freeman, C. Theoretical Study of Structural and Electronic Properties of H-Silsesquioxanes. *J. Phys. Chem. B* **1998**, *102*, 8704–8711.
72. Park, S. S.; Xiao, C.; Hagelberg, F.; Hossain, D.; Pittman, C. U.; Saebo, S. Endohedral and Exohedral Complexes of Polyhedral Double Four-Membered-Ring (D4R) Units with Atomic and Ionic Impurities. *J. Phys. Chem. A* **2004**, *108*, 11260–11272.
73. Jug, K.; Gloriov, I. P. Mechanism of Silsesquioxane Growth. *Phys. Chem. Chem. Phys.* **2002**, *4*, 1062–1066.
74. Sulaiman, S.; Zhang, J.; Goodson, I. T.; Laine, R. M. Synthesis, Characterization and Photophysical Properties of Polyfunctional Phenylsilsesquioxanes: $[\text{o-RPhSiO}_{1.5}]_8$, $[\text{2,5-R}_2\text{PhSiO}_{1.5}]_8$, and $[\text{R}_3\text{PhSiO}_{1.5}]_8$. Compounds with the Highest Number of Functional Units/unit Volume. *J. Mater. Chem.* **2011**, *21*, 11177.
75. Laine, R. M.; Sulaiman, S.; Brick, C.; Roll, M.; Tamaki, R.; Asuncion, M. Z.; Neurock, M.; Filhol, J.-S.; Lee, C.-Y.; Zhang, J.; et al. Synthesis and Photophysical Properties of Stilbeneoctasilsesquioxanes. Emission Behavior Coupled with Theoretical Modeling Studies Suggest a 3-D Excited State Involving the Silica Core. *J. Am. Chem. Soc.* **2010**, *132*, 3708–3722.
76. Salom, C.; Horta, A.; Hernandez-Fuentes, I.; Pierola, I. F. Poly(phenylsiloxanes) Electronic Spectra *Macromolecules*, 1987, *20*, 696-698.
77. Suzuki, M.; Nakata, Y.; Nagai, H.; Okutani, T.; Kushibiki, N.; Murakami, M. Light Emission Properties of Poly(diphenylsilylenemethylene) and Poly(diphenylsilaxane) by UV Laser Irradiation. *Mater. Sci. Eng. B* **1997**, *49*, 172–174.
78. Gan, Y.; Dong, D.; Carlotti, S.; Hogen-Esch, T.E. “Enhanced Fluorescence of Macrocyclic Polystyrene,” *J. Am. Chem. Soc.* 2000, *122*, 2130-2131.
79. Phillips, H.; Furgal, J. C.; Goodson III, T.; Laine, R. M.; Dunietz, B.; Geva, E.; Unpublished Results
80. Bahrami, M.; Furgal, J. C.; Hashemi, H.; Ehsani, M.; Jahani, Y.; Goodson III, T.; Kieffer, J.; Laine, R. M. Synthesis and Characterization of Nano-Building Blocks $[\text{o-RStilbeneSiO}_{1.5}]_{10,12}$ (R = Me-, MeO-, NBoc- and CN. Unexpected Photophysical Properties Arising from Apparent Asym-Metric Cage Functionalization as Supported by Modelling Studies. *Manuscr. Submitt.* **2015**.

Chapter 5

Modification of 3-D molecular mixtures of [vinylSiO_{1.5}]₁₀/[vinyl-SiO_{1.5}]₁₂, Functionalization to [R-stilbenevinylSiO_{1.5}]_{10/12}, and Photophysical Properties

5.1 Original Publication Information

Jung, J.H.; Furgal, J.C.; Goodson, III, T.; Mizumo, T.; Schwartz, M.; Chou, K.; Vonet, J.F.; Laine, R.M.; *Chem. Mater.* **2012**, *24* (10), 1883–1895, DOI: 10.1021/cm300587s.

Modifications have been made to the original document in order to adapt the content to the proper format. It should also be noted that the lead author contributed the synthesis and characterization of these materials, with my contribution attributed to the detailed photophysical property analysis (i.e. two photon absorption and steady state absorption and fluorescence).

5.2 Abstract

Fluoride ion catalyzed rearrangement of $-\text{[vinylSiO}_{1.5}]_n-$ oligomers and polymers in THF provides essentially quantitative conversion to mixtures of the 3-D cage compounds [vinylSiO_{1.5}]₁₀ and [vinylSiO_{1.5}]₁₂ with small amounts of the [vinylSiO_{1.5}]₁₄ cage. These mixtures are easily transformed into their respective styrenyl analogs by metathesis with *p*-R-styrene to give 100 % conversion to the Generation 1 (GEN1) compounds [*p*-R-styrenylSiO_{1.5}]_{10/12}. The R = Br compounds are then easily modified by Heck coupling with *p*-R-styrene in > 90 % yields and ≈ 100 % conversion to the Generation 2 (GEN2) compounds [*p*-R-stilbenevinylSiO_{1.5}]_{10/12}. These studies were designed to map structure-photophysical properties in these 3-D molecules with the goal of finding replacements for C₆₀ and C₇₀ electron acceptor compounds currently in use in most hybrid organic photovoltaics. Photophysical characterization indicates that the GEN2 compounds have average band gaps that are slightly smaller than their T₈ analogs. However, the C₆F₅ derivative offers blue shifted absorption with very red shifted emission belying what might be expected for this type of moiety.

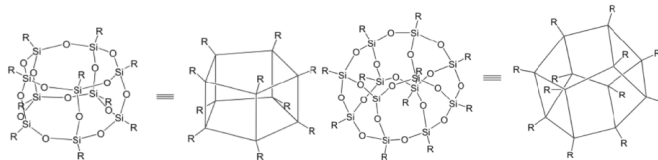
Initial cyclic voltammetry studies suggest that the GEN2 C₆F₅ derivative has HOMO-LUMO energies that may, through further modification, provide energy levels that meet our target objectives.

In addition, solvent studies targeting absorption and emission behavior find emission behavior in poor solvents for R = H, Me, MeO that suggests some form of aggregation. This aggregation red-shifts emission perhaps arising from partial interdigitation of *p*-R-stilbenevinyl groups. Because these molecules are three dimensional; moieties opposite the points of interdigitation emit as they do in good solvents leading to emissions that broadened greatly. Furthermore, because we have previously observed what appears to be 3-D conjugation in the excited state, these results suggest the potential to promote charge transport in three dimensions perhaps similar to C₆₀/C₇₀. Alternately, these same materials may serve as novel emitters for light emitting diodes.

5.3 Introduction

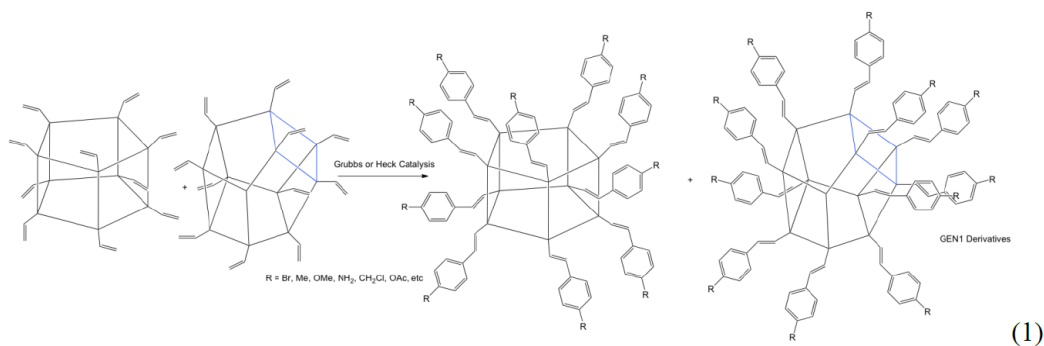
Silsesquioxane (SQ) cage chemistry has recently received a great deal of attention because of the many benefits that can be derived from SQs' potential to offer high degrees of functionalization coupled with thermal stabilities improved by the heat capacity inherent in their silica cores and their high solubility in multiple organic solvents allowing ease of purification. To date this area of research has been the subject of some 17 reviews.¹⁻¹⁷ Most of these reviews focus on the chemistry of the octahedral compounds [RSiO_{1.5}]₈ (where R = R'SiMe₂O and R/R' = alkyl, aryl, alkenyl, alkynyl, etc.).

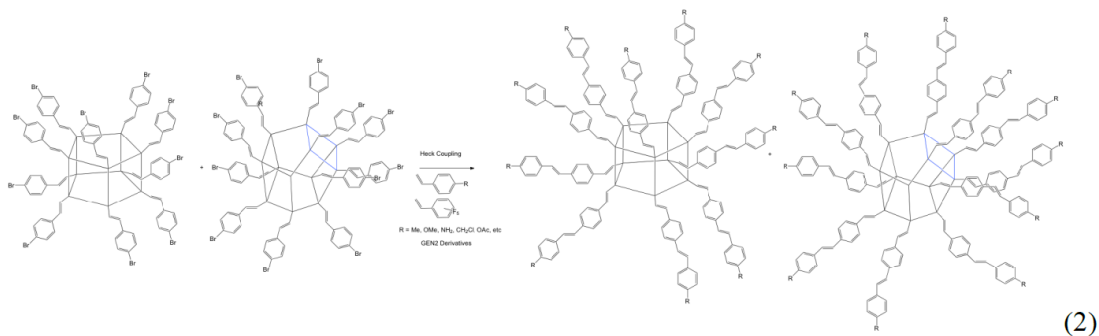
Research by Bassindale et al.,¹⁸⁻²⁰ Rikowski et al.,²¹ and Mabry, Bowers et al.²² described the influence of various bases on the formation of SQ cages with some evidence suggesting F⁻ catalytically scrambles the R groups. In recent work, we demonstrated that this route provides an excellent method of making mixed functional cages; not mixed functional [R¹SiO_{1.5}]_{8-x}[R²SiO_{1.5}]_x but [R¹SiO_{1.5}]_{10-x}[R²SiO_{1.5}]_x and [R¹SiO_{1.5}]_{12-x}[R²SiO_{1.5}]_x cages almost exclusively.²³⁻²⁵ Most recently we learned to make large quantities of [vinylSiO_{1.5}]_{10/12} mixtures from the T resin, [vinylSiO_{1.5}]_x.²⁴



Previously, we reported using $[\text{vinylSiO}_{1.5}]_8$ to synthesize $[\text{p-RStyrlSiO}_{1.5}]_8$ where $\text{R} = \text{H}, \text{Me}, \text{MeO}, \text{Br}, \text{NH}_2$ and the corresponding vinylstilbenes, $[\text{RStilCH=CH}_2\text{SiO}_{1.5}]_8$.^{26,27} We also characterized their photophysical properties in detail as these materials appear to exhibit some form of conjugation in the excited state.^{24,26} A further motivation comes from work of Sellinger et al.,²⁸ who describe Heck cross-coupling of $[\text{vinylSiO}_{1.5}]_8$ with organic moieties conjugated to the SQ silica cage. The resulting compounds offer exceptional improvements in their electron and hole transport properties when used as components in organic light emitting diodes (OLED) compared with simple organics as reviewed recently.¹⁴

In this report, we continue efforts to expand our knowledge of the photophysical properties of these systems as potential new components in the development of OLEDs but also as highly stable, easily modified and robust components for hybrid photovoltaics. In particular, our long term goal is to find materials that can replace components such as the C_{60} and C_{70} fullerenes (e.g. PCBM) currently used in many hybrid photovoltaics given their very high cost and potential toxicity especially as singlet oxygen generators.^{29,30} In this vein, we report here efforts to functionalize $[\text{vinylSiO}_{1.5}]_{10/12}$ via reactions (1) and (2).





More specifically, our objective in the current studies is to map the photophysical properties especially of the GEN2 compounds of reaction (2) to compare the effects (if any) of the larger cage sizes on emissive behavior, two photon cross-sections and also on their HOMO-LUMO energies via cyclic voltammetry for the reasons mentioned just above. We use the term “map” because the properties of these types of 3-D molecules are for the most part unknown and consequently, we must develop a detailed understanding of many of their properties as a prelude to learning to tailor their properties to meet our stated objectives.

As we will see below, for some types of functionalization, the photophysical behavior observed differs very little from the T₈ compounds; however, for others there is a considerable difference. Indeed the C₆F₅ derivatives offer novel behavior that for the present is inexplicable.

5.4 Experimental Procedures

Synthetic methods and characterization procedures are given above in Chapter 2.

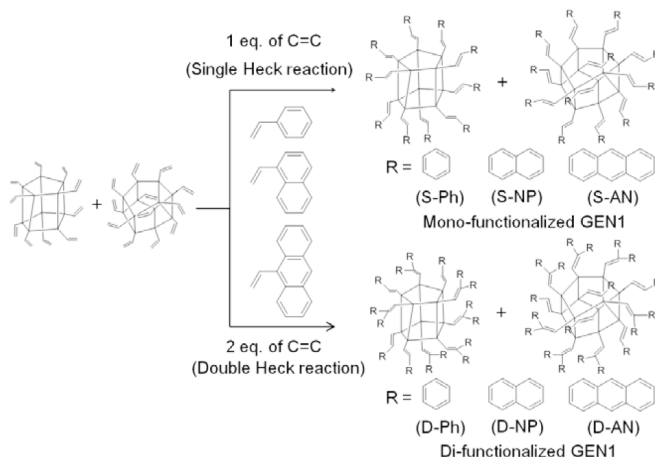
5.5 Results and Discussion

In the following sections we first discuss our synthetic approaches to generating T_{10/12} compounds with very high degrees of functionalization and thereafter their photophysical properties. Because both sets of compounds have very similar chemical and physical properties we have not found simple methods of separating the T₁₀ from the T₁₂ compounds. Thus, at the outset it is important to realize that these compounds can be considered to be relatively well-defined oligomers rather than discrete molecular species although the distinction may seem small. Consequently, we are exploring average properties though the differences may not be particularly great. Also note that in the

current studies we see small amounts of T₁₄ compounds. The exact structure of this component is unknown but see Baney and Itoh.²

As seen with the T₈ compounds, we are able to install layers of organic functionality starting from the silica cage out. In a future paper, we will develop routes to the further functionalization of the GEN2 compounds developed here, to produce GEN3 compounds that come closer to meeting our stated objectives.

Because our starting points for the compounds made here are vinyl functionalized species, two pathways can be explored for further modification; Heck or metathesis cross-coupling. Sellinger et al.^{14,28} report using Heck coupling to mono- and partially di-functionalize [vinylSiO_{1.5}]₈. Using their work as the starting point, we explored the use of Heck coupling to synthesize mono- (S) and di- (D) functionalized vinylT_{10/12} (Scheme 5.1).



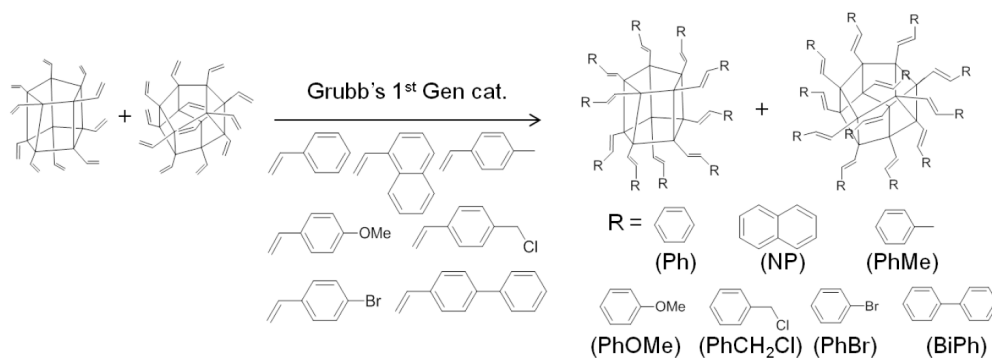
Scheme 5.1. Heck coupling reactions of vinylT_{10/12} (GEN1).

Table 5.1 summarizes our findings indicating that with the exception of anthracene, functionalization, even with efforts to limit coupling to mono-functionalization, gave significant di-functionalization. Furthermore, under the conditions used, it was not possible to obtain complete di-functionalization as also reported by Sellinger et al.²⁸ albeit for the vinylT₈.

Table 5.1. Characterization of T_{10/12} GEN 1 Mono (S) and Double (D) Heck coupling compounds.

R group	TGA				m/z (Ag ⁺ adduct)				GPC	
	Ceramic yield (%)		Ave. Substit.	T _{d5%} °C	T ₁₀		T ₁₂		M _n	PDI
	found	Calc.			MALDI		MALDI			
Vinyl	75.4	75.9	--	240	900.0	899.2	1056.0	1057.5	950	1.03
S-Ph	34.8	38.7	1.2	420	1890.4	Ph ₁₃	2124.4	Ph ₁₄	1550	1.05
D-Ph	29.7	26.0	1.6	385	2350.0	Ph ₁₉	2660.4	Ph ₂₁	1590	1.07
S-NP	27.3	29.3	1.1	480	2286.3	NP ₁₁	2696.4	NP ₁₃	1620	1.07
D-NP	21.4	18.1	1.6	455	3050.8	NP ₁₇	3460.2	NP ₁₉	1700	1.08
S-AN	23.1	23.5	1.0	445	2661.5	AN ₁₀	3171.3	AN ₁₂	1820	1.08
D-AN	23.6	14.7	1.0	445	2661.8	AN ₁₀	3171.8	AN ₁₂	1890	1.17

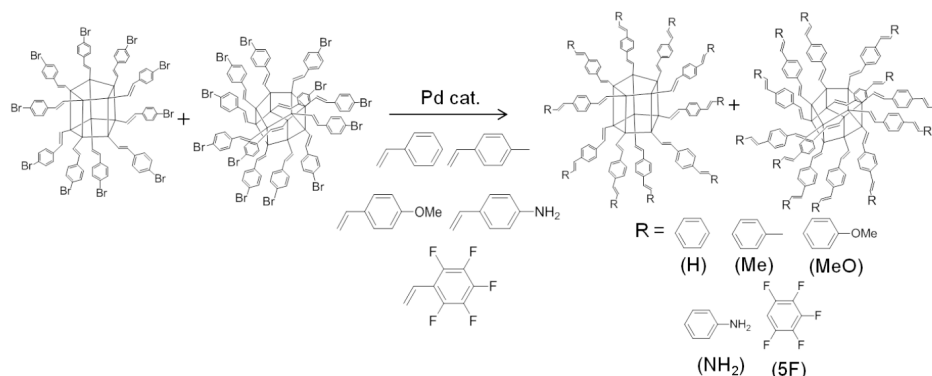
In contrast to the Heck coupling reactions, the metathesis products give analyses (Table 5.2) expected for 100 % cross-coupling and mono-functionalization (Scheme 5.2). As such, and in particular, the *p*-bromophenyl derivative was scaled to 10 g quantities to serve as the starting point for all GEN2 compounds (Scheme 5.3).



Scheme 5.2. Metathesis reactions of vinylT_{10/12} (GEN1).

Table 5.2. Characterization of T_{10/12} GEN1 materials produced by metathesis.

R group	TGA				m/z (Ag ⁺ adduct)				GPC	
	Ceramic yield (%)		Ave. Subst.	T _{d5%} °C	T ₁₀		T ₁₂		M _n	PDI
	actual	calc			MALDI	Calc.	MALDI	Calc.		
Ph	38.8	38.7	1.0	430	1659.0	1660.7	1970.0	1971.3	1540	1.06
NP	28.7	29.3	1.0	415	2164.0	2161.3	2574.8	2572.0	1650	1.05
PhMe	35.8	35.5	1.0	330	1800.9	1801.0	2140.0	2139.6	1600	1.04
PhOMe	31.9	32.4	1.0	395	1960.4	1961.0	2332.0	2331.6	1630	1.03
PhCH ₂ Cl	30.7	29.5	1.0	340	2144.7	2145.4	2552.0	2552.9	1860	1.04
BrPh	25.0	25.7	1.0	335	2452.0	2449.7	2920.3	2918.1	1830	1.06
BiPh	25.4	26.0	1.0	340	2422.1	2421.7	2885.7	2884.5	2150	1.04



Scheme 5.3. Heck coupling reaction of *p*-Br-StyrenylvinylT_{10/12} (GEN2).

Table 5.3. Characterization of T_{10/12} stilbenevinylSQ (GEN2) compounds.

R'	TGA				m/z (Ag ⁺ adduct)				GPC	
	C.Y. (%)		Ave. Subst.	T _{d5%} °C	T ₁₀		T ₁₂		M _n	PDI
	Found	Calc.			MALDI	Calc.	MALDI	Calc.		
H	23.3	23.4	1.0	390	2680.7	2681.5	3195.1	3196.2	3200	1.04
Me	21.5	22.1	1.0	385	2820.1	2821.7	3362.8	3364.5	3500	1.03
MeO	20.9	20.9	1.0	350	2981.0	2981.7	3555.2	3556.5	3530	1.04
NH ₂	22.1	22.6	1.0	390	2832.3	2831.6	3376.9	3376.4	4100	1.03
5F	17.0	17.3	1.0	345	3581.6	3581.0	4276.4	4275.6	4140	1.05

In general the TGA, MALDI and GPC data are all in agreement with those expected for the compounds isolated. It should be noted that the calculated ceramic yields (C.Y.) in

Table 5.3, are those calculated for the average degree of substitution as determined by the MALDI data and not theoretical values for single and di-substitution.

It is also important to note that the MALDI intensity data used to calculate the average degree of substitution depend on the ease of ionization of each particular species. While these are not necessarily the same for given degrees of substitution, they are viewed as being qualitatively the same. Consequently, there may be some error in the average degree of substitution observed which may account for some slight discrepancies in the CY data.

It should also be noted that because all SQ cages are spherical, they occupy different hydrodynamic volumes than what might be expected for oligomers of similar atomic mass. Therefore, the polystyrene standards used to calibrate the GPC, will not give calculated M_n values representative of the actual SQ molecular masses.

5.5.1 FTIR Studies

Figure 5.1 provides two representative spectra for GEN1 *p*-MeOStrySQ and GEN2 for C_6F_5 stilbenevinylSQ. The cage structure is maintained throughout the syntheses as witnessed by the strong ν Si-O bands near 1100 cm^{-1} , aside from this specific band, the remaining IR bands are typical of those found in aromatic compounds.

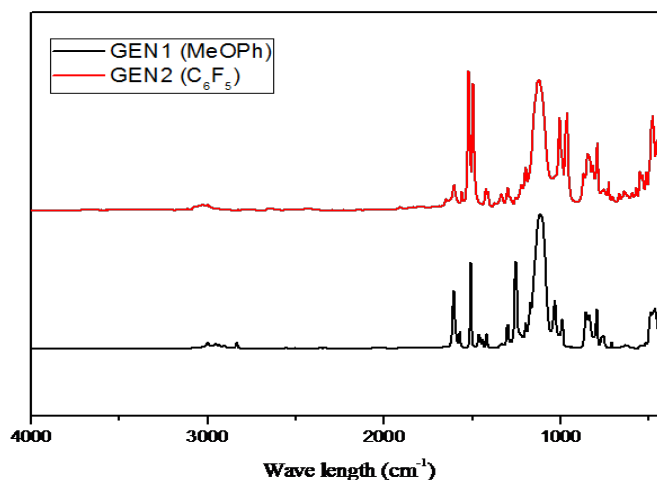


Figure 5.1. Representative FTIR for GEN1 *p*-MeOStrySQ and GEN2 C_6F_5 stilbenevinylSQ.

5.5.2 GPC studies

GPC data for GEN1 and GEN2 SQs are given in Table 5.1 and Table 5.3. Figure 5.1 provides representative GPC chromatograms for vinylSQ, styrenylSQs (GEN1) made by different methods and stilbenevinylSQ (GEN2). These materials show narrow molecular weight distributions, indicating that they retain their cage structures. Note that the three different styrenylSQs show the same retention times, even though they have different numbers of phenyl groups, because SQ cages are rigid and spherical molecules of approximately the same hydrodynamic radii.

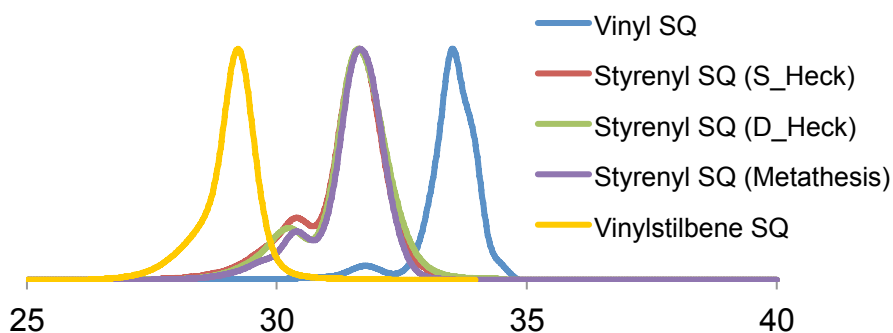


Figure 5.2. GPC traces of vinylSQs and styrenylSQs and stilbenevinylSQ (GEN2).

5.5.3 DSC Studies

Figure 5.3 shows representative DSC traces of GEN1 StyrenylSQs and GEN2 stilbenevinylSQs. As seen in Figure 5.3, GEN1 compounds present endotherms indicative of melting near 100 °C for the second scan. Hot stage optical microscopy also shows that these materials melt over a 100-120 °C range as might be expected for T_{10/12} mixtures. However, the GEN2 compounds do not show melting behavior in the DSC and decompose at temperatures >200 °C.

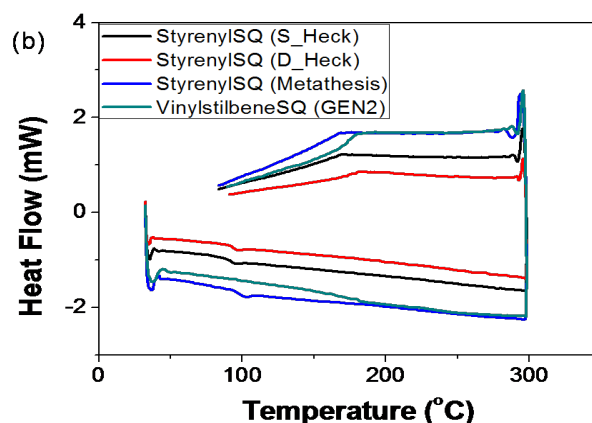


Figure 5.3. DSC traces of selected styrenylSQs and stilbenevinylSQ (GEN2), second scan.

5.5.4 Photophysical Studies

The following work is divided into two sections, steady state spectroscopy and two-photon absorption measurements.

5.5.4.1 *Steady-State Spectroscopy*

Figure 5.4-Figure 5.6 provide absorption and emission spectra (THF) for selected GEN1 compounds with the data shown in Table 5.4 and Table 5.5. The absorption spectra for both the single and double Heck phenyl and naphthalene compounds exhibit distinct band structure, with absorption maxima being nearly the same for both single and double Heck derivatives. These values are $\lambda_{\text{max}} = 254 \pm 2$ vs. 258 ± 2 nm for the phenyls respectively, and $\lambda_{\text{max}} = 302 \pm 2$ nm for both naphthalenes. Furthermore, the doubly functionalized compound emission spectra are slightly red-shifted as might be expected for cross-conjugated moieties due to slightly extended excited state conjugation. Both the single and double Heck phenyl and naphthalene compounds give similar spectra respectively.

In contrast, while mono functionalized anthracene offers the most red-shifted absorption at $\sim 374 \pm 2$ nm and emission at $\lambda_{\text{max}} = 465 \pm 2$ nm. Its emission is featureless possibly resulting from charge transfer or from an averaging of the emission signals. All of the absorption and emission spectra were taken at concentrations of 10^{-6} to 10^{-7} molar where formation of excimers/exciplexes between two cages is unlikely. However, it is

possible that internal excimers form. Zhang et al. report formation of T-type excimers on zinc (II) acetate w/*N,N'*-Bis(anthracen-9-ylmethyl)propane-1,3-diamine ligands, which give broad emission bands similar to those found here, suggesting the possibility of internal T- type excimer formation on the cages.³⁴ We believe this is not occurring as the individual moieties are almost 90 ° apart on the surface of the cage and even with some rotation are unlikely to be able to approach each other.

A comparison between the molar extinction coefficients of S-anthracene and D-anthracene, of $4.2 \times 10^4 \text{ M}^{-1} \text{ cm}^{-1}$ and $4.8 \times 10^4 \text{ M}^{-1} \text{ cm}^{-1}$ respectively reveals just a slight increase in absorption efficiency of the doubly substituted versus the singly substituted. This is consistent with the double and single species both being approximately only singly substituted. As a comparison, the D-naphthalene showed an increase in molar extinction coefficient compared to that of S-naphthalene, $9.6 \times 10^4 \text{ M}^{-1} \text{ cm}^{-1}$ and $1.0 \times 10^4 \text{ M}^{-1} \text{ cm}^{-1}$ respectively, evidence of increased substitution as seen in Table 5.1, which gives a substitution of 1.2 for the S-and 1.6 for the D-naphthalene.

The calculated fluorescent quantum yield (QY) was 13% for S-anthracene. This contrasts with a literature QY for vinylanthracene linked to aliphatic carbons of 80%.³⁵ The lower than expected QY for the S-anthracene system may arise because of a photoinduced electron transfer (PET) fluorescence quenching process, which may also be evident in the solvent study of the S-anthraceneSQ.³⁶ The S-anthracene QY is $\approx 2\%$ in acetonitrile, likely arising from non-radiative decay enhanced by the smaller, more polar acetonitrile solvent.

In general the Stokes shift differences between the mono- and di-substituted compounds are small, with no general trends observed for the GEN1 compounds.

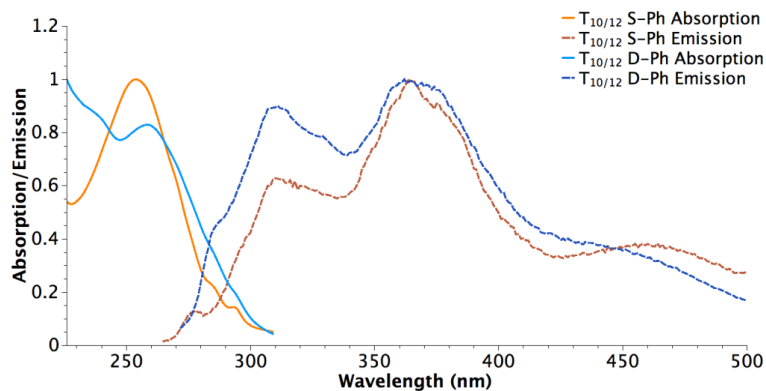


Figure 5.4. UV-vis absorption and PL spectra for GEN1 T_{10/12} R = S-Ph, and D-Ph in THF.

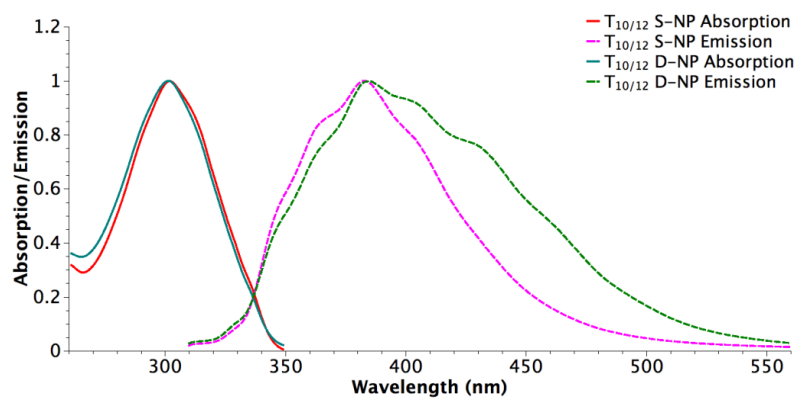


Figure 5.5. UV-vis absorption and PL spectra of GEN1 T_{10/12} R = S-NP and D-NP (THF).

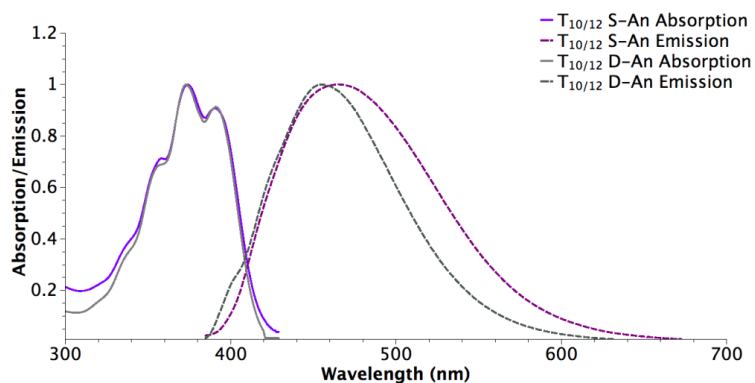


Figure 5.6. UV-vis absorption and PL spectra of GEN1 T_{10/12} R = S-An and D-NP (THF).

The lack of structure in the anthracene systems prompted us to examine the effects of solvent polarity on emission behavior with the intent of enhancing CT behavior if it existed. Thereafter we decided that it would be wise to explore the effects of good, bad and polar or nonpolar solvents on the photophysical behavior of several of our GEN2 compounds.

Table 5.4. Absorption and Emission Maxima for GEN1 compounds.

	Absorption(nm)	Emission(nm)	Stokes Shift (cm ⁻¹)
T _{10/12} R = S-Ph	254	310, 364	7112
T _{10/12} R = D-Ph	258	311, 362	6501
T _{10/12} R = S-NP	302	384	7071
T _{10/12} R = D-NP	302	386	7206
T _{10/12} R = S-An	374	465	4135
T _{10/12} R = D-An	374	455	3663

Table 5.5. Photophysical data for GEN1 compounds.

	$\Phi_{PL(x)}$	Cross-section per Chromophore $\delta(\text{GM})$ at 795 nm
T _{10/12} R = S-Ph	0.03	-
T _{10/12} R = S-NP	0.03	~0.01
T _{10/12} R = S-An	0.13	~0.001

For the anthracene moieties, there is a noticeable solvent effect for emission on going from 95:5% acetonitrile:THF to the less polar THF solvent. This was studied by dilution with THF from the 95% acetonitrile sample, with a 25% reduction in concentration and amount of acetonitrile per measurement as shown in Figure 5.7. The emission spectrum shifts from $\lambda_{\text{max}} = 492 \pm 2$ nm in acetonitrile to $\lambda_{\text{max}} = 465 \pm 2$ nm in THF, with ~25% reduction in intensity with each dilution of THF.

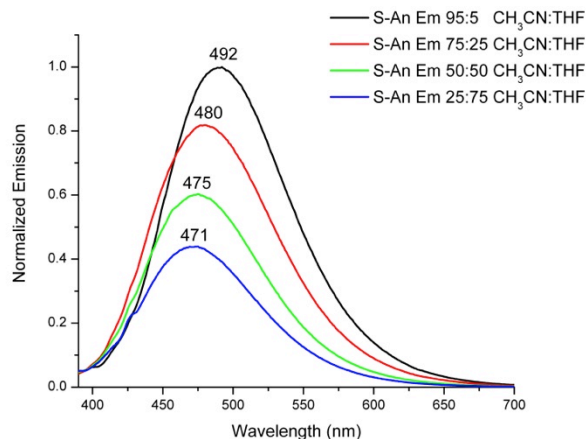


Figure 5.7. Solvent study of GEN1 T_{10/12} R = S-An by sequential dilution with THF to reduce the amount of acetonitrile and the overall concentration.

In contrast, samples prepared with equimolar concentrations with different ratios of acetonitrile:THF evinced no shifts at all; although fluorescence quenching was notable with a decrease in intensity on going from THF to acetonitrile. We suggest that this arises due to differences in solvent interactions with the chromophore (Figure 5.8, Table 5.6), as noted just above. As acetonitrile concentration increases, a second band appears $\lambda_{\text{max}} \approx 415 \pm 2$ nm and the emission becomes more structured as was originally expected. This emission is similar to that expected for vinylanthracene.³⁴

Further analysis in hexane:THF mixtures shows a similar trend, with higher hexane concentrations giving the lowest intensities, and THF the highest. The spectra show slight blue shifts with increased hexane concentration, attributable to poorer solvation, though the general shape and intensity trends are similar to those of acetonitrile.

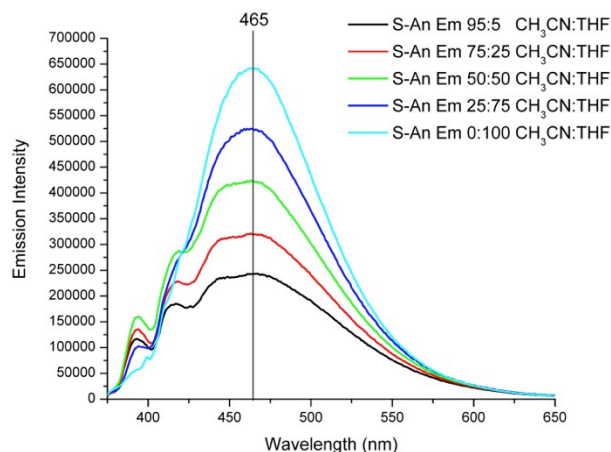


Figure 5.8. GEN1 T_{10/12} R = An emission spectra at different acetonitrile:THF ratios (1 μM).

Table 5.6. Emission solvent study comparing GEN1 T_{10/12} R = S-An in acetonitrile, hexanes and THF.

Acetonitrile:THF	95:5	75:25	50:50	25:75	0:100
T _{10/12} S-An ^(S)	492	480	475	471	465
T _{10/12} S-An ^(C)	465				
Hexane:THF	20:1	15:5	5:15	0:100	
T _{10/12} S-An ^(C)	452	456	458	465	

(S)= Serial dilution study, (C)= Constant concentration studies.

Figure 5.9 and Figure 5.10 show Gen2 compound absorption and emission behavior (THF) with the data tabulated in Table 5.7. In keeping with what is generally expected, aromatic rings with more polar substituents, (e.g. R = NH₂, OMe), are red-shifted compared to less polar substituents, (e.g. R = H, Me). In part this arises from a switch from π - π^* transitions dominating the photophysical properties to charge transfer (CT) behavior as seen in the T₈ vinyl systems.^{26,27}

The UV/Vis and PL spectra for T_{10/12} R = NH₂ were also examined as a function of the solvents acetonitrile, THF and cyclohexane as seen in Figure 5.11 and Table 5.8. As expected, acetonitrile with 5% THF added to improve solubility leads to a 32 nm red-shift compared to THF alone because of CT stabilization in the more polar solvent. The

absorption spectra for all three solvents are essentially the same, with cyclohexane with 5% THF and THF samples having identical emissions.

The absorption of $T_{10/12}$ R = NH₂ in THF, acetonitrile and cyclohexane reveals a $\lambda_{\text{max}} \approx 363 \pm 2$ nm within error limits the same as the $\lambda_{\text{max}} \approx 360 \pm 2$ nm seen for the T₈ analog.^{26,27} In THF, both the T₈ and T_{10/12} systems exhibit featureless emissions at $\lambda_{\text{max}} \approx 486 \pm 2$ nm. In acetonitrile, the T₈ analog exhibits a structureless emission at $\lambda_{\text{max}} \approx 507 \pm 2$ nm, whereas the T_{10/12} system emits at 517 ± 2 nm. We believe that this slight red-shift for the T_{10/12} system is real compared to the emissions in THF. One possible interpretation is that the average band gap for the mixture is slightly lower in energy than that for the T₈ compound. One might expect some change in band gap if the cages interact electronically with the organic functional groups as we have suggested elsewhere.^{26,27} In this instance, this behavior would suggest the larger GEN2 cages have slightly smaller band gaps.

The most unusual compound, however, is the GEN2 T_{10/12} R = C₆F₅ derivative. This compound exhibits a λ_{max} of absorption that is blue-shifted from 333 ± 2 nm for R = H to 316 ± 2 nm, see Table 5.7 and Figure 5.9. This shift is anticipated based on the electron withdrawing character of C₆F₅. However, the emission is red-shifted to a λ_{max} of 443 ± 2 nm which is even greater than the R = OMe analog with (Figure 5.10). This is surprising since one would expect that the emission would also be blue-shifted. The Stokes shift at 9173 cm^{-1} is the largest of any GEN2 compounds. The source of this exceptional red-shift is unclear at present, but clearly indicative of the unusual photophysical properties in these systems.

Another important difference between the T₈ and T_{10/12} amino systems resides in the emission quantum efficiencies (Φ_{PLx}) compared against the standard Bis-MSB (1,4-bis(2-methylstyryl)benzene) ($\Phi_{\text{PLx}} = 95\%$). The Φ_{PLx} of the T₈ R = NH₂ is somewhat lower $\Phi_{\text{PL(x)}}$ than the T_{10/12} R = NH₂ compounds, 5% vs. 7% respectively, which is significant in the calculation of the two-photon cross-section discussed below. All GEN2 T_{10/12} compounds except the R = NH₂ have slightly lower $\Phi_{\text{PL(x)}}$ than their T₈ counterparts. The molar extinction coefficients (ϵ)/chromophore for these compounds are T₈ $3.43 \times 10^4 \text{ M}^{-1} \text{ cm}^{-1}$ and T_{10/12} $3.64 \times 10^4 \text{ M}^{-1} \text{ cm}^{-1}$, suggesting that increasing the chromophore density in the same volume does not influence overall absorption. This indicates absorption is linearly

additive. The somewhat lower $\Phi_{\text{PL}(x)}$ probably arises from some self-absorption but this again is not particularly significant. The molar extinction coefficients are all listed in Table 5.7.

Table 5.7. Absorption and Emission Maxima for GEN2 compounds.

$T_{10/12}R =$	Absorption (± 2 nm)	Emission (± 2 nm)	Stokes Shift (cm^{-1})	$\Phi_{\text{PL}x}$	ϵ ($\text{M}^{-1} \text{cm}^{-1}$)
H	333	387	3988	0.2	3.94×10^5
Me	333	393	4316	0.1	3.77×10^5
OMe	343	418	5402	0.07	4.01×10^5
NH ₂	363	483	7056	0.07	4.00×10^5
C ₆ F ₅	316	445	9173	0.01	4.84×10^5
T ₈ C ₆ F ₅	317	434	8504	0.03	2.44×10^5

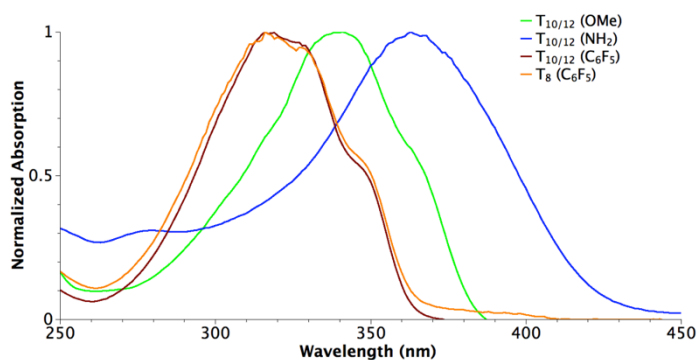


Figure 5.9. UV-vis absorption spectra of selected GEN2 vinylstilbene compounds in THF.

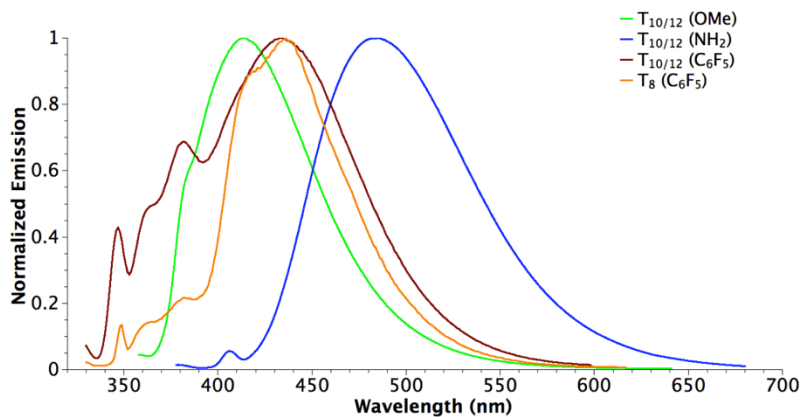


Figure 5.10. PL emission spectra of selected GEN2 vinylstilbene compounds in THF.

Table 5.8. UV/vis absorption and PL for 4-aminovinylstilbene Gen2 SQ as a function of solvent.

	Absorption (± 2 nm)	Emission (± 2 nm)
Acetonitrile (5% THF)	363	516
Cyclohexane (5% THF)	365	483
THF	363	483

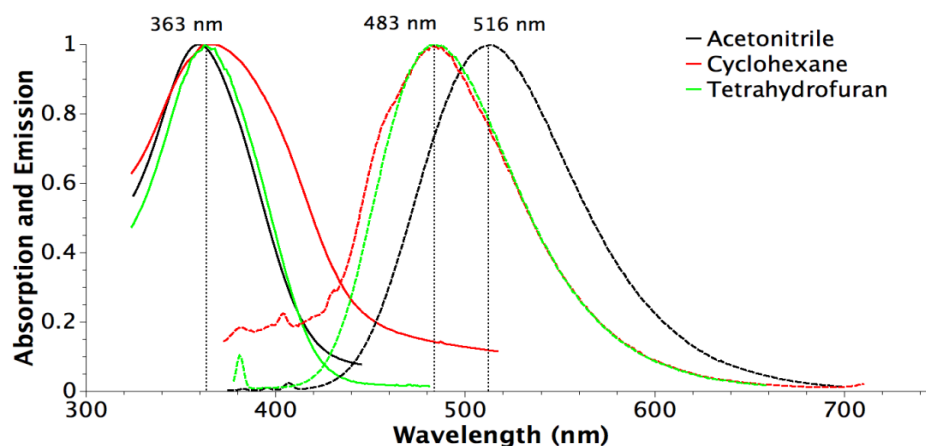


Figure 5.11. UV/vis absorption and PL spectrum of GEN2 T_{10/12} R = NH₂.

The effects of solvation on the UV/Vis and PL spectra for T_{10/12} R = H were assessed in THF, acetonitrile, and hexane, with spectra shown in Figure 5.12 and Figure 5.13 respectively, with emission λ_{max} data given in Table 5.9. This study compared the effects of solvent on both solubility and potential charge transfer properties.

A comparison of λ_{max} for T_{10/12} R = H in 95:5 acetonitrile:THF vs acetonitrile shows a 57-nm red shift (444 ± 2 nm) from THF (387 ± 2 nm) as a function of acetonitrile content, Figure 5.12. In these studies, a single concentration was made ($0.86 \mu\text{M}$) in 95:5 acetonitrile:THF, which was successively diluted with acetonitrile, eventually to ~ 0 % acetonitrile.

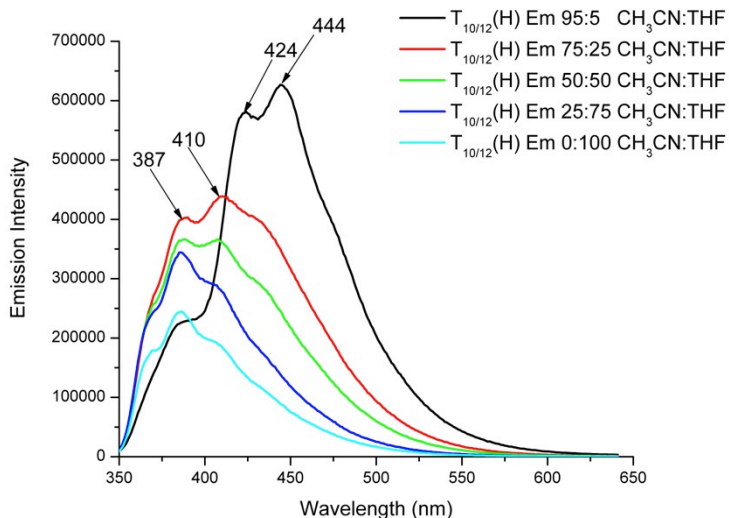


Figure 5.12. Emission studies of $T_{10/12}$ R = H in acetonitrile/THF mixtures at constant $0.86 \mu\text{M}$ concentration.

The fluorescence intensity diminishes on moving to pure THF as expected with dilution. One possible explanation for this shift in emission is that acetonitrile promotes CT behavior; however, the band structure is retained contradicting this explanation. Additional solvent effect studies were then run to further explore this effect.

In the first one, R = H samples at constant $0.86 \mu\text{M}$ concentration provide a somewhat different trend, in which the lowest intensities are observed in 95:5 acetonitrile:THF and the most intense in THF. However, there are no changes in λ_{max} , suggesting that the Figure 5.12 shifts arise as a result of poorer solvent interactions.

Consequently, we decided to move to emission studies with poorer solvents as seen in Figure 5.13 and Figure 5.14. Figure 5.13 shows that at 20:1 hexanes:THF a new peak appears at 477 ± 2 nm. The breadth of the peak suggests aggregation.³⁷ However, at higher THF concentrations this “aggregate peak” disappears as solubility improves. It is important to note that the original emission

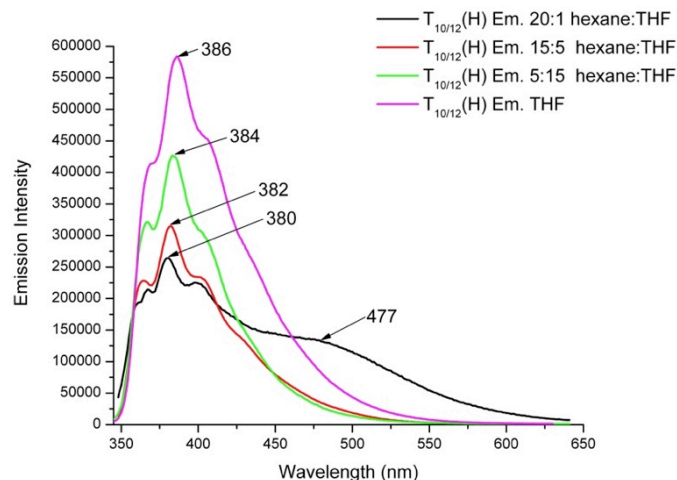


Figure 5.13. Emission studies of $T_{10/12}$ R=H in hexane/THF at constant $0.86 \mu\text{M}$ concentration.

band is still present but slightly blue-shifted compared with the THF sample. An explanation for this blue shift is discussed below. While intriguing, the Figure 5.13 data represent a single data point. Thus, additional studies were run at different hexane:THF ratios closer to the 20:1 value in Figure 5.13. Thus at 10:1, 20:1 and 30:1 ratios of hexane:THF at three concentrations, 0.85 , 0.43 and $0.28 \mu\text{M}$ respectively, we again see (Figure 5.14) the apparent formation of aggregates with a $\lambda_{\text{max}} \approx 492 \text{ nm}$. The original THF emission centered at $\lambda_{\text{max}} \approx 379 \text{ nm}$ appears to be of almost equal intensity.

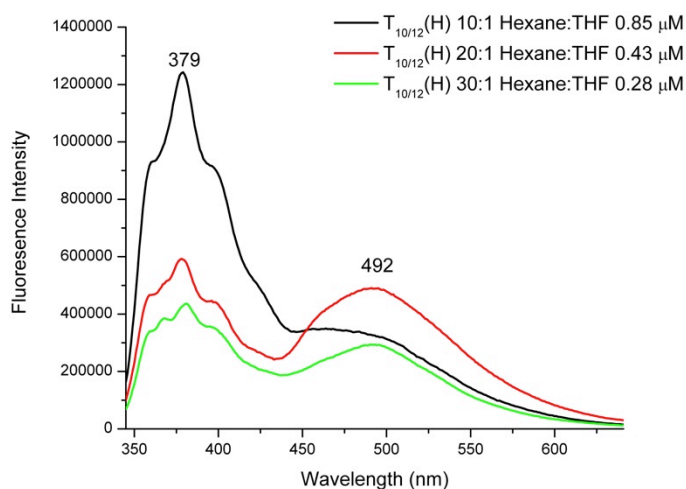


Figure 5.14. $T_{10/12}$ R = H emission in 10:1, 20:1 and 30:1 hexane:THF at various concentrations, suggesting “aggregate” formation.

A final study, run in MeOH (Figure 5.15), shows the same behavior, although the ratio of intensities now favors the 492 nm peak. The fact that two poor solvents at both ends of the “spectrum,” hexane and MeOH, bring about formation of the same red shifted, featureless emission.

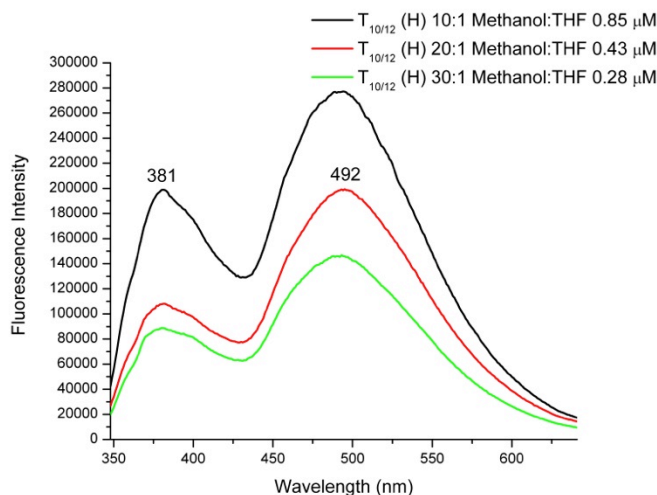


Figure 5.15. Emission spectra of $T_{10/12}$ R=H in 10:1, 20:1 and 30:1 MeOH:THF at various concentrations, showing “aggregate” formation.

The simplest explanation is that an interdigitated excimer forms such as suggested in Figure 5.16, though the interdigitation may be more complex and involve multiple cages. It can be seen that the 3-D nature of the compounds will greatly limit the degree of overlap between two cages. Given that the same emissions are exhibited in two very different but poor solvents seems to support this conclusion. A further conclusion can be drawn based on the observation of emission from the original moieties, albeit blue shifted.

The fact that interdigitation is first likely to occur between two cages only across a narrow set of moieties in a “face-to-face” conformation; thus, moieties opposite the point(s) of interdigitation will retain their emissive behavior. If we then suggest that there is a real electronic interaction between the moieties on the original cages and the cage itself as we have described elsewhere;^{24,26,27} then removing the interdigitated moieties from the overall electronic structure would diminish this interaction leading to the observed blue shift.

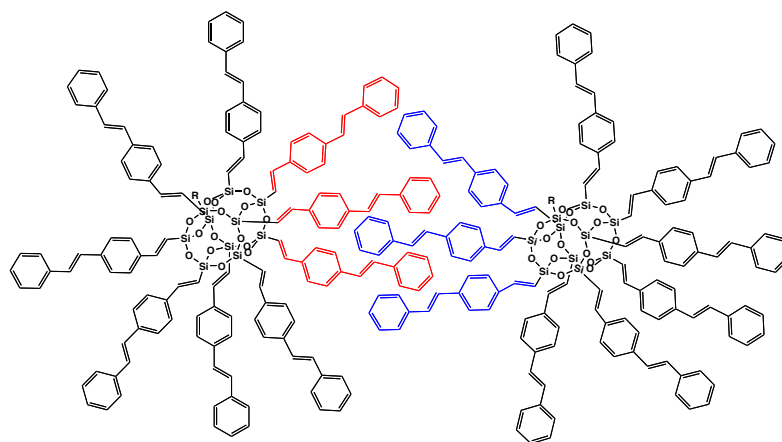


Figure 5.16. Possible aggregation or exciplex formation between two GEN2 stilbenevinylSQs.

While this behavior is reminiscent of emissions from solid state aggregate materials,³⁸ there is an aspect of these emissions that may have some import with respect to our above stated objectives. One possible benefit from this type of interaction is that emission now extends from approximately 350 nm out to 550 nm suggesting the potential for a single system to become a white light emitter with further functionalization and optimization of processing. It is important to add that we have seen evidence that suggests 3-D conjugation in the excited state.^{24,26,27} As such, it may be that some types of aggregates will offer hole and electron transport properties that are superior to 2-D aromatics.³⁹⁻⁴⁴ The potential for such behavior may already exist as reviewed recently by Sellinger et al.¹⁴ Clearly more work needs to be done here, but the potential appears to exist for some very novel materials and photophysics.

As a further extension of the above studies, we examined the effects of solvents on the emissive behavior of T₈ stilbenevinylSQs finding no effect in acetonitrile:THF mixtures, see Table 5.9. We also extended our studies to T₈/T_{10/12} mixtures in MeOH:THF finding that some interactions are observed as noted in Table 5.10 with much reduced red shifts for T₈ vs T_{10/12} which suggests weaker aggregation. This can be anticipated from the fact that the T_{10/12} cages are slightly larger, and offer smaller angles between chromophores ($\sim 72^\circ$ T₁₀, $\sim 60^\circ$ T₁₂ vs. $\sim 90^\circ$ T₈) allowing better interdigitation.

Table 5.9. Emission (nm) of T₈ and T_{10/12} stilbenevinylSQs (± 2 nm) in Acetonitrile:THF.

Acetonitrile:THF	95:5	75:25	50:50	25:75	0:100
T _{10/12} R = H ^S	444	410	410	387	387
T _{10/12} R = Me ^S	402	-	398	394	393
T ₈ R = H ^S	386	-	384	-	385
T ₈ stilbene ^S	357	-	358	358	358
T _{10/12} R = H ^C	387				

(S)= Serial Dilution study, (C)= Constant concentration study.

Table 5.10. Emission (nm) of T₈ and T_{10/12} stilbenevinylSQs (± 2 nm) in hexane:THF or MeOH:THF of varying concentrations.

Hexane:THF	10:1	20:1	30:1	Aggregate λ_{\max}
Concentration (μ M)	0.85	0.43	0.28	--
T _{10/12} R = H	379			492
T ₈ R = H ^S	380			-
Methanol:THF				
Concentration (μ M)	1.1	0.55	0.36	--
T _{10/12} R = H	381			492
T ₈ R = H	384			420/442

Finally, we also explored the effects of solvents on the emissive behavior of other T_{10/12} *p*-stilbenevinylSQs as seen in Table 5.11. The only clear cases for aggregation are for the R = Me and R = OMe compounds which exhibit shifts from an average $\lambda_{\max} \approx 390$ nm ± 5 nm (Me) 405 ± 5 nm R = OMe in hexane:THF mixtures to $\lambda_{\max} \approx 460/454$ R = Me/OMe nm in MeOH:THF at 20:1, see Note that no temperature dependence was observed for R = Me emission and no evidence of excimer formation was observed for the anthracene derivatives.

Table 5.11. Emission of T₈ and T_{10/12} vinylstilbene molecules (± 2 nm) in hexane:THF or MeOH:THF at constant concentrations, (*)= “Aggregate”.

Hexane:THF	20:1	15:5	5:15	0:100
T _{10/12} R = H	380 (477)*	382	384	386
T _{10/12} R = Me	385	390	393	395
T _{10/12} R = OMe	402	396	406	413
T ₈ R = H	380	381	384	385
T _{10/12} R = S-An	452	456	458	464
Methanol:THF				
	20:1			
T _{10/12} R = H	379 (492)*			
T _{10/12} R = Me	460			
T _{10/12} R = OMe	454			
T ₈ R = H	384 (420/442)*			
T _{10/12} R = S-An	456			

It is now well recognized that ordering of molecules in π - π stacking ensembles (e.g. J and H aggregates) provide structures that allow control and fine tuning of electron and/or hole (exciton) transport properties. In turn, this control permits their employ in multiple important applications ranging from dye sensitization in photography to electrochromic and electroluminescent to organic photovoltaic to non-linear optical devices, etc.³⁸⁻⁴⁴

In general, most molecules that exhibit strong π - π stacking interactions are relatively planar and aromatic. To the best of our knowledge, no one has explored the effects of such interactions in 3-D molecules. We believe that the above results may be of value in developing new components for both OLEDs and/or organic photovoltaics if properly explored.

5.5.4.2 Two-Photon Absorption Measurements (TPA)

TPA cross-sections were determined for selected GEN1 and GEN2 compounds. The GEN1 compounds do not exhibit any TPA properties (Table 5.5) as might be expected since they do not contain polarizable groups necessary to obtaining high TPA cross-sections. The double Heck and the phenyl compounds were not studied since the double

Heck had similar functionalization to the single products, and the phenyl absorption band at 254 nm made it difficult to study by our TPEF method.

TPA cross-sections for selected GEN2 compounds are plotted as a function of wavelength and are shown in Figure 5.17, with results given in Table 5.12. The cross-section values per chromophore are given in Table 5.13. TPA values can provide a measure of the degree of enhanced absorption per chromophore and coupling between donor and acceptor regions,^{45,46} leading to some measure of understanding of the potential photocurrent of photovoltaic devices that might incorporate these compounds as components.^{26,27}

The data presented here suggest that the TPA cross-sections for the GEN2 T_{10/12} increase with conjugation and electron donating ability of the R-substituent on the chromophore. Thus on changing from R=H to NH₂ results in an 800 fold increase in cross-section per cage. It is important to note that measured TPA cross-sections depend on the fluorescence quantum efficiency (ϕ_{PL}) as these values are part of the cross-section calculation, which uses an “action cross-section” (based on fluorescence comparison with a standard), which is then multiplied by the quantum yield to give the corrected value based on the fluorescence efficiency.^{31,32} A 1 % difference in ϕ_{PL} can affect the cross-section by as much as 100 GM. This is particularly evident when comparing the difference between the previously published results on the T₈ cages and these new larger cages.^{26,27}

If the T₈ and T_{10/12} R = NH₂ substituted cages are compared (those with the highest cross sections), it is interesting to note that due to the lower quantum yield of the T₈ species, the cross-section at 770 nm is higher than that for T_{10/12}, 100 GM vs 68 GM respectively per chromophore. *These values may arise as a consequence of different cage geometries*, which orient the chromophores differently by angle and proximity to one another leading to changes in fluorescence efficiency. Interestingly, the maximum cross-section arises from a lower energy excitation (770 nm) than expected from the single photon absorption (363 nm), suggesting that we are accessing a lower energy state.

The maximum TPA would be expected to exist around 725 nm or double the one photon absorption, which may be the case, but do to limits in instrumentally accessible wavelengths, was not explored. Since a lower energy state can be accessed, this may explain the large Stokes shift in the single photon fluorescence through relaxation before emission. Since the T_8 cage is more symmetrical than the $T_{10/12}$ cages, it can be rationalized that the chromophore orientations may change fluorescence properties.^{26,27} SQs in general give enhanced TPA cross-sections compared to single chromophores due to the enhanced dipole-moment term from the electrophilic nature of the cage.^{26,45-47}

The TPA analyses for the $R = C_6F_5$ species are not as expected. Table 5.12 compares the cross-sections between the T_8 and $T_{10/12}$ $R = C_6F_5$ compounds. The per chromophore values are 9 GM for the T_8 and 17 GM for the $T_{10/12}$. These findings are surprising given the strong electron withdrawing character of the substituent.^{26,27} If we assume that for the $R = NH_2$ compounds the cage acts as a strong electron withdrawing center enabling CT behavior in these systems, the introduction of $R = C_6F_5$ should provide two withdrawing sites competing for the electron populating the excited state. Such a situation should reduce the CT behavior significantly leading to lower TPA cross-sections, which is contrary to what is found. Recognizing that the TPA data for the $R = C_6F_5$ moiety is well below that of the $R = NH_2$ substituted GEN2 compounds it is still surprising to see any TPA cross-section values at all. This again may relate to the emission red shift for which we have no explanation as yet.

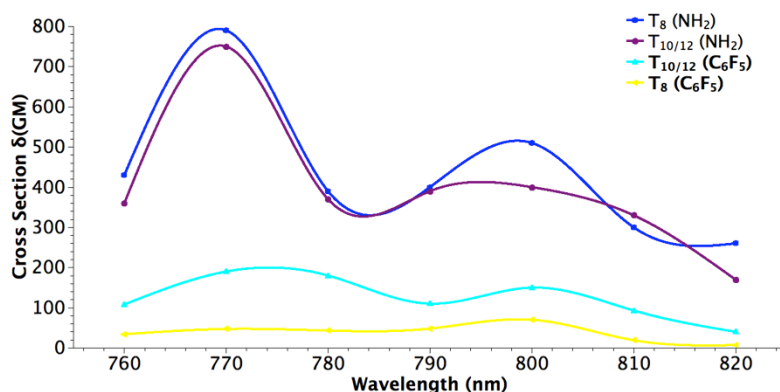


Figure 5.17. Two-photon absorption spectra of selected GEN2 vinylstilbene compounds in THF.

Table 5.12. Two-photon studies of GEN2 compounds with respective cross-sections given.

Two-photon cross section in δ (GM) (10^{-50} cm ⁴ s photon ⁻¹)								
SQ	650	760	770	780	790	800	810	820
T _{10/12} R = H	4	-	8	7	5	6	4	.3
T _{10/12} R = Me	12	-	10	9	6	7	5	8
T _{10/12} R = OMe	33	-	18	21	19	23	16	5
T _{10/12} R = NH ₂	80	360	750	370	390	400	330	170
T _{10/12} R=C ₆ F ₅	110	108	190	180	110	150	93	40
T ₈ R = NH ₂	-	430	790	390	400	510	300	260
T ₈ R = C ₆ F ₅	-	34	47	43	48	70	19	7

Table 5.13. Two-photon laser wavelengths studied and respective cross-section per chromophore on GEN2 SQs.

SQ	Wavelength (± 2 nm)	Cross-section/Chromophore δ (GM)
T _{10/12} R = H	770	~1
T _{10/12} R = Me	650	~1
T _{10/12} R = OMe	650	3
T ₈ R = NH ₂	770	100
T _{10/12} R = NH ₂	770	68
T ₈ R = C ₆ F ₅	800	9
T _{10/12} R = C ₆ F ₅	770	17

5.5.5 SQs as Electron Acceptors in Photovoltaics

The design rationale of the above materials for photovoltaic applications as electron accepting materials is based on the knowledge that SQs in their unfunctionalized state (H-SQ) contain an electrophilic core (equivalent to CF₃) and a centralized core LUMO; suggesting that SQs should be capable of accepting electrons. The challenge with bare SQs is that their band gaps and HOMO-LUMO energy levels are much too high (~ 6 eV) for use in photovoltaic devices, unless they were designed to work in the deep UV. Therefore we proposed that organic functionalization could be used to tune the electronic

properties of these materials to align with the desired energy levels for use in functional devices. Our efforts started from the basic set of mappable R-stilbenevinylSQs mentioned above, since they are effective models of Poly(phenylenevinylene) PPV based materials and we could easily tune the absorption spectra and TPA properties also important for efficient photovoltaic materials.

In order to probe the HOMO-LUMO levels in this first set of GEN2 compounds, we conducted cyclic voltammetry studies in films cast from dichlorobenzene as discussed in Chapter 2. These studies are viewed as a qualitative analysis of the redox behavior of these molecules. Figure 5.18 provides an overview of the data measured.

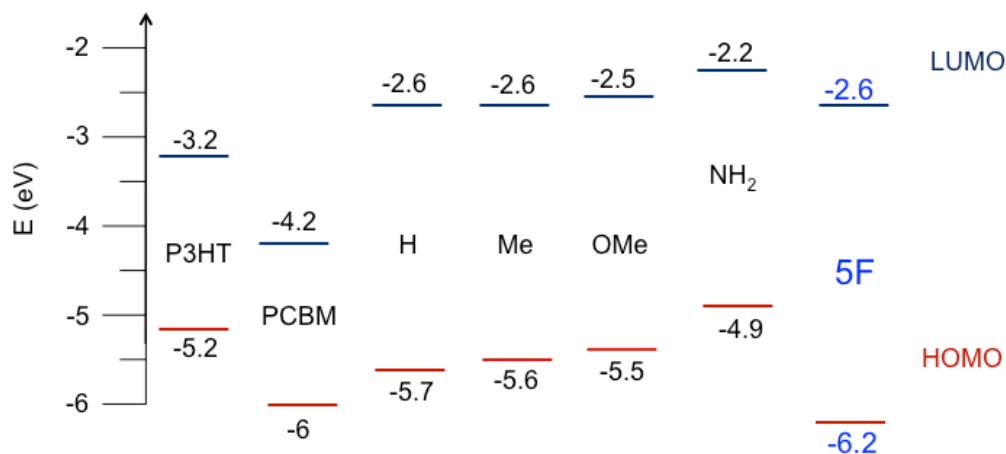


Figure 5.18. Cyclic Voltammetry studies of selected GEN2 compounds, with published data for P3HT and PCBM added.

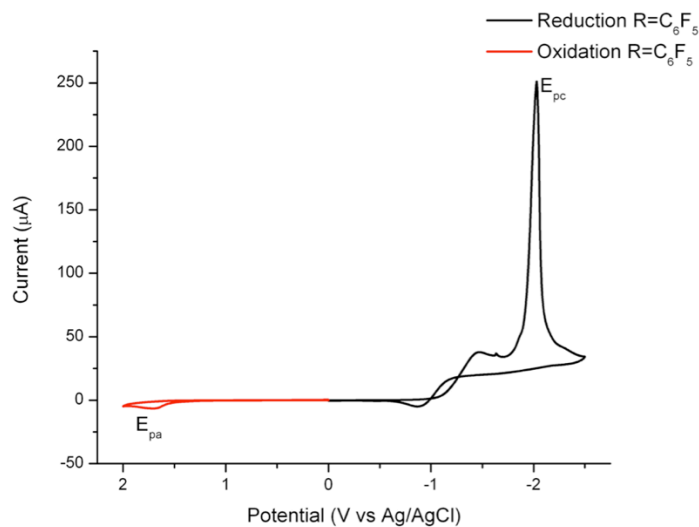


Figure 5.19. Cyclic Voltammety oxidation and reduction curves of pentafluorostilbenevinylSQ (5F).

The literature suggests that a potential replacement for PCBM derivatives should have a LUMO that is actually somewhat higher than -4.2 eV, preferably in the -3.8 to -3.4 eV in order to optimize V_{oc} .⁴⁸⁻⁵⁰ The HOMO and LUMO of C_{60} are given in Figure 5.20 with their respective reversible redox potentials given in Figure 5.21 for comparison.

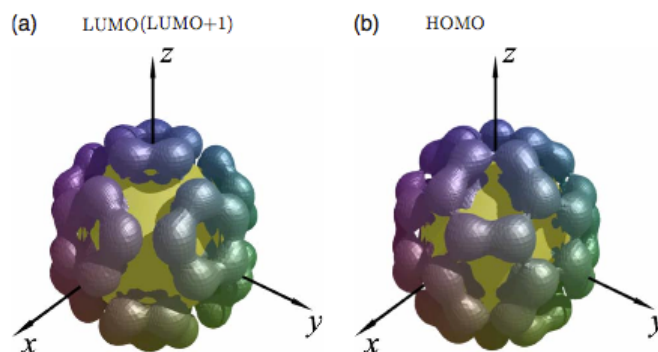


Figure 5.20. LUMO and HOMO orbitals of C_{60} .⁵¹

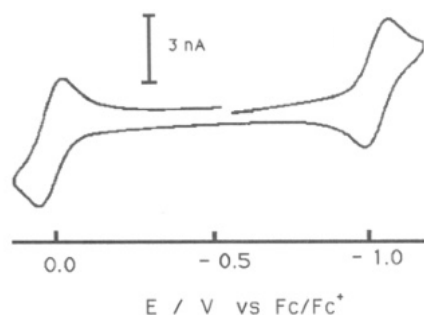


Figure 5.21. Cyclic voltammogram of oxidation and reduction of C_{60} .⁵²

Though our materials may be tunable as replacements for photovoltaics, a further pitfall is that our materials to date do not exhibit the important reversible redox behavior present in PCBM and necessary for efficient solar devices. Thus, in view of our current efforts, we must reduce the LUMO of one of the above compounds and develop an understanding of why these materials do not exhibit reversible redox behavior. Furthermore, we find that incorporating low energy organics onto the the SQ core effectively moves the redox behavior to the organic components as opposed to simply adjusting the energy levels of the cage itself. This is notwithstanding the obvious need to learn to process good devices with these new compounds, which still may be a difficult task.⁵³

5.6 Conclusions

Our stated objective in this work was to synthesize and then map the photophysical properties of sets of three-dimensional molecules derived from vinyl T_{10} SQ and vinyl T_{12} SQ mixtures as GEN1 and GEN2 compounds. These mapping studies are considered as a first step in exploring their potential utility as components on organic electronic and photonic materials. As we anticipated, based on early studies of the vinyl T_8 SQs the synthesized compounds were all quite soluble in multiple organic solvents and easily purified by traditional methods. Although a mixture is used, the analytical results indicate that it is possible to obtain 100 % conversions to target GEN1 and then GEN2 products.

The photophysical behavior of these compounds is mostly similar to that of the T_8 compounds with some clear exceptions. In particular the $T_{10/12}$ systems are able to

interdigitate in poor solvents exhibiting behavior that appears to indicate aggregation. Given their 3-D structures, this aggregation appears to be 3-D in nature and most likely differs considerable from aggregates formed from traditional organic molecules.

The photophysical data suggest that the mixed $T_{10/12}$ systems have slightly smaller band gaps than those measured for the T_8 analogs. Furthermore, they show a higher propensity to interdigitate perhaps because of the slightly larger cage sizes. However, TPA data suggest slightly lower cross-sections except for the C_6F_5 compounds, which offer very unexpected properties.

Given our previous finding of the existence of conjugation through the center of the cage for these types of systems in the excited state, the aggregation data suggest some novel potential for 3-D hole/electron transport properties perhaps reminiscent of fullerene type compounds and with further modification allowing their use in place of fullerene PCBM derivatives in photovoltaic devices.

References:

1. Voronkov, M.G.; Lavrent'yev, V.I.; "Polyhedral Oligosilsesquioxanes and Their Homo Derivatives," *Top. Curr. Chem.* **1982**, *102*, 199-236
2. Baney, R.H.; Itoh, M.; Sakakibara, A.; Suzuki, T.; "Silsesquioxanes," *Chem. Rev.*, **1995**, *95*, 1409-30.
3. Loy, D.A.; Shea, K.J.; "Bridged Polysilsesquioxanes. Highly Porous Hybrid Organic-Inorganic Materials," *Chem. Rev.*, **1995**, *95*, 1431-42.
4. Calzaferri, G.; "Silsesquioxanes," in Tailor-made Silicon-Oxygen Compounds, from molecules to materials, R. Corriu and P. Jutzi eds. Publ. Friedr. Vieweg&SohnmbH, Braunschweig/Weisbaden, Germany **1996**, 149-169.
5. Lichtenhan, J.; "Silsesquioxane-based Polymers," in Polymeric Materials Encyc., J.C. Salmone Ed. Vol. 10, CRC Press, N.Y., **1996**, 7768-77.
6. Provatas, A.; Matison, J.G.; "Synthesis and applications of silsesquioxanes," *Trends Polym. Sci.* **1997**, *5*, 327-33.
7. G. Li, L. Wang, H. Ni, C. U. Pittman, "Polyhedral Oligomeric Silsesquioxane (POSS) Polymers and Copolymers: A Review," *J. Inorg. and Organomet. Polymers*, **2001**, *11*, 123-151.
8. Duchateau, R.; "Incompletely Condensed Silsesquioxanes: Versatile Tools in Developing Silica-Supported Olefin Polymerization Catalysts," *Chem. Rev.* **2002**, *102*, 3525-3542.
9. Abe, Y.; Gunji, T.; "Oligo- and polysiloxanes" *Prog. Poly. Sci.* **2004**, *29*, 149-182.
10. Phillips, S.H.; Haddad, T.S.; Tomczak, S.J. "Developments in Nanoscience: polyhedral oligomeric silsesquioxane (POSS)-polymers," *Current Opinion in Solid State and Mater. Sci.* **2004**, *8*, 21-29.

11. Kannan, R. Y.; Salacinski, H. J.; Butler, P. E.; Seifalian, A. M.; "Polyhedral Oligomeric Silsesquioxane Nanocomposites: The Next Generation Material for Biomedical Applications," *Acc. Chem. Res.* **2005**, *38*, 879-884.
12. Laine, R.M. "Nano-building blocks based on the [OSiO_{1.5}]₈ silsesquioxanes," *J. Mater. Chem.*, **2005**, *15*, 3725 – 44.
13. Lickiss, P.D.; Rataboul, F., "Fully Condensed Polyhedral Silsesquioxanes: From Synthesis to Application," *Adv. Organomet. Chem.*, **2008**, *57*, 1-116.
14. Chan, K. L.; Sonar, P.; Sellinger, A. "Cubic silsesquioxanes for use in solution processable organic light emitting diodes (OLED)," *J. Mater. Chem.* **2009**, *19* 1-19.
15. Wu, J.; Mather, P. T.; "POSS Polymers: Physical Properties and Biomaterials Applications," *Polymer Reviews*, **2009**, 25–63.
16. Cordes, D. B.; Lickiss, P. D.; Franck, R.; "Recent Developments in the Chemistry of Cubic Polyhedral Oligosilsesquioxanes," *Chem. Rev.* **2010**, *10*, 2081–2173 (2010).
17. Laine, R. M.; Roll, M. F.; "Polyhedral Phenylsilsesquioxanes," *Macromolecules*, **2011**, *44*, 1073-1220.
18. Bassindale, A. R.; Liu, Z.; MacKinnon, I. A.; Taylor, P. G.; Yang, Y.; Light, M. E.; Horton, P. N.; Hursthouse, M. B.; "A higher yielding route for T8 silsesquioxane cages and X-ray crystal structures of some novel spherosilicates," *Dalton Transactions*, **2003** 2945-2949.
19. Bassindale, A.R.; Pourny, M.; Taylor, P.G.; Hursthouse, M.B.; Light, M.E. "Fluoride-Ion Encapsulation within a Silsesquioxane Cage." *Angew. Chem. Int. Ed.* **2003**, *42*, 3488-3490.
20. Bassindale, A.R.; Parker, D.J.; Pourny, M.; Taylor, P.G.; Horton, P.N.; Hursthouse, M.B. "Fluoride Ion Entrapment in Octasilsesquioxane Cages as Models for Ion Entrapment in Zeolites. Further Examples, X-Ray Crystal Structure Studies, and Investigations into How and Why They May Be Formed." *Organometallics*, **2004**, *23*, 4400-4405.
21. Rikowski, E.; Marsmann, H.C., "Cage Rearrangement of Polysilsesquioxanes," *Polyhedron*, **1997**, *16*, 3357-3361.
22. Anderson, S. E.; Bodzin, D. J.; Haddad, T. S.; Boatz, J. A.; Mabry, J. M.; C. Mitchell, M. T. Bowers, "Structural Investigation of Encapsulated Fluoride in Polyhedral Oligomeric Silses-quioxane Cages Using Ion Mobility Mass Spectrometry and Molecular Mechanics," *Chem. Mater.* **2008**, *20*, 4299-4309.
23. Ronchi, M.; Sulaiman, S.; Boston, N. R.; Laine, R. M.; "Fluoride catalyzed rearrangements of polysilsesquioxanes, mixed Me,Vinyl T₈, Me,Vinyl T₁₀ and T₁₂ cages," *Applied Organometallic Chemistry*, **2010**, *24*, 551–557.
24. Asuncion, M. Z.; Laine, R.M. "Fluoride Rearrangement Reactions of Polyphenyl- and Polyvinylsilsesquioxanes as a Facile Route to Mixed Functional Phenyl, Vinyl T₁₀ and T₁₂ Silsesquioxanes," *J. Am. Chem. Soc.* **2010**, *132* 3723–3736.
25. Jung, J. H.; Laine, R.M. "Beads on a chain (BOC) polymers formed from the reaction of NH₂PhSiO_{1.5}]_x[PhSiO_{1.5}]_{10-x} and [NH₂PhSiO_{1.5}]_x[PhSiO_{1.5}]_{12-x} mixtures (x = 2-4) with the diglycidyl ether of bisphenol A," *Macromolecules*, **2011**, *44*, 7263-7272.
26. Sulaiman, S.; Brick, C.; Roll, M.; Bhaskar, A.; Goodson, T.; Zhang, J.; Laine, R. M. "Molecules with Perfect Cubic Symmetry as Nanobuilding Blocks for 3-D Assemblies. Elaboration of Octavinylsilsesquioxane. Unusual Luminescence Shifts

- May Indicate Extended Conjugation Involving the Silsesquioxane Core.” *Chem. Mater.* **2008**, *20*, 5563.
27. Laine, R. M.; Sulaiman, S.; Brick, C.; Roll, M.; Tamaki, R.; Asuncion, M. Z.; Neurock, M.; Filhol, J.-S.; Lee, C.-Y.; Zhang, J.; Goodson, T.; Ronchi, M.; Pizzotti, M.; Rand, S. C.; Li, Y. “Synthesis and Photophysical Properties of Stilbeneoctasilsesquioxanes. Emission Behavior Coupled with Theoretical Modeling Studies Suggest a 3-D Excited State Involving the Silica Core.” *J. Am. Chem. Soc.* **2010**, *132*, 3708-3722.
 28. Sellinger, A.; Tamaki, R.; Laine, R.M.; Ueno, K.; Tanabe, H.; Williams, E.; Jabbour, G.E. “Heck Coupling of Haloaromatics with Octavinylsilsesquioxane: Solution Processable Nanocomposites for application in electroluminescent devices,” *Chem. Comm.*, **2005**, 3700-3702.
 29. Usenko, C. Y.; Harper, S. L.; Tanguay, R. L.; “*In vivo* evaluation of carbon fullerene toxicity using embryonic zebrafish,” *Carbon*, **2007**, *45* 1891–1898.
 30. Sera, N.; Tokiwa, H.; Miyata, N. “Mutagenicity of the fullerene C⁶⁰-generated singlet oxygen dependent formation of lipid peroxides,” *Carcinogenesis*, **1996**, *17*, 2163-2169.
 31. Maciejewski, A.; Steer, R. P. “Spectral and photophysical properties of 9,10-diphenylanthracene in perfluoro-n-hexane: the influence of solute—solvent interactions,” *J. Photochem.* **1986**, *35*, 59.
 32. Xu, C.; Webb, W. W. “Measurement of two-photon excitation cross sections of molecular fluorophores with data from 690 to 1050 nm.” *J. Opt. Soc. Am. B.* **1996**, *13*, 481.
 33. Bhaskar, A.; Ramakrishna, G.; Lu, Z.; Twieg, R.; Hales, J. M.; Hagan, D. J.; Van Stryland, E.; Goodson, T. “Investigation of Two-Photon Absorption Properties in Branched Alkene and Alkyne Chromophores.” *J. Am. Chem. Soc.* **2006**, *128*, 11840-11849.
 34. Zhang, G.; Yang, G.; Wang, S.; Chen, Q.; Ma, J.S., “A Highly Fluorescent Anthracene-Containing Hybrid Material Exhibiting Tunable Blue–Green Emission Based on the Formation of an Unusual “T-Shaped” Excimer (pages 3630–3635),” *Chem. Eur. J.* **2007**, *13*, 3630 – 3635.
 35. Bonneau, R.; Carmichael, I.; Hug, H.G. “Molar Absorption Coefficients of Transient Species in Solution.” *Pure & Appl. Chem.*, **1991**, *63*, 289-299.
 36. Eaton, D.F. “Reference Materials for Fluorescence Measurement” *Pure & Appl. Chem.*, **1988**, *60*, 1107-1114.
 37. Jenekhe S. A.; Osaheni, J. A. “Excimers and Exciplexes of Conjugated Polymers,” *Science*, **1994**, *265*, 765-768.
 38. Bolton, O.; Lee, K.; Kim, H.-J.; Lin, K. Y.; Kim, J.; “Activating efficient phosphorescence from purely organic materials by crystal design,” *Nature Chemistry*, **2011** *3*, 205-210 and references therein.
 39. Cariati, E.; Macchi, R.; Roberto, D.; Ugo, R.; Galli, S.; Masciocchi, N.; Sironi, A., “Sequential Self-Organization of Silver(I) Layered Materials with Strong SHG by J Aggregation and Intercalation of Organic Nonlinear Optical Chromophores through Mechanochemical Synthesis,” *Chem. Mater.*, **2007**, *19*, 3704–3711.

40. Arai, Y.; Segawa, H.; "Cl⁻ Complexation Induced H- and J-Aggregation of *meso*-Tetrakis(4-sulfonatothienyl)porphyrin Diacid in Aqueous Solution" *J. Phys. Chem. B*, **2011**, *115*, 7773–7780.
41. Yi, J.; Chen, Z.; Xiang, J.; Zhang, F.; "Photocontrollable J-Aggregation of a Diarylethene–Phthalocyanine Hybrid and Its Aggregation-Stabilized Photochromic Behavior," *Langmuir*, **2011**, *27*, 8061–8066.
42. Slavnova; T. D.; Chibisov, A. K.; Görner, H.; "Kinetics of Salt-Induced J-aggregation of Cyanine Dyes," *J. Phys. Chem. A* **2005**, *109*, 4758-4765.
43. Chaudhuri,, D.; Li, D.; Che, Y.; Shafran, E.; Gerton, J. M.; Zang, L.; Lupton, J. M.; "Enhancing Long-Range Exciton Guiding in Molecular Nanowires by H-Aggregation Lifetime Engineering," *Nano Lett.* **2011**, *11*, 488–492.
44. Deng, Y.; Li, Y.; Wang, X.; "Colloidal Sphere Formation, H-Aggregation, and Photoresponsive Properties of an Amphiphilic Random Copolymer Bearing Branched Azo Side Chains," *Macromolecules* **2006**, *39*, 6590-6598
45. Ramakrishna, G.; Bhaskar, A.; Goodson, T. G. "Ultrafast Excited State Relaxation Dynamics of Branched Donor- π -Acceptor Chromophore: Evidence of a Charge-Delocalized State," *J. Phys. Chem. B.* **2006**, *110*, 20872.; Haley, J. E.; Krein, D. M.; Monahan, J. L.; Burke, A. R.; McLean, D. G.; Slagle, J. E.; Fratini, A.; Cooper, T. M. "Photophysical Properties of a Series of Electron-Donating and -Withdrawing Platinum Acetylide Two-Photon Chromophores." *J. Phys. Chem. A* **2010**, *115*, 265-273.
46. Varnavski, O.; Yan, X.; Mongin, O.; Blanchard-Desce, M.; Goodson, T. "Strongly Interacting Organic Conjugated Dendrimers with Enhanced Two-Photon Absorption." *J. Phys. Chem. C.* **2006**, *111*, 149-162.
47. Goodson, T. G. "Optical Excitations in Organic Dendrimers Investigated by Time-Resolved and Nonlinear Optical Spectroscopy." *Acc. Chem. Res.* **2005**, *38*, 99.
48. Kim, K-H.; Kang, H.; Nam, S. Y.; Jung, J.; Kim, P. S.; Cho, C-H.; Lee, C.; Yoon, S. C.; Kim, B. J. "Facile Synthesis of *o*-Xylenyl Fullerene Multiadducts for High Open Circuit Voltage and Efficient Polymer Solar Cells," *Chem. Mater.* **2011**, *23*, 5090–5095.
49. He, Y.; Chen, H.-Y.; Hou, J.; Li, Y.; "Indene-C60 Bisadduct: A New Acceptor for High-Performance Polymer Solar Cells," *J. Am. Chem. Soc.* **2010** *132*, 1377-1382.
50. Lenes, M.; Wetzelaer, G-J. A. H.; Kooistra, F. B.; Veenstra, S. C.; Hummelen, J. C.; Blom; P. W. M. "Fullerene Bisadducts for Enhanced Open-Circuit Voltages and Efficiencies in Polymer Solar Cells," *Adv. Mater.* **2008**, *20* 2116-2119.
51. Oku, T.; Nomura, K.; Suzuki, A.; Kikuchi, K. "Effect of perylenetetracarboxylic dianhydride layer as a hole blocking layer on photovoltaic performance of polyvinylcarbazole: C60 bulk heterojunction thin films" *Thin Solid Films*, **2012**, *520*, 2545.
52. Mirkin, M. V.; Bulhoes, L. O. S.; Bard, A. J. "Determination of the kinetic parameters for the electroreduction of fullerene C60 by scanning electrochemical microscopy and fast scan cyclic voltammetry" *J. Am. Chem. Soc.* **1993**, *115*, 203.
53. Jung, J.-H.; Furgal, J.; Goodson, T.; Laine, R. M.; unpublished work

Chapter 6

Analyzing Structure-Photophysical Property Relationships for Isolated T₈, T₁₀ and T₁₂ Stilbenevinyl Silsesquioxanes

6.1 Original Publication Information

Furgal, J.C.; Jung, J.H.; Goodson, T.; Laine, R.M. *J. Am. Chem. Soc.*, 2013, *135*, 12259-12269, DOI: 10.1021/ja4043092.

6.2 Abstract

Silsesquioxanes (SQs) are of considerable interest for hybrid electronic and photonic materials. However, to date, their photophysical properties have not been studied extensively, thus their potential remains conjecture. Here we describe the first known efforts to map structure-photophysical properties as a function of cage symmetry and size by comparing identically functionalized systems.

Our focus here is on the solution photophysical properties of the title stilbenevinylSQs, which were characterized using single photon absorption, two-photon absorption, fluorescence emission and fluorescence lifetime kinetics. We offer here the first detailed photophysical study of the larger pure T₁₀ and T₁₂ silsesquioxanes and show photophysical properties that differ as a function of size; especially in their fluorescence behavior, indicating that cage size and/or symmetry can strongly affect photophysical properties. We also find that they offer excitation dependent emission (evidence of rare “red-edge” effects). The T₁₀ stilbenevinylSQ offers up to a 10-fold increase in two-photon absorption cross-section per chromophore over a free chromophore, signifying increased electronic coupling. The SQ cage compounds show “rise times” of 700 – 1000 fs and low anisotropy (~ 0.1) in fluorescence lifetime kinetic studies. These results indicate excited state energy transfer, unobserved for the free chromophores, and unexpected for systems with “inert” silica cores, and for 3-D hybrid molecular species.

These findings provide the first detailed photophysical study of chromophore functionalized T_{10} and T_{12} silsesquioxanes, and show that SQs may be considered a separate class of compounds/materials for anticipated novel properties of value in developing new components for electronic and photonic applications.

6.3 Introduction

Silsesquioxanes (SQs) are of considerable interest for hybrid electronic and photonic materials applications.¹⁻⁴ They have gained recent attention due to their unique 3-D oriented functional groups,⁵⁻⁸ potential for high degrees of functionalization,⁹⁻¹⁵ and high thermal stabilities deriving from the heat capacity of the silica core.^{15,16} SQs functionalized with conjugated organic groups offer high absorption, unexpected emissive properties, tunable band gaps, and charge delocalization.^{3,4,9,17,18} Until recently most work on SQs has focused on the T_8 compounds, with more than 17 reviews on the subject, with minimal emphasis given to the T_{10} and T_{12} compounds described herein.^{3,12,14,19-32}

To date, very little work has targeted mapping the photophysical properties of SQs as a function of structure and symmetry, let alone cage sizes. In part, this is because the synthetic tools and separation methods that allow the synthesis and isolation of well-defined compounds were not sufficiently refined. We report here the development of both synthesis and separation methods that provide access to the pure, individual, stilbenevinylSQ cage compounds.^{4,9,15,17,33} Strong motivation for the current work arises because their photophysical behaviors often differ considerably from pure organics. Thus, there is considerable potential to develop SQs with entirely different photonic/electronic properties of potential value for multiple applications as alternatives to organic components currently in commercial use or being considered for commercial use.

Most review articles to date give little attention to the larger cages. Indeed very few studies of the larger cage systems have been reported.^{9,14,19,33-35} Recent, facile access to the T_{10} and T_{12} cages was occasioned by the discovery of F^- catalyzed rearrangement of T_8 cages, T-resins or directly from $RSi(OEt)_3$.^{9,33-35} This method allows isolation in high purity of the higher cage compounds after a simple two day reaction, though usually as a mixture of cage sizes.

F⁻ catalysis offers a distinct advantage over the slow syntheses (weeks) and low yields (5-30%) reported for many T₈ cages.^{3,12,23,30,36,37} Thus, our current efforts focused on isolating larger cage sizes and thereafter mapping their respective properties.^{9,33}

The few reports that discuss the separation of T₁₀ and T₁₂ SQs typically discuss their removal (as by-products) during the purification of T₈ SQs.^{5,14,30,38} Thus, we report here the synthesis, purification and detailed studies of the photophysical properties of the model systems, *p*-Rstilbenevinyl T₈, T₁₀ and T₁₂ SQs. The first paper in this series developed a synthetic approach to mixed T_{10/12} *p*-RstilbenevinylSQs and mapped their basic photophysical properties in solution. Since our previous study looked at cage mixtures, we sought to ascertain the properties of the pure T₁₀ and T₁₂ *p*-RstilbenevinylSQs, since the mixture offered properties that often differed from those of the *p*-Rstilbenevinyl T₈ SQs.^{9,17} Figure 6.1 depicts stilbenevinylSQs prepared and purified in the current studies. These compounds serve as models for beads on a chain (BoC) oligomer and polymer systems explored briefly below and in accompanying papers. These same models can be considered a first step in characterizing the photophysical properties of dendronized BoCs, see accompanying papers.^{39,40} Finally they also serve to provide baseline properties for the design of next generation cage systems.

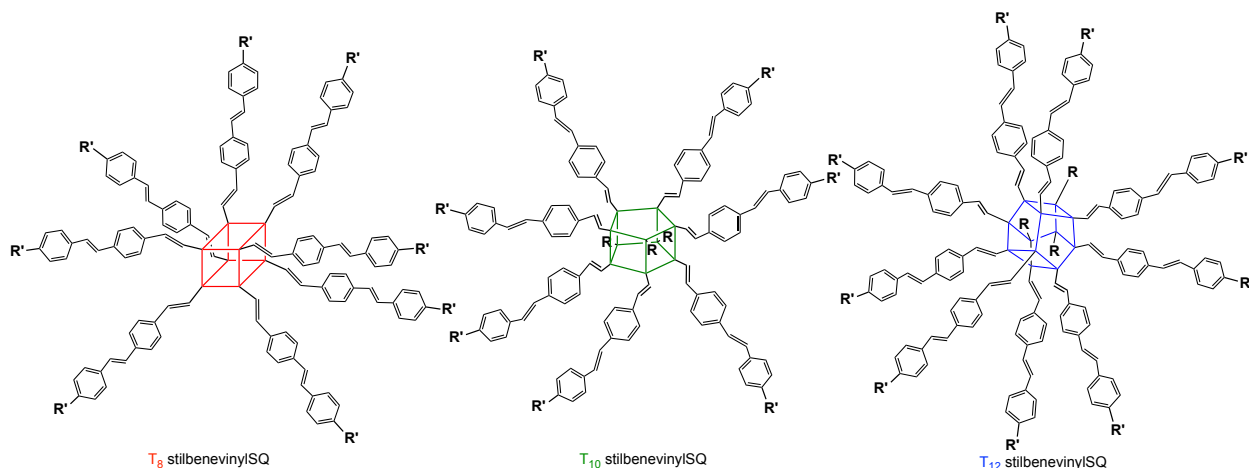


Figure 6.1. StilbenevinylSQ cages, R = stilbenevinyl, R' = H.

The photophysical mapping efforts encompassed emissive behavior, two photon absorption cross-sections, fluorescence lifetime kinetics and initial solid-state (film) studies.⁴¹⁻⁴⁹ These properties have not been studied extensively for any hybrid 3-D

molecules, let alone SQs. In-depth studies have been done on fullerenes;⁵⁰⁻⁵³ however, only simple steady state spectroscopic studies of hybrid molecules such as carboranes, are reported and show lessening conjugation on going from *o* to *m* to *p* as evidenced by a blue shifting emission.^{54,55}

A further objective of the work reported here was to identify properties that allow selected compounds to be designed and synthesized as possible components for hybrid photovoltaic and related photonic and electronic applications. One outcome of our design efforts is reported in a coincidentally submitted paper where we find that rigid organic linkers provide improved 3-D conjugation.⁴⁰

The first step in these studies used tetrabutylammonium fluoride (TBAF) catalyzed rearrangement to generate vinylT_{10/12} mixtures. Thereafter metathesis with *p*-Brstyrene followed by Heck cross-coupling with *p*-Rstyrene provided high yields of the T₁₀ and T₁₂ stilbenevinylSQs. Only at this juncture were the mixtures amenable to separation via a combination of selective precipitation and/or GPC, as discussed just below.

The isolated compounds were then characterized by MALDI-ToF, ²⁹Si NMR, steady state spectroscopy, two-photon absorption (TPA) spectroscopy, and fluorescence lifetime kinetics. We also offer some comparison to theoretical calculations in regards to the types of interactions possible with the chromophore and cage. This overall analysis offers the first in-depth study of the photophysical properties of T₁₀ and T₁₂ silsesquioxanes, which can offer significant value in photonic and electronic applications due to their robust nature, absorption efficiencies, and unique 3D-symmetries.

6.4 Experimental Procedures

Synthetic methods and characterization procedures are given above in Chapter 2.

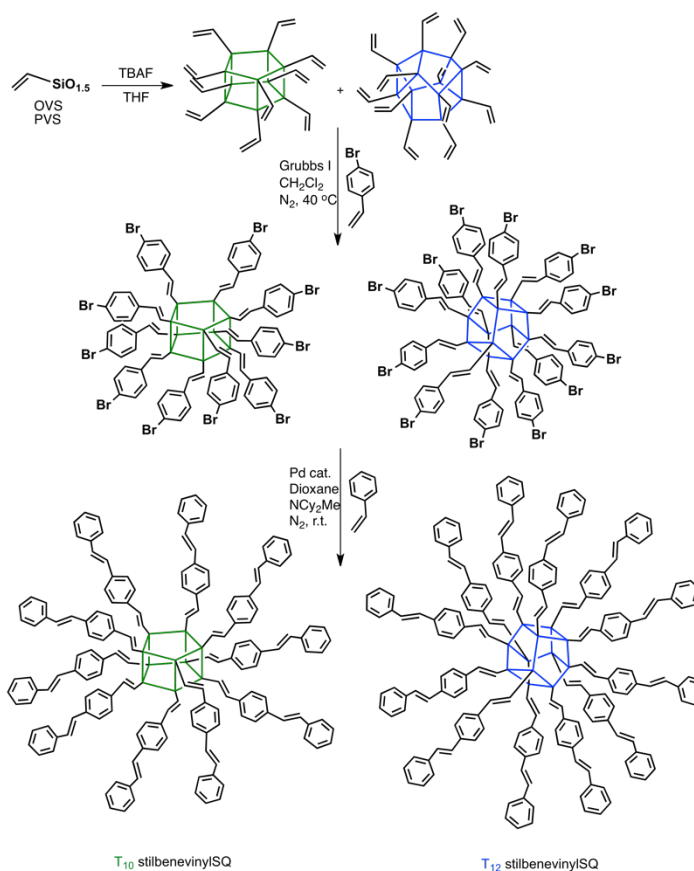
6.5 Results and Discussion

In the following sections, we begin by discussing the synthesis of T_{10/12} stilbenevinylSQs via metathesis and Heck cross-coupling reactions. F⁻ catalyzed rearrangement generates an approximately 1:1 equilibrium mixture of T₁₀ and T₁₂.^{9,33} We then discuss separating T₁₀ and T₁₂ stilbenevinylSQs by GPC and/or selective precipitation. Thereafter we detail the solution-based photophysical properties of the pure

SQs as compared to *p*-triethoxysilylvinylstilbene, *p*-vinylstilbene and the T₈ analog.¹⁷ These studies include determining steady state absorptions and emissions, TPA and fluorescence lifetime kinetics. Solid state photophysical properties will be the subject of future paper, where we will report on novel aggregation.⁵⁶

6.5.1 Synthesis and Separations

Scheme 6.1 illustrates the general synthesis of the T_{10/12} stilbenevinylSQ mixtures, see the experimental section for details.

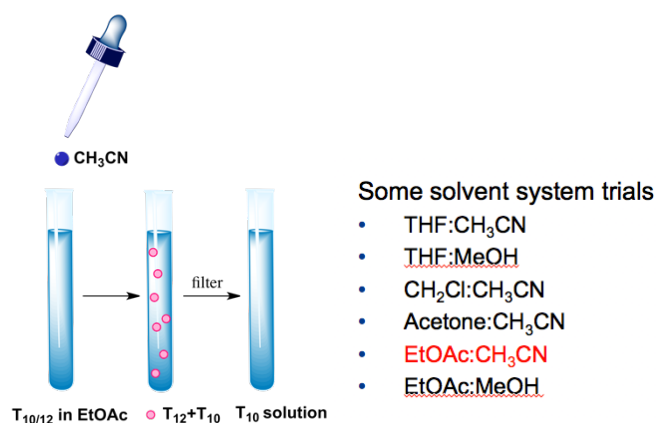


Scheme 6.1. Synthesis of T_{10/12} stilbenevinylSQs.

Separation of SQs with different cage sizes is in general an unexplored area given previous difficulties in synthesizing the larger cages, especially the T₁₀ SQs. Thus, to date only a few research groups have explored the larger SQ cages.^{5,9,14,30,33,34,38,57} As noted above, our motivation for the current studies came from unexpected differences observed in the photophysical properties of the stilbenevinyl T_{10/12} compared to the T₈ analogs.

To this end, our separation efforts extend original work of Kawakami et al.³⁴ Our first attempts assessed direct separation of the vinylT_{10/12} mixed starting materials, however such separations proved difficult due to their high solubility in most solvents combined with oil formation on precipitation into water. We also attempted to separate the individual cages at the 4-bromostyrenyl T_{10/12} stage. While partially successful, separation was not easily reproduced and offered < 90% purities. Thus successful, reproducible separations at purities >95% (MALDI-ToF) came only at the stilbenevinylSQ stage.

Our separation method (see experimental Chapter 2) takes advantage of solubility differences likely due symmetry differences. Both the T₁₀ stilbenevinylSQs and the PhenylSQs,²⁴⁶ are more soluble than the T₈ and T₁₂ compounds and can be separated selectively in high purity but only at 5 mg scales (~5% purified recovery). This follows efforts to separate these compounds via silica gel column chromatography, affinity chromatography using dodecaphenylSQ as the column media, gel permeation chromatography (GPC), and selective solubility. Only GPC and selective solubility approaches work well with the latter providing better separation of T₁₀, due to its higher solubility. Thus, GPC was better for purifying T₁₂ after T₁₀ removal. Up to eight iterations were necessary to purify T₁₂ without GPC. Only two iterations were necessary to purify T₁₀. Figure 6.2 provides a schematic of solubility-based separations.



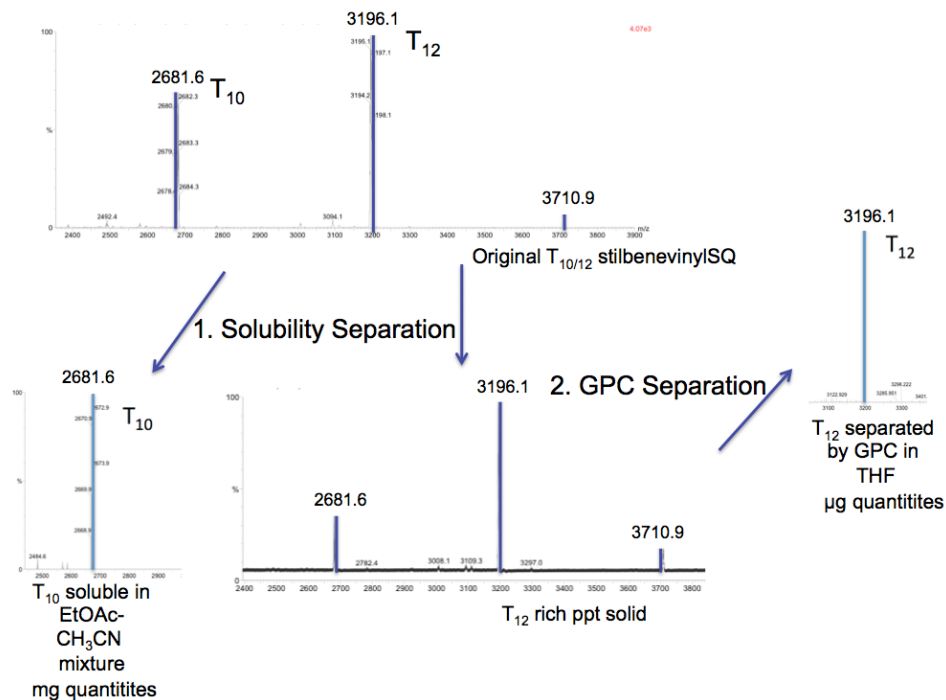


Figure 6.2. Solvent study and MALDI-ToF analysis of separated mixed stilbenevinylSQs.

The separated materials were characterized as described below and in the experimental. The most notable verifications of purity are MALDI-TOF mass spectral analysis and ^{29}Si NMR. Figure 6.3a and b compare the T_{10} and T_{12} stilbenevinylSQs MALDI-TOF spectra showing successful separation. Table 6.1 shows the ^{29}Si NMR ppm shift for selected species, with the spectra shown in Figure 6.4 and Figure 6.5 offering corroborative proof of the separation efficiency.

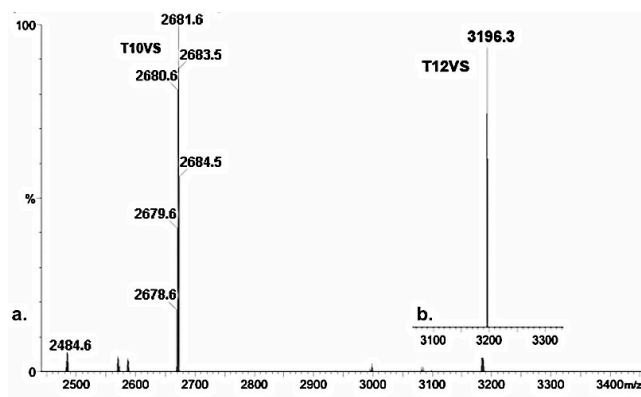


Figure 6.3a and b. MALDI-ToF Comparison of the separated T_{10} and T_{12} stilbenevinylSQ compounds.

Table 6.1. ^{29}Si NMR for separated stilbenevinylSQ cages.

Compound	Chemical Shift (ppm)
T ₈ stilbenevinylSQ	-78.17
T ₁₀ stilbenevinylSQ	-78.85
T ₁₂ stilbenevinylSQ	-78.69, -80.44

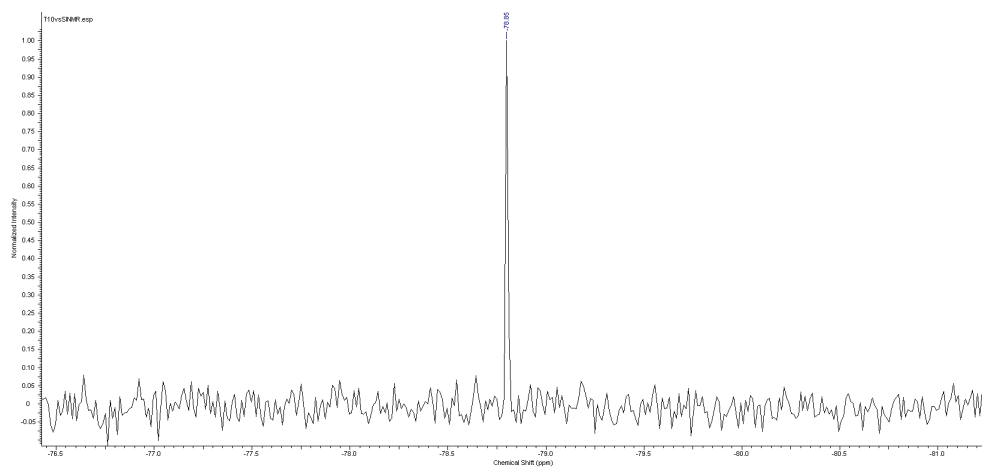


Figure 6.4. ^{29}Si NMR of T₁₀ stilbenevinylSQ in CDCl_3 .

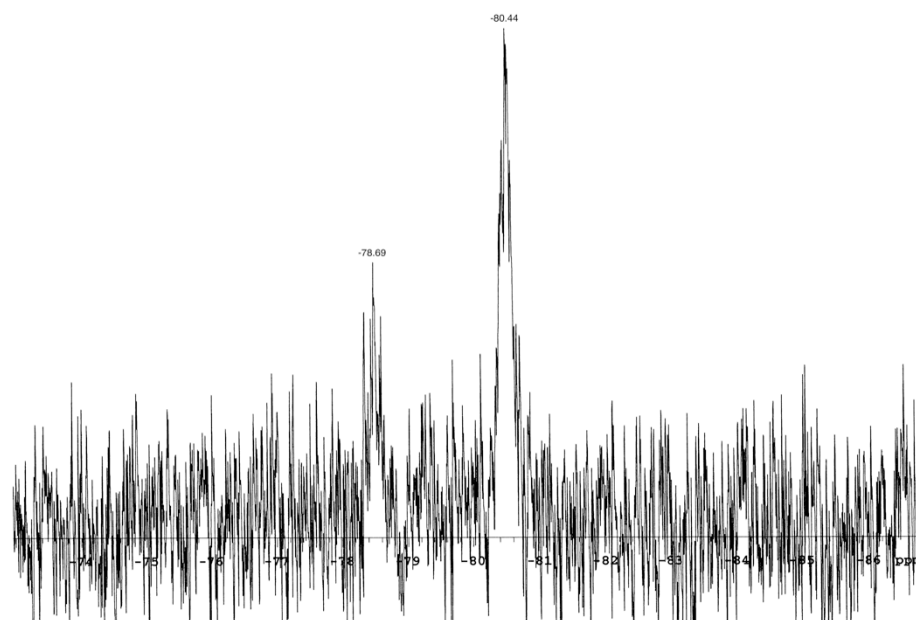


Figure 6.5. ^{29}Si NMR of T₁₂ stilbenevinylSQ in CDCl_3 .

6.5.2 Photophysical Characterization

6.5.2.1 Steady State Spectroscopy

Successful separation allowed us to map the photophysical properties. The first step was to compare the absorption (Figure 6.6a) and emission spectra (Figure 6.6b) of the individual T₁₀ and T₁₂ compounds.⁹ The absorption spectra show similar band structures and maxima for all the cage species (T_{8,10,12}) with absorption peaks at 320, 333, and 352 nm. Figure 6.6b shows the emission spectra of the stilbenevinylSQs normalized to the same absorption value ($\lambda_{\text{max}} = 0.6$).

Surprisingly, stilbenevinylT₁₂ gives the lowest emission intensities with $\Phi_{\text{PL}} = 11\%$, despite having the greatest number of chromophores. This suggests that there is more non-radiative decay through self absorption with the greater number of chromophores.⁵⁹ Indeed, this would be expected if we also recall that the “bite” angle for this molecule averages 60° (vs. 72° T₁₀ and 90° T₈) placing the functional groups in closer proximity to each other improving the opportunity for self-absorption.²¹ The *p*-triethoxysilylvinylstilbene shows the highest quantum yield at 38%. Table 6.2 shows the molar extinction coefficients, absorption and emission maxima and quantum yields.

Photophysical characterization at different excitation wavelengths suggests the existence of two emissive states in stilbenevinylSQs at low concentrations (< 1 μM in THF). Figure 6.7a compares the excitation spectra for the T₁₀ and T₁₂ stilbenevinylSQs for two different emission wavelengths, which is of importance in our two-photon absorption study below (450, 387 nm). Both give similar excitation spectra, with only the 450 nm excitation spectrum showing a slight shoulder between 380 – 420 nm. This is initial evidence of the existence of multiple emissive states in these molecules.

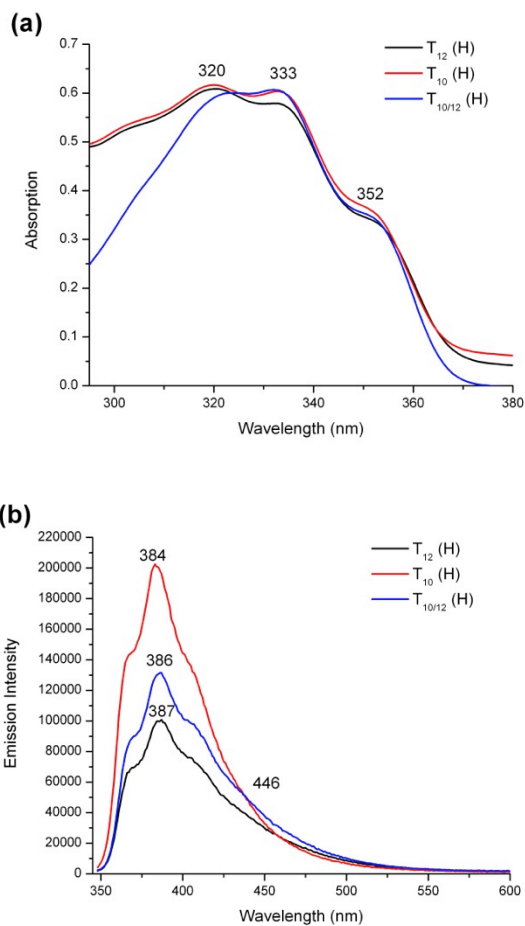


Figure 6.6a. Absorption spectra of stilbenevinylSQs, **b.** Emission spectra (THF, $\sim 3 \times 10^{-7}$ M).

Table 6.2. Comparison of $T_{8,10,12}$ (H)-stilbenevinylSQ steady state properties in THF.

	Abs. λ_{\max} (nm)	Em. λ_{\max} (nm)	ϵ ($M^{-1} \text{ cm}^{-1}$)	Φ_{PL} %
T_8 (H)	335	385	286000	36
T_{10} (H)	333	383	358000	19
T_{12} (H)	333	386	430000	11
$T_{10/12}$ (H)	333	387	394000	15
<i>p</i> -triethoxysilyl-VS	329	380	38200	38
<i>p</i> -vinylstilbene	328	373	35800	28

The shoulder seen in the excitation spectrum may give rise to the red shifted emissive state in the 436 to 450 nm range, since Figure 6.7b shows that the relative intensities of the fluorescence

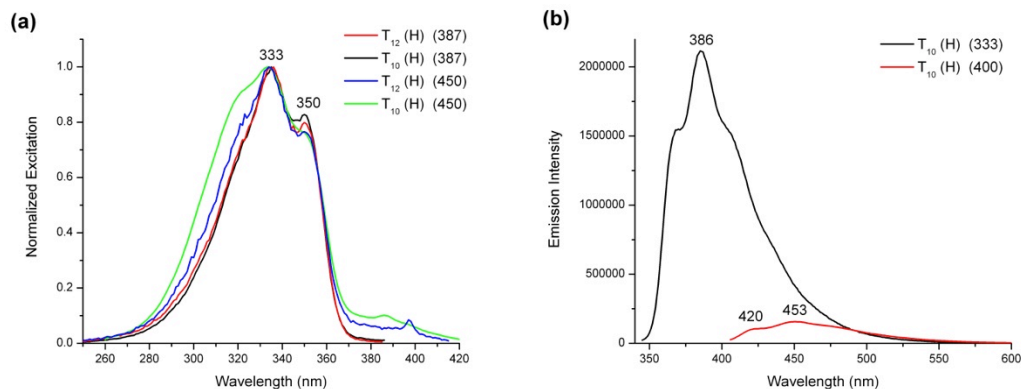


Figure 6.7a. Comparison of excitation spectra for T₁₀ and T₁₂ stilbenevinylSQ with emission held at 387 and 450 nm, **b.** Comparison of emission of T₁₀ stilbenevinylSQ with excitation at 333 or 400 nm, (THF, $\sim 2 \times 10^{-7}$ M).

spectra correlate well with the amplitude of the shoulder. This figure compares the emission spectra from different excitation bands (333 and 400 nm). Note that a red shift is observed on shifting the excitation wavelength to higher values. Excitation at < 375 nm provides emission $\lambda_{\text{max}} = 385$ nm. In contrast, excitation at > 375 nm red shifts the emission to $\lambda_{\text{max}} \approx 450$ nm. This excitation based spectral shift is found in all cages, and slightly observable in the *p*-triethoxysilylvinylstilbene ($< 1\%$), however it is not seen in the *p*-vinylstilbene. These spectral shifts are unusual for organic systems, but since we are dealing with rigid 3-D hybrid materials, with chromophores oriented in space, various excited state energy transfer processes are possible, allowing access to red shifted emissive states.

This red shift can potentially be attributed to a “red-edge” effect, typically observed for locked fluorophores with a well-defined dipole moment in highly viscous solvents, however it has also been observed for fluorophores attached to rigid substrates, and often results from lower rotational diffusion.⁵⁹⁻⁶¹ Since SQs are very rigid substrates that would force fluorophores into certain conformations based on a structure that may be thought of

as a nearly solvent free environment, and that also show dipolar effects (see TPA), what is observed appears to be a novel example of the “red-edge” effect.

The 450 nm emission is close to the emission maximum found in solid state analyses, discussed further below.⁵⁶ but due to the low concentrations used it is unlikely that molecules are in close enough proximity to interact as if they were in the solid state (i.e. aggregates). However theoretical calculations and kinetic studies suggest chromophore-chromophore interactions may still be possible.^{62,63} Another explanation could be that the organic group emissions in the solid state and in any aggregates that form are quenched, so that the 450 nm emission dominates the 387 nm band. The low energy-tailing present in the 387 nm emission suggests that the 450 nm emission is present regardless of excitation wavelength, but is masked by the higher Φ_{PL} of the 387 nm emission.

6.5.2.2 Two Photon Absorption

Two-photon spectroscopy was used to compare the polarization and non-linear absorption properties of the separated cages, *p*-triethoxysilylvinylstilbene and those of *p*-vinylstilbene. Table 6.3 and Table 6.4 compare the two-photon cross-sections at three laser excitation wavelengths (650, 740 and 800 nm). The 800 nm excitation shows the greatest differences between cross-sections, with T_{10} giving the largest cross-section at ~42 GM/mol. This suggests the T_{10} cage has the largest change in dipole moment on excitation.⁶⁴⁻⁶⁶ Due to their different symmetries, the two structural formats will have different two-photon selection rules based on orbital geometry, and thus different polarization dynamics, likely accounting for the different TPA cross-section values.^{67,68}

Table 6.3. Comparison of TPA data for $T_{8,10,12}$ (H)-stilbenevinylSQs (cross-sections GM/mol).

Sample	Conc. (M)	800 nm δ (GM)	740 nm δ (GM)	650 nm δ (GM)
$T_{10/12}$ (H)	1.94E-06	30	52	41
T_{12} (H)	1.42E-06	7	40	63
T_{10} (H)	1.57E-06	42	55	57
T_8 (H)	2.35E-06	2.0	16	26
<i>p</i> -triethoxysilyl-VS	1.03E-05	0.2	1.1	N/A

<i>p</i> -vinylstilbene	1.04E-05	N/A	0.5	2
-------------------------	----------	-----	-----	---

Table 6.4. TPA data for $T_{8,10,12}$ (H)-stilbenevinylSQs (cross-sections GM/chromophore).

Sample	800 nm/chrom δ (GM)	740 nm/chrom δ (GM)	650 nm/chrom δ (GM)
$T_{10/12}$ (H)	2.7	4.7	3.8
T_{12} (H)	0.6	3.3	5.3
T_{10} (H)	4.2	5.5	5.7
T_8 (H)	0.3	2.0	3.3

This then represents a relatively novel observation given that few 3-D molecular species are available with identical moieties and overall compositions that also offer quite different geometries. Thus, our results are the first examples for such classes of compounds.

Figure 6.8 shows the two-photon excited fluorescence (TPEF) spectra at 800 nm, with T_{10} showing the highest fluorescence intensity at equal concentrations. The interesting observation is that with 740 and 800 nm excitation, the emission wavelength is \sim 450 nm, which is similar to the one photon emission band from excitation at 370 and 400 nm (Table 6.5). Figure 6.9 shows the log- log plot for cross-section calculations at 740 nm, with a slope of two guaranteeing a quadratic dependence on excitation energy.

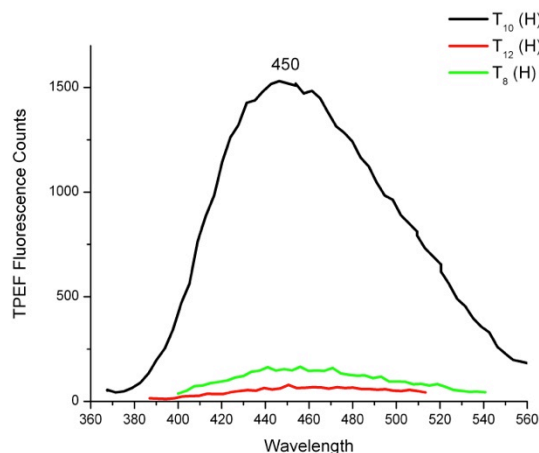


Figure 6.8. TPEF plot comparing $T_{8,10,12}$ stilbenevinylSQs at 800 nm excitation.

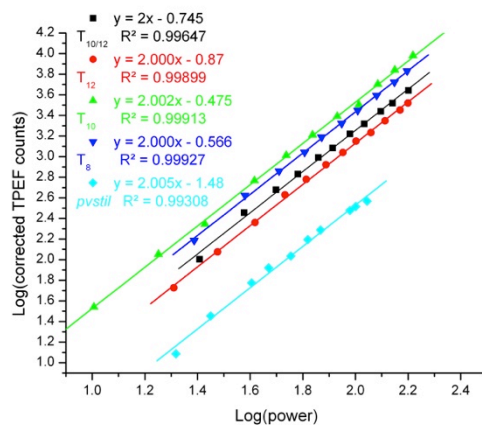


Figure 6.9. Log-Log plot for TPA cross-sections at 740 nm (SI).

Table 6.5. TPEF emission maxima at different two-photon excitation wavelengths.

Sample	800 nm	740 nm	650 nm
T _{10/12} (H)	455	466	410
T ₁₂ (H)	453	473	411
T ₁₀ (H)	458	461	415
T ₈ (H)	452	464	407
<i>p</i> -triethoxysilyl-VS	439	432	-
<i>p</i> -vinylstilbene	-	395	395

Two-photon spectroscopy at 650 nm shows emission maxima between 407 and 415 nm for the single cage SQs, most consistent with one photon emission from excitation at 335 nm, with only a 20 nm red shift as opposed to 60 nm for the other excitations (Table 6.3 and Table 6.4). The TPA cross-sections are comparable to those found at 740 nm excitation. The *p*-triethoxysilylvinylstilbene gives a cross-section at 800 nm and 740 nm of 0.2 and 1.1 GM respectively, however data at 650 nm is unavailable at this time. Also note that the cross-sections of this compound are smaller than the per chromophore values for the cages. A further important observation is that *p*-vinylstilbene itself does not show a TPA excitation or cross-section at 800 nm, and only a small cross-section at 740 nm of 0.5 GM. A cross-section of 2 GM is reasonable for excitation at 650 nm, however it is still nearly half that of the per chromophore values for the cage compounds. *Therefore, depending on the wavelength (i.e. 740 nm), the cages offer at least a ten-fold*

TPA enhancement over their organic counterparts and at least two-fold over their hybrid model. TPA enhancements of the SQs at 650 nm are only double that of organic alone.

This TPA observation suggests that the SQs offer greater electronic coupling, especially at longer wavelengths, which is important for efficient energy transfer processes, such as electron/hole pair separation. This polarization is 3D in nature, and thus is likely highly symmetry dependent. A larger two-photon cross-section also scales with a higher absorption efficiency at low excitation intensity, which is related to the large density of chromophores surrounding the core, which is contained in a small unit volume with spherical diameter of ~1.5 nm. This allows for molecules to more efficiently absorb light over a broad range of light intensity and give enhanced cross-sections.

Since these molecules have two emission states dependent on the excitation wavelength, it is necessary to take into account the quantum yield differences between the emission bands for an accurate TPA cross-section calculation. Table 6.6 shows the QYs for the two emission bands, in which the red-shifted emission band (450 nm) is \approx 10% of the 386 nm emission band.

Table 6.6. T_{8,10,12} StilbenevinylSQ quantum yield values for 387 and 450 nm emission bands.

Sample	QY ₃₈₇	QY ₄₅₀
T _{10/12} (H)	0.15	0.012
T ₁₂ (H)	0.11	0.011
T ₁₀ (H)	0.19	0.018
T ₈ (H)	0.36	0.039
<i>p</i> -triethoxysilyl-VS	0.38	-
<i>p</i> -vinylstilbene	0.24	-

6.5.2.3 Fluorescence Lifetime Kinetics

Fluorescence upconversion measurement analyses were carried out in THF. Analyses were done at excitation wavelengths of 286 and 400 nm, and then collected at 385 and/or 450 nm to measure the fluorescence kinetics for each of the two states

described above, and to investigate the potential for charge transfer.⁶⁹⁻⁷¹ The long component lifetimes were run for hundreds of ps for each compound.

Table 6.7, Figure 6.10 and Figure 6.11 compare lifetimes for the stilbenevinylSQs as compared to *p*-triethoxysilylvinylstilbene and *p*-vinylstilbene with an excitation at 286 nm and an emission collection at 450 nm. These studies were done to probe the red shifted fluorescence band shown above and show that within error,

Table 6.7. Fluorescence lifetime data for $T_{8,10,12}$ StilbenevinylSQ at 286 nm excitation and 450 nm collection (isotropy).

	T_1 (fs)	A_1	T_2 (ps)	A_2	T_3 (ps)	A_3
T_8	760	-0.36	16±2	0.33	209±47	0.46
T_{10}	840	-0.29	15±4	0.39	167±47	0.54
T_{12}	950	-0.29	11±4	0.18	155±20	0.62
$T_{10/12}$	900	-0.21	17±6	0.14	170±35	0.55
<i>p</i> -triethoxysilyl-VS	0	0	6.1±0.9	0.16	252±6	0.98
<i>p</i> -vinylstilbene	0	0	2.9±0.5	0.37	49±5	0.38

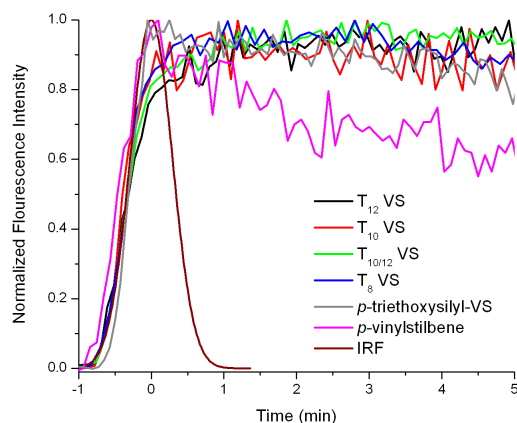


Figure 6.10. Comparison of short fluorescence lifetime components of $T_{8,10,12}$ stilbenevinylSQs with the instrument response function at 286 nm.

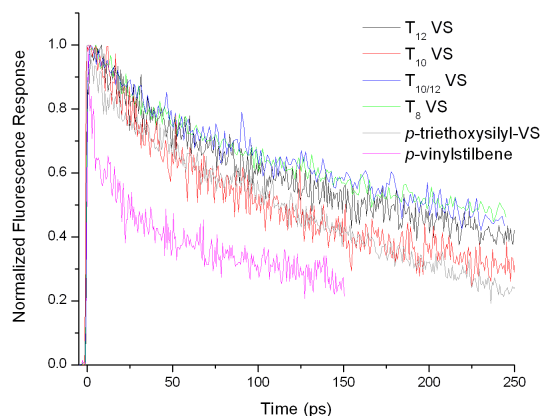


Figure 6.11. Comparison of long decay fluorescence lifetime components of stilbenevinylSQs.

all the cages give similar lifetimes for their short (T_2) and long (T_3) components. Note that in Figure 6.11, the T_{10} stilbenevinylSQ shows a stronger T_2 component, which results in its long decay being below, but parallel to those of the other stilbenevinylSQs. This can be attributed to the symmetry differences in the T_{10} system, which likely also contribute to its enhanced TPA cross-section over the other cage sizes. The *p*-triethoxysilylvinylstilbene gives a lifetime that is just slightly longer than those for the SQ cages (~ 252 ps), which can be attributed to the higher QY.

The outlier in this study was *p*-vinylstilbene (free chromophore), which shows much shorter lifetimes of 2.9 and 49 ps respectively. This is expected since the degree of rotational diffusion should be largest in the free chromophore.⁵⁹ This may also suggest a shorter-lived excited state than the hybrid systems, likely due to the influence of silicon.

The “rise time” (T_1) was determined for these compounds, which is the onset time for fluorescence to occur from the probed state and often indicative of an excited state process.^{59,69,71-73} Excitation at 286 nm and emission collection at 450 nm gave a rise time of a few hundred femto seconds, suggesting the 450 nm comes from a lower energy excited state.

This suggests that it takes time after the molecule is excited to fluoresce from that state, giving evidence for an energy transfer process.⁵⁹ Two compounds shown in Table

6.7 and Figure 6.10 that did not show a rise time were the free chromophore systems (*p*-triethoxysilylvinylstilbene and *p*-vinylstilbene). Our analysis shows that the shortest rise times are observed for the T₈ stilbenevinyl system at 760 fs, while the T₁₀ gives a rise time of 840 fs and the T₁₂ a rise time of 950 fs, suggestive of Förster energy transfer.⁷⁴⁻⁷⁶

There are two primary charge transfer mechanisms that may be expected in these molecules, but may or may not be related to these rise times, as other solvent and symmetry effects are plausible.⁷⁷ The first is a Dexter energy transfer from the stilbenevinyl groups to the cage. The second is Förster type hopping between chromophores, which could occur on the same cage, or between cages. Our rise times discussed above are on the time scale where Förster energy transfer (FRET) takes place, which would suggest it as an energy transfer mechanism for these systems.⁷⁴⁻⁷⁶ This however does not rule out the possibility of a Dexter type energy transfer from chromophore to cage, as this transfer would be faster than the instrument response function (650 fs) and could not be observed by our methods. Therefore, it is possible that both mechanisms proceed, but further analysis and computational modeling is necessary.

In order to gain a better understanding of the FRET system, we calculated the Förster radii for the compounds.^{59,74} For the calculation, we used the assumption that the dipolar angles would scale with the angles between the chromophores discussed above, and the integral of the overlap between absorption and emission spectra Appendix C. We calculate the Förster radius R₀ to be ~12 Å for T₈, 10 Å for T₁₀, and 8.6 Å for T₁₂. If we then approximate the distance between chromophores from a combination of similar crystal structures and computational modeling, we get values for the centroid-centroid distance of two adjacent chromophores to be ~12, 14, 16 Å respectively.¹¹² Back calculation of the expected lifetimes can then be calculated to be on the order of a few hundred femtoseconds to a few ps, depending on the exact distance (r) chosen between chromophores. From our analysis, the best energy transfer would likely occur within the first few carbons on the cage side of the chromophores (~7-9 Å between chromophores), which are within the Förster radii discussed above, and may involve the face of the cage. Förster energy transfer between the outside ends of the chromophores (> 20 Å) is unlikely for these systems.

Early theoretical modeling attempts suggest that Förster hopping between chromophores on the same cage is most likely at 10^{-7} M concentrations,^{62,63} which would also be expected for the solid state, and is observed in its emission data. Their calculations show that charge transfer by this method is solvent stabilized. However, unpublished experimental analyses of single chromophore (mono-stilbenevinylSQ) systems suggests that if this is true, it is not necessarily between chromophores on the same cage, since similar steady state spectra are observed for the fully functionalized systems.⁵⁶ In order to fully understand the mechanisms by which this rise time occurs, we are assessing the photophysical properties of single chromophore SQs, allowing for simplification of the energy transfer possibilities.⁵⁶

Table 6.8 shows the fluorescence lifetimes of $T_{10/12}$ stilbenevinylSQ taken previously. This compound was excited at 286 nm and probed at 385 nm, the main fluorescence band. The $T_{10/12}$ compound shows lifetimes of 20 and 140 ps respectively, which is within error for that found in the study above. No rise time was observed for this excitation-probe pair, suggesting that this fluorescence is directly from the chromophore emission.

Table 6.8. Fluorescence lifetimes of selected $T_{10/12}$ StilbenevinylSQ components excited at 286 nm with fluorescence collection at 385 nm.

	T_1 (ps)	A_1	T_2 (ps)	A_2
$T_{10/12}$	20±5	0.27	140±82	0.39

Figure 6.12 and Table 6.9 show the fluorescence lifetimes of the stilbenevinylSQs with excitation at 400 nm and emission probing at 450 nm. As this was our first kinetic analysis of stilbenevinylSQ based materials, a more careful analysis is needed for the 400 nm excitation data, since this is an off band wavelength.⁵⁶

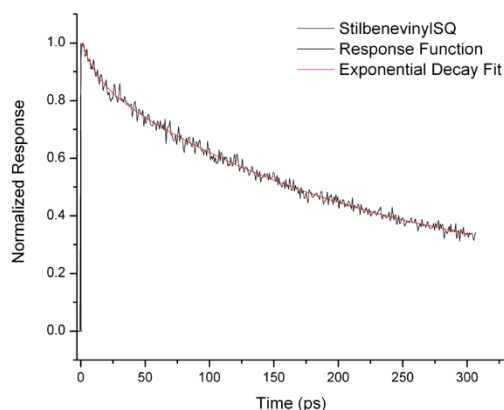


Figure 6.12. Fluorescence decay of $T_{10/12}$ (H) at 400 nm excitation, and 450 nm collection.

Table 6.9. Fluorescence lifetimes of the $T_{8,10,12}$ StilbenevinylSQ systems using fluorescence upconversion spectroscopy from excitation at 400 nm and collection at 450 nm.

	T_1 (ps)	A_1	T_2 (ps)	A_2
T_8	361	3.5	-	-
T_{10}	11 ± 3	0.14	419 ± 120	0.64
T_{12}	1.2 ± 0.2	0.18	86 ± 9	0.23
$T_{10/12}$	20 ± 6	0.28	140 ± 80	0.39

Polarized excitation measurements for these materials give fluorescence anisotropy for the stilbenevinylSQs. The anisotropy shows the directionality of the materials, such that a more symmetrical and less freely moving material gives a higher anisotropy value (max of 0.4).^{78,79} The anisotropy was measured for the 286 nm excitation and 450 nm collection. The T_8 compound shows higher anisotropy (0.3/0.4) than the T_{10} (0.1) or T_{12} (0.15). This means that the highest symmetry and lowest directional dependence is observed for the T_8 system (Figure 6.13). The *p*-triethoxysilylvinylstilbene also shows medium anisotropy that decays from 0.2 to nearly zero in 250 ps.

The $T_{10/12}$ stilbenevinylSQ mixture also shows low anisotropy similar to the T_{10} . The anisotropy does not decay significantly during the 250 ps measurement time. The decrease in anisotropy for regular organic systems can be attributed to two factors

including: increased rotational diffusion, and/or increased energy transfer processes.⁵⁹ The likelihood of radiationless energy transfer likely increases in the larger cage systems due to the closer proximity of the chromophores even under μM concentrations.⁸⁰⁻⁸² The only extensively studied 3-D systems are those of fullerenes, which offer excellent charge delocalization and show even lower anisotropy values of ~ 0.5 .⁵⁰ Therefore, we can speculate that the larger SQs also show charge delocalization in 3-D based on a combination of known properties of organic systems and observations from fullerenes.

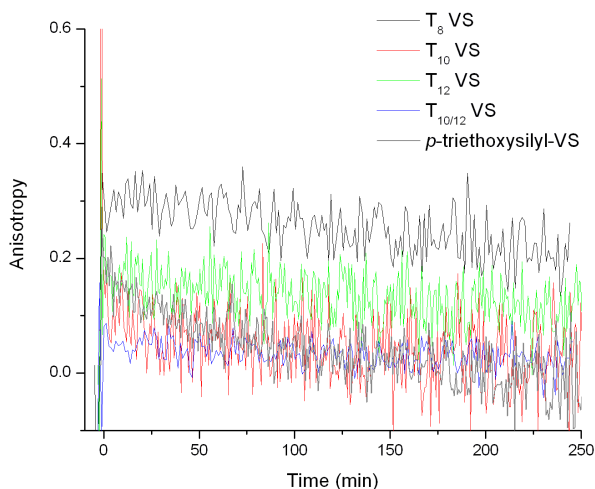


Figure 6.13. Fluorescence anisotropy measured at 286 nm excitation and 450 nm fluorescence collection for stilbenevinylSQs.

6.5.3 Summary of Findings

In the above studies we:

- (1) Developed novel methods for separating T_{10} and T_{12} stilbenevinylSQs by selective solubility/precipitation methods by exploiting the geometric differences between the cages.
- (2) Find that higher chromophore densities per cage decrease fluorescence quantum yields, contrary to expectations, but likely due enhanced self-absorption leading to non-radiative decay processes.
- (3) Find single-photon and two-photon excitation dependent emissions that can be attributed to “red edge” effects.

- (4) Find that of the three cage sizes and symmetries studied; the T_{10} stilbenevinylSQs offer the highest TPA cross-sections, indicative of the strongest electronic coupling and polarization.
- (5) Find that SQ cage compounds show “rise times” of 700 – 1000 fs and low anisotropies (~ 0.1) in fluorescence upconversion lifetime kinetic studies, indicative of excited state energy transfer process, (Internal delocalization or FRET type energy transfer), which is unobserved for the free chromophore, unexpected for a system with an “inert” silica core, and unexpected for 3-D hybrid molecular species.

6.5.4 Additions and Future Work

Figure 6.14 provide SEM micrographs of the T_{10} stilbenevinylSQ systems in the solid state. Compounds were cast from toluene onto a copper foil surface and air dried to form spherulitic structures. The largest spherulites are $\sim 30 \mu\text{m}$ in diameter, and are clearly made up of smaller spheres of 500 nm to $2 \mu\text{m}$, which would be anticipated from interdigitation of 3-D structures.

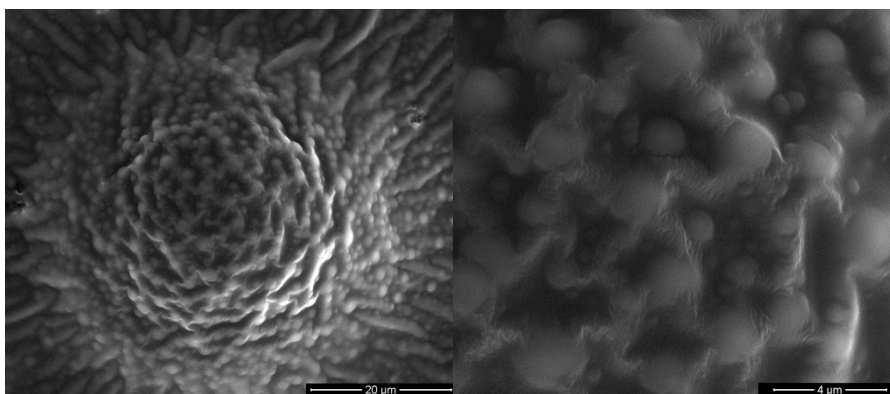


Figure 6.14. a and b. SEM images of T_{10} stilbenevinylSQ aggregates.

Atomic force microscopy and near-field scanning optical microscopy (AFM/NSOM) of the T_{10} stilbenevinylSQ was also undertaken as an early attempt to image the change in fluorescence spectrum based on cluster size. Figure 6.15 shows an AFM image of a $2 \mu\text{m}$ sized aggregate. Figure 6.16 shows an image of the fluorescence intensity given off the same aggregate using NSOM with a two-photon excitation of 810 nm. Figure 6.17 shows the fluorescence spectrum obtained from NSOM analysis. This fluorescence spectrum was fit with a Gaussian curve and shows a $\lambda_{\text{max}} = 450 \text{ nm}$, similar to that obtained in two-photon solvent studies, and also single photon solid-state fluorescence studies for the stilbenevinylSQ compounds. This suggests that in both single-photon and two-photon

excited films, the solid-state interactions are similar. The AFM and NSOM images reinforce our interdigitation theory, in that one could imagine we are probing one of the small spheres that make up the spherulite shown in the SEM image above. Future work should continue to look at the aggregates of other cage sizes, as well as going toward single molecule imaging of the stilbenevinylSQ system.

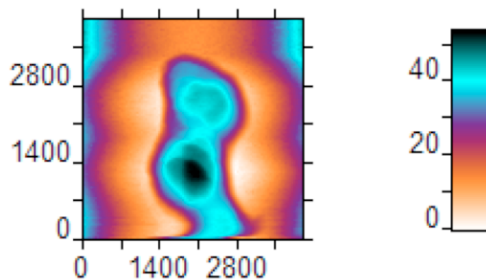


Figure 6.15. AFM image of T₁₀ stilbenevinylSQ aggregates on mica (nm).

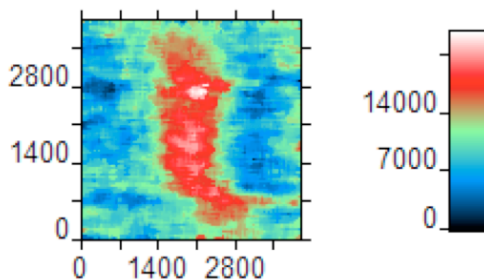


Figure 6.16. NSOM image of T₁₀ stilbenevinylSQ aggregates on mica (nm).

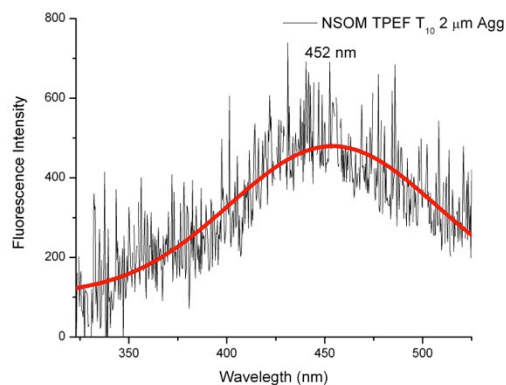


Figure 6.17. NSOM-TPEF spectrum of T₁₀ stilbenevinylSQ taken on a USB-2000 Ocean Optics Spectrophotometer, with Gaussian fit.

6.6 Conclusions

The separated T_{10} and T_{12} stilbenevinylSQs show properties that are unique to their cage sizes and symmetries. First, we see decreases in fluorescence quantum yield with increasing cage sizes, indicative of self-quenching effects likely due to cage symmetry and/or chromophores proximity. Second, stilbenevinylSQs show excitation dependent emission in both one-photon and two-photon absorption studies, evident of a “red edge” effect, an unusual result normally observed for fluorophores attached to 2-D rigid substrates.

The current studies represent observation of red-edge effects in 3-D molecular structures and suggest a new class of hybrid materials offering switchable emissions. Third, the T_{10} stilbenevinylSQ exhibits the highest enhanced TPA cross-section, implying the highest polarizability (charge separation), which can be attributed directly to its symmetry. This is again a first example of the effects of symmetry in a class of 3-D molecules that are essentially identical in all other aspects. Lastly, fluorescence lifetime kinetics and anisotropy measurements show that stilbenevinylSQs offer charge delocalization in the excited state through a likely combination of Förster and Dexter energy transfer processes, while the free chromophores do not. The process by which this transfer occurs will be under further investigation, but can be described as through cage (cage-chromophore), through space (chromophore-chromophore) or by both processes simultaneously.

The observation of 3D charge delocalization, high absorption efficiency and high cross-sections show that we can potentially tailor SQs for use in electronic and photonic applications. This is the first study mapping the detailed photophysical properties of T_{10} and T_{12} silsesquioxanes and the first evidence of quite different photophysical properties based solely on cage size and symmetry.

References:

1. Hartmann-Thompson, C. Polyhedral Oligomeric Silsesquioxanes in Electronics and Energy Applications. In *Applications of Polyhedral Oligomeric Silsesquioxanes SE - 7*; Hartmann-Thompson, C., Ed.; Advances in Silicon Science; Springer Netherlands, 2011; Vol. 3, pp. 247–325 LA – English.

2. Kaneko, Y.; Coughlin, E. B.; Gunji, T.; Itoh, M.; Matsukawa, K.; Naka, K. Silsesquioxanes: Recent Advancement and Novel Applications. *Int. J. Polym. Sci.* **2012**, *2012*, 1–2.
3. Chan, K. L.; Sonar, P.; Sellinger, A. Cubic Silsesquioxanes for Use in Solution Processable Organic Light Emitting Diodes (OLED). *J. Mater. Chem.* **2009**, *19*, 9103.
4. Laine, R. M.; Sulaiman, S.; Brick, C.; Roll, M.; Tamaki, R.; Asuncion, M. Z.; Neurock, M.; Filhol, J.-S.; Lee, C.-Y.; Zhang, J.; et al. Synthesis and Photophysical Properties of Stilbeneoctasilsesquioxanes. Emission Behavior Coupled with Theoretical Modeling Studies Suggest a 3-D Excited State Involving the Silica Core. *J. Am. Chem. Soc.* **2010**, *132*, 3708–3722.
5. Roll, M. F.; Kampf, J. W.; Kim, Y.; Yi, E.; Laine, R. M. Nano Building Blocks via Iodination of [PhSiO 1 . 5] N , Forming High-Surface-Area , Thermally Stable , Microporous Materials via Thermal Elimination of I 2. *J. Am. Chem. Soc.* **2010**, *132*, 10171–10183.
6. Choi, J.; Yee, A. F.; Laine, R. M. Organic/Inorganic Hybrid Composites from Cubic Silsesquioxanes. Epoxy Resins of Octa(dimethylsiloxylethylcyclohexylepoxide) Silsesquioxane. *Macromolecules* **2003**, *36*, 5666–5682.
7. Samthong, C.; Laine, R. M.; Somwangthanaroj, A. Synthesis and Characterization of Organic/inorganic Epoxy Nanocomposites from Poly(aminopropyl/phenyl)silsesquioxanes. *J. App. Poly. Sci.* **2013** *128* 3601-3608.
8. Lin, W.; Chen, W.; Wu, W.; Niu, Y.; Jen, A. Synthesis and Optoelectronic Properties of Starlike Polyfluorenes with a Silsesquioxane Core. *Macromolecules* **2004**, *37*, 2335–2341.
9. Jung, J. H.; Furgal, J.; Iii, T. G.; Mizumo, T.; Schwartz, M.; Chou, K.; Vonet, J.-F.; Laine, R. M. 3-D Molecular Mixtures of Catalytically Functionalized [vinylSiO1.5]10/ [vinylSiO1.5]12. Photophysical Characterization of Second Generation Derivatives. *Chem. Mater.* **2012**, *24*, 1883–1895.
10. Neumann, D.; Fisher, M.; Tran, L.; Matisons, J. G. Synthesis and Characterization of an Isocyanate Functionalized Polyhedral Oligosilsesquioxane and the Subsequent Formation of an Organic–Inorganic Hybrid Polyurethane. *J. Am. Chem. Soc.* **2002**, *124*, 13998–13999.
11. Hong, B.; Thoms, T. P. S.; Murfee, H. J.; Lebrun, M. J. Highly Branched Dendritic Macromolecules with Core Polyhedral Silsesquioxane Functionalities. *Inorg. Chem.* **1997**, *36*, 6146–6147.
12. Laine, R. M.; Roll, M. F. Polyhedral Phenylsilsesquioxanes. *Macromolecules* **2011**, *44*, 1073–1109.
13. Kim, Y.; Koh, K.; Roll, M. F.; Laine, R. M.; Matzger, A. J. Porous Networks Assembled from Octaphenylsilsesquioxane Building Blocks. *Macromolecules* **2010**, *43*, 6995–7000.
14. Baney, R. H.; Itoh, M.; Sakakibara, A.; Suzuki, T. Silsesquioxanes. *Chem. Rev.* **1995**, *95*, 1409–1430.
15. Sulaiman, S.; Zhang, J.; Goodson, I. T.; Laine, R. M. Synthesis, Characterization and Photophysical Properties of Polyfunctional Phenylsilsesquioxanes: [o-

- RPhSiO_{1.5}]₈, [2,5-R₂PhSiO_{1.5}]₈, and [R₃PhSiO_{1.5}]₈. Compounds with the Highest Number of Functional Units/unit Volume. *J. Mater. Chem.* **2011**, *21*, 11177.
16. Laine, R. M.; Soles, C. L.; Krug, D. J.; Wook Ro, H.; Popova, V. Silsesquioxane Derived Hard, Hydrophobic, and Thermally Stable Thin Films and Coatings for Tailorable Protective and Multi-Structured Surfaces and Interfaces **2010**.
 17. Sulaiman, S.; Bhaskar, A.; Zhang, J.; Goodson, T.; Laine, R.M. Blocks for 3-D Assemblies. Elaboration of Octavinylsilsesquioxane. Unusual Luminescence Shifts May Indicate Extended Conjugation Involving the Silsesquioxane Core. *Chem. Mater.* **2008**, *20*, 5563–5573.
 18. Lo, M. Y.; Zhen, C.; Lauters, M.; Jabbour, G. E.; Sellinger, A. Organic-Inorganic Hybrids Based on Pyrene Functionalized Octavinylsilsesquioxane Cores for Application in OLEDs, *J. Am. Chem. Soc.* **2007**, *129*, 5808–5809.
 19. Voronkov, M.; Lavrent'yev, V. Polyhedral Oligosilsesquioxanes and Their Homo Derivatives. *Top. Curr. Chem.* **1982**, *102*, 199–236.
 20. Loy, D.; Shea, K. Bridged Polysilsesquioxanes. Highly Porous Hybrid Organic/Inorganic Materials, *Chem. Rev.* **1995**, *95*, 1431–1442.
 21. Calzaferri, G.; Corriu, R.; Jutzi, P. *Tailor-made Silicon-Oxygen Compounds, from molecules to materials*; 1996; p. 149.
 22. Lichtenhan, J. In *Tailor-made Silicon-Oxygen Compounds*; Salmone, J. C., Ed.; CRC Press: New York, 1996; pp. 7768–7777.
 23. Provatas, A.; Matisons, J. G. Synthesis and Applications of Silsesquioxanes. *Trends. Polym. Sci.* **1997**, *5*, 327–333.
 24. Li, G.; Wang, L.; Ni, H.; Pittman Jr, C.U. Polyhedral Oligomeric Silsesquioxane (POSS) Polymers and Copolymers: A Review. *J. Inorg. and Organomet. Polymers* **2002**, *11*, 123–154.
 25. Duchateau, R. Incompletely Condensed Silsesquioxanes: Versatile Tools in Developing Silica-Supported Olefin Polymerization Catalysts. *Chem. Rev.* **2002**, *102*, 3525–42.
 26. Phillips, S. H.; Haddad, T. S.; Tomczak, S. J. Developments in Nanoscience: Polyhedral Oligomeric Silsesquioxane (POSS)-Polymers. *Curr. Opin. Solid State Mater. Sci.* **2004**, *8*, 21–29.
 27. Abe, Y.; Gunji, T. Oligo- and Polysiloxanes. *Prog. Poly. Sci.* **2004**, *29*, 149–182.
 28. Kannan, R. Y.; Salacinski, H. J.; Butler, P. E.; Seifalian, A. M. Polyhedral Oligomeric Silsesquioxane Nanocomposites: The next Generation Material for Biomedical Applications. *Acc. Chem. Res.* **2005**, *38*, 879–84.
 29. Laine, R. M. Nanobuilding Blocks Based on the [OSiO_{1.5}]_x (x= 6, 8, 10) Octasilsesquioxanes. *J. Mater. Chem.* **2005**, *15*, 3725.
 30. Lickiss, P. D.; Rataboul, F. Fully Condensed Polyhedral Oligosilsesquioxanes (POSS): From Synthesis to Application. *Adv. Organomet. Chem.* **2008**, *57*, 1–116.
 31. Wu, J.; Mather, P. T. POSS Polymers: Physical Properties and Biomaterials Applications. *Poly. Rev.* **2009**, *49*, 25–63.
 32. Cordes, D. B.; Lickiss, P. D.; Rataboul, F. Recent Developments in the Chemistry of Cubic Polyhedral Oligosilsesquioxanes. *Chem. Rev.* **2010**, *110*, 2081–173.

33. Asuncion, M. Z.; Laine, R. M. Fluoride Rearrangement Reactions of Polyphenyl- and Polyvinylsilsesquioxanes as a Facile Route to Mixed Functional Phenyl, Vinyl T₁₀ and T₁₂ Silsesquioxanes. *J. Am. Chem. Soc.* **2010**, *132*, 3723–36.
34. Miyazato, A.; Pakjamsai, C.; Kawakami, Y. Octa, Deca, and dodeca(4-Nitrophenyl) Cage Silsesquioxanes via 4-Trimethylsilylphenyl Derivatives. *Dalton Trans.* **2010**, *39*, 3239–44.
35. Ronchi, M.; Sulaiman, S.; Boston, N. R.; Laine, R. M. Fluoride Catalyzed Rearrangements of Polysilsesquioxanes, Mixed Me, Vinyl T₈, Me, Vinyl T₁₀ and T₁₂ Cages. *Appl. Organomet. Chem.* **2009**, *24*, 551–557.
36. Harrison, D. P.; Hall, C. Preparation and Characterization of Octasilsesquioxane Cage Monomers. *Main Group Met. Chem.* **1997**, *20*, 515.
37. Agaskar, P. New Synthetic Route to the Hydridospherosiloxanes O_h-H₈Si₈O₁₂ and D_{5h}-H₁₀Si₁₀O₁₅. *Inorg. Chem.* **1991**, 2707–2708.
38. Brown, J. F. The Polycondensation of Phenylsilanetriol, *J. Am. Chem. Soc.* **1965**, *87*, 4317-4324.
39. Jung, J. H.; Furgal, J. C.; Clark, S. C.; Schwartz, M. C.; Chou, K.; Laine, R. M. “Copolymerization of [p-IPhSiO_{1.5}]₈, I8OPS] with Divinyl (DVB)- and Diethynylbenzene (DEB) gives Beads on a Chain (BoC) Polymers with Functionalized Beads. The DEB Systems Exhibit through Chain, Extended 3-D Conjugation in the Excited State.” *Macromolecules*, **2013**, *46*, 7580-7590.
40. Furgal, J.C.; Jung, J.H.; Clark, S.C.; Goodson III, T.; Laine, R.M. “Beads on a Chain (BoC), Phenylsilsesquioxane (SQ), Conjugated Polymers Via F⁻ Catalyzed Rearrangements and ADMET and Reverse Heck Cross-coupling Reactions; through chain, extended conjugation in 3-D,” *Macromolecules* **2013**, *46*, 7591-7604.
41. Varnavski, O.; Yan, X.; Mongin, O.; Blanchard-Desce, M.; Goodson, T. Strongly Interacting Organic Conjugated Dendrimers with Enhanced Two-Photon Absorption. *J. Phys. Chem. C* **2006**, *111*, 149–162.
42. Goodson, T. G. Optical Excitations in Organic Dendrimers Investigated by Time-Resolved and Nonlinear Optical Spectroscopy. *Acc. Chem. Res.* **2005**, *38*, 99.
43. Xu, C.; Webb, W. W. Measurement of Two-Photon Excitation Cross Sections of Molecular Fluorophores with Data from 690 to 1050 Nm. *J. Opt. Soc. Am. B* **1996**, *13*, 481.
44. Haley, J. E.; Krein, D. M.; Monahan, J. L.; Burke, A. R.; McLean, D. G.; Slagle, J. E.; Fratini, A.; Cooper, T. M. Photophysical Properties of a Series of Electron-Donating and -Withdrawing Platinum Acetylide Two-Photon Chromophores. *J. Phys. Chem. A* **2010**, *115*, 265–273.
45. Jha, P. C.; Das, M.; Ramasesha, Two-Photon Absorption Cross Sections of Trans-Stilbene, and 7,8-Disubstituted Stilbenes in Different Molecular Conformations: A Model Exact Study. *S. J. Phys. Chem. A* **2004**, *108*, 6279–6285.
46. Varnavski, O.; Goodson III, T. G. Femtosecond Fluorescence Dynamics and Molecular Interactions in a Water-Soluble Nonlinear Optical Polymeric Dye. *Chem. Phys. Lett.* **2000**, 688–696.
47. Ramakrishna, G.; Bhaskar, A.; Goodson III, T. Ultrafast Excited State Relaxation Dynamics of Branched Donor-Pi-Acceptor Chromophore: Evidence of a Charge-Delocalized State. *J. Phys. Chem. B* **2006**, *110*, 20872–8.

48. Flynn, D. C.; Ramakrishna, G.; Yang, H.; Northrop, B. H.; Stang, P. J.; Goodson III, T. G. Ultrafast Optical Excitations In Supramolecular Metallacycles with Charge Transfer Properties *J. Am. Chem. Soc.* **2010**, *132*, 1348–1358.
49. Raymond, J. E.; Goodson, T. Single-Particle Two-Photon Absorption Imaging and Enhancement Determination for Organic Nanoparticles. *J. Phys. Chem. Lett.* **2011**, *2*, 329–333.
50. Fedorov, A.; Berberan-Santos, M. N.; Lefevre, J.-P.; Valeur, B. Picosecond Time-Resolved and Steady-State Studies of the Polarization of the Fluorescence of C 60 and C 70. *Chem. Phys. Lett.* **1997**, *267*, 467–471.
51. Brusatin, G.; Signorini, R. Linear and Nonlinear Optical Properties of Fullerenes in Solid State Materials. *J. Mater. Chem.* **2002**, *12*, 1964–1977.
52. Amendola, V.; Mattei, G.; Cusan, C.; Prato, M.; Meneghetti, M. Fullerene Non-Linear Excited State Absorption Induced by Gold Nanoparticles Light Harvesting. *Synth. Met.* **2005**, *155*, 283–286.
53. Liu, Z.; Xu, Y.; Zhang, X.; Zhang, X.; Chen, Y.; Tian, J. Porphyrin and Fullerene Covalently Functionalized Graphene Hybrid Materials with Large Nonlinear Optical Properties. *J. Phys. Chem. B.* **2009**, 9681–9686.
54. Peterson, J. J.; Simon, Y. C.; Coughlin, E. B.; Carter, K. R. Polyfluorene with P-Carborane in the Backbone. *Chem. Comm.* **2009**, 4950–2.
55. Peterson, J. J.; Werre, M.; Simon, Y. C.; Coughlin, E. B.; Carter, K. R. Carborane-Containing Polyfluorene: O- Carborane in the Main Chain. *Macromolecules* **2009**, *42*, 8594–8598.
56. Furgal, J. C.; Abeyasinge, N.; Yi, E.; Goodson, T.; Laine, R. M. *Unpublished Results*
57. Rikowski, E.; Marsmann, H. C. *Polyhedron* **1997**, *16*, 3357–3361.
58. Bahrami, M.; Hashemi, H.; Ma, X.; Kieffer, J.; Laine, R. M. Why Do the [PhSiO_{1.5}]_(8,10,12) Cages Self-Brominate Primarily in the Ortho Position? Modeling Reveals a Strong Cage Influence on the Mechanism. *Phys. Chem. Chem. Phys.* **2014**, *16*, 25760–25764.
59. Lakowicz, J. *Principles of Fluorescence Spectroscopy*; Third.; Springer Science+Business Media: New York, 2006; pp. 47, 243, 358–359, 588.
60. Demchenko, A. P. The Red-Edge Effects: 30 Years of Exploration. *Luminescence* **2002**, *17*, 19–42.
61. Józefowicz, M.; Heldt, J. R. Excitation-Wavelength Dependent Fluorescence of Ethyl 5-(4-Aminophenyl)-3-Amino-2,4-Dicyanobenzoate. *J. Fluoresc.* **2011**, *21*, 239–45.
62. Phillips, H.; Zheng, S.; Hyla, A.; Laine, R.; Goodson, T.; Geva, E.; Dunietz, B. D. Ab Initio Calculation of the Electronic Absorption of Functionalized Octahedral Silsesquioxanes via Time-Dependent Density Functional Theory with Range-Separated Hybrid Functionals. *J. Phys. Chem. A* **2012**, *116*, 1137–1145.
63. Zheng, S.; Phillips, H.; Geva, E.; Dunietz, B. D. Ab Initio Study of the Emissive Charge-Transfer States of Solvated Chromophore-Functionalized Silsesquioxanes. *J. Am. Chem. Soc.* **2012**, *134*, 6944–7.
64. Dick, B.; Hohlneicher, G. Importance of Initial and Final States as Intermediate States in Two-Photon Spectroscopy of Polar Molecules. *J. Chem. Phys.* **1982**, *76*, 5755–5760.

65. Goodson, T. G. Optical Excitations in Organic Dendrimers Investigated by Time-Resolved and Nonlinear Optical Spectroscopy. *Acc. Chem. Res.* **2005**, *38*, 99–107.
66. Bhaskar, A.; Ramakrishna, G.; Lu, Z.; Twieg, R.; Hales, J. M.; Hagan, D. J.; Stryland, E. Van; Goodson, T. Investigation of Two-Photon Absorption Properties in Branched Alkene and Alkyne Chromophores *J. Am. Chem. Soc.* **2006**, *128*, 11840–9.
67. Andrews, D. L.; Ghoul, W. A. Polarization Studies in Multiphoton Absorption Spectroscopy. *J. Chem. Phys.* **1981**, *75*, 530.
68. Craig, D. P.; Thirunamachandran, T. *Molecular Quantum Electrodynamics: An Introduction to Radiation Interaction*; 1984; p. 120.
69. Holt, N. E.; Kennis, J. T. M.; Fleming, G. R. Femtosecond Fluorescence Upconversion Studies of Light Harvesting by β -Carotene in Oxygenic Photosynthetic Core Proteins. *J. Chem. Phys.* **2004**, *108*, 19029–19035.
70. Ceroni, P.; Balzani, V. The Exploration of Supramolecular Systems and Nanostructures by Photochemical Techniques. *J. Phys. Chem. B* **2012**, *78*, 21–39.
71. Langhals, H.; Esterbauer, A. J.; Walter, A.; Riedle, E.; Pugliesi, I. Resonant Energy Transfer in Orthogonally Arranged Chromophores. *J. Am. Chem. Soc.* **2010**, 16777–16782.
72. Kleiman, V. Ultrafast Dynamics of Electronic Excitations in a Light-Harvesting Phenylacetylene Dendrimer. *J. Phys. Chem. B* **2001**, *105*, 5595–5598.
73. Ito, A.; Stewart, D. J.; Knight, T. E.; Fang, Z.; Brennaman, M. K.; Meyer, T. J. Excited-State Dynamics in Rigid Media: Evidence for Long-Range Energy Transfer. *J. Phys. Chem. B* **2013**, *117*, 3428–3438.
74. Varnavski, O. P.; Ostrowski, J. C.; Sukhomlinova, L.; Twieg, R. J.; Bazan, G. C.; Goodson, T. Coherent Effects in Energy Transport in Model Dendritic Structures Investigated by Ultrafast Fluorescence Anisotropy Spectroscopy. *J. Am. Chem. Soc.* **2002**, *124*, 1736–43.
75. Varnavski, O.; Leanov, a.; Liu, L.; Takacs, J.; Goodson, T. Femtosecond Luminescence Dynamics in a Nonlinear Optical Organic Dendrimer. *Phys. Review B* **2000**, *61*, 12732–12738.
76. Loura, L. M. S. Simple Estimation of Forster Resonance Energy Transfer (FRET) Orientation Factor Distribution in Membranes. *Int. J. Mol. Sci.* **2012**, *13*, 15252–70.
77. Albrecht, C. Lakowicz, J. Principles of Fluorescence Spectroscopy, 3rd Edition. *Anal. Bioanal. Chem.* **2008**, *390*, 1223–1224.
78. Kusba, J.; Lakowicz, J. Definition and Properties of the Emission Anisotropy in the Absence of Cylindrical Symmetry of the Emission Field: Application to the Light Quenching Experiments. *J. Chem. Phys.* **1999**, *111*, 89–99.
79. Jablonski, A. On The Notion of Emission Anisotropy. *Bull. l'Acad. Pol. Sci. Ser A* **1960**, *8*, 259–264.
80. Baumann, J.; Fayer, M. D. Excitation Transfer in Disordered Two- Dimensional and Anisotropic Three-Dimensional Systems: Effects of Spatial Geometry on Time-Resolved Observables. *J. Chem. Phys.* **1986**, *85*, 4087–4107.
81. Jablonski, A. Anisotropy of Fluorescence of Molecules Excited by Excitation Transfer. *Acta. Phys. Pol. A* **1970**, *38*, 453–458.

82. Van Der Meer, B. W.; Coker III, G.; Chen, S.-Y. *Resonance energy transfer theory and data*; Wiley-VCH: New York, 1991.

Chapter 7

Beads on a Chain (BoC), Phenylsilsesquioxane (SQ), Polymers Via F⁻ Catalyzed Rearrangements and ADMET or Reverse Heck Cross-coupling Reactions; through chain, extended conjugation in 3-D with potential for dendronization.

7.1 Original Publication Information

Furgal, J.C.; Jung, J.H.; Clark, S.C.; Goodson III, T.; Laine, R.M. *Macromolecules* **2013**, *46*, 7591-7604, DOI: 10.1021/ma401423f

7.2 Abstract

In this paper, we assess the utility of complementary routes to silsesquioxane based compounds using F⁻ catalyzed coupling to synthesize [vinylSiO_{1.5}]_xPhSiO_{1.5}]_{10-x/12-x} mixtures followed by co-polymerization with divinylbenzene (via ADMET), or using reverse Heck coupling with 1,4-dibromobenzene and 4,4'-dibromo-stilbene to prepare lightly branched, non-linear BOC systems. In an accompanying paper, we describe the use of Heck and Suzuki coupling to synthesize model conjugated p-R-stilbeneSQ BOCs starting from [*p*-IPh₈SiO_{1.5}]₈ and coupling with divinylbenzene (DVB) and 1,4-diethynylbenzene (DEB) finding extended 3-D conjugation in the DEB polymers.

We find that the reverse Heck coupling (where the linker contains the bromo moieties) works best for these systems giving BoC oligomers with M_n of ~ 6 kDa, in which extended excited state conjugation is observed for 1,4-dibromobenzene linked systems through ~50+ nm red shifts in the emission spectra compared with DVB linked systems and model compounds.

We compare and contrast the photophysical properties of the two sets of BOCs and the system where the conjugation length of the linker changes from divinylbenzene to divinylstilbene. We find that for a linker with a longer conjugation length, a red shifted absorption and emission is observed, however the difference in emission is much larger for the 1,4-dibromobenzene linked system as compared to the model compounds,

suggesting that a more rigid linker contributes to better orbital overlap with the cage and/or phenyl groups, increasing excited state conjugation interactions.

7.3 Introduction

Polyhedral silsesquioxanes (SQs) $[\text{RSiO}_{1.5}]_x$ ($x = 8, 10, 12$) are a versatile class of organosilicon compounds that offer 3-D symmetry in nano-scale structures. As noted in the 17 reviews on these materials,¹⁻¹⁷ they have found applications in multiple areas including: components in polymer nanocomposites,¹⁸ homogeneous and heterogeneous catalysis,¹⁹⁻²¹ models for silica surfaces,²² low-k dielectrics,²³ antimicrobials,²⁴ emitting layers in organic light-emitting diodes (OLEDs),^{25,26} omniphobic films,²⁷ and coatings.²⁸ The basis for all of these studies arises because of their advantageous properties. For example, SQ based materials often offer thermal stabilities >350 °C, high resistance to oxidation, high functional group densities (up to 24) groups on a 0.5 nm dia. SQ cage, with a total diameter of ~ 1.5 nm and facile purification because they are typically highly soluble.²⁹

Our discovery of 3-D excited state communication between conjugated moieties on $[-\text{SiO}_{1.5}]_8$, $[-\text{SiO}_{1.5}]_{10}$, and $[-\text{SiO}_{1.5}]_{12}$ cage systems prompted an exploration of the potential to introduce conjugated tethers between cages to prepare BoC oligomers and polymers that also exhibit conjugation through the tethers. Our initial study provides the first example of conjugation between SQ cages via a conjugate linker, Figure 7.1:³⁰

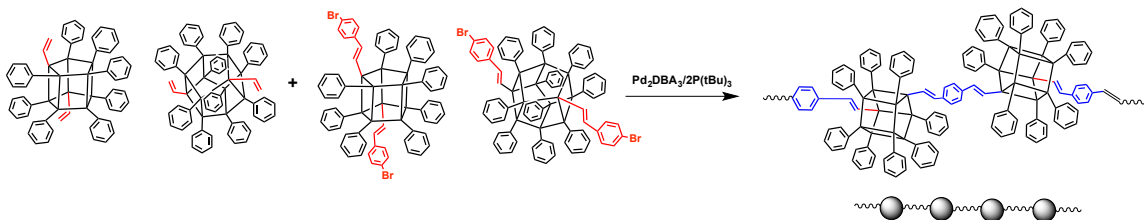


Figure 7.1. Heck cross-coupling synthesis of a BoC oligomer with 1,4-divinyl bridges between phenylT₁₀ and phenylT₁₂ SQs.³⁰

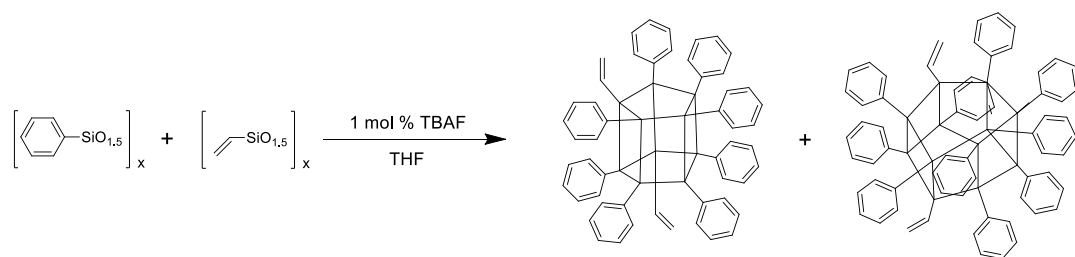
Given that oligomeric and polymeric systems that show extended conjugation are now in use or being contemplated for use in multiple applications in organic electronics and photonics; the development of BoC counterparts might provide a completely new approach to materials with similar or quite different but useful properties. To this end, we

are exploring the development of synthetic tools targeting the optimization of synthetic routes to BoC systems and their photophysical properties.

One particular focus of the photophysical properties efforts targets mapping their electronic and photonic properties for OLED and photovoltaic applications. Motivation for this work comes from work by Sellinger et al, who describe Heck cross-coupling of $[\text{vinylSiO}_{1.5}]_8$ with organic moieties conjugated to the SQ silica cage and Jabbour et al. who describe multifunctional SQ emitter based OLED components.^{25,26,31}

We have previously reported using $[\text{vinylSiO}_{1.5}]_8$ to synthesize $[p\text{-RStylSiO}_{1.5}]_8$ where R = H, Me, MeO, Br, NH₂, C₆F₅ and the corresponding stilbenevinyls, $[\text{RStilCH}=\text{CH}_2\text{SiO}_{1.5}]_8$.^{32,33} We coincidentally detailed their photophysical properties, as these compounds also exhibit some form of 3-D conjugation in the excited state.³²⁻³⁴

More recent work has targeted using the T₁₀ and T₁₂ cages that recently became available through our discovery of facile, high yield routes that use F⁻ to catalytically exchange RSiO_{1.5} units between different $[\text{RSiO}_{1.5}]_n$ cages and/or T resins, Scheme 7.1. This discovery was prompted by studies by Bassindale et al,³⁵⁻³⁷ and Mabry, Bowers et al.³⁸



Scheme 7.1. Synthesis of vinyl/phenyl mixed functional SQ compounds by F⁻ catalysis.

Thus F⁻ catalysis provides an excellent route to mixed functional cages $[\text{R}^1\text{SiO}_{1.5}]_{10/12}$ - $[\text{R}^2\text{SiO}_{1.5}]_x$ almost exclusively.^{30,39} This method also provides access to $[\text{vinylSiO}_{1.5}]_{10/12}$, to $[p\text{-RStylSiO}_{1.5}]_{10/12}$ and then (where R = Br) to $[p\text{-RStilCH}=\text{CH}_2\text{SiO}_{1.5}]_{10/12}$. These compounds permit us to map (for the first time) their photophysical properties to explore the potential differences that may arise as a consequence of different cage sizes and symmetries compared with the T₈ compounds we explored previously.³²⁻³⁴ A primary focus in these studies was to continue to explore their potential to exhibit 3D-excited state

conjugation.⁴⁰ A further opportunity presents itself given that by controlling the number of reactive groups on the cage, we have now devised routes to oligomeric and polymeric versions of the same cages; the immediate objective of the work reported here and in accompanying papers.^{41,42}

To date, most polymer studies have explored the effects of introducing monofunctional SQs as endcaps and/or pendant groups on polymer backbones or the use of polyfunctional SQs to make 3-D highly crosslinked nanocomposites.⁴³⁻⁵¹ In contrast, only a few groups including Kawakami et al. and Kakimoto et al. have used partially condensed cages to generate SQ based polymer systems with cages in the backbone.⁵²⁻⁵⁸ Thus the literature offers only a few, brief examples of the general class of polymers wherein the SQ cage is part of the polymer backbone, herein termed “beads on a chain” (BoC) polymers.^{1,59}

SQs are not the only 3-D molecules that offer unique photophysical properties. Coughlin et al. compare the effects of *ortho* and *para* carborane cages linked with fluorene units.^{60,61} They find that *ortho* substituted cages show extended conjugation in the excited state with fluorescence red shifts from monomer units of ~30 nm, with only slight changes in the absorption spectrum. However, they find that *para* substituted carboranes show minimal emission red shifts, suggesting minimal extended conjugation from this orientation. This suggests that similar orientational effects may be in place for SQ derived polymers.

We now find that F⁻ catalyzed cage rearrangements provide a facile route to di and tri-functional SQs {e.g. [vinylSiO_{1.5}]_xPhSiO_{1.5}]_{10-x/12-x}} that are thereafter amenable to copolymerization. In these studies and those in two complementary papers submitted coincidentally^{41,42} we have sought to develop efficient synthetic tools that provide access to related types of BoC polymers.

The first route to BoCs, described by Asuncion et al. is presented in Scheme 7.1.³⁰ This initial example compared the absorption and emission behavior of the resulting 1,4-divinylbenzene linked BoCs with unlinked model compounds showing nearly identical absorptions but emission red shifts of >50 nm for the BoCs, suggesting 3-D excited state

conjugation *through* the cages and *through* the conjugated bridges. This surprising result is the basis for all the current studies as it suggests the potential to perhaps make semiconducting polymers. A further example by Jung et al. used F^- catalyzed cage rearrangement to make $[(NH_2Ph)_{2,3}(Ph)SiO_{1.5}]_{10/12-2,3}$ SQs and then react them DGEBA (diglycidylether bisphenol A) to make “linear” epoxy resins.⁵⁹ Here we assess additional copolymerization routes to BoCs using ADMET and reverse Heck coupling with 4,4'-dibromobenzene and 4,4'-dibromostilbene as the cross-coupling components. The latter allows us to extend the conjugation of the linker.

7.4 Experimental Procedures

Synthetic methods and characterization procedures are given above in Chapter 2.

7.5 Results and Discussion

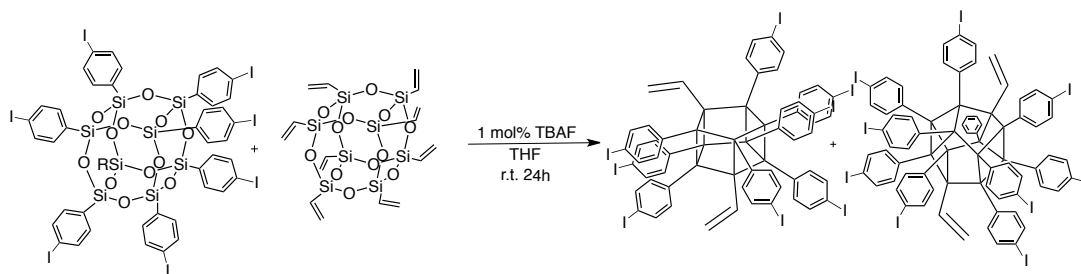
As noted above, we are attempting to develop optimal synthetic tools that allow the facile synthesis of conjugated BoC oligomers and polymers using catalytic copolymerization methods. Here we explore the potential utility of ADMET and reverse Heck catalytic crosscoupling as additional routes to BoCs and in particular to materials with novel photophysical properties. An additional and equally important goal is to assess the effects of increasing the conjugation length of the linker between SQ cages as a means of probing the potential for extended conjugation in $[(vinyl)_2(Ph)_{n-2}SiO_{1.5}]_n$ or $[(vinyl)_2(p-IPh)_{n-2}SiO_{1.5}]_n$ ($n = 10, 12$) BOC oligomers and polymers. Further, this work extends earlier efforts to delineate the nature of excited state, electronic communication between SQ cages as seen previously in the form of significant emission red-shifts, and also in accompanying papers where the linker is divinylbenzene (DVB) or 1,4-diethynylbenzene (DEB).

In the following sections, we describe ADMET copolymerization of divinyl(*x*-phenyl)SQ ($x = 8, 10$) and divinyl(*x*-iodophenyl)SQ with divinylbenzene (mixture of isomers). We then discuss further functionalization of the IPh groups by Heck cross-coupling with styrene and methoxystyrene. As in the accompanying paper, this step represents a model for the dendronization of BoC oligomers and polymers. Finally we describe the reverse Heck cross-coupling co-polymerization of divinyl(*x*-phenyl)SQ with

dibromobenzene and 4,4'-dibromostilbene as still a fourth alternative to BoC polymers.³⁰ Thereafter we delineate the photophysical properties of these BOC systems.^{41,42}

7.5.1 Syntheses of [(vinyl)₂(Ph)_{n-2}SiO_{1.5}]_n and [(vinyl)₂(*p*-IPh)_{n-2}SiO_{1.5}]_n (n = 10, 12)

The first step was to develop a basic route to the starting materials via F⁻ (tBu₄NF, TBAF) catalyzed exchange of [PhSiO_{1.5}]₈ (OPS) or [*p*-IPhSiO_{1.5}]₈ (I₈OPS) with [vinylSiO_{1.5}]₈ (OVS) using methods reported previously (Scheme 7.2).³⁰ These reactions were run at a 4.4:1 ratio to favor formation of ≈ two vinyl groups/cage.



Scheme 7.2. F⁻ catalyzed rearrangement reaction of I₈OPS and OVS.

Figure 7.2 and Figure 7.3 show the MALDI spectra of [(vinyl)₂(Ph)_{n-2}SiO_{1.5}]_n and [(vinyl)₂(*p*-IPh)_{n-2}SiO_{1.5}]_n (n = 10, 12). The spectra show equilibrium mixtures of compounds, (both cage sizes and functionalities). Table 7.1 and Table 7.2 show the expected and actual masses for the different MALDI species. Note that in the phenyl system, T₁₀ cages tend to form preferentially by rearrangement, whereas the iodophenyl system seems to favor T₁₂ cages per the Figure 7.2 MALDI. It is important to note that Figure 7.3 shows peaks missing iodo groups, which may result from the ionization process.⁶⁷

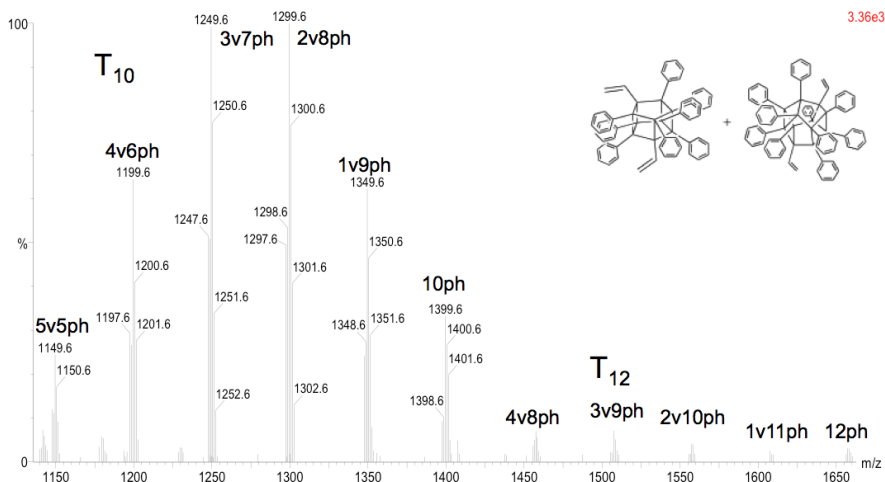


Figure 7.2. MALDI-ToF spectrum of $[(\text{vinyl})_2(\text{Ph})_{n-2}\text{SiO}_{1.5}]_n$ ($n = 10, 12$).

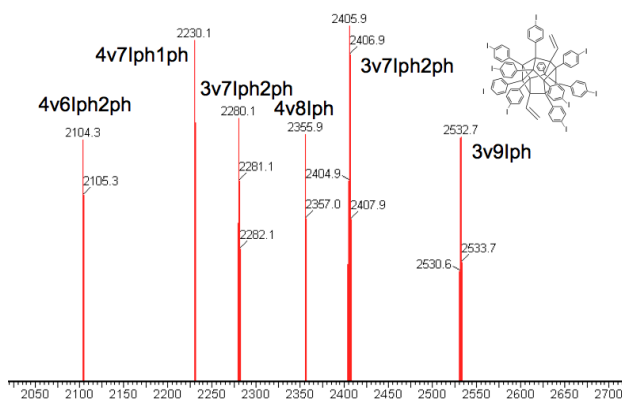


Figure 7.3. MALDI-ToF spectrum of $[(\text{vinyl})_2(\text{IPh})_{n-2}\text{SiO}_{1.5}]_n$ ($n = 10, 12$).

Table 7.1. MALDI-ToF data for $[(\text{vinyl})_2(\text{Ph})_{n-2}\text{SiO}_{1.5}]_n$ ($n = 10, 12$) w/ Ag^+ ion.[†]

Peak	Found (Da)	Calculated (Da)	Relative Peak Intensities (%)
$[\text{Si}_{10}\text{O}_{15}(\text{C}_2\text{H}_3)_5(\text{C}_6\text{H}_5)_5]$	1149.6	1148.8	37
$[[\text{Si}_{10}\text{O}_{15}(\text{C}_2\text{H}_3)_4(\text{C}_6\text{H}_5)_6]$	1199.6	1198.8	75
$[\text{Si}_{10}\text{O}_{15}(\text{C}_2\text{H}_3)_3(\text{C}_6\text{H}_5)_7]$	1249.6	1248.8	100
$[\text{Si}_{10}\text{O}_{15}(\text{C}_2\text{H}_3)_2(\text{C}_6\text{H}_5)_8]$	1299.6	1298.8	100
$[\text{Si}_{10}\text{O}_{15}(\text{C}_2\text{H}_3)_1(\text{C}_6\text{H}_5)_9]$	1349.6	1348.9	73
$[\text{Si}_{10}\text{O}_{15}(\text{C}_6\text{H}_5)_{10}]$	1399.6	1398.9	40
$[\text{Si}_{12}\text{O}_{18}(\text{C}_2\text{H}_3)_4(\text{C}_6\text{H}_5)_8]$	1457.6	1456.2	5
$[\text{Si}_{12}\text{O}_{18}(\text{C}_2\text{H}_3)_3(\text{C}_6\text{H}_5)_9]$	1507.5	1506.1	4

[Si ₁₂ O ₁₈ (C ₂ H ₃) ₂ (C ₆ H ₅) ₁₀]	1557.5	1556.1	3
[Si ₁₂ O ₁₈ (C ₂ H ₃) ₁ (C ₆ H ₅) ₁₁]	1607.5	1606.0	2
[Si ₁₀ O ₁₅ (C ₆ H ₅) ₁₂]	1657.5	1657.1	3

[†]Error in reported intensities is $\pm 5\%$

Table 7.2. MALDI-ToF data for [(vinyl)₂(IPh)_{n-2}SiO_{1.5}]_n (n = 10, 12) without Ag⁺ ion.[†]

Peak	Found (Da)	Calculated (Da)	Relative Peak Intensities (%)
[Si ₁₂ O ₁₈ (C ₂ H ₃) ₄ (IC ₆ H ₅) ₆ (C ₆ H ₅) ₂]	2104.3	2103.3	78
[Si ₁₂ O ₁₈ (C ₂ H ₃) ₄ (IC ₆ H ₅) ₇ (C ₆ H ₅) ₁]	2230.1	2229.3	97
[Si ₁₂ O ₁₈ (C ₂ H ₃) ₃ (IC ₆ H ₅) ₇ (C ₆ H ₅) ₂]	2280.1	2279.1	82
[Si ₁₂ O ₁₈ (C ₂ H ₃) ₄ (IC ₆ H ₅) ₈]	2355.9	2356.2	78
[Si ₁₂ O ₁₈ (C ₂ H ₃) ₃ (IC ₆ H ₅) ₈ (C ₆ H ₅) ₁]	2405.9	2405.2	100
[Si ₁₂ O ₁₈ (C ₂ H ₃) ₃ (IC ₆ H ₅) ₉]	2532.7	2532.2	75

[†]Error in reported intensities is $\pm 5\%$

Table 7.3 records the TGA data showing reasonable agreement with theory, where the theoretical ceramic yields (CY%) for the phenyl system were calculated from an average molecular weight. The average molecular weight was in turn found using the compositions and peak intensities in the MALDI spectra suggesting an average vinyl functionality of 2.5 for the combined cage sizes. If we instead calculate the average vinyl functionality based on the found CY of 52.6%, it comes out to be 3.1 vinyl groups per cage on average.

Table 7.3. GPC and TGA data for difunctional SQ monomers for polymerization.

	GPC			TGA			
	M _n (kDa)	M _w (kDa)	PDI	Ceramic yield (wt %, Found)	Ceramic yield (wt %, Theory MALDI)	T _{d5%} (°C)	Avg. vinyl Func.
[(vinyl) ₂ (Ph) _{n-2} SiO _{1.5}] _n	1.4	1.5	1.06	52.6	51.4	372	3.1
[(vinyl) ₂ (IPh) _{n-2} SiO _{1.5}] _n	2.4	2.5	1.05	28.4	29.7 ^a	404	2.2

^aCalculated based on the MALDI-ToF spectrum given in the supporting information.

Therefore, we calculated an average molecular weight of 1176.6 g/mol for [(vinyl)₂(Ph)_{n-2}SiO_{1.5}]_n mixture, which then gave a CY of 51.4 wt %. This value is 1.2 % lower than the found value of 52.6 wt %, suggesting that the weighted average method of calculating the molecular weights favors a monomer with greater organic functionality, but is a reasonable estimate for determining the average functionality by MALDI.

The CY for the IPh system was calculated using the same method and found to be 29.7 wt %^a, with an average molecular weight of 2121.2 g/mol and average vinyl functionality of 2.7. The actual CY % for the IPh system is 1.3 % lower than the calculated value, suggesting a slightly higher organic component (i.e. more Iphenyl) than used to calculate the actual value. The biggest challenge with MALDI-ToF analysis of the IPh derivative is that up to three iodo groups are missing in some cage species upon ionization. Therefore it is anticipated that there would be error in the calculated ceramic yield. As above, the average functionality was also calculated based on the actual CY of 29.7%, which gave an average vinyl functionality of 2.9 per cage.

Basically the CY calculations allow us to suggest that the resulting BoCs are likely to be highly branched. Furthermore, because the functional groups are also likely to be randomly distributed on the cage, the most reasonable perspective is that these polymers are closer to being globular in shape rather than linear which may have some implications for electron and hole transport processes.

Figure 7.4 and Table 7.3 compare the GPCs of both divinylSQs, with analyses showing a low PDI for both rearranged products. The MWs determined by GPC are not exact as GPC calibration uses polystyrene standards, and the BoC systems have quite different hydrodynamic volumes and the cages themselves offer very similar hydrodynamic volumes as they can be considered to be decorated spheres joined by short linkers. Thus, we assume that there is a consistent error in the GPC derived MWs and PDIs.

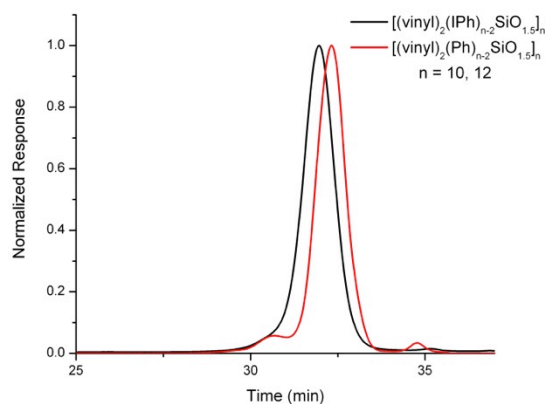
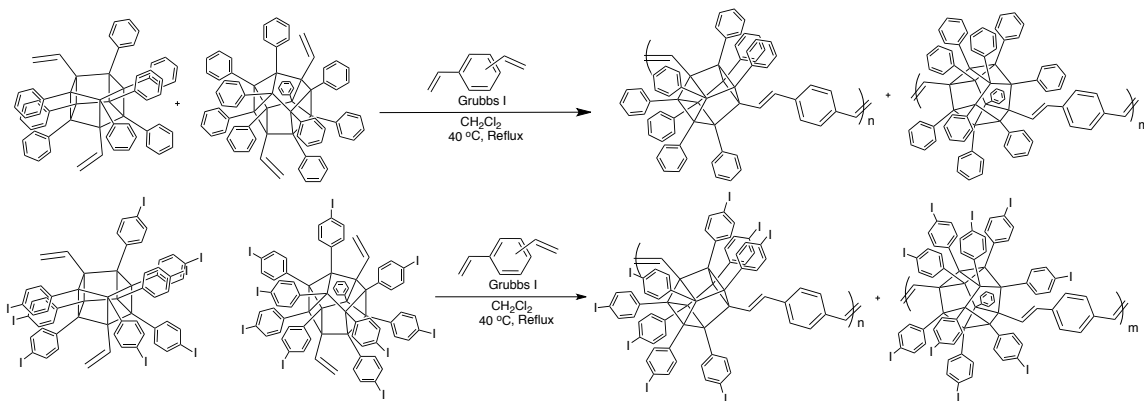


Figure 7.4. GPC analysis of $[(\text{vinyl})_2(\text{IPh})_{n-2}\text{SiO}_{1.5}]_n$ and $[(\text{vinyl})_2(\text{Ph})_{n-2}\text{SiO}_{1.5}]_n$, ($n = 10, 12$).

7.5.2 Synthesis of Polymers by Metathesis

The $[(\text{vinyl})_2(p\text{-IPh})_{n-2}\text{SiO}_{1.5}]_n$ and $[(\text{vinyl})_2(\text{Ph})_{n-2}\text{SiO}_{1.5}]_n$ ($n = 10, 12$) compounds were copolymerized with divinylbenzene (DVB using a Grubb's type I catalyst, ADMET) (Scheme 7.3, polymers **A** and **B**). The DVB used was a mixture of 1,3- and 1,4- isomers in a 2:1 ratio. As found in an accompanying paper, the conjugation length of the resulting copolymers is found to be short given that the 1,3-isomer does not imbue extended conjugation. This has a direct result on the resulting photophysical properties as we discuss in the accompanying paper and below. An additional influence will be on the solubility of the resulting copolymer, which in turn can affect the observed molecular weights.



Scheme 7.3. ADMET coupling of DVB with phenyl and iodophenyl vinyl SQs generating BoC polymers **A** and **B**.

Table 7.4 gives the GPC and TGA data for polymers **A** and **B**. By GPC (Figure 7.5), both sets of oligomers have DPs of 6-10 units with PDIs of 1.6 and 1.7 respectively, typical for ADMET

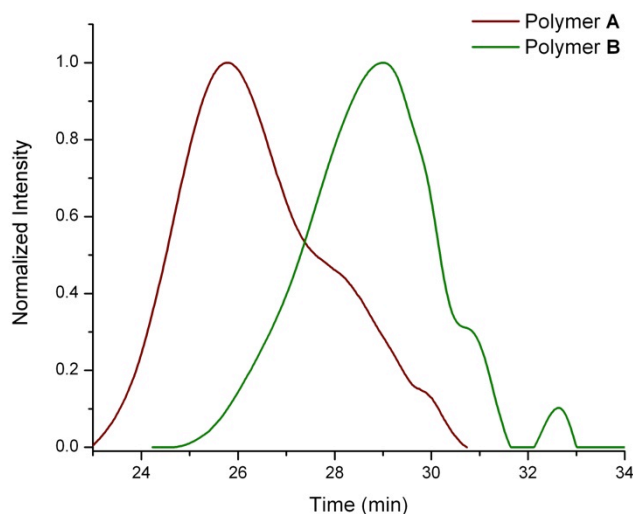


Figure 7.5. GPC analysis of polymers A and B, see copolymerizations.⁶⁸ The DPs can be calculated via three methods, the first uses the average repeat unit MW found from MALDI-ToF analysis, the second uses the TGA determined functionalization, and the third uses the GPC determined Mn of the starting cages, $[(\text{vinyl})_2(\text{Ph})_{n-2}\text{SiO}_{1.5}]_n$. The first values were calculated based on the average repeat units for each polymer by the MALDI-ToF analysis above (1176.6 g/mol phenyl, and 2121.2 g/mol IPh, DP \approx 6-10 units). The other methods give similar results. Note that *the resulting copolymers are certainly not linear* compared to the polystyrene standards and thus the DPs are likely underestimated.

Table 7.4. Characterization of BOC polymers synthesized by ADMET.

	GPC			TGA		
	Mn (KDa)	Mw (KDa)	PDI	Ceramic yield (%) (Experimental)	Ceramic yield (%) (Theoretical)	T _{d(5%)} (°C)
Polymer A	18	31	1.7	28.7	28.9	374
Polymer B	8.2	13	1.6	45.3	46.4	350

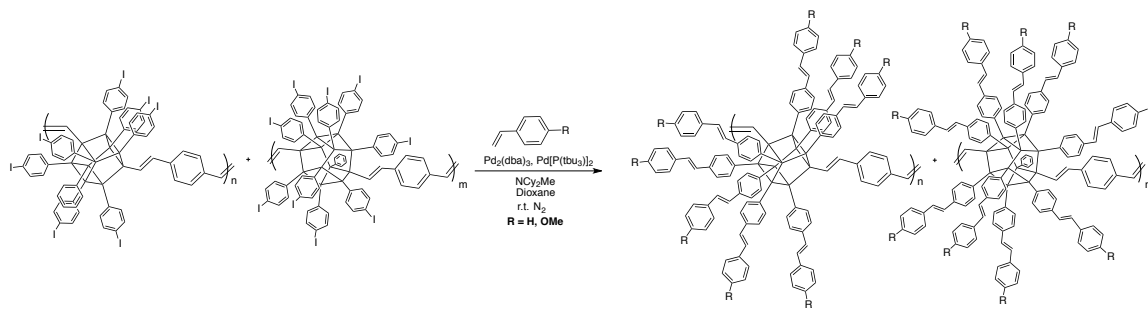
The theoretical ceramic yields were also calculated using the above repeat units and are 46.4 and 28.9% respectively. The actual values are within the error of the method of analysis and the uncertainty of the DP, and are 45.3 wt % for the phenyl and 28.7 wt % for the IPh monomer. In both cases, the theoretical values underestimate the amount of organic functionalization in the polymer systems. If we calculate the CY with two organic end-capped units instead, the calculated theoretical CY is 45.6 wt %, which most closely resembles the found value for polymer **B**. A similar calculation for polymer **A** CY gives 28.7 wt %, which is also closer to the found value with T_{d5%} (air) are 380° and 400 °C respectively.

The monomers for these reactions are formed by thermodynamic equilibration of SQ cages with two different functionalities in solution, so it should be noted that the position of the vinyl groups on each of the mixed cages must vary again pointing to the BoC oligomers being far from linear. In principle this may increase their solubility. It also may mean that some fraction of the oligomers are actually cyclics. All of the resulting

materials are soluble in THF, CH₂Cl₂, toluene, ethyl acetate and acetone. The IPh polymers tend to be more soluble.

7.5.3 Functionalization of Polymer A with R-styrene

Polymer **A** was further functionalized with either styrene, or *p*-methoxystyrene via Heck cross-coupling (Scheme 7.4) as a model for future dendronization studies and to probe/map the changes in photophysical properties as discussed below. All reactions were run at ambient under N₂ in dry 1,4-dioxane.



Scheme 7.4. Synthesis of R-styrene functionalized oligomers from polymer **A**.

Table 7.5 gives the GPC and CY wt % data for polymers **C** and **D**. The GPC (Figure 7.6) of the styrene functionalized oligomer (Polymer **C**) has a PDI similar to the unfunctionalized starting material of 1.8, but shows an M_n value that is ≈ half (Figure 7.6), while the PDI of polymer **D**, is much larger at 3.2. This is potentially a consequence of the significant differences in hydrodynamic volumes of polymers **A** and **C** and points to the issues we note above about observed MWs. The GPC traces of both polymers **C** and **D** are very similar in shape suggesting that they offer similar amounts of functionality. This would infer that double Heck coupling is not observed for linking chains together in either polymerization product, (see photophysical analysis).^{8,26,50,14}

The difference between actual and theoretical ceramic yields is similar to that found in the starting material, which suggests that complete or nearly complete conversion of “I” to styrene results. ¹H NMR analyses give complex peak patterns in the aromatic regions that make it difficult to establish the extent of reaction.

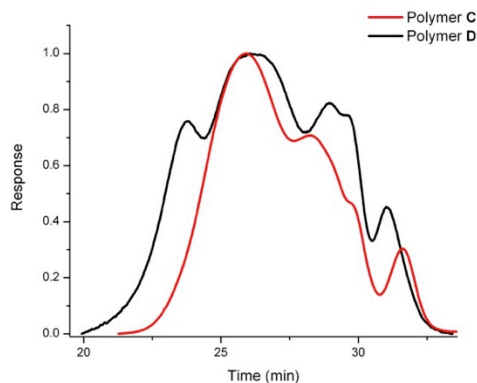


Figure 7.6. GPC analysis of polymers C and D, with characterization data given in **Table 7.5**.

Table 7.5. GPC and TGA characterization of Polymers C and D.

	GPC			TGA		
	Mn (kDa)	Mw (kDa)	PDI	Ceramic yield (%) (Experimental)	Ceramic yield (%) (Theoretical)	T _{d(5%)} (°C)
Polymer C	9.5	17	1.8	29.5	28.7	333
Polymer D	8	26	3.2	27.5	26.0	272

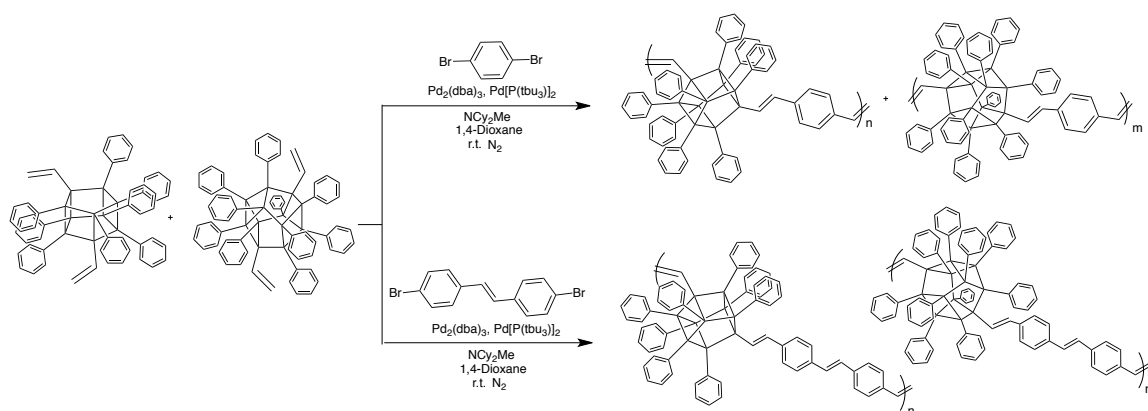
7.5.4 Synthesis of Polymers by Reverse Heck Cross-coupling

The approach used here, Heck cross-coupling with 1,4-dibromobenzene or 4,4'-dibromostilbene (Scheme 7.5), generates fully conjugated BoCs with 1,4-DVB and 4,4'-divinylstilbene linkers in contrast to the metathesis approach used above, polymers **E** and **F**. This method reduces the overall synthesis to two steps vs the three step approach of Ascuncion et al.³⁰

Table 7.6 gives the GPC and TGA data for these compounds. The GPCs exhibit PDIs expected for step-growth type polymerization (Figure 7.7) with average DPs of 5-7, calculated as discussed above for the DVB system. Since this polymerization uses reverse Heck coupling, the possibility of double functionalization at one vinyl group always exists, as found by Sellinger et al.^{8,50} However, from our TGA analysis of polymer **E**, it

appears as if there are no double-Heck reactions taking place, since the actual and theoretical CY are 45.8 and 46.4 wt % respectively. If we in fact consider end capping of the polymer chain with monovinyl functionalized material, the theoretical CY becomes 46.1%.

A further argument against double Heck reactions is that these reactions were run at room temperature, where double Heck reactions have not been observed.^{26,33} The found and theoretical CYs for polymer **F** are 43.7 and 41.8 wt % respectively, suggesting that on average they are fully functionalized without double Heck coupling. The shorter than anticipated chain lengths are likely a result of end capping the polymer chains with monofunctional units [(vinyl)₁(Ph)_{n-1}SiO_{1.5}]_n (n = 10, 12) as observed in the MALDI-ToF spectrum above.



Scheme 7.5. Synthesis of BoC polymers **E** and **F** through Heck cross-coupling with 1,4-dibromobenzene and 4,4'-dibromostilbene.

Table 7.6. GPC and TGA characterization of polymers **E** and **F**.

	GPC			TGA		
	Mn (kDa)	Mw (kDa)	PDI	Ceramic yield (%) (Experimental)	Ceramic yield (%) (Theoretical)	T _{d(5%)} (°C)
Polymer E	6.0	11	1.8	45.8	46.4	489
Polymer F	5.3	12	2.3	43.7	41.8	162

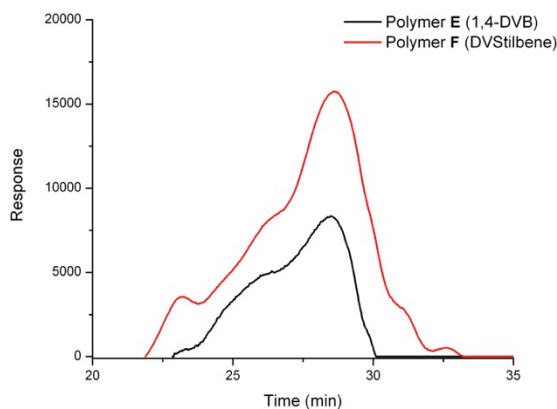
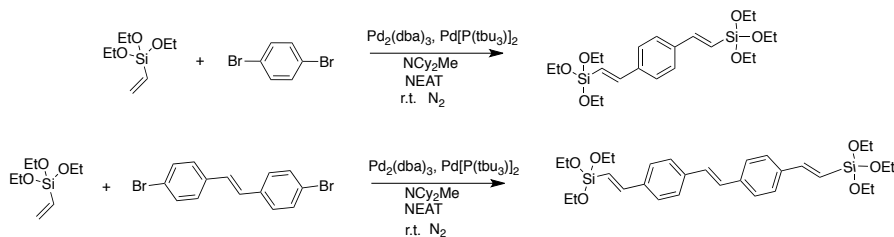


Figure 7.7. GPC of polymers E and F, with 1,4-dibromobenzene and 4,4'-dibromostilbene linkers.

7.5.5 Model Compound Syntheses

A set of model compounds were synthesized, Scheme 7.6, as standards enabling comparison of photophysical properties with those of oligomers **E** and **F**. Thus, bis-vinyltriethoxysilylbenzene (DVB model) was synthesized using literature methods.⁴⁷ 4,4'-bis-vinyltriethoxysilylstilbene (model **2**) was synthesized by self-metathesis of 4-bromostyrene followed by Heck coupling with vinyltriethoxysilane, see experimental section. Both model compounds were purified by vacuum distillation and characterized by NMR and GPC.



Scheme 7.6. Synthesis of bis-vinyltriethoxysilylbenzene and 4,4'-bis-vinyltriethoxysilylstilbene model compounds **1** and **2**.

7.5.6 Photophysical Studies

The steady state absorption and emission properties of the model compounds and oligomers are shown in Figure 7.8, Figure 7.9 and Table 7.7 and compared with data from the oligomers made by metathesis. The photophysical properties of Polymer **A** show an absorption $\lambda_{\text{max}} = 298 \text{ nm}$ and fluorescence λ_{max} at 347 nm, only slightly red

shifted from Model **1**. Polymer **B** shows the same maxima. The R-stilbene derivatives of the metathesis oligomers (polymers **C** and **D**), offer photophysical properties similar to single cages functionalized with stilbene or *p*-methoxystilbene as expected given the preponderance of 1,3 divinylbenzene used as the linker, surprisingly however, polymer **D** gives a quite high quantum yield of 39%, which is higher than that recorded for a methoxystilbene cage on its own of 4%.⁶⁹ These results are a negative proof in that without conjugation through the linker, extended conjugation between cages is impossible and one observes only the photophysical properties of the isolated SQs.

Figure 7.9a and b and Table 7.7 compare the absorption and emission properties of the reverse Heck based polymers (**E** and **F**) and model compounds. Figure 7.9a shows the absorption and emission of the 1,4-DVB linked oligomer (**E**) and model **1**. *Note the 60+ nm red shift in emission between the two.* This differs considerably from the metathesis generated oligomers, but is identical to our first paper in this area, where the BoC oligomers were made using a different synthetic method.³⁰

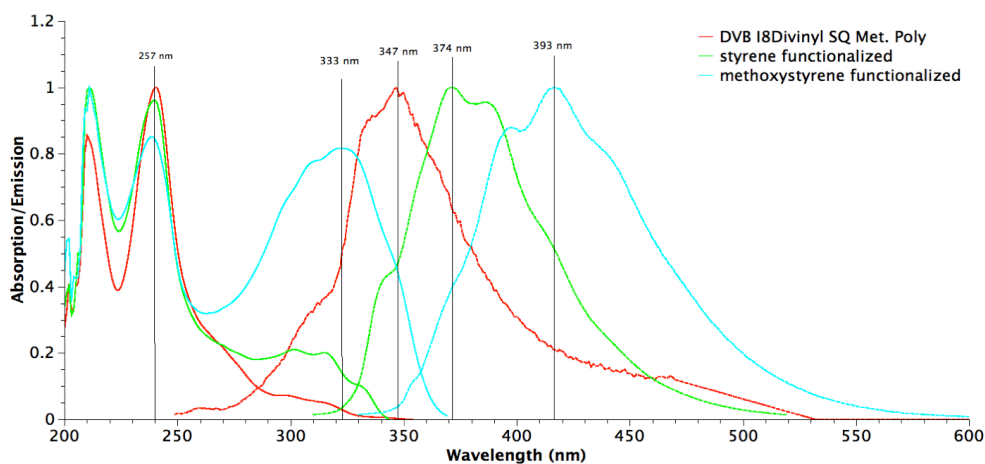


Figure 7.8. Steady-state absorption and emission comparison of ADMET linked BoC polymers.

Table 7.7. Steady-state absorption and emission properties of the BoC polymers (excitation at λ_{\max}).

Polymers	λ_{\max}	PL $_{\max}$	Φ_{PL}	$\epsilon \text{ M}^{-1} \text{ cm}^{-1}$	$\delta(\text{GM})$
A	298	347	0.09	86000	-
B	298	348	0.01	54662	-
C	315	374	0.07	104000	-
D	333	393	0.39	494375	-
E	297	410	0.02	15150	1.8
F	356	426	0.18	74700	12
Model 1	285, 297	344	0.04	-	-
Model 2	353	406	0.69	-	-

Model 1 and Polymer E both offer absorption $\lambda_{\max} \approx 298$ nm, while their emissive $\lambda_{\max} \approx 344$ and 410 nm respectively (Figure 7.9a). This observation is further evidence for excited state 3-D conjugation in systems containing conjugated organic bridges. We term this excited state conjugation because no shift is seen in the absorption spectra for these compounds given that we do not observe ground state conjugation as observed in traditional π -conjugated polymers. It is also important to note that this shift in absorption is observed for the same polymer synthesized by an alternate approach,³⁰ as well as an unpublished method which incorporates Model 1 into the polymer backbone through TBAF catalyzed polymerization,⁷⁰ which further reinforces the fact that these observations are not a consequence of impurities or side-products in any particular synthetic approach.

One reasonable explanation is that excited state conformational changes allow better orbital overlap in the excited state, and thus lower the system LUMO and its apparent band-gap. This in turn leads to emission red shifts. The fluorescence quantum yield for this compound was 2%, whereas that of the model compound was 4%.

Figure 7.9b shows the absorption and emission of the 4,4'-stilbene linked polymer F and Model 2. Again, the absorptions of the model compound and oligomer are quite similar, with

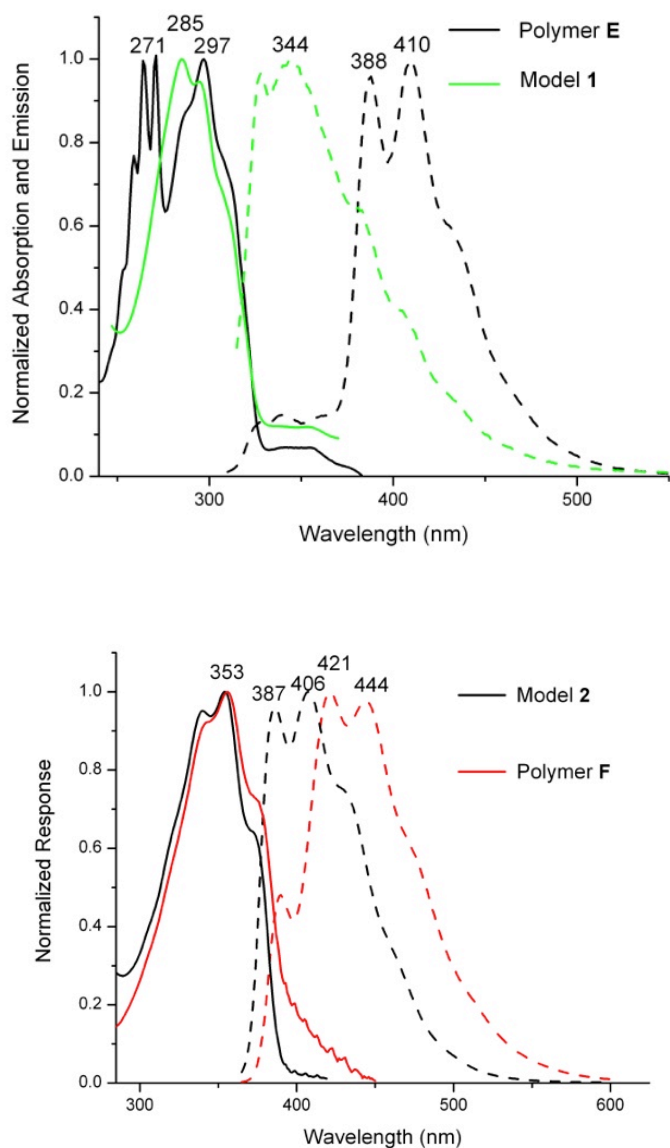


Figure 7.9. Absorption and emission comparison of **a.** polymer **F** and model **1**, and **b.** polymer **E** and model **2**.

only a slight change in band structure. The red shift between them is ~ 20 nm, which is smaller than found for the shorter linker. This may be due to increased torsional flexibility with the vinyl groups in the longer linker that decreases orbital overlap and thus the excited state conjugation length.⁷¹ The QY for polymer **F** is 18%, while the linker, e.g. Model **2**, has a QY of 69%.

In support of this conjecture, *we have now made the 9,9-dimethylfluorene linked system and find much better overlap, greater red shifts and higher emission quantum efficiencies as discussed further below* and data presented in Table 7.8.⁷⁰

7.5.7 Two-photon Spectroscopy

Our objective is to develop optimal synthetic tools and map the photophysical properties of the resulting conjugated BoCs. Thus, the systems studied here represent the first steps in developing better BoC systems, as noted just above with the 9,9-dimethylfluorene compounds. Thus, we did not anticipate nor did we find TPA properties that were particular noteworthy in contrast to several simple aminostilbeneSQ systems reported elsewhere.^{13-15,22}

The two-photon absorption (TPA) cross-sections were determined for polymers **E** and **F** at 650 nm. TPA cross-sections are a measure of the compounds polarizability or separation of charge within a molecular species. Therefore compounds with clear donor-acceptor separation have a higher (>300 GM) TPA cross-sections.^{62,72,73} These materials were expected to have low cross-sections (<10 GM) because there are no donor-acceptor interactions.

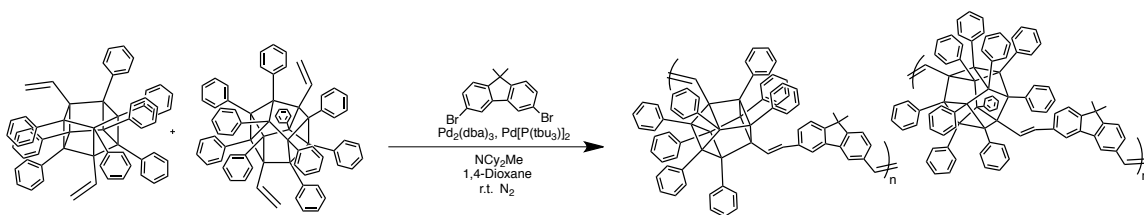
The cross-sections were determined by comparison with 1,4-bis(2-methylstyryl)benzene as a standard using the TPEF method discussed above. The TPA cross-sections were calculated to be 1.8 GM for polymer **E** and 12 GM for polymer **F** at 650 nm excitation. These values indicate (as expected) low polarizability and were not explored further. Of notable mention however, is that the TPEF emission spectra show red shifts in emission from those of single photon. The λ_{max} of TPEF emission for polymers **E** and **F** are 439±2 and 451±2 nm respectively. This would suggest the presence of an excited state that is “dark” or not allowed in single photon excitation. A further explanation of this effect will be presented in future papers.

7.5.8 Comparison of Steady State Spectroscopy for BoC Polymers

To better explain the emission spectral shifts observed for BoC polymers, we compare the absorption and emission maxima for the polymers in this paper, an accompanying paper and recent, unpublished materials. Table 7.8 shows the absorption,

emission and quantum yields for each model system and the corresponding oligomers. Note that the DVB polymers consisting of mixed 1,3- and 1,4- divinylbenzene linkers show absorption and emission maxima similar to their combined monomer species and organic linker, while 1,4-divinylbenzene and 1,4-diethynylbenzene linkers show > 30 and < 60 nm red-shifts in their emission spectra. However, the absorption spectra remain consistent regardless of linker. This is also true for a $[\text{vinyl}_x(\text{stilbenevinyl})_{n-x}]_{\text{SQ}}$ ($n = 8, 10$) linked BOC system, which shows an absorption similar to its parent stilbenevinylSQ compounds at 336 nm, but a shift in emission maximum from 387 ± 2 nm, to 440 ± 2 nm.⁷⁰

More recently, we have explored the use of 2,7-dibromo-9,9-dimethylfluorene as the linker for $[(\text{vinyl})_2(\text{Ph})_{n-2}\text{SiO}_{1.5}]_n$ ($n = 10, 12$) based BOC polymers (Scheme 7.7), and using bis-triethoxysilyl-9,9-dimethylfluorene as the model compound. This polymer exhibits the first example with a meaningful red shift in the absorption spectrum (Figure 7.10).⁷⁰ The absorption λ_{max} shifts to 410 ± 2 nm compared to the model system and the fluorene-OVS coupled system (if the phenyl band is ignored). The emission spectrum of the dimethylfluorene linked polymer also red shifts by nearly 70 nm from the model compound. These linker trends are presented in Table 7.8. Thus, the above argument about flexibility seems to be valid of our first example with a rigid linker holds for other systems.



Scheme 7.7. Synthesis of phenyl-fluoreneSQ BoC polymer.

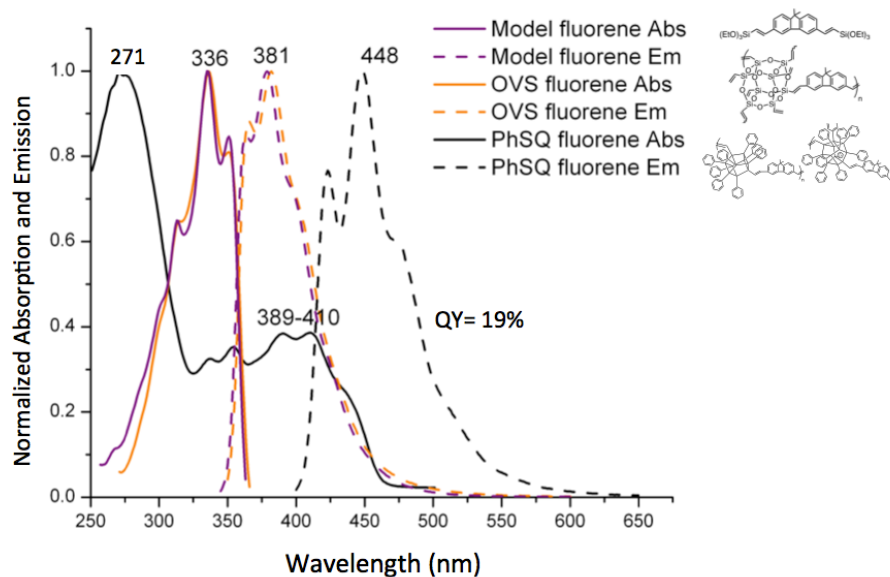


Figure 7.10. Absorption and emission of dimethylfluorene polymer derivatives.

Still another aspect of the photophysical properties comes from the effects of introducing model dendrons, which will be discussed in a subsequent publication. As mentioned in the accompanying paper, the lowest occupied molecular orbital (LUMO) of the polymer systems, suggests communication through the conjugated tethers.

Table 7.8. Spectral data for T₈ iodophenyl based monomers with divinylbenzene or diethynylbenzene linkers, A-F and 2,7-dibromo-9,9-dimethylfluorene linked polymers in THF.

	R	UV λ_{\max} (nm) (± 2 nm)	PL λ_{\max} (nm) (± 2 nm)	Φ_{PL} (%)
Monomers	Monomer A (H) ^a	315	359, 391	11
	Monomer B (OMe) ^a	327	409	12
	Monomer C (NH ₂) ^a	353	446	6
DEB polymers	Polymer IX (H) ^a	315	400, 423	12
	Polymer X (OMe) ^a	327	447	5
	Polymer XI (NH ₂) ^a	350	484	1
	Polymer XII (OMe, NH ₂) ^a	327	464	1
DVB polymers	Polymer V (H) ^a	315	375, 397	23
	Polymer VI (OMe) ^a	321	422	19
	Polymer VII (NH ₂) ^a	350	443	2
	Polymer VIII (OMe, NH ₂) ^a	324	425	4
	A	298	347	9
	B	298	348	1
	C	315	374	7
1,4-DVB polymers	D	333	393	-
	E	297	410	2
	F	356	426	18
	Model 1	285	344	-
	Model 2	353	406	-
Flourene Systems	T _{8/10} stilbenevinyl polymer	336	409, 440	3
	Fluorene model	336	381	-
	Fluorene-OVS-polymer	336	381	-
	Phenyl-fluorene polymer	371, 389, 410	422, 448	19

^a See reference for further polymer information.⁴¹

7.6 Conclusions

As part of our objectives in developing optimal synthetic tools for the synthesis of 3-D conjugated BoCs, we have determined that the reverse Heck coupling of dibromo linkers to [vinylSiO_{1.5}]_x[PhSiO_{1.5}]_{10-x/12-x} mixtures provides a very facile route to 3-D conjugated BoCs that are easily purified and offer a basic starting point for the synthesis of more complex BoC systems with easily tuned properties.

We note that in particular, the use of F⁻ catalyzed rearrangement of two types of SQs provides a simple route to mixed functional cages that provide potential access to an exceptional number of new SQs that can be used to probe a wide variety of photonic and electronic properties.

These systems mark an important new ability to synthesize 3-D materials through multifunctional SQs with differing functionality on demand. We have clearly shown the

difference in fluorescence spectral effects that come from systems with 1,3-,1-4- mixed divinylbenzene and 1,4-dibromobenzene, with 1,4-dibromobenzene showing 40-50 nm red shifts compared with divinylbenzene, giving evidence to excited state energy transfer dynamics we refer to as 3-D excited state conjugation. These effects are less prominent in systems with longer organic conjugated linkers, likely due to weaker orbital overlap from inherent flexibility, and limiting the proximity of phenyl-phenyl interactions. The stilbenefunctionalized DVB linked polymers show absorption and emission characteristics inherent to non-polymeric systems. Due to our understanding and ability to make multiply functionalized SQ cages, more complex systems are imagined, which could offer ideal properties for electronic applications such as photovoltaic devices.

Indeed, our initial studies in the current set of papers mapping the relationships between cage structure, symmetry and linker structure on photophysical properties provide the basis for making important advances in absorption, emission and quantum efficiencies in these systems with *the initial results from the 9,9-dimethylfluorene system providing next generation properties.*⁷¹

References:

1. Voronkov, M.G.; Lavrent'yev, V.I.; "Polyhedral Oligosilsesquioxanes and Their Homo Derivatives," *Top. Curr. Chem.* **1982**, *102*, 199-236
2. Baney, R.H.; Itoh, M.; Sakakibara, A.; Suzuki, T.; "Silsesquioxanes," *Chem. Rev.*, **1995**, *95*, 1409-30.
3. Loy, D.A.; Shea, K.J.; "Bridged Polysilsesquioxanes. Highly Porous Hybrid Organic-Inorganic Materials," *Chem. Rev.*, **1995**, *95*, 1431-42.
4. Calzaferri, G.; "Silsesquioxanes," in Tailor-made Silicon-Oxygen Compounds, from molecules to materials, R. Corriu and P. Jutzi eds. Publ. Friedr. Vieweg&SohnmbH, Braunschweig/Weisbaden, Germany **1996**, 149-169.
5. Lichtenhan, J.; "Silsesquioxane-based Polymers," in Polymeric Materials Encyc., J.C. Salmone Ed. Vol. 10, CRC Press, N.Y., **1996**, 7768-77.
6. Provatas, A.; Matisons, J.G.; "Synthesis and Applications of Silsesquioxanes," *Trends Polym. Sci.* **1997**, *5*, 327-33.
7. G. Li, L. Wang, H. Ni, C. U. Pittman, "Polyhedral Oligomeric Silsesquioxane (POSS) Polymers and Copolymers: A Review," *J. Inorg. and Organomet. Polymers*, **2001**, *11*, 123-151.
8. Duchateau, R.; "Incompletely Condensed Silsesquioxanes: Versatile Tools in Developing Silica-Supported Olefin Polymerization Catalysts," *Chem. Rev.* **2002**, *102*, 3525-3542.
9. Abe, Y.;Gunji,T.; "Oligo- and polysiloxanes"*Prog. Poly. Sci.* **2004**, *29*, 149-182.

10. Phillips, S.H.; Haddad, T.S.; Tomczak, S.J. "Developments in Nanoscience: Polyhedral oligomeric silsesquioxane (POSS)-polymers," *Current Opinion in Solid State and Mater. Sci.* **2004**, *8*, 21-29.
11. Kannan, R. Y.; Salacinski, H. J.; Butler, P. E.; Seifalian, A. M.; "Polyhedral Oligomeric Silsesquioxane Nanocomposites: The Next Generation Material for Biomedical Applications," *Acc. Chem. Res.* **2005**, *38*, 879-884.
12. Laine, R.M. "Nano-building Blocks Based on the [OSiO_{1.5}]₈ Silsesquioxanes," *J. Mater. Chem.*, **2005**, *15*, 3725 – 44.
13. Lickiss, P.D.; Rataboul, F., "Fully Condensed Polyhedral Silsesquioxanes: From Synthesis to Application," *Adv. Organomet. Chem.*, **2008**, *57*, 1-116.
14. Chan, K. L.; Sonar, P.; Sellinger, A. "Cubic Silsesquioxanes for use in Solution Processable Organic Light Emitting Diodes (OLED)," *J. Mater. Chem.* **2009**, *19* 1-19.
15. Wu, J.; Mather, P. T.; "POSS Polymers: Physical Properties and Biomaterials Applications," *Polymer Reviews*, **2009**, 25–63.
16. Cordes, D. B.; Lickiss, P. D.; Franck, R.; "Recent Developments in the Chemistry of Cubic Polyhedral Oligosilsesquioxanes," *Chem. Rev.* **2010**, *10*, 2081–2173 (2010).
17. Laine, R. M.; Roll, M. F.; "Polyhedral Phenylsilsesquioxanes," *Macromolecules*, **2011**, *44*, 1073-1220.
18. 19. Kannan, R. Y.; Salacinski, H. J.; Butler, P. E.; Seifalian, A. M. "Polyhedral Oligomeric Silsesquioxane Nanocomposites: The Next Generation Material for Biomedical Applications." *Acc. Chem. Res.* **2005**, *38*, 879-884.
19. 20. Kim, Y.; Koh, K.; Roll, M. F.; Laine, R. M.; Matzger, A. J. "Porous Networks Assembled from Octaphenylsilsesquioxane Building Blocks." *Macromolecules* **2010**, *43*, 6995-7000.
20. Feher, F. J.; Blanski, R. "Olefin Polymerization by Vanadium-Containing Silsesquioxanes: Synthesis of a Dialkyl-oxo-vanadium (V) Complex that Initiates Ethylene Polymerization." *J. Am. Chem. Soc.* **1992**, *114*, 5886-5887.
21. Duchateau, R.; Abbenhuis, H. C. L.; van Santen, R. A.; Meetsma, A.; Thiele, S. K.- H.; van Tol, M. F. H. "Half-Sandwich Titanium Complexes Stabilized by a Novel Silsesquioxane Ligand: Soluble Model Systems for Silica-Grafted Olefin Polymerization Catalysts." *Organometallics* **1998**, *17*, 5222.
22. Feher, F. J.; Newman, D. A.; Walzer, J. F. "Silsesquioxanes as Models for Silica Surfaces." *J. Am. Chem. Soc.* **1989**, *111*, 1741-1748.
23. Leu, C. M.; Reddy, M.; Wei, K.-H.; Shu, C.-F. "Synthesis and Dielectric Properties of Polyimide-Chain-End Tethered Polyhedral Oligomeric Silsesquioxane Nanocomposites." *Chem. Mater.* **2003**, *15*, 2261-2265.
24. Chojnowski, J.; Fortuniak, W.; Rościszewski, P.; W erel, W.; Lukasiak, J.; Kamysz, W.; Halasa, R. "Polysilsesquioxanes and Oligosilsesquioxanes Substituted by Alkylammonium Salts as Antibacterial Biocides." *J. Inorg. Organomet. Polym. Mater.* **2006**, *16*, 219-230.
25. Chan, K. L.; Sonar, P.; Sellinger, A. "Cubic Silsesquioxanes for use in Solution Processable Organic Light Emitting Diodes (OLED)." *J. Mat. Chem.* **2009**, *19*, 9103-9120.

26. Sellinger, A.; Tamaki, R.; Laine, R. M.; Ueno, K.; Tanabe, H.; Williams, E.; Jabbour, G. E. "Heck Coupling of Haloaromatics with Octavinylsilsesquioxane: Solution Processable Nanocomposites for application in electroluminescent devices." *Chem. Comm.* **2005**, 3700-3702.
27. Pan, S.; Kota, A. K.; Mabry, J. M.; Tuteja, A. "Superomniphobic Surfaces for Effective Chemical Shielding." *J. Am. Chem. Soc.* **2012**, *135*, 578–581.
28. Gromilov, S. A.; Basova, T. V.; Emel'yanov, D. Y.; Kuzmin, A. V.; Prokhorova, S. A. Layer "Arrangement in the Structure of Octakis-(trimethylsiloxy)octasilsesquioxane and Dodecakis-(trimethylsiloxy)octasilsesquioxane." *J. Struct. Chem. (Engl. Trans.)* **2004**, *45*, 471-475.
29. Laine, R. M. "Nano-building Blocks Based on the [OSiO_{1.5}]₈ Silsesquioxanes." *J. Mater. Chem.* **2005**, *15*, 3725-3744.
30. Asuncion, M. Z.; Laine, R. M. "Fluoride Rearrangement Reactions of Polyphenyl- and Polyvinylsilsesquioxanes as a Facile Route to Mixed Functional Phenyl, Vinyl T₁₀ and T₁₂ Silsesquioxanes." *J. Am. Chem. Soc.*, **2010**, *132*, 3723-3736.
31. Froehlich, J. D.; Young, R.; Nakamura, T.; Ohmori, Y.; Li, S.; Mochizuki, A.; Lauters, M.; Jabbour, G. E. "Synthesis of Multi-Functional POSS Emitters for OLED Applications." *Chem. Mater.* **2007**, *19*, 4991–4997.
32. Sulaiman, S.; Brick, C.; Roll, M.; Bhaskar, A.; Goodson, T.; Zhang, J.; Laine, R. M. "Molecules with Perfect Cubic Symmetry as Nanobuilding Blocks for 3-D Assemblies. Elaboration of Octavinylsilsesquioxane. Unusual Luminescence Shifts May Indicate Extended Conjugation Involving the Silsesquioxane Core." *Chem. Mater.* **2008**, *20* (5563-5573).
33. Sulaiman, S.; Zhang, J.; Goodson III, T.; Laine, R. M. "Synthesis, Characterizations and Photophysical Properties of Polyfunctional Phenylsilsesquioxanes: [*o*-RPhSiO_{1.5}]₈, [2,5-R₂PhSiO_{1.5}]₈, and [R₃PhSiO_{1.5}]₈. Compounds with the Highest Number of Functional Units/unit Volume." *J. Mat. Chem.*, **2011**, *21*, 11177.
34. Laine, R. M.; Sulaiman, S.; Brick, C. T. R.; Asuncion, M. Z.; Neurock, M.; Filhol, J.-S.; Lee, C.-Y.; Zhang, J.; Goodson, T.; Ronchi, M.; Pizzotti, M.; Rand, S. C.; Li, Y. "Synthesis and Photophysical Properties of Stilbeneoctasilsesquioxanes. Emission Behavior Coupled with Theoretical Modeling Studies Suggest a 3-D excited State Involving the Silica Core." *J. Am. Chem. Soc.* **2010**, *132*, 3708-3722.
35. Bassindale, A. R.; Parker, D. J.; Pourny, M.; Taylor, P. G.; Horton, P. N.; Hursthouse, M. B. "Fluoride Ion Entrapment in Octasilsesquioxane Cages as Models for Ion Entrapment in Zeolites. Further Examples, X-Ray Crystal Structure Studies, and Investigations into How and Why They May Be Formed." *Organometallics* **2004**, *23*, 4400-4405.
36. Bassindale, A. R.; Pourny, M.; Taylor, P. G.; Hursthouse, M. B.; Light, M. E. "Fluoride-Ion Encapsulation within a Silsesquioxane Cage." *Angew. Chem. Int. Ed.* **2003**, *42*, 3844-3490.
37. Aziz, Y. El; Bassindale, A. R.; Taylor, P. G.; Horton, P. N.; Stephenson, R. A.; Hursthouse, M. B. "Facile Synthesis of Novel Functionalized Silsesquioxane

- Nanostructures Containing an Encapsulated Fluoride Anion,” *Organometallics* **2012**, *31*, 6032–6040.
38. Anderson, S. E.; Bodzin, D. J.; Haddad, T. S.; Boatz, J. A.; Mabry, J. M.; Mitchell, C.; Bowers, M. T. Structural Investigation of Encapsulated Fluoride in Polyhedral Oligomeric Silsesquioxane Cages Using Ion Mobility Mass Spectrometry and Molecular Mechanics. *Chem. Mater.* **2008**, *20* 4299-4309.
 39. Ronchi, M.; Sulaiman, S.; Boston, N. R.; Laine, R. M. Fluoride catalyzed rearrangements of polysilsesquioxanes, mixed Me,Vinyl T₈, Me,Vinyl T₁₀ and T₁₂ cages. *App. Organomet. Chem.* **2010**, *24*, 551-557.
 40. Jung, J.H.; Furgal, J.C.; Goodson, III, T.; Mizumo, T.; Schwartz, M.; Chou, K.; Vonet, J.F.; Laine, R.M.; “3-D Molecular Mixtures of Catalytically Functionalized [vinylSiO_{1.5}]₁₀/[vinylSiO_{1.5}]₁₂. Photophysical Characterization of Second Generation Derivatives,” *Chem. Mater.*, **2012**, *24* (10), 1883–1895.
 41. Jung, J. H.; Furgal, J.C.; Clark, S. C.; Schwartz, M. C.; Chou, K. Laine, R. M. Copolymerization of [p-IPhSiO_{1.5}]₈, I₈OPS] with Divinyl (DVB)- and Diethynylbenzene (DEB) gives Beads on a Chain (BoC) Polymers with Functionalized Beads. The DEB Systems Exhibit through Chain, Extended 3-D Conjugation in the Excited State. *Submitted*.
 42. Furgal, J.C.; Jung, J.H.; Goodson, T.; Laine, R.M. “Analyzing Structure-Photophysical Property Relationships of Isolated T₈, T₁₀, and T₁₂ Stilbenevinyl Silsesquioxanes.” *Submitted*
 43. Zheng, L.; Farris, R. J.; Coughlin, E. B. “Synthesis of Polyethylene Hybrid Copolymers Containing Polyhedral Oligomeric Silsesquioxane Prepared with Ring-Opening Metathesis Copolymerization” *J. Poly. Sci. Part A: Poly. Chem.* **2001**, *39*, 2920–2928.
 44. Xu, W.; Chung, C.; Kwon, Y. “Synthesis of Novel Block Copolymers Containing Polyhedral Oligomeric Silsesquioxane (POSS) Pendent Groups via Ring-opening Metathesis Polymerization (ROMP).” *Polymer* **2007**, *48*, 6286–6293.
 45. Pyun, J.; Matyjaszewski, K. “Synthesis of Nanocomposite Organic/Inorganic Hybrid Materials Using Controlled/“Living” Radical Polymerization” *Chem. Mater.* **2001**, *13*, 3436–3448.
 46. Chen, R.; Feng, W.; Zhu, S.; Botton, G.; Ong, B.; Wu, Y. “Surface-initiated Atom Transfer Radical Polymerization of Polyhedral Oligomeric Silsesquioxane (POSS) Methacrylate from Flat Silicon Wafer” *Polymer* **2006**, *47*, 1119–1123.
 47. Thompson, D. B.; Brook, M. A. “Rapid Assembly of Complex 3D Siloxane Architectures,” *J. Am. Chem. Soc.* **2008**, *130*, 32-33.
 48. Sulaiman, S.; Brick, C. M.; De Sana, C. M.; Katzenstein, J. M.; Laine, R. M.; Basheer, R. A.;” Tailoring the Global Properties of Nanocomposites. Epoxy Resins with Very Low Coefficients of Thermal Expansion,” *Macromolecules* **2006**, *39*, 5167-5169.
 49. Roh, H. W.; Popova, V.; Chen, L.; Forster, A. M.; Ding, Y.; Alvine, K. J.; Krug, D. J.; Laine, R. M.; Soles, C. L. “Cubic Silsesquioxanes as a Green, High-Performance Mold Material for Nanoimprint Lithography” *Adv. Mater.* **2011**, *23*, 414–420.
 50. Nuyken, O.; Böhner, R.; Erdmann, C. Oxetane photopolymerization– A System with Low Volume Shrinkage. *Macromol. Symp.* **1996**, *107*, 125–128.
 51. Schwartz, M. C.; Clark, S. C.; Doan, P.; Furgal, J. C.; Laine, R. M. “Unpublished results”
 52. Li, Z.; Kawakami, Y.; “Formation of Incompletely Condensed

- Oligosilsesquioxanes by Hydrolysis of Completely Condensed POSS via Reshuffling,” *Chem. Lett.*, **2008**, *37*, 804-05.
53. Lichtenhan, J. D.; Vu, N. Q.; Carter, J. A.; Gilman, J. W.; Feher, F. J.; “Silsesquioxane-Siloxane Copolymers from Polyhedral Silsesquioxanes,” *Macromolecules*, **1993**, *26*, 2141-2142.
 54. Morimoto, Y.; Watanabe, K.; Ootake, N.; Inagaki, J. Yoshida, K.; Ohguma, K. Silsesquioxane Derivatives and Process or Production Therefore. U.S. Patent Application 20040249103A1, Sept 2002.
 55. Seino, M.; Hayakawa, T.; Ishida, Y.; Kakimoto, M.; Watanabe, K.; Oikawa, H. Hydrosilylation Polymerization of Double-Decker- Shaped Silsesquioxane Having Hydrosilane with Dienes. *Macromolecules*, **2006**, *39*, 3473–3475.
 56. Yoshida, K.; Hattori, T.; Ootake, N.; Tanaka, R.; Matsumoto, H. Silsesquioxane-Based Polymers: Synthesis of Phenylsilsesquioxanes with Double-Decker Structure and Their Polymers. In *Silicon Based Polymers*; Ganachaud, F., Boileau, S., Boury, B., Eds.; Springer: Dordrecht, 2008; pp. 205-211.
 57. Wu, S.; Hayakawa, T.; Kikuchi, R.; Grunzinger, S. J.; Kakimoto, M.; Oikawa, H. Synthesis and Characterization of Semiaromatic Poly- imides Containing POSS in Main Chain Derived from Double-Decker- Shaped Silsesquioxane. *Macromolecules*, **2007**, *40*, 5698–5705.
 58. Hoque, M. A.; Kakihana, Y.; Shinke, S.; Kawakami, Y. Polysiloxanes with Periodically Distributed Isomeric Double-Decker Silsesquioxane in the Main Chain. *Macromolecules* **2009**, *42*, 3309–3315.
 59. Jung, J. H.; Laine, R. M.; “Beads on a Chain (BOC) Polymers Formed from the Reaction of $\text{NH}_2\text{PhSiO}_{1.5}[\text{PhSiO}_{1.5}]_{(10-x)}$ and $[\text{NH}_2\text{PhSiO}_{1.5}(\text{x})][\text{PhSiO}_{1.5}]_{(12-x)}$ Mixtures (x=2-4) with the Diglycidyl Ether of Bisphenol A,” *Macromolecules*, **2011**, *44*, 7263-7272.
 60. Peterson, J. J.; Werre, M.; Simon, Y. C.; Coughlin, E. B.; Carter, K. R. “Carborane Containing Polyfluorene: o- Carborane in the Main Chain.” *Macromolecules* **2009**, *42*, 8594-8598.
 61. Peterson, J. J.; Simon, Y. C.; Coughlin, E. B.; Carter, K. R. “Polyfluorene with p-carborane in the backbone.” *Chem. Comm.* **2009**, 4950–4952.
 62. Maciejewski, A.; Steer, R. P. “Spectral and Photophysical Properties of 9,10-Diphenylanthracene in Perfluoro-n-hexane: The Influence of Solute—solvent Interactions,” *J. Photochem.* **1986**, *35*, 59.
 63. Xu, C.; Webb, W. W. “Measurement of Two-photon Excitation Cross Sections of Molecular Fluorophores with Data from 690 to 1050 nm.” *J. Opt. Soc. Am. B.* **1996**, *13*, 481.
 64. Bhaskar, A.; Ramakrishna, G.; Lu, Z.; Twieg, R.; Hales, J. M.; Hagan, D. J.; Van Stryland, E.; Goodson, T. “Investigation of Two-Photon Absorption Properties in Branched Alkene and Alkyne Chromophores.” *J. Am. Chem. Soc.* **2006**, *128*, 11840-11849.
 65. Roll, M. F.; Asuncion, M. Z.; Kampf, J.; Laine, R. M.; “para-Octaiodophenylsilsesquioxane, $[p\text{-IC}_6\text{H}_4\text{SiO}_{1.5}]_8$, a Nearly Perfect Nano-building Block.” *ACS Nano*, **2008**, *2*, 320-326.
 66. Cornelius, M.; Hoffmann, F.; Fröba, M. Periodic Mesoporous Organosilicas with a Bifunctional Conjugated Organic Unit and Crystal-like Pore Walls. *Chem.*

- Mater.* **2005**, 6674–6678.
67. Lipstman, S.; Muniappan, S.; Goldberg, I. “Supramolecular Reactivity of Porphyrins with Mixed Iodophenyl and Pyridyl meso-Substituents.” *Cryst. Growth Des.* **2008**, 8, 1682–1688.
 68. Odian, G. *Principles of Polymerization*; 4th ed.; Wiley: Hoboken, 2004.
 69. Bahrami, M.; Furgal, J. C.; Goodson III, T.; Laine, R. M. *Unpublished Results*.
 70. Furgal, J.C.; Goodson, T.; Laine, R.M. *Unpublished Results*.
 71. Ali, B.; Jabar, S.; Salih, W.; Al Tamimi, R. K.; Al Attar, H.; Monkman, A. P. “Synthesis and Spectroscopic Characterization Studies of Low Molecular Weight Light Emitting PPV Segmented Copolymers.” *Opt. Mater.* **2009**, 32, 350–357;
 - Tang, S.; Zhang, J. “First Principles Investigation on the Key Factors of Broad Absorption Spectra and Electronic Properties for Oligothiophene and its Derivatives for Solar Cells.” *Int. J. Quantum Chem.* **2011**, 111, 2089–2098;
 - Rothberg, L. J.; Yan, M. *Photophysics of Phenylenevinylene Polymers. Synth. Met.* **1996**, 80, 41–58;
 - Gierschner, J.; Mack, H.-G.; Luer, L.; Oelkrug, D. *Fluorescence and Absorption Spectra of Oligophenylenevinylenes: Vibronic Coupling, Band Shapes, and Solvatochromism. J. Chem. Phys.* **2002**, 116, 8596.
 72. Kogej, T.; Beljonne, D.; Meyers, F. Mechanisms for Enhancement of Two-photon Absorption in Donor–acceptor Conjugated Chromophores. *Chem. Phys. Lett.* **1998**, 298, 1–6.
 73. Xu, F.; Wang, Z.; Gong, Q. Synthesis, Characterization, and Optical Properties of Two-photon-absorbing Octupolar Molecule with an s-Triazine Core. *Opt. Mater.* **2007**, 29, 723–727.

Chapter 8

Summary and Future Work

8.1 Summary and Insights

In this dissertation, we have demonstrated new routes to functionalized silsesquioxanes starting from rice hull ash, the synthesis of decaphenylsilsesquioxanes in high yields, the mechanism of fluoride-catalyzed rearrangement, the functionalization and photophysical properties of T₁₀ and T₁₂ stilbene and stilbenevinylSQs, and finally the development of beads on a chain (BoC) polymers with unique photophysical properties.

In Chapter 1 we proposed four questions to answer throughout the work of this dissertation. The findings of these questions are summarized here. The first question asked was could we find the optimized reaction conditions and the mechanism of converting PhT₈ to PhT₁₀ by fluoride catalysis (Chapter 4)? We find that the mechanism of TBAF catalyzed rearrangement is very complex, but we have gained strong insight into its pathways through experiment and computation. The reaction outcome depends on solvent, catalyst, water, concentration of starting materials, time, and temperature; of which we have found optimal conditions to favor the T₁₀ cage being 60 mM PhT₈ in dichloromethane with 5 mol% TBAF at room temperature for 24 h. Modeling studies of this reaction show that a hybrid fluoride catalyst with water pathway is the most thermodynamically favorable by up to 24 kcal/mol, and that solvent choice plays a role in the final product equilibrium.

The second question proposed was whether PhT₁₀ SQs can be made in high isolated yields from waste/byproduct materials such as rice hull ash (RHA) derived Ph-spirosiloxanes and polyphenylsilsequioxanes through TBAF (F⁻) catalyzed rearrangement (Chapters 3 and 4)? We demonstrated a simple method to make mono-Ph-spirosiloxanes [PhSi(OR)₃] from RHA derived spiro-siloxane by nucleophilic substitution at low temperature, a new “greener” method to R-alkoxysilanes. We also find that using the above optimized reaction conditions for F⁻ rearrangement that we can convert any

[PhSiO_{1.5}]_n or [PhSi(OR)₃] to PhT₁₀ SQs in >50% isolated yield, the highest ever reported and that PhT₁₀ offers much higher solubility over PhT₈ and PhT₁₂ making it a highly desirable alternative for further functionalization and processing.

The third question proposed was whether we could determine the intramolecular interactions present in chromophore functionalized SQs by two photon absorption and fluorescence upconversion (Chapters 5 and 6)? The first step was to synthesize and develop separation methods for T₁₀ and T₁₂ R-stilbenevinylSQs so that mapping studies could be done. We find that higher chromophore densities per cage show a decrease in fluorescence quantum yields (36, 19, 11% for T₈, T₁₀ and T₁₂ respectively), likely due enhanced self-absorption through chromophore interactions leading to non-radiative decay processes. We also find that of the three cage sizes and symmetries studied, the T₁₀ stilbenevinylSQs offer the highest TPA cross-sections of 5.5 GM per chromophore, indicative of strong intramolecular electronic coupling (i.e. charge separation) and polarization. Lastly, we find that SQ cage compounds show “rise times” of 700 – 1000 fs and low anisotropies (~0.1) in fluorescence upconversion lifetime kinetic studies, indicative of an excited state energy transfer process, (Internal delocalization or FRET type energy transfer), which is unobserved for the free chromophore, unexpected for a system with an “inert” silica core, and unexpected for 3-D hybrid molecular species.

The final question was whether we could make chromophore-functionalized silsesquioxanes that are suitable replacements for electron accepting materials (i.e.PCBM) in organic photovoltaics (Chapters 5 and 7)? The rationale for using SQs in photovoltaic applications as electron accepting materials stems from the knowledge that SQs in their unfunctionalized state (H-SQ) contain an electrophilic core (equivalent to CF₃) and a centralized core LUMO; suggesting that SQs should be capable of accepting electrons, as discussed in Section 1.6. The challenge with bare SQs is that their band gaps and HOMO-LUMO energy levels are much too high (~ 6 eV) for use in photovoltaic devices, unless they were designed to work in the deep UV. Therefore, we used a series of T_{10/12} R-stilbenevinylSQs, where R = H, Me, OMe, NH₂ and 5F to map the photophysical and electronic properties of SQs for potential use in hybrid/organic photovoltaic devices. Stilbenevinyl was chosen due to its simplicity both in synthesis and

photophysics as well as it being an analog of a common photovoltaic material poly(phenylenevinylene) (PPV). We used the R-group to control their absorption and fluorescence wavelengths, and TPA cross-sections. The most interesting compound was the C₆F₅, which showed a reasonable TPA cross section of 17 GM per chromophore, and unexpected red shifts in fluorescence of 50 nm from R = H. Though we were not successful in showing that SQs could be used as a replacement for PCBM, our results show that they should be capable of accepting electrons, and that the band gap and HOMO-LUMO energy level of SQs can be tuned through their organic groups, with C₆F₅ showing the most promising results toward PCBM replacement.

8.2 Future Work

In Chapter 3 we showed that we could synthesize R-spirosiloxanes from the agricultural waste product rice hull ash. This was achieved through the nucleophilic substitution of R-Li at spiro-siloxane, which occurs at low temperature (-78 °C) through a pentacoordinated intermediate that must be quenched by an electrophile to maintain a mono-substituted product. The trouble with this reaction is that it often results in an equilibrium mixture of product and starting material that are difficult to separate. Future work in this area must look at novel methods to separate these materials or adjust the reaction conditions to push the equilibrium toward the products. One method could be to use bi-phasic reaction conditions for in-situ separation, in which the product is soluble in one solvent, and the starting materials soluble in another.

In our study, we found that alkylLi reagents did not result in nucleophilic substitution at spiro-siloxane. The reasons for this are not clear, but could be due to the basicity of alkyl groups favoring removal of protons over reacting nucleophilically. Future work should look at whether changing the reaction solvent or conditions such as concentration would allow for the synthesis of alkyl-spirosiloxane derivatives.

In Chapter 4 we showed potential mechanistic pathways for the F⁻ catalyzed rearrangement of silsesquioxanes. However, further work is necessary to make our analysis more concrete. Future work in the area of mechanistic development should look extensively at the influence of solvent on the product equilibria and energy stabilization of intermediates by both experimental and computational methods. We are also missing

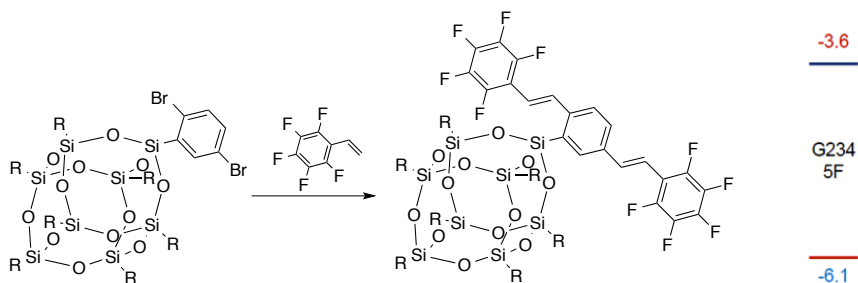
reaction transition states, which would allow us to better judge which of the three reaction pathways proposed offers the most favorable kinetics. Modeling studies or alternative mass spec techniques such as ion mobility could be used to follow reaction intermediates. Since we modeled reaction enthalpies instead of free energies the entropic component of these studies is missing, therefore developing reliable computational methods to analyze free energies would be ideal. The use of other fluoride sources should also be explored (i.e. N,N,N-Trimethyl-1-adamantylammonium fluoride) to get an understanding of how different salts influence the mechanism.¹ Lastly, the methods developed in Chapter 4 should be extended to other systems such as [vinylSiO_{1.5}] to see if reaction conditions can be developed to favor specific cage sizes (i.e. [vinylSiO_{1.5}]₁₀) and whether its mechanism of formation is consistent.

In Chapters 5 and 6 we compared the photophysical properties of T₈, T₁₀ and T₁₂ stilbenevinylSQs in solution, finding that they interdigitated/aggregate in “poor” solvents, similar to what we would expect to find in the solid state. Future work in this area should look at the solid state dynamics of these systems (i.e. films with near field scanning optical microscopy, NSOM), continuing our efforts mentioned at the end of Chapter 6. This would allow for a better understanding of the way these molecules aggregate on surfaces and how this changes their photophysical properties.

In Chapter 7 we showed the development of conjugated organic linked BoC polymers. Future work should look further into the development of BoCs with rigid conjugated linkers for possible applications in photonic applications, since we find that the more rigid dimethylfluorene structure shows both ground state and excited state conjugation. We should also look at the synthesis of BoCs by direct rearrangement of SQ cages with bis-triethoxysilyl-R linkers, removing the cross coupling step for polymerization, and allowing for easier manipulation of polymer chain length. Lastly, as mentioned below, future work should look at the development of alternating donor acceptor BoC polymers for photovoltaic applications.

In expanding our work done in Chapters 5 and 7, our group has done preliminary studies using SQs as additives and/or replacements for components in photovoltaic devices.² These SQs were developed to compliment PCBM as acceptor materials in a

P3HT:PCBM BJH system. One of the most promising of these materials was di-styryl-pentafluorophenyl₈SQ (Scheme 8.1), which has HOMO-LUMO energy levels intermediate those of P3HT and PCBM (Scheme 8.1 and Figure 5.18), allowing it to act as a cascade component aiding in electron transfer. We find that up to 30 wt.% SQ offered a slight increase in power conversion efficiency (PCE) of 4.1 to 4.2%, Figure 8.1 and a 3-fold improvement in the photocurrent (Figure 8.2). Using this SQ on its own as a replacement for PCBM resulted in low PCE of ~0.004%.



Scheme 8.1. Synthesis of di-styryl-pentafluorophenyl₈SQ and its HOMO-LUMO energy levels.

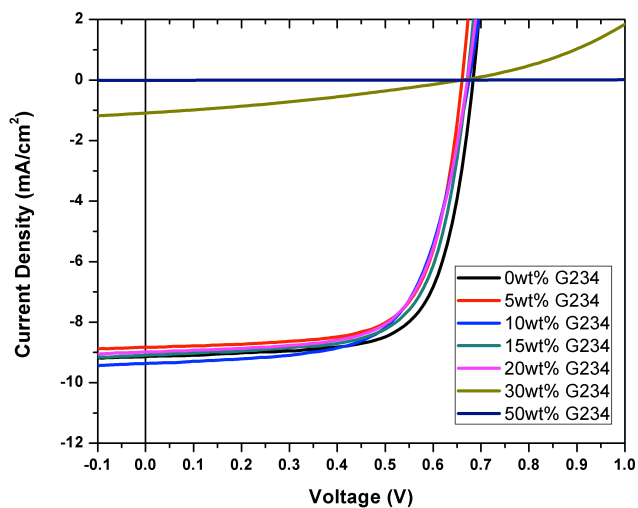


Figure 8.1. J-V curves of OPV devices fabricated with a mixture of P3HT, PCBM, and di-styryl-pentafluorophenyl₈SQ, with device configuration of glass/ITO/PEIE/active layer/MoO₃/Ag.

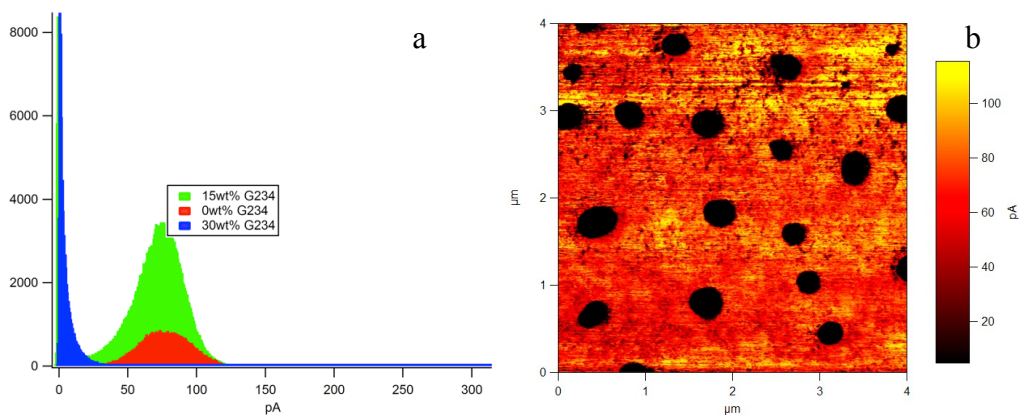
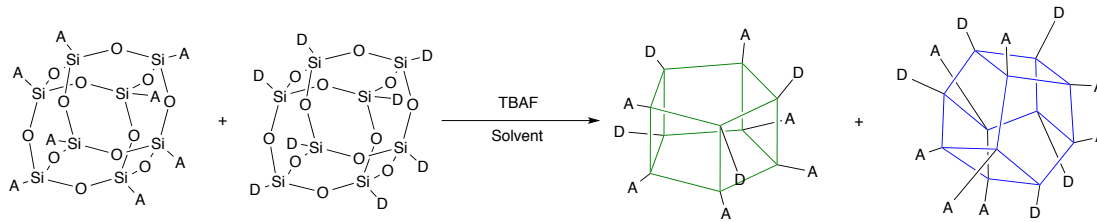


Figure 8.2. a. Photocurrent histogram showing an increase in photocurrent up to 15 wt.% SQ, b. Conductive AFM measurement of the mixed P3HT:PCBM:SQ film with SQs theorized to be in black.

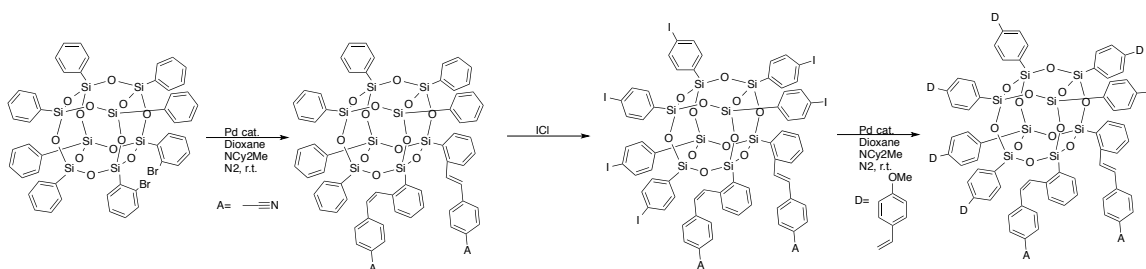
In order to further the development of SQs for energy harvesting applications, we must focus our efforts on making materials that offer higher absorption potential, ideal band gaps, and efficient charge transfer through exciton diffusion. One of the ways that researchers have been improving energy harvesting polymers is through the incorporation of donor and acceptor units within a polymer backbone.³ Using donor-acceptor polymers within one polymeric backbone enables broad spectrum absorption since each subunit would likely absorb in separate regions, efficient charge transfer since the materials would have stronger intrinsic dipoles, and also better interfacial interactions due to their ability to have better phase interactions in multi-component systems.

One could imagine that SQs could also be functionalized in a way that enables them to function as donor-acceptor materials. The first method would incorporate a donor (p-type) chromophore at one or more corners on the SQ cage, and acceptors (n-type) chromophores on the remaining corners. This can be achieved by F^- catalyzed scrambling of donor and acceptor SQs (Scheme 8.2), resulting in a statistical distribution of functionality, controlled by the initial ratio of the two cages.



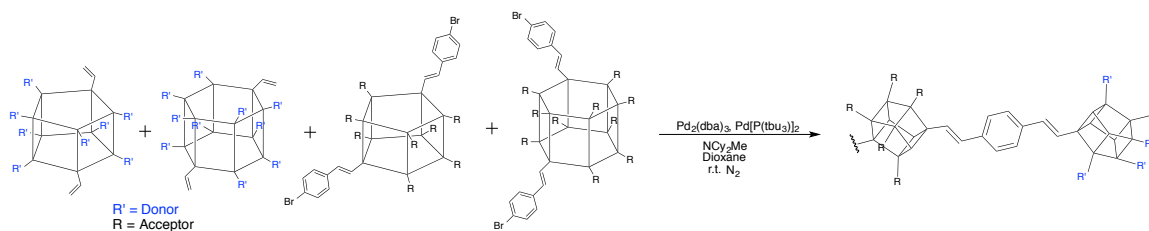
Scheme 8.2. Synthesis of mixed donor-acceptor SQs through F^- catalyzed rearrangement.

Though the rearrangement is effective at making difunctional cages, the statistical distributions may not be desired, our group has recently shown that bromination of phenylSQ cages by Br₂ is quite selective. In that after one *ortho*-bromine is attached, the second bromine is selectively added to the *ortho*-carbon on the neighboring phenyl ring.⁴ These two bromines could then be functionalized with a chromophore group with ideal characteristics. After functionalization the remaining phenyl groups can be iodinated in the *para*-position and then functionalized through cross coupling reactions with a different chromophore group (Scheme 8.3). This sort of control would allow for an intrinsic dipole to be formed through the core of the SQ, similar to those observed in conjugated polymers.



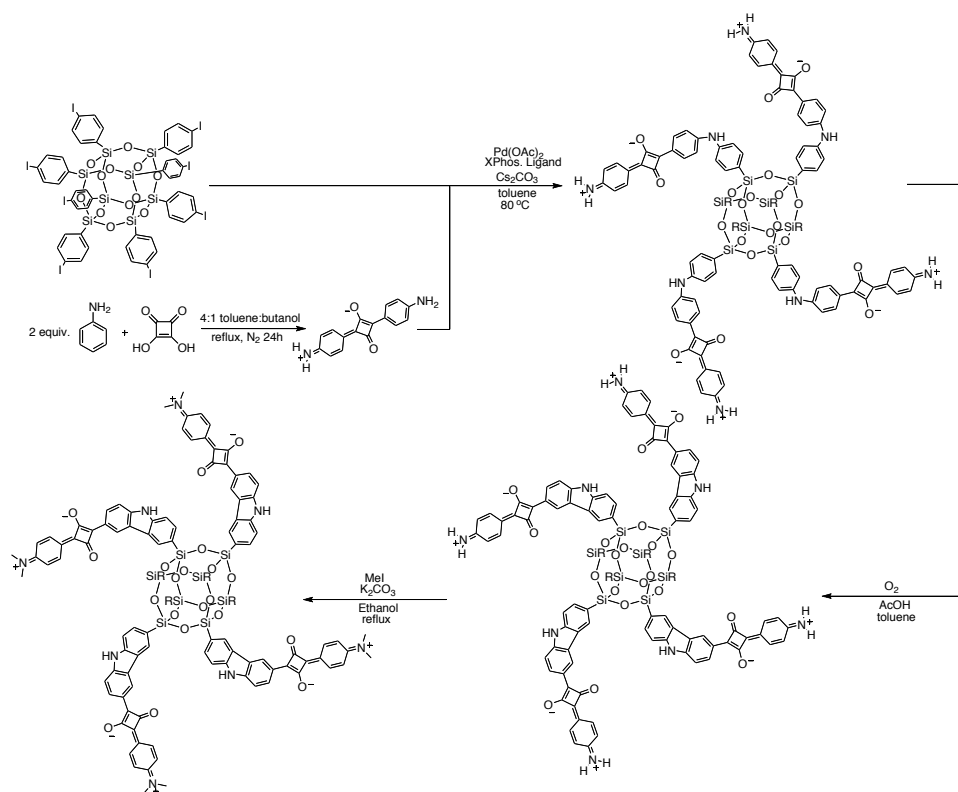
Scheme 8.3. Controlled functionalization of SQs with donor and acceptor moieties.⁵

The second major adaptation of donor-acceptor polymer type SQs would be developing them as beads on a chain (BoC) polymers/oligomers, which should allow for behavior and processability similar to organic systems. This could be achieved by methods analogous to those in Chapter 7. We would first use the F⁻ catalyzed rearrangement to scramble two sets of silsesquioxanes; for example a p-type SQ could be scrambled with a bromostyrene functionalized silsesquioxane and an n-type SQ could be scrambled with a vinylSQ. To obtain a “linear” polymer, the ratio should be controlled to give only two cross-linkable groups per cage (4.4:1). The n-type and p-type cages with their respective cross-linkable groups can then be reacted through Heck cross-coupling to form BoCs (Scheme 8.4). The reason for the two different functionalities is so that truly alternating donor-acceptor BoCs can be made, whereas if we made both cages with the same functionality a random copolymer would be obtained. After these donor-acceptor materials have been made, an in-depth analysis of their photophysical and electronic properties (i.e. absorption, emission, TPA, CV, etc) is necessary.



Scheme 8.4. Synthesis of donor-acceptor BoC polymers.

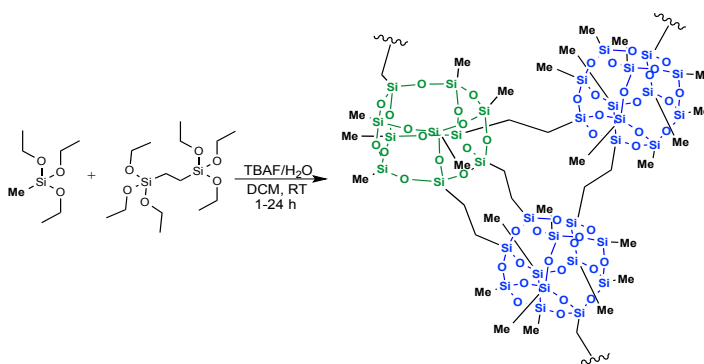
Another area that SQs could be developed is for dye sensitized solar cells. These devices typically use a thin layer of organic or inorganic dye on an oxide surface (TiO_2), with ion transfer taking place through a liquid or plasma electrolyte, much like the inner workings of a liquid electrolyte battery.⁶ These devices have been able to achieve PCE's of >11%, but have limited lifetimes, and typically poor utilization of the solar spectrum.⁷ Scheme 8.5 shows how squaraines may be used in conjunction with SQs to give dye materials that absorb over a large portion of the visible and near IR spectral range (450-800 nm). The stability of the cage, and conjugation to the cage should allow for further stability of the already robust squaraine molecules.⁸⁻¹¹



Scheme 8.5. Example synthetic methodology for developing squaraine functionalized SQs.

Polymeric materials with high surface areas ($>750 \text{ m}^2/\text{g}$) and microporosity (average pore sizes $< 2 \text{ nm}$) have been driven by their potential applications including gas storage, catalysis, separations, and nano-reactors.^{12,13} The techniques described here can also be extended to the use of SQs for high surface area materials, since their unique 3D structure allows functionalization at each corner in a well-defined manner, hyper-branched polymer systems with uniform pore diameters can be imagined. In recent work our group reported that the $\text{B}(\text{C}_6\text{F}_5)_3$ catalyzed Piers-Rubinsztajn (oxysilylation) reaction of a cubic symmetry Q-cage $[(\text{HMe}_2\text{SiOSiO}_{1.5})_8]$ with ethoxysilanes in hexane form irreversible microporous 3-D networks with surface areas $> 700 \text{ m}^2/\text{g}$ and micropore sizes of $\sim 0.6 \text{ nm}$.¹⁴ One of the limitations of this method is its sensitivity to water. Though we find that the above method works well to give high surface area materials, we set out to develop a method that could achieve higher surface areas, still be microporous and be insensitive to water.

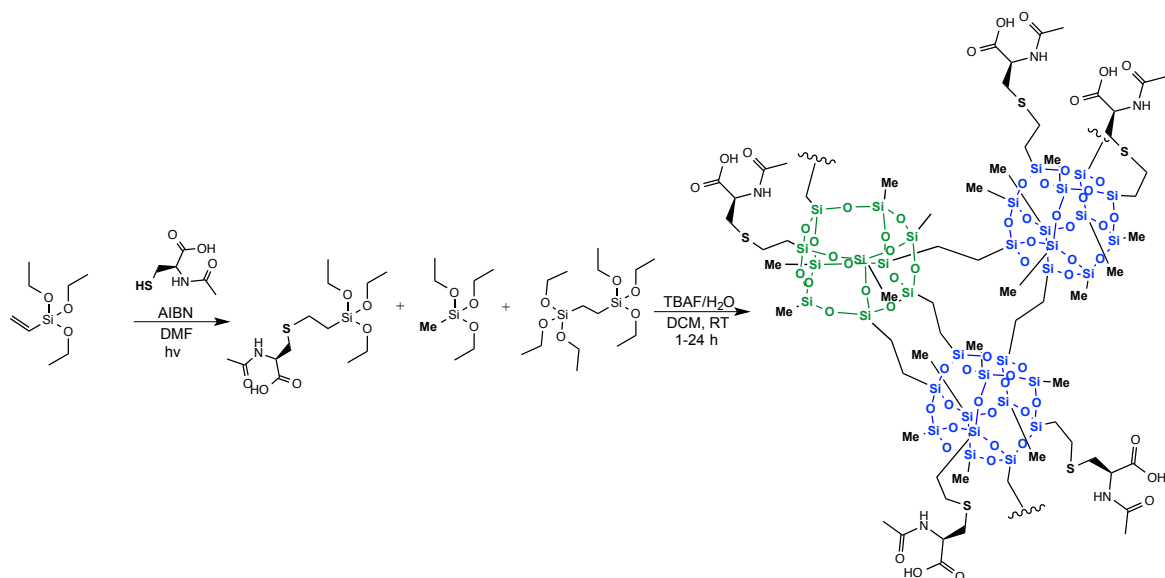
Scheme 8.6 shows how high surface area hyper-branched co-polymer SQ systems are made through F^- catalyzed cage formation using the in-situ cage formability of methyltriethoxysilane and bis-triethoxysilyl ethane.¹⁵ The advantages to this method are that it depends on water for hydrolysis and condensation reactions to occur, gels form within 24 h and can be simply filtered off and dried in-vacuo. Initial results have shown surface areas as high as $1300 \text{ m}^2/\text{g}$, which is about $900 \text{ m}^2/\text{g}$ higher than an average zeolyte and with average pore sizes of $\sim 0.8 \text{ nm}$. They offer low bulk densities (0.06 g/mL), stabilities $> 250 \text{ }^\circ\text{C}$, and solvent uptake (THF) of up to 600 % by mass.



Scheme 8.6. Synthesis of high surface area materials based with methyl functionality by fluoride catalyzed cage formation.

One important application of high surface area materials is for chiral separation columns. Many drug molecules are synthesized as a mixture of isomers and though strong effort is given to synthesizing single enantiomers, often the most cost effective method of separation is through chiral columns. This is important since one isomer of a drug may be an active pharmaceutical with therapeutic value, while the other isomer may be detrimental to one's health (i.e. thalidomide). Many chiral functionalized column materials have been developed over the years, but they are often costly and specialized for the separation of certain molecules.¹⁶ Effective separations are best achieved with chiral stationary phase materials that offer a minimum of three simultaneous intermolecular interactions with the chiral molecule, including hydrogen bonding, π -bond to π -bond interactions, dipole stacking, inclusion complexing, and the interactions caused by steric bulk.^{17,18}

High surface area SQs offer potential functionalization to chiral stationary phase materials. One method could employ amino acid functionalized silsesquioxanes, since amino acids are inherently chiral and SQs can be made with high surface areas, increasing intermolecular interactions with the molecules being separated. Scheme 8.7 below shows a proposed synthetic pathway to high surface area materials encompassing the amino acid methodology (with N-acetyl-L-cysteine).¹⁹ These materials could then be packed in a standard HPLC column and used for separation of various chiral molecules.



Scheme 8.7. High surface chiral separation polymers based on N-acetyl-L-cysteine functionalized silsesquioxanes by thiol-ene functionalization followed by fluoride catalyzed polymer formation.

References:

- Harmok, K. M.; Southworth, B. a; Wilson, K. E.; Keefer, P. K. N-Trimet Hyl- 1- Adamantylammonium Fluoride, a Completely Anhydrous Quaternary Ammonium Fluoride Salt. *J. Org. Chem.* **1993**, *58*, 7294–7295.
- Jung, J. H. Synthesis and Characterization of Conjugated Silsesquioxanes (SQs) and Their Beads on a Chain (BoC) Polymers, University of Michigan, 2013.
- Kularatne, R. S.; Magurudeniya, H. D.; Sista, P.; Biewer, M. C.; Stefan, M. C. Donor-Acceptor Semiconducting Polymers for Organic Solar Cells. *J. Polym. Sci. Part A Polym. Chem.* **2013**, *51*, 743–768.
- Bahrami, M.; Furgal, J. C.; Hashemi, H.; Ehsani, M.; Jahani, Y.; Goodson III, T.; Kieffer, J.; Laine, R. M. Synthesis and Characterization of Nano-Building Blocks [o-RStilbeneSiO_{1.5}]_{10,12} (R = Me-, MeO-, NBoc- and CN. Unexpected Photophysical Properties Arising from Apparent Asym-Metric Cage Functionalization as Supported by Modelling Studies. *Manuscr. Submitt.* **2015**.
- Zhang, X.; Furgal, J.C.; Laine, R.M. *Unpublished Results*
- Khalil Ebrahim Jasim (2011). Dye Sensitized Solar Cells - Working Principles, Challenges and Opportunities, Solar Cells - Dye-Sensitized Devices, Leonid A. Kosyachenko (Ed.), ISBN: 978-953-307-735-2, InTech
- Paek, S.; Choi, H.; Kim, C.; Cho, N.; So, S.; Song, K.; Nazeeruddin, M. K.; Ko, J. Efficient and Stable Panchromatic Squaraine Dyes for Dye-Sensitized Solar Cells. *Chem. Commun. (Camb).* **2011**, *47*, 2874–2876.
- Wang, S.; Hall, L.; Diev, V. V.; Haiges, R.; Wei, G.; Xiao, X.; Djurovic, P. I.; Forest, S. R.; Thompson, M. E. N,N-Diarylanilinosquaraines and Their Application to Organic Photovoltaics. *Chem. Mater.* **2011**, *23*, 4789-4798.

9. Dirk, C. W.; Herndon, C. W.; Cervantes-Lee, F.; Selnau, H.; Martinez, S.; Kalamegham, P.; Tan, A.; Camps, G.; Velez, M.; Zyss, J.; Ledoux, I.; Cheng, L.-T. Squarylium Dyes: Structural Factors Pertaining to the Negative Third-Order Nonlinear Optical Response. *J. Am. Chem. Soc.* **1995**, *117*, 2214-2225.
10. Watanabe, T.; Ueda, S.; Inuki, S.; Oishi, S.; Fujii, N.; Ohno, H. O. One-pot synthesis of carbazoles by palladium-catalyzed N-arylation and oxidative coupling. *ChemComm* **2007**, 4516-4518.
11. Kinashi, K.; Lee, K.-P.; Matsumoto, S.; Ishida, K.; Ueda, Y. Alkyl substituent effects on J- or H-aggregate formation of bisazomethine dyes. *Dyes and Pigments* **2011**, *92*, 783-788.
12. Kim, Y.; Koh, K.; Roll, M. F.; Laine, R. M.; Matzger, A. J. Porous Networks Assembled from Octaphenylsilsesquioxane Building Blocks. *Macromolecules* **2010**, *43*, 6995-7000.
13. Zhang, C.; Babonneau, F.; Bonhomme, C.; Laine, R. M.; Soles, C. L.; Hristov, H. A.; Yee, A. F. Highly Porous Polyhedral Silsesquioxane Polymers. Synthesis and Characterization. *J. Am. Chem. Soc.* **1998**, *120*, 8380-8391.
14. Pan, D.; Yi, E.; Doan, P.; Furgal, J. C.; Schwartz, M.; Clark, S.; Goodson III, T.; Laine, R. M. Microporous Inorganic/Organic Hybrids via Oxysilylation of a cubic symmetry nanobuilding block [(HMe₂SiOSiO_{1.5})₈] with R_xSi(OEt)_{4-x}. *Manuscript in Preparation*.
15. Furgal, J. C.; Yamane, H.; Odykirk, T.; Yi, E.; Laine, R. M. *Manuscript in Preparation*.
16. *Chiral Separations Methods and Protocols*; Gubitz, G., Schmid, M., Ed.; 1st ed.; *From Methods in Molecular Biology*, Humana Press: Totowa, NJ, 2004; pp. 29-60 and 173-182.
17. Yuki, H.; Okamoto, Y.; Okamoto, I. Resolution of Racemic Compounds by Optically Active Poly(triphenylmethyl-methacrylate), *J. Am. Chem. Soc.* **1980**, *78*, 6358.
18. Lipkowitz, K. B. Atomistic modelling of enantioselection in chromatography. *J. Chrom. A*, **2001**, 417-442.
19. Murray, F.; Furgal, J.C.; Laine, R.M. *Unpublished Results*

Appendices

Appendix A. Guide to geometry optimization, single point energy, and excited state energy calculations in the Gamess software Package

Building Your Molecule (Chemdraw, Avogadro, or Import Crystal Structure)

1. Open Chemdraw
2. Draw your molecule
3. Optimize your structure (Structure → cleanup structure)
4. Save structure as (cml) format (File → save as → scroll to .cml)
(you may also prefer to build your 3D structure directly in Avogadro, or import a crystal structure)

Working in Avogadro (rough geometry optimization and making input files)

1. Open Avogadro
2. Draw your molecule, or import .cml file from Chemdraw (File → Open)
3. If desired go to (Extensions → optimize geometry) for rough optimization

Input files

1. To generate an input file go to (Extensions → Gamess → Input Generator), this will open a Games Input screen
2. Decide type of information to calculate in the basic menu, if it is not listed it may be selected in the advanced setup menu.

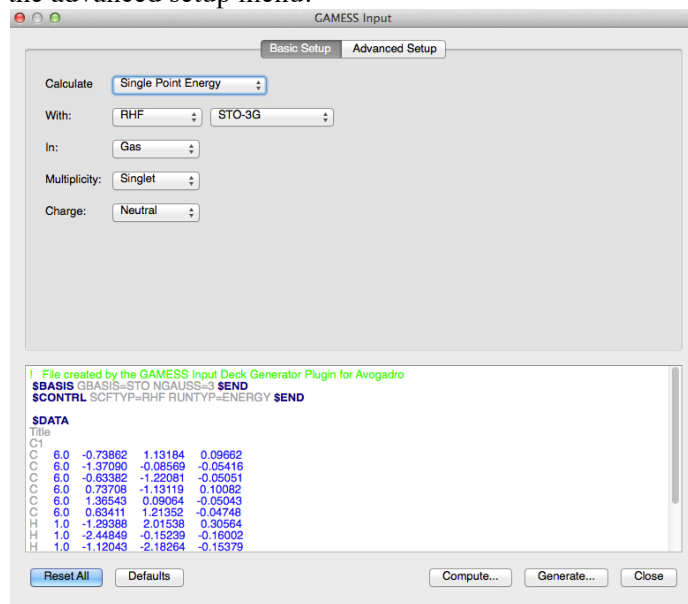


Figure A.1. Example basic input for benzene single point energy.

3. Decide the method of calculation/basis set (i.e. B3LYP, MP2, RHF..., and 6-31G(d,p)...)?
4. Gas Phase or Solvent (select water and change later (iv))?
5. Charge of molecule?
6. Once selected go to the advanced setup menu
 - a. If Geometry optimization
 - i. For small molecules select (Data → and pick the point group of the molecule) “For most large molecules the point group can be left as C1” *It may also be possible to calculate this (i.e. benzene C6h)*

- ii. Select (System → and input your desired time and memory (typically 60 min, and 1000 megawords of memory works for medium sized molecules)
- iii. If gas phase, select (Generate in the bottom right corner, and save as a **filename containing no spaces**)
- iv. If solution phase, you will need to change water in your input file box given at the bottom of the display to the solvent code you would like to use (i.e. methylene chloride is CH₂Cl₂), this uses a PCM or dielectric constant based solvation method. Then select (Generate in the bottom right corner, and save as a **filename containing no spaces**)

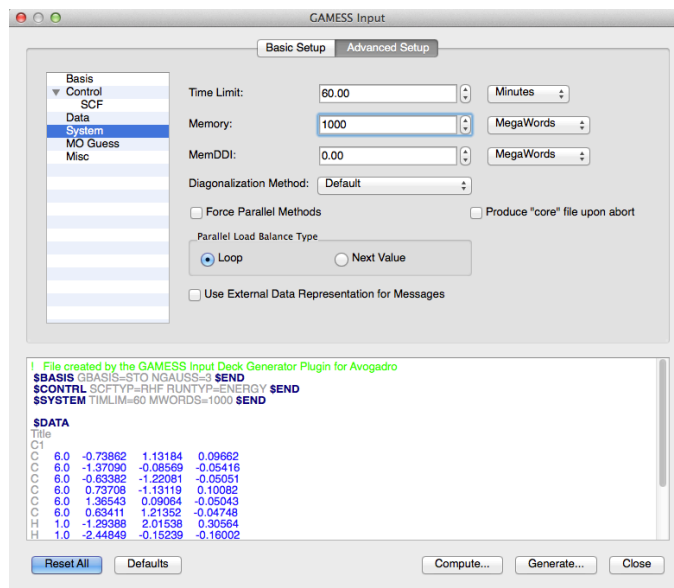


Figure A.2. Setting up time and memory requirements.

- b. If Single Point Energy
 - i. Follow same steps as above for Geometry Optimization
 - ii. You may wish to import a geometry optimized file for this calculation
- c. If Configuration Interactions (excited state...)
 - i. After basic setup, go to the advanced tab
 - ii. Go to (Control)
 1. Select (Runtype → Energy)
 2. SCF Type (None (CI))
 3. CI: (CI Singles) for CIS calculations
 - iii. Data tab same as mentioned above for Geo Opt
 - iv. Go to (System)
 1. Time: 60 min
 2. Mem: 1000 megawords
 3. MemDDI: 500 megawords (or what is needed)
 - v. If gas phase, select (Generate in the bottom right corner, and save as a **filename containing no spaces**)
 - vi. If solution phase see iv of Geo Opt

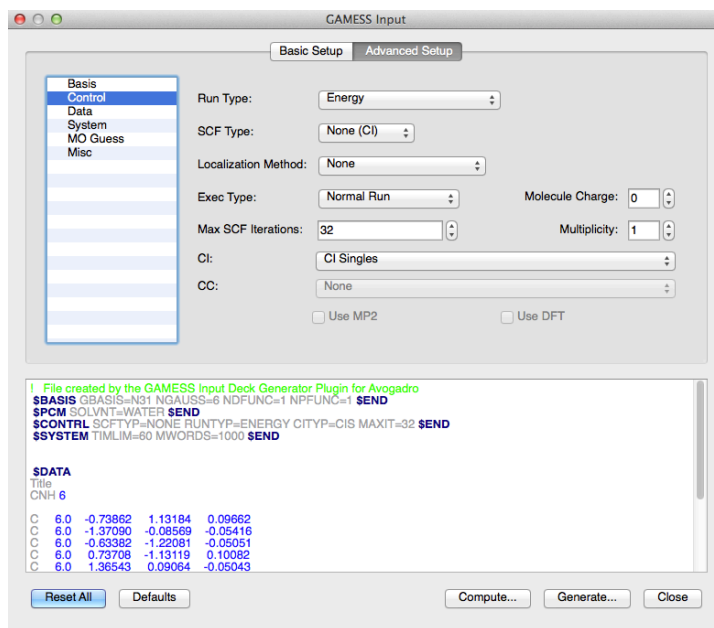


Figure A.3. Example for setting up CIS calculations.

Open input file in Gamess

1. Open Gamess
2. Select (Add+)
3. Select your input file
4. When the processor dialog box pops up, select (2 processors)
5. Wait for your file to complete
6. Then right click on the file once complete to visualize in MacMolPlt, or open the log file to view the output, you may also wish to use Gabedit (discussed later)

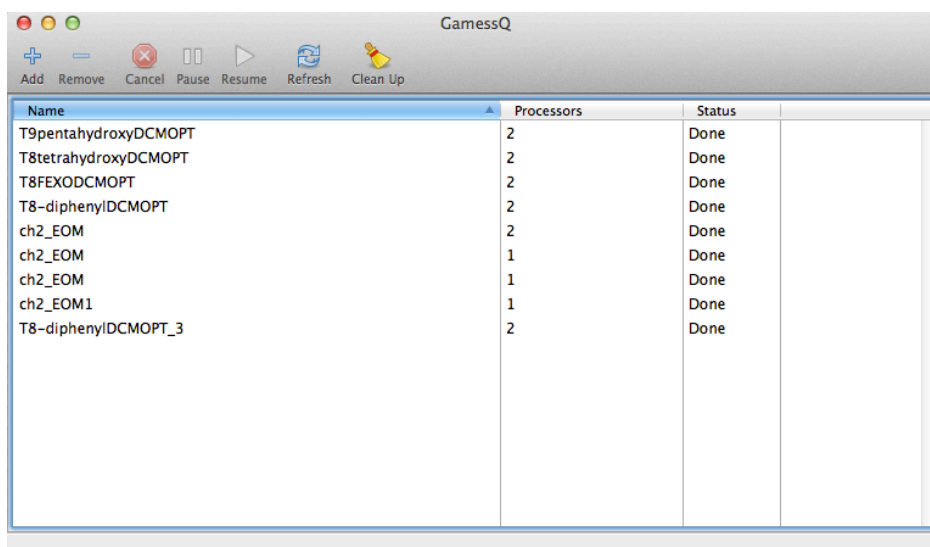


Figure A.4. GamessQ file que GUI interface.

Appendix B. Third Harmonic Generation Fluorescence Upconversion Setup:

(Laser Safety Glasses Must be Worn Throughout Process)

1. Optimize the FOG 100 system in 2nd harmonic mode using C-30 at 480 nm collection; ~70,000+ cps and ~350 mw power after BBO should be obtained before attempting 3rd harmonic mode (record all optics positions carefully)
2. Block laser beam at Tsunami
3. Place the 3rd harmonic generation optics set on the table markings
 - a. The mirror directing the laser beam into the 2nd harmonic optics set will need to be carefully removed, noting its position
 - b. The mirror directing the beam into 3rd harmonic optics set should already be in place
4. Move the mirror (M1) at the output of the Tsunami to the position noted on the table for 3rd harmonic generation

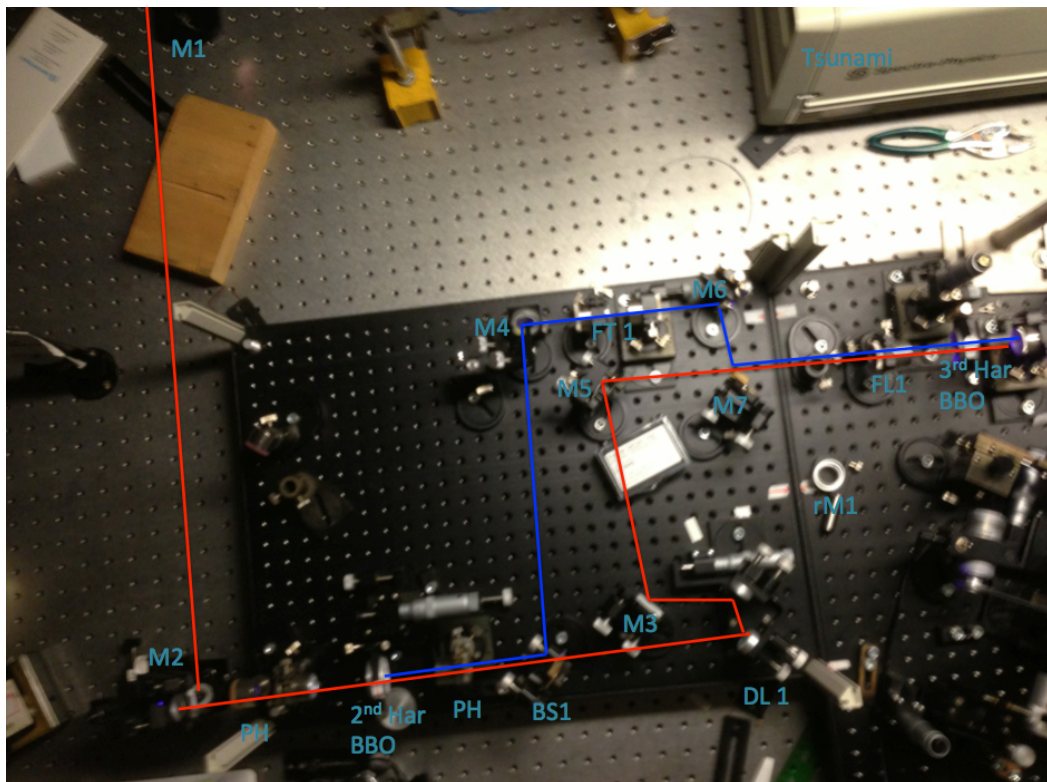


Figure B.1. 3rd harmonic upconversion table setup.

5. Set all optics as follows for initial startup
 - a. Replace the standard 2nd harmonic BBO with 3rd harmonic BBO crystal
 - b. 3rd harmonic delay line barek (8.85, DL1), Focusing lense into sample (6.55, 11.30 for 2nd harmonic), 3rd harmonic BBO (5.95), 2nd harmonic BBO (5.40), move sample cell position from -1.5 (2nd) to + 2.5 (3rd)
6. Unblock laser beam and adjust the beam into the iris (PH) on the 3rd harmonics optics set (note do this at low power, this is very tedious and takes time)

7. Turn up power and adjust 2nd harmonic crystal until the most intense blue beam is obtained (>170 mW), the beam then hits a wavelength selective splitter (BS1), separating 2nd harmonic (blue) and the incident (red) beams
 - a. The optics should be reasonably aligned, if not, shifting of the 3rd harmonic box, M1 or the mirrors in the optics set may be necessary
 - b. Check the input power (~700 mw), blue after BS1 ~ 200 mw, red after BS1 ~380 mw, red after DL1 ~362 mw, blue at UPC setup 172 mw, red 359 mw
8. Adjust the 3rd harmonic BBO angle so that the back reflection lines up with the markings on the inside panel of the standard UPC setup

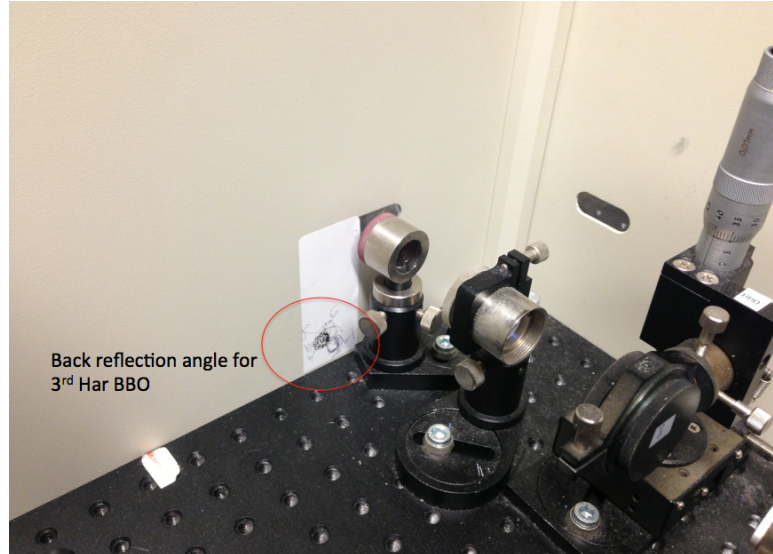


Figure B.2. 3rd harmonic upconversion reflection angle.

9. Adjust the delay line
 - a. Very carefully remove the side panels between the 3rd harmonic generation optics set and the standard UPC setup
 - i. Check the distance between the beams directly at the 3rd harmonic BBO, they should be ~0.4 cm apart with blue on left (see template)
 - ii. Remove the iris before the 3rd harmonic generation crystal and replace with mirror rM1 (usually loose in the box)
 - iii. Carefully direct this mirror so that the beam hits the two spots marked on the wall, one corresponding to the red beam, one for the blue (see below)
 - iv. Make adjustments accordingly to the optics to be sure the beams are in proper positioning

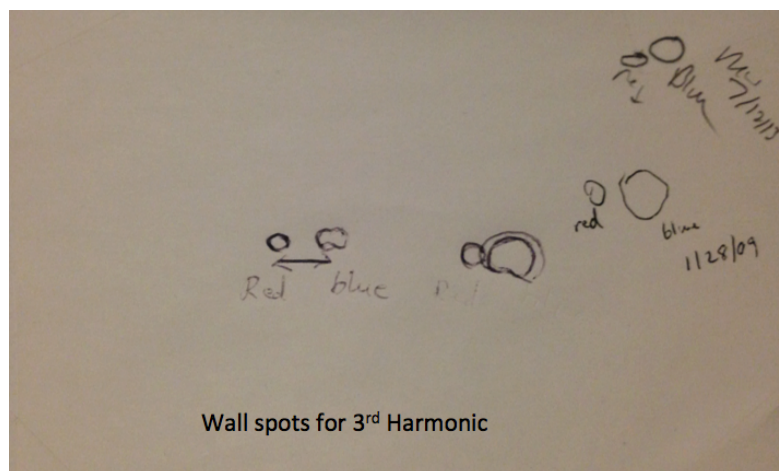


Figure B.3. 3rd harmonic upconversion wall spot positions.

- b. Use a 1 mm sample cuvette filled with a saturated solution of Rh6G in methanol to observe feature changes (i.e. while adjusting delay line watch for a “flash” or quick change in brightness (start with 8.85 mm then slowly move +/- 2 mm)
 - i. If the optimal spot is found (“flash”) then move on to step 10.
 - ii. If flash is not found adjustments have to be made to the horizontal spacing and possibly vertical alignment between the two beams, and then repeating the above steps
10. Remove the mirror added in step 7 and adjust the 3rd harmonic crystal slightly until the maximum output is achieved (~12 mW)
 - a. Check that the beam is going through the beam splitter and then to the optical delay line and sample holder (following the same path as 2nd harmonic, this is very important)
 - i. Insert pinhole before the sample holder (see below) to block off residual 400 nm, otherwise your sample will be excited with both wavelengths

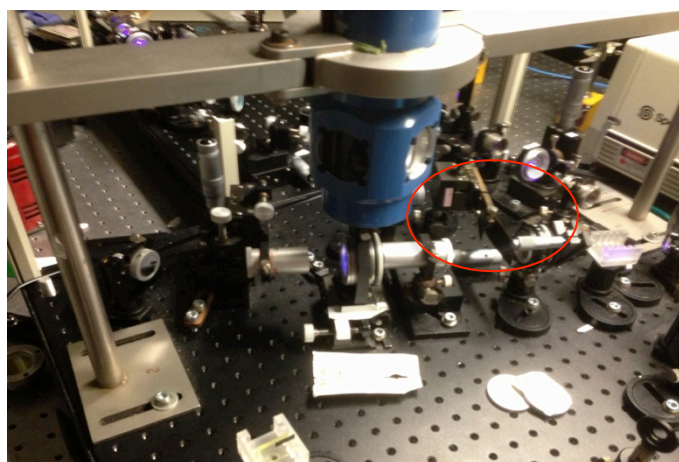


Figure B.4. 3rd harmonic upconversion pinhole position.

- ii. If it is not in relatively the same positions as those first achieved in 2nd harmonic optimization, then the 3rd harmonics optics set will need to be adjusted to compensate for the difference, try not to adjust the main system as it will be very difficult to go back to 2nd harmonic after doing so
 - iii. If necessary only adjust (slightly) the mirror directing 3rd harmonic beam into the sample holder, but do not change the path for the red beam
- 11. Adjust the main system as usual to get fluorescence counts (i.e. 2nd harmonic mode) with C-30, or stilbene which has better absorption at 286 nm
 - a. The overlap between the delay line beam and fluorescence beam will be slightly different than for 2nd harmonic (see card) and will need to be adjusted with the end mirror after the sample holder
 - b. Adjust the sum frequency crystal until counts are obtained on the system
 - i. Max with C-30 ~1500 cps
 - c. Note: to obtain collection wavelengths below 400 nm, a standard such as exalite should be used (i.e. ~370 nm); however it is difficult to jump over the 400 nm collection region due to beam leakage so be patient
- 12. Run scans as usual

Removing 3rd Harmonic Optics Set

1. Move 3rd harmonic optics set back to the end of the table
2. Replace 3rd harmonic BBO crystal with 2nd harmonic BBO crystal
3. Replace iris in front of BBO crystal
4. Replace beam elevation change mirror in front of the iris
5. Replace M1 to its previous position in front of the Tsunami
6. Set all optics to their recorded 2nd harmonic positions
7. Adjust input beam into the iris and verify it is following the correct path

Note: for further information/tricks consult Dr. Oleg Varnavski and/or his notebooks

Appendix C. Supplemental Reaction Schemes, Mass Spec and NMR Data for Chapter 3:

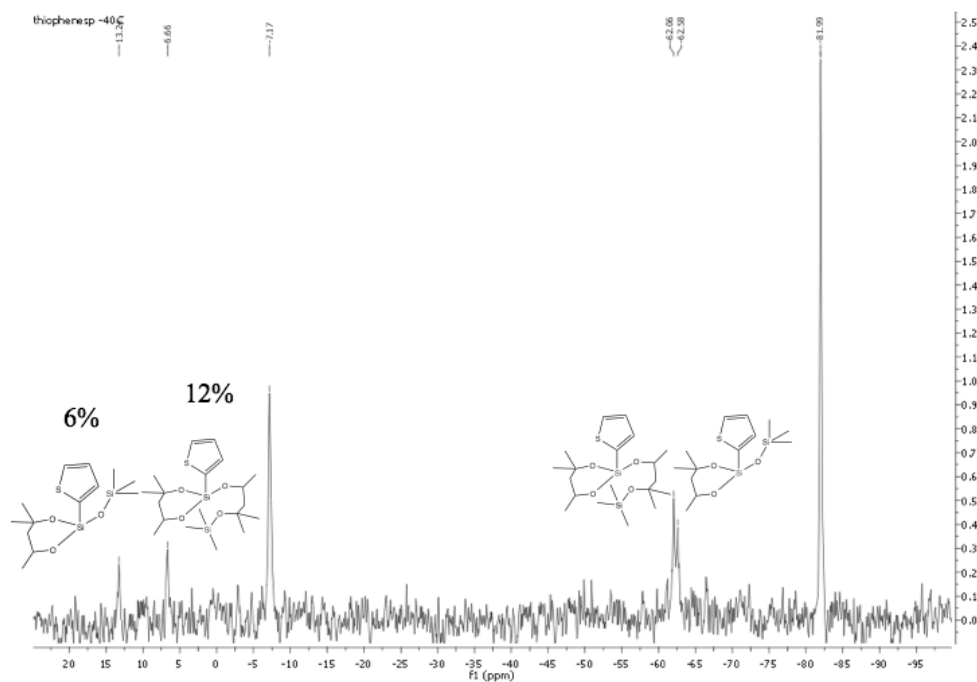
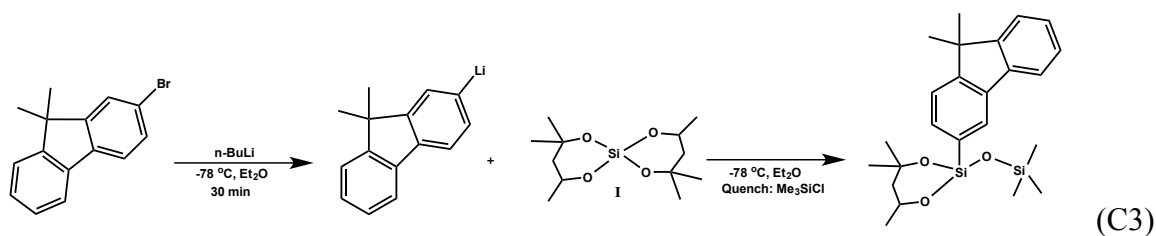
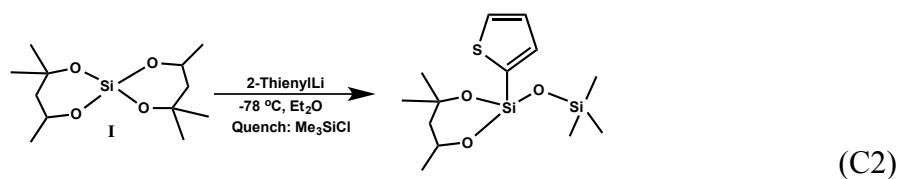
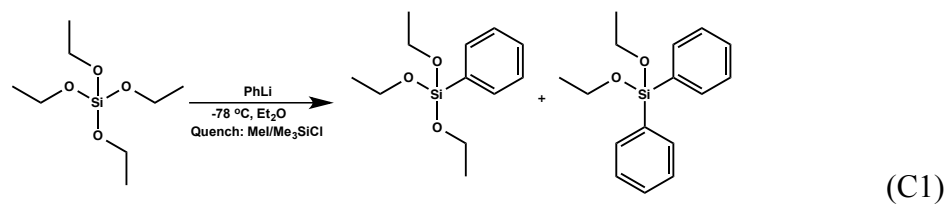


Figure C.1. ²⁹Si NMR of 1:1.2 2-thienylli:I (IX) quenched with Me₃SiCl at -78 °C.

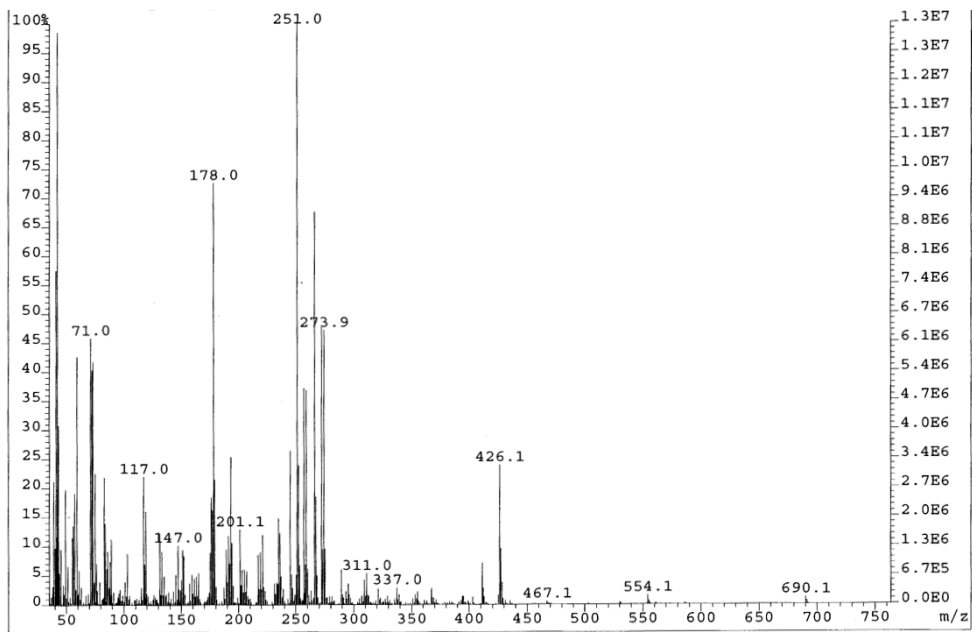


Figure C.2. EI MS of 1:1.2 9,9-dimethylfluorenylLi:I (**IX**) quenched with Me₃SiCl at -78 °C.

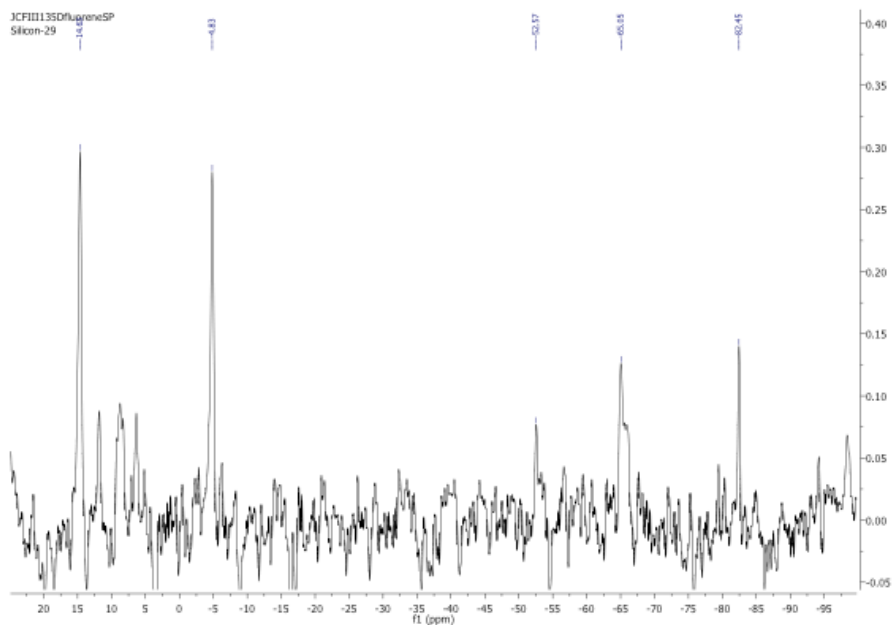


Figure C.3. ²⁹Si NMR of 1:1.2 9,9-dimethylfluorenylLi:I (**IX**) quenched with Me₃SiCl at -78 °C.

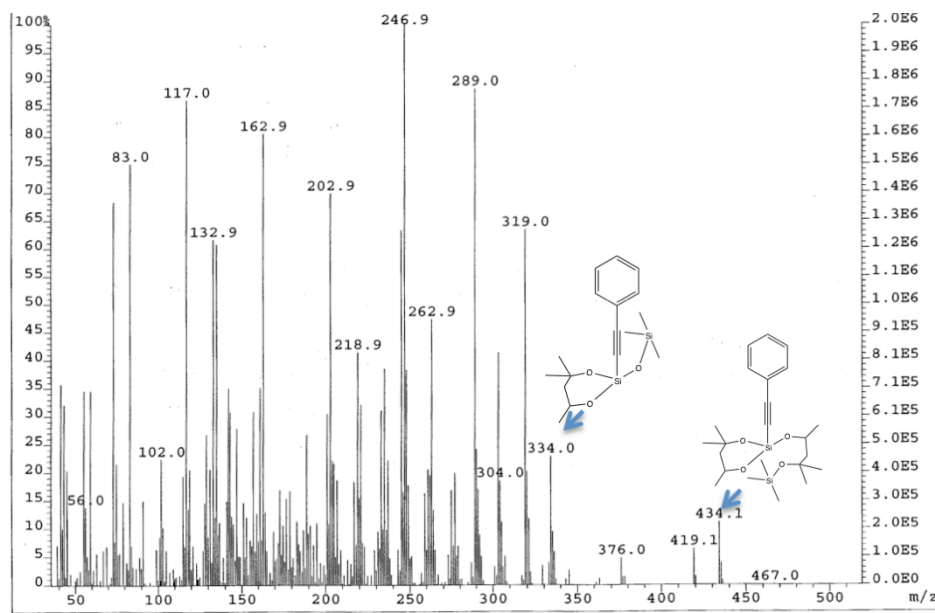


Figure C.4. EI MS of 1:1.2 Li-phenylacetylide:I (VII) quenched with Me₃SiCl at -78 °C.

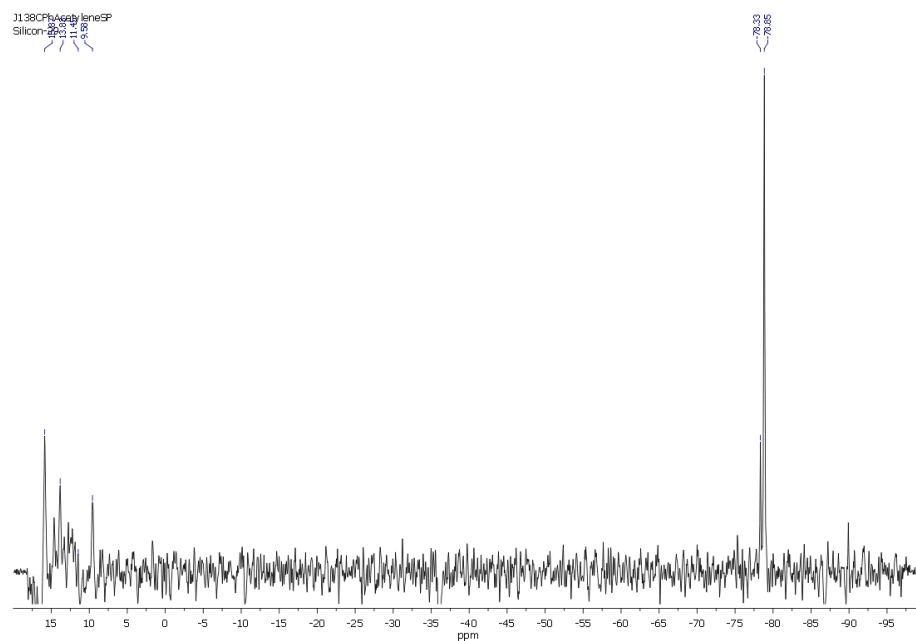


Figure C.5. ²⁹Si NMR of 1:1.2 Li-phenylacetylide:I (VII) quenched with Me₃SiCl at -78 °C.

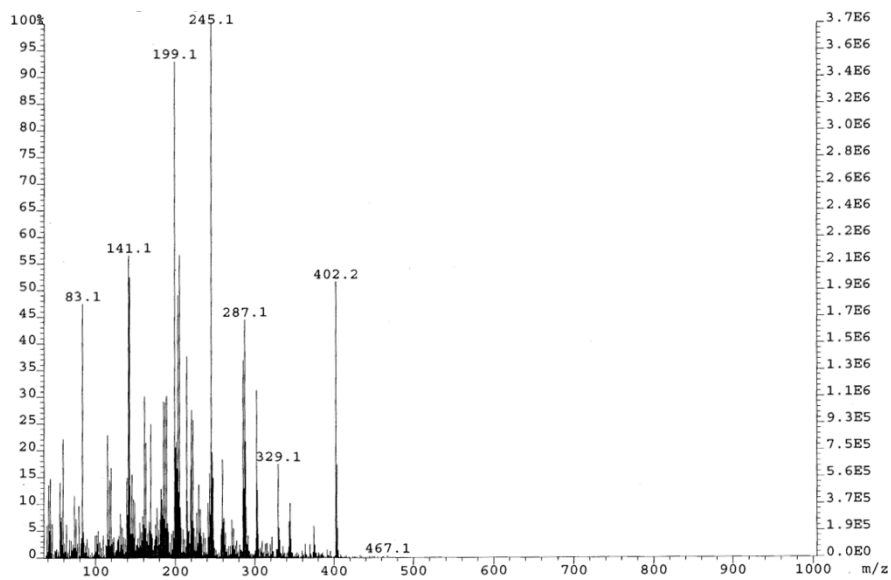


Figure C.6. EI MS of 1:1.2 methylnaphthalenylLi:I (**X**) quenched with Me₃SiCl at -78 °C.

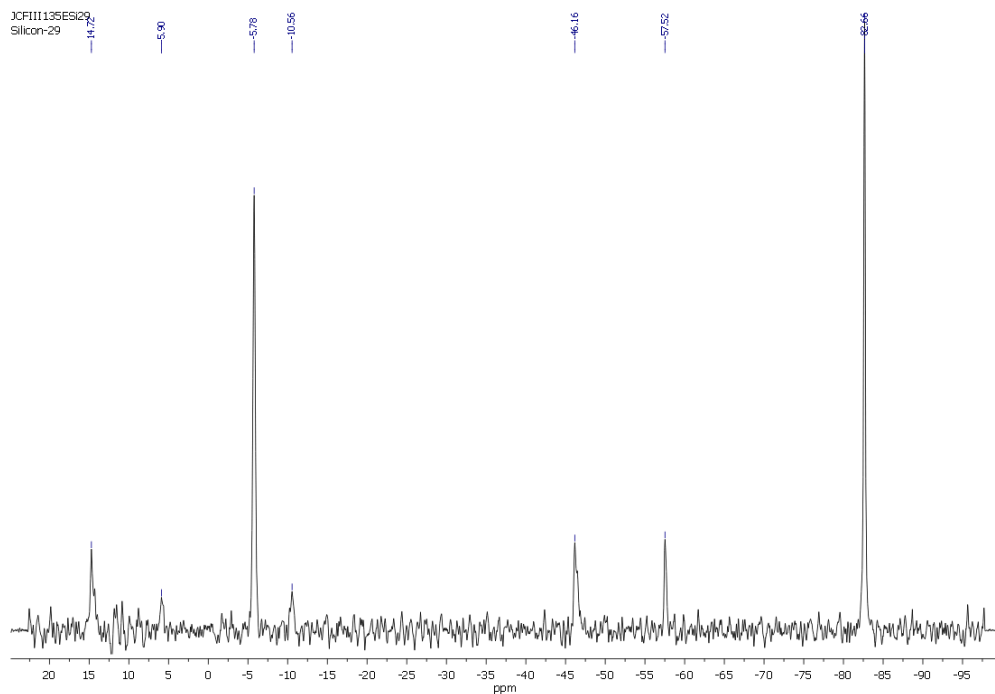


Figure C.7. ²⁹Si NMR of 1:1.2 methylnaphthalenylLi:I (**X**) quenched with Me₃SiCl at -78 °C.

Appendix D. Förster radius determination from Chapter 6:

k = dipole orientation in radians, n = refractive index of solvent, Q_D = fluorescence quantum yield, J is the overlap integral between absorption and emission.

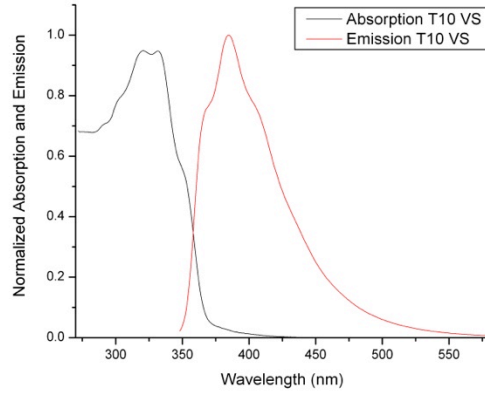


Figure D.1. Absorption and emission of T₁₀ stilbenevinylSQ.

$$R_0^6 = \frac{9000(\ln 10)\kappa^2 Q_D J(\lambda)}{128\pi^5 N n^4}$$

$$R_0 = 0.211[\kappa^2 n^{-4} Q_D J(\lambda)]^{1/6} \quad (\text{in angstroms})$$

$$= 0.211[(1.24^2)(1.404^{-4})(0.19)(1.5 \times 10^{10} \text{ M}^{-1} \text{ cm}^{-1} \text{ nm}^4)]^{1/6}$$

$$= 10 \text{ \AA for } T_{10}$$

$$= 8.6 \text{ \AA } T_{12}$$

$$= 12 \text{ \AA } T_8$$

$$= 9.9 \text{ \AA } T_{10/12}$$

Calculations of theoretical Rise Times:

$$\tau_{hop} = \tau_{ET} = T_D \left[\frac{R_0}{r} \right]^6$$

Where τ_{hop} is the expected rise time, T_D is the lifetime of the free donor system, R_0 is the FRET radius and r is the distance between chromophores.

Table D.1. Approximate distances for (r) in Å and hopping time estimate based on (r) value given.

	Distance between first carbons	Phenyl Centroid	Chromophore Centroid Distances	(r) Å used in T_{hop} calculation	T_{hop} (fs)
T8	5.2	6.6	16	9.5	720
T10	5.1	6.4	14	8.2	880
T12	4.9	5.9	12	7.3	1080

References

1. Jablonski, A. Anisotropy of Fluorescence of Molecules Excited by Excitation Transfer. *Acta. Phys. Pol. A* **1970**, *38*, 453–458.
2. Van Der Meer, B. W.; Coker III, G.; Chen, S.-Y. *Resonance energy transfer theory and data*; Wiley-VCH: New York, 1991.

Appendix E. MALDI-ToF data for Chapter 4.

Table E.1. Possible peak orientations and formulas for OPS rearrangement. Peaks in bold and italics are those observed in MALDI-ToF spectrometry, $(\text{PhSiO}_{1.5})_a(\text{H}_2\text{O})_{0.5b}$.

		Ph	Ph+108	Ph+Ag+F-
a (PhSiO _{1.5})	b (H ₂ O _{0.5})	Ph	Ph+108	Ph+Ag+F-
1	3	156.06	265.06	284.06
2	0	258.08	367.08	386.08
2	2	276.1	385.1	404.1
2	4	294.11	403.11	422.11
3	3	414.14	523.14	542.14
3	5	432.16	541.16	560.16
4	0	516.16	625.16	644.16
4	2	534.17	643.17	662.17
4	4	552.19	661.19	680.19
4	6	570.21	679.21	698.21
5	3	672.22	781.22	800.22
5	5	690.24	799.24	818.24
5	7	708.25	817.25	836.25
6	0	774.24	883.24	902.24
6	2	792.25	901.25	920.25
6	4	810.27	919.27	938.27
6	6	828.29	937.29	956.29
6	8	846.3	955.3	974.3
7	1	912.29	1021.29	1040.29
7	3	930.3	1039.3	1058.3
7	5	948.32	1057.32	1076.32
7	7	966.33	1075.33	1094.33
7	9	984.35	1093.35	1112.35
8	0	1032.32	1141.32	1160.32
8	2	1050.33	1159.33	1178.33
8	4	1068.35	1177.35	1196.35
8	6	1086.37	1195.37	1214.37
8	8	1104.38	1213.38	1232.38
8	10	1122.4	1231.4	1250.4
9	1	1170.9	1279.9	1298.9
9	3	1188.9	1297.9	1316.9
9	5	1206.9	1315.9	1334.9
9	7	1224.9	1333.9	1352.9

9	9	1242.9	1351.9	1370.9
9	11	1260.9	1369.9	1388.9
10	0	1291	1400	1419
10	2	1309	1418	1437
10	4	1327	1436	1455
10	6	1345	1454	1473
10	8	1363	1472	1491
10	10	1381	1490	1509
10	12	1399	1508	1527
11	1	1429.1	1538.1	1557.1
11	3	1447.1	1556.1	1575.1
11	5	1465.1	1574.1	1593.1
11	7	1483.1	1592.1	1611.1
11	9	1501.1	1610.1	1629.1
11	11	1519.1	1628.1	1647.1
11	13	1537.1	1646.1	1665.1
12	0	1549.2	1658.2	1677.2
12	2	1567.2	1676.2	1695.2
12	4	1585.2	1694.2	1713.2
12	6	1603.2	1712.2	1731.2
12	8	1621.2	1730.2	1749.2
12	10	1639.2	1748.2	1767.2
12	12	1657.2	1766.2	1785.2
12	14	1675.2	1784.2	1803.2